



University
of Glasgow

Aree, P. (2000) *Small-signal stability modelling and analysis of power systems with electronically controlled compensation*. PhD thesis.

<http://theses.gla.ac.uk/2600/>

Copyright and moral rights for this thesis are retained by the author

A copy can be downloaded for personal non-commercial research or study, without prior permission or charge

This thesis cannot be reproduced or quoted extensively from without first obtaining permission in writing from the Author

The content must not be changed in any way or sold commercially in any format or medium without the formal permission of the Author

When referring to this work, full bibliographic details including the author, title, awarding institution and date of the thesis must be given

**Small-Signal Stability Modelling and Analysis
of Power Systems with Electronically
Controlled Compensation**

by

P. Aree

A Thesis submitted to the

Department of Electronics and Electrical Engineering

of

The University of Glasgow

for the degree of Doctor of Philosophy

April 2000

© Pichai Aree

To my mother for her love, strong encouragement and support throughout my life

and

To all my teachers for their supports and guidance

Abstract

Flexible AC Transmission Systems (FACTS) equipment is currently being incorporated into the power system for controlling key network parameters aiming at improving the power system steady-state and dynamic performances. The vast array of power system analysis tools used by planners and system operators, on a daily basis, for the successful running of the network are to be upgraded to include comprehensive modelling for FACTS plant components. Commensurate with this global objective, this research work is aimed at developing comprehensive power system models of FACTS devices suitable for small-signal stability studies. The FACTS components covered in this research are the Static Var Compensator (SVC) and the Thyristor-Controlled Series Capacitor (TCSC). More specifically, the modelling of these devices combined with advanced modelling of synchronous generators has positioned the current work in the area of small-signal stability modelling and analysis of power systems with electronically controlled compensation. The work has been developed within the framework of the block-diagram methodology because it yields physical insight and offers the opportunity to gain fundamental knowledge of the dynamic interactions taking place between synchronous generators and FACTS plant components.

The key issues of synchronous generator modelling, from the viewpoint of small-signal stability analysis, are addressed in this thesis. In particular, the impact of synchronous generator modelling order, with emphasis on system damping, is discussed in depth. Various representations of salient-pole synchronous generators are used to enable a variety of models suitable for small-signal stability studies. The models range from synchronous generators with no damper windings, to cases when one damper winding is included in each of the rotor axes, i.e. d and q -axis. The drive behind the study is to settle the issue of what is a suitable number of machine damper windings to be used in small-signal stability analysis that adequately represents the system model with a good level of reliability while keeping engineering complexity manageable. The context of this discussion belongs to the realm of FACTS-upgraded power systems networks. The system models developed are used for a rigorous explanation of the dynamic interactions taking place between synchronous generators and between synchronous generators and these FACTS devices. The influence of SVC and TCSC plant components on the generator dynamic characteristic of the d and q -axis flux linkages are explored.

Acknowledgements

I would like to express my sincere gratitude to my advisor, Dr. Enrique Acha, for his continued guidance, encouragement, thoughtful support, and understanding during my doctoral studies. I am also very grateful to the members of staff of the Electronics and Electrical Engineering Department for providing an excellent environment for study and research.

I would also like to thank all my postgraduate colleagues for their supports and friendships.

I gratefully acknowledge the scholarship given to me by The Royal Thai Government, Thailand, during my PhD studies.

Thanks are also due to Thammasat University for granting me study leave to carry out my PhD research.

To my family, especially my mother, I express my deepest thanks for their unending love, encouragement and support. To my wife, Kalaya, for her love, understanding.

Table of Contents

| | page |
|---|------|
| Abstract | iii |
| Acknowledgements | iv |
| Table of Contents | v |
| List of Figures | ix |
| List of Tables | xiii |
| Abbreviations | xiv |
| <i>Chapter 1: Introduction</i> | |
| 1.1 Power system stability | 1 |
| 1.2 Small-signal stability | 1 |
| 1.3 Small-signal stability in small-scale power systems | 2 |
| 1.4 Small-signal stability in large-scale power systems | 4 |
| 1.5 Small-signal stability of power systems including FACTS devices | 6 |
| 1.6 Main aims of the PhD research project | 6 |
| 1.7 Main contributions | 7 |
| 1.8 Transaction-grade publications | 8 |
| 1.9 Outline of the thesis | 8 |
| 1.10 References | 9 |
| <i>Chapter 2: Power Systems and Electronically Controlled Compensation</i> | |
| 2.1 Introduction | 15 |
| 2.2 Synchronous machine modelling | 16 |
| 2.2.1 Phasor and mathematical representation of a synchronous generator | 18 |
| 2.2.2 Synchronous generator frame-of-reference | 20 |
| 2.2.3 Power relationships | 21 |
| 2.2.4 Dynamics equations of motion | 22 |
| 2.3 Electrical network | 22 |
| 2.4 Generating units | 22 |
| 2.4.1 Turbine-governor system | 23 |
| 2.4.2 Excitation system | 23 |

| | |
|--|----|
| 2.5 FACTS devices | 24 |
| 2.5.1 Static var compensators | 28 |
| 2.5.1.1 SVC control scheme | 29 |
| 2.5.2 Thyristor-controlled series compensators | 30 |
| 2.5.2.1 Basic characteristic of TCSC | 31 |
| 2.5.2.2 TCSC control scheme | 33 |
| 2.6 Conclusions | 34 |
| 2.7 References | 34 |

Chapter 3: Small-Signal Modelling of a Synchronous Generator-SVC System in a Single-Machine Environment

| | |
|--|----|
| 3.1 Introduction | 40 |
| 3.2 System under study | 41 |
| 3.3 Mathematical representation of the system under study | 41 |
| 3.4 Representation of system model | 42 |
| 3.5 Analysis of the interactions between a synchronous generator and a SVC | 45 |
| 3.6 Analysis of the SVC impact on the synchronous generator dynamic characteristic | 46 |
| 3.6.1 Effect of changes in initial operating conditions and SVC location | 46 |
| 3.6.2 Effect of changes in firing angle | 47 |
| 3.6.2.1 Variation in electrical power ΔP_{ed} | 47 |
| 3.6.2.2 Variation in electrical power ΔP_{eq} | 48 |
| 3.6.2.3 Variation in electrical power ΔP_{svc} | 48 |
| 3.7 Analysing the generator's impact on SVC | 48 |
| 3.8 Assessing the SVC's effects on the generator dynamic performance | 49 |
| 3.8.1 Electrical power ΔP_{ed} | 49 |
| 3.8.2 Electrical power ΔP_{eq} | 52 |
| 3.8.3 Electrical power ΔP_{svc} | 53 |
| 3.9 Conclusions | 54 |
| 3.10 References | 54 |

Chapter 4: Evaluation and Application of the Small-Signal Block-Diagrams Models

| | |
|---|----|
| 4.1 Introduction | 57 |
| 4.2 Fundamental evaluation of the small-signal system models | 57 |
| 4.2.1 Characteristic of the additional transfer function and coefficients | 58 |
| 4.2.2 An investigation of the power characteristic of the flux linkages in the d and q -axes | 62 |
| 4.2.3 Assessment of the overall system model | 64 |
| 4.3 An investigation of the generator dynamic performance | 66 |
| 4.3.1 Generator performance with no SVC | 67 |
| 4.3.2 Generator performance with SVC voltage control loop | 69 |
| 4.3.3 Generator dynamic performance with SVC voltage and damping control loops | 73 |
| 4.4 Conclusions | 75 |
| 4.5 References | 76 |

Chapter 5: Small-Signal Stability of the Synchronous Generator-SVC in a Multi-Machine Environment

| | |
|--|----|
| 5.1 Introduction | 78 |
| 5.2 System under study | 79 |
| 5.3 Representation of system model | 79 |
| 5.4 Overall assessment of system models | 83 |
| 5.4.1 Generator dynamic interactions | 83 |
| 5.4.2 Generator-SVC dynamic interactions | 85 |
| 5.5 Multi-machine study case | 88 |
| 5.5.1 System dynamic performance with various operating conditions | 88 |
| 5.5.2 System dynamic performance with SVCs | 92 |
| 5.6 Conclusions | 98 |
| 5.7 References | 99 |

**Chapter 6: Small-Signal Modelling of Synchronous Generator-TCSC System in
a Single-Machine Environment**

| | |
|--|-----|
| 6.1 Introduction | 101 |
| 6.2 System under study | 101 |
| 6.3 Representation of system model | 102 |
| 6.4 TCSC characteristic and control scheme | 103 |
| 6.5 Analysing the dynamic interactions between the synchronous generator and TCSC | 105 |
| 6.6 Assessing the generator dynamic performance with TCSC effects included | 105 |
| 6.6.1 Electrical power ΔP_{ed} | 105 |
| 6.6.2 Electrical power ΔP_{eq} | 108 |
| 6.6.3 Electrical power ΔP_{csc} | 108 |
| 6.7 Comparison of damping capabilities between SVCs and TCSCs | 108 |
| 6.8 Conclusions | 114 |
| 6.9 References | 114 |

Chapter 7: Conclusions and Suggestions for Further Research work

| | |
|---|-----|
| 7.1 General | 116 |
| 7.2 Suggestions for further research work | 118 |
| 7.3 References | 119 |

Appendix A: Derivation of the Small-Signal Transfer-function Block Diagram

| | |
|--|-----|
| Model of the Synchronous generator-SVC System | 122 |
|--|-----|

Appendix B: Derivation of the Small-Signal Transfer-function Block Diagram

| | |
|--|-----|
| model of the n Synchronous generators and m SVC Systems | 136 |
|--|-----|

Appendix C: Derivation of the Small-Signal Transfer-function Block Diagram

| | |
|---|-----|
| Model of the Synchronous generator-TCSC System | 149 |
|---|-----|

Appendix D: System Parameters 156

List of Figures

| | |
|---|----|
| Figure 2-1 Modelling structure of a synchronous machine | 16 |
| Figure 2-2 Machine equivalent circuits after applying Park's transformation | 16 |
| Figure 2-3 Phasor representation of the synchronous generator for transient operation | 19 |
| Figure 2-4 Machine and network frame-of-reference | 21 |
| Figure 2-5 Generating unit | 22 |
| Figure 2-6 Simplified model of the steam turbine governor system | 23 |
| Figure 2-7 Structure of the excitation system | 24 |
| Figure 2-8 FC-TCR structure of the SVC | 25 |
| Figure 2-9 Configuration of the TCSC | 25 |
| Figure 2-10 Configuration of the SPS | 26 |
| Figure 2-11 Configuration of the STATCOM | 26 |
| Figure 2-12 Configuration of the SSSC | 27 |
| Figure 2-13 Configuration of the UPFC | 27 |
| Figure 2-14 Configuration of the IPC | 28 |
| Figure 2-15 Typical configuration of a SVC System | 28 |
| Figure 2-16 Voltage-current composite characteristics of the SVC | 29 |
| Figure 2-17 SVC block diagram model | 30 |
| Figure 2-18 Configuration of the TCSC in thyristor-blocked mode | 31 |
| Figure 2-19 Configuration of the TCSC in thyristor-bypassed mode | 31 |
| Figure 2-20 Configuration of the TCSC in phase-controlled mode | 32 |
| Figure 2-21 Operating range of the TCSC | 32 |
| Figure 2-22 TCSC block diagram control | 33 |
| Figure 3-1 System under study | 41 |
| Figure 3-2 Detailed block diagram of the generator-SVC system | 44 |
| Figure 3-3 Block diagram of the generator-SVC system with the SVC placed at generator's terminal bus | 44 |
| Figure 3-4 Electrical power loops of the synchronous generator-SVC system | 45 |
| Figure 3-5 Frequency response of $\Delta P_{ed}/\Delta\delta$ with and with no SVC | 51 |
| Figure 3-6 Plots of electrical power generated by the d -axis flux linkage with various AVR gains | 52 |
| Figure 3-7 Frequency response of $\Delta P_{eq}/\Delta\delta$ with and with no SVC | 52 |
| Figure 3-8 Frequency response of $\Delta P_{svc}/\Delta\delta$ with SVC | 53 |

| | |
|--|----|
| Figure 4-1 Frequency response characteristic of the transfer function $\Delta E''_q/\Delta\alpha$ through the $g_{svc2}(s)$ branch | 60 |
| Figure 4-2 Frequency response characteristic of the transfer function $\Delta E''_q/\Delta\alpha$ through the K_{svc3} branch and AVR | 61 |
| Figure 4-3 Frequency response characteristic of the transfer function $\Delta E''_d/\Delta\alpha$ through the $g_{svc2d}(s)$ | 61 |
| Figure 4-4 Frequency response of $\Delta P_{ed}/\Delta\delta$ with Model 1-3 | 63 |
| Figure 4-5 Frequency response of $\Delta P_{eq}/\Delta\delta$ with Model 1-2 | 63 |
| Figure 4-6 Frequency response characteristic of $\Delta e_t/\Delta e_{err}$ | 64 |
| Figure 4-7 Step response of the generator output voltage ΔE_t resulting from applying a step change to Δe_{t-ref} | 65 |
| Figure 4-8 Frequency response characteristic of $\Delta e_t/\Delta e_{err}$ | 66 |
| Figure 4-9 Open-loop frequency response between $\Delta e_t/\Delta e_{err}$ for two tie-line reactance values | 67 |
| Figure 4-10 Open loop frequency response between $\Delta e_t/\Delta e_{err}$ for two electrical output powers | 69 |
| Figure 4-11 Open-loop frequency response between $\Delta e_t/\Delta e_{err}$ for cases with SVC and with no SVC | 70 |
| Figure 4-12 Open-loop frequency response between $\Delta e_t/\Delta e_{err}$ for different SVC voltage control loop gains | 71 |
| Figure 4-13 Open-loop frequency response between $\Delta e_t/\Delta e_{err}$ for cases with SVC and with no SVC | 72 |
| Figure 4-14 Open-loop frequency response between $\Delta e_t/\Delta e_{err}$ for different SVC voltage control loop gains | 73 |
| Figure 4-15 Open-loop frequency response between $\Delta e_t/\Delta e_{err}$ with and with no SVC damping control loop | 74 |
| Figure 4-16 Open-loop frequency response between $\Delta e_t/\Delta e_{err}$ with SVC damping control loop | 75 |
| Figure 5-1 Representation of the system under study | 79 |
| Figure 5-2 Block diagram of the i^{th} machine and the i^{th} SVC in a multi-machine system | 82 |
| Figure 5-3 System under study (2-generator system) | 83 |
| Figure 5-4 Open-loop frequency response between Δe_t and Δe_{err} of machine 1 | 84 |
| Figure 5-5 Open-loop frequency response between Δe_t and Δe_{err} of machine 2 | 84 |

| | |
|--|-----|
| Figure 5-6 System under study (2-generator, 1-SVC system) | 85 |
| Figure 5-7 Open-loop frequency response between Δe_t and Δe_{err} of machine 1 with Model 1-3 | 86 |
| Figure 5-8 Step responses of machine 1's voltage (Δe_t) with Models 1 and 3 | 87 |
| Figure 5-9 Step responses of machine 1's voltage (Δe_t) with Models 1 and 2 | 88 |
| Figure 5-10 System with various operating conditions | 89 |
| Figure 5-11 Open-loop frequency response between Δe_t and Δe_{err} of machine 1 with Z_1 and Z_2 changing from $0+j0.25$ to $0.05+j0.25$ p.u. | 90 |
| Figure 5-12 Open-loop frequency response between Δe_t and Δe_{err} of machine 2 with Z_1 and Z_2 changing from $0+j0.25$ to $0.05+j0.25$ p.u. | 90 |
| Figure 5-13 Open-loop frequency response between Δe_t and Δe_{err} of machine 1 with Z_1 and Z_2 changing from $0+j0.1$ to $0+j0.25$ p.u. | 91 |
| Figure 5-14 Open-loop frequency response between Δe_t and Δe_{err} of machine 2 with Z_1 and Z_2 changing from $0+j0.1$ to $0+j0.25$ p.u. | 91 |
| Figure 5-15 System under study (2-generator, 2-SVC systems) | 92 |
| Figure 5-16 Open-loop frequency response between Δe_t and Δe_{err} of machine 1 | 93 |
| Figure 5-17 Open-loop frequency response between Δe_t and Δe_{err} of machine 2 | 93 |
| Figure 5-18 Step response of output voltage Δe_t of machine 1 | 94 |
| Figure 5-19 Step response of output voltage Δe_t of machine 2 | 95 |
| Figure 5-20 Open-loop frequency response between Δe_t and Δe_{err} of machine 1 with two different gains of SVC voltage control loop | 96 |
| Figure 5-21 Open-loop frequency response between Δe_t and Δe_{err} of machine 2 with two different gains of SVC voltage control loop | 96 |
| Figure 5-22 Step response of output voltage Δe_t of machine 1 with two different gains of SVC voltage control loop | 97 |
| Figure 5-23 Step response of output voltage Δe_t of machine 2 with two different gains of SVC voltage control loop | 98 |
| Figure 6-1 System under study | 102 |
| Figure 6-2 Detailed block diagram model of the generator-TCSC system | 103 |
| Figure 6-3 TCSC configuration | 103 |
| Figure 6-4 TCSC Impedance characteristic(X_{csc}) | 104 |
| Figure 6-5 Derivative of the TCSC impedance characteristic(X_{csc}) | 104 |
| Figure 6-6 Frequency response of $\Delta P_{ed}/\Delta\delta$ with and with no TCSC | 107 |
| Figure 6-7 Frequency response of $\Delta P_{eq}/\Delta\delta$ with and with no TCSC | 107 |
| Figure 6-8 Frequency response of $\Delta P_{csc}/\Delta\delta$ with TCSC | 109 |

| | |
|--|-----|
| Figure 6-9 Frequency response of $\Delta P_{ed}/\Delta\delta$ | 110 |
| Figure 6-10 Frequency response of $\Delta P_{eq}/\Delta\delta$ | 110 |
| Figure 6-11 Open-loop frequency response between Δe_t and Δe_{err} | 111 |
| Figure 6-12 Open-loop frequency response between Δe_t and Δe_{err} | 113 |
| Figure A-1 Vector diagram of the synchronous generator-SVC system | 122 |
| Figure A-2 Block-diagram model of synchronous generator-SVC system with Model 1 | 130 |
| Figure A-3 Block-diagram model of synchronous generator-SVC system with Model 2 | 133 |
| Figure A-4 Block-diagram model of synchronous generator-SVC system with Model 3 | 135 |
| Figure B-1 Block-diagram model of n machine and m SVC system | 148 |
| Figure C-1 Vector diagram of a synchronous generator-TCSC system | 149 |
| Figure C-2 Block-diagram model of synchronous generator-TCSC system with Model 1 | 155 |

List of Tables

| | |
|---|-----|
| Table 2-1 Generator models for various d and q -axis combinations | 17 |
| Table 3-1 Summary of synchronous generators and SVC equations required for small-signal stability analysis | 42 |
| Table 3-2 System operating conditions | 50 |
| Table 4-1 System operating conditions (Section 4.1) | 59 |
| Table 4-2 System operating conditions (Section 4.2) | 68 |
| Table 6-1 System operating conditions | 106 |
| Table 6-1 System operating conditions | 112 |

Abbreviations

Synchronous generator

E_q'' = q -axis component of the subtransient internal e.m.f. proportional to total flux linkage in the d -axis damper winding

E_q' = q -axis component of the transient internal e.m.f. proportional to field winding flux linkage

E_d'' = d -axis component of the subtransient internal e.m.f. proportional to the total flux linkage in the q -axis damper winding

E_{fd} = generator field voltage

e_t = generator terminal voltage in d - q axis frame-of-reference

E_t = generator terminal voltage in D - Q axis frame-of-reference

i_g = generator armature current in d - q axis frame-of-reference

I_g = generator armature current in D - Q axis frame-of-reference

X_d, X_q = synchronous reactance in d and q -axis, respectively

X_d', X_q' = transient synchronous reactance in d and q -axis, respectively

X_d'', X_q'' = subtransient synchronous reactance in d and q -axis, respectively

τ'_{do} = open circuit d -axis transient time constant

τ''_{qo} = open circuit q -axis subtransient time constant

δ = rotor angle

ω = rotor speed

f_o = nominal frequency

P_e = electrical power injected into the grid system

P_m = mechanical power supplied by the prime mover to the generator

H = inertia constant

D = damping coefficient

L_l = stator leakage inductance

L_{fd} = field winding leakage inductance

L_{kd} = d -axis equivalent damper winding leakage inductance: $k=1,2,\dots,n$.

L_{kq} = q -axis equivalent damper winding leakage inductance: $k=1,2,\dots,n$.

L_{ad} = d -axis stator to rotor mutual inductance

L_{aq} = q -axis stator to rotor mutual inductance

L_{fkd} = differential leakage inductance proportional to the fluxes that link one or more damper windings with the field but no with the stator: $k=1,2,\dots,n$.

R_{fd} = field resistance

R_{kd} = d -axis damper winding resistance: $k=1,2,\dots,n$.

R_{kq} = q -axis damper winding resistance: $k=1,2,\dots,n$.

Static var compensator

v_{svc} = SVC terminal voltage in $d-q$ axis frame of reference

V_{svc} = SVC terminal voltage in $D-Q$ axis frame of reference

i_{svc} = SVC output current in $d-q$ axis frame of reference

I_{svc} = SVC output current in $D-Q$ axis frame of reference

$B_L(\alpha)$ = varying inductive susceptance as a function of firing angle

B_C = capacitive susceptance

X_L = inductive reactance

X_C = capacitive reactance

α = SVC firing angle

Reactive tie-line system

X_t = reactive tie-line reactance

X_{t1}, X_{t2} = reactive tie-line reactance subjected to $X_t = X_{t1} + X_{t2}$

i_t = current injected at the infinite bus

v_∞ = infinite bus voltage

Excitation control system

e_{t-ref} = generator terminal voltage reference

K_a = automatic voltage regulator gain

τ_a = automatic voltage regulator time constant

SVC control system

$v_{svc-ref}$ = SVC terminal voltage reference

K_r = SVC voltage regulator gain

τ_r = SVC regulator time constant

K_i, K_p = PI controller gain

τ_ω = time constant of washout element

TCSC control system

$i_{csc-ref}$ = TCSC current reference

K_c = TCSC voltage regulator gain

τ_c = TCSC regulator time constant

Operators

Δ = Incremental change

S = Laplace operator

Chapter 1

Introduction

1.1 Power system stability

An electrical power system consists of many individual elements, connected together to form a large, complex system capable of generating, transmitting and distributing electrical energy over large geographical areas. A major concern in power system operation is to assess the system's ability to remain stable after it has undergone a disturbance such as a fault in electrical network and sudden increase or decrease in load demands. Most stability problems are concerned with studying the behaviour of synchronous machines after they have been perturbed [1-6].

If an unbalance between supply and demand is created by a change in load, in generation, or in network conditions, a new network state is reached. The interval taken to adjust to the new condition is called the *transient period*. The system behaviour during this period is termed the *dynamic system performance* [7], which is of critical concern in defining system stability. The main criterion for stability assessment is to verify whether or not all synchronous machines maintain synchronism at the end of the transient period. The system only becomes stable if the oscillatory response exhibited during the transient period is damped and the system settles down to a new safe, operating point.

For many years, power engineers have categorised disturbances into small and large disturbances [1, 2, 6]. Random, small perturbations in system loading occur very frequently and an assessment of the ability of the system to return spontaneously to its initial operating state comes under the category of steady-state stability or small-signal stability. On the other hand, short-circuits on high voltage transmission networks or the loss of a major generating unit or transmission line are examples of large disturbances. When one of these large impacts occur, one or more synchronous machines may come out of step, i.e. lose synchronism. The problem is known in the literature as *transient stability*.

1.2 Small-signal stability

In order to study the power system dynamic behaviour from the small-signal stability viewpoint, realistic and flexible mathematical models to represent the system adequately need to be

established. If a disturbance is assumed to be sufficiently small, then a linearisation process of the non-linear equations that describe the power system dynamics may be carried out [1-3]. Once the system equations are linearised around a base operating point, the transfer functions of each system component are established and suitably connected to represent the system under study. The system performance can be studied by drawing out key information contained in the model, by resorting to well-known analytical techniques used widely in classical engineering, such as root locus, frequency responses and step responses. However, in power system engineering this approach has only been used in the study of small systems. For large systems, the non-linear set of differential equations that describe the network, in linearised form, is expressed in state-space form and the stability characteristics are determined by examining the eigenvalues and eigenvectors of the state-space matrix [1, 3-5]. This has become the only practical way in which small-signal stability studies are conducted today since numerically efficient, comprehensive algorithms have been developed over many years. The drawback of this method [1] is that it relies, exclusively, on mathematical abstraction to achieve a global result and it contributes no physical insight to the study.

1.3 Small-signal stability in small-scale power systems

Power systems have been growing continuously to meet higher load demands and, at various stages of the evolution process, system stability has become the stumbling block for sustainable growth [1, 8]. In the 1920s, the fast-acting, high-gain Automatic Voltage Regulator (AVR) was introduced to improve transient stability and voltage regulation. In the late 1960s, the Power System Stabiliser (PSS) was developed to overcome the adverse effects introduced by AVRs at certain frequency range of operation. A great many studies [8-13] in the area of small-signal stability have been conducted over a number of years to assess how the AVR affects the steady-state dynamic performance of regulated power systems. A block-diagram approach, which yields great physical insight, originally developed by Heffron and Phillips [9] and advanced further by Demello and Concordia [10], has been used for these kinds of studies. The block-diagram model was developed to represent a system under study where a synchronous generator connects to an infinite bus through an external tie-line reactance. The block-diagram model leads to an excellent explanation of how the AVR interacts dynamically with the generator and influences the generator's behaviour. The model also illustrates, in a diagrammatic form, the potential of using a PSS to supply an additional signal into the excitation control system for enhanced stability. These fundamental studies introduced very valuable knowledge in power system dynamics and formed a good basis for dealing with larger, complex systems.

Although the original Heffron-Phillips block-diagram model was a popular tool in the past, nowadays it is found unsuitable because the model only accounts for a simple representation of the synchronous generator, where only the effect of generator main field winding is included. Due to the low order model of the generator being used, there is an incomplete representation of the dynamic interaction taking place between the generator and the network. It has been recognised that this may lead to unreliable assessments of system model. From this standpoint, higher order generator models, with an increased number of damper windings, have been used more recently [14-18]. In particular, this has been the case in the design of excitation controls for enhancing system stability, because the successful tuning of these controls is critically dependent on the quality of the model used. A rigorous study of the inclusion of the damper winding effects into the generator block-diagram representation has already been conducted in [14-16]. Although the number of damper windings to be included in the model is, up to a point, arbitrary; in practice, it is limited by the difficulty to solve the large number of differential equations describing the system in an efficient manner [17-19]. Various orders of generator representations have been suggested in the open literature and whether higher or lower degrees are preferable may be open to argument [20]. Many factors play a role in the selection, for example, electrical proximity of the tie-line impedance between generators, severity of the disturbance and the type of excitation control, etc., influence the requirement of the generator model accuracy. From this viewpoint, the key concern is to select the simplest machine models that still yield sufficient accuracy of results and are amenable to meaningful small-signal stability analysis.

Once a satisfactory representation of the transfer-function block-diagram model of the power system has been established, its performances can be analysed by using a variety of methods such as the synchronising and damping coefficients method, root-locus plots, frequency domain analysis, etc. The essence of these methods is outlined below:

- The synchronising and damping coefficients method offers a very traditional way to investigate the stability of synchronous machines [1]. The electrical torque is expressed in terms of synchronising and damping torques which are useful in assessing small-signal stability. System instability can be of two forms: (i) Steady increases in rotor angle due to lack of sufficient synchronising torque, (ii) rotor oscillations of increasing amplitude due to lack of sufficient damping torque. This method has been widely used because it yields physical insight into power system stability problems.
- The Frequency response method is a very useful technique for assessing the steady-state response and for predicting and adjusting system dynamic performances without resorting to the explicit solution of the system differential equations that govern the system. The amplitude

and the phase angle of the resulting transfer function are plotted as a function of system frequency, which changes with operating conditions. The evaluation of system stability is indicated by gain and phase margins.

- The root-locus method is normally used for representing variations in system parameters and operating conditions. Whether or not the system is stable can be determined by examining the roots obtained from solving the characteristic system equation, i.e. $1+G(S)H(S)=0$.
- The state-space analysis is widely used in connection with system studies described by n -non-linear differential equations. The stability characteristics are determined by examining the eigen-values and eigen-vectors of the system matrix [1].
- Very recently, a new frequency domain based methodology has been developed in [21], termed Individual Channel Analysis and Design (ICAD). It is a very promising tool aimed at the analysis and design of single and multi-variable systems. ICAD has been applied to small-signal stability analysis of a single-machine infinite-bus system, where the role of the PSS is investigated with the aid of the block-diagram approach [22].

1.4 Small-signal stability in large-scale power systems

Early power system dynamic studies were based on the concept of a single-machine infinite-bus system. In the 1950's and mid 1960's these studies were found to be satisfactory. However, as the size of power systems continued to grow due to increasing interconnections, power system dynamic studies became much more involved [5, 23-36]. The state-space approach was introduced some years ago to deal with systems containing a large number of synchronous machines. The fundamental concept in this methodology is to use the system state variables to incorporate the dynamics of all power system components. The generator variables are blended seamlessly with the network variables by resorting to axis transformations [1, 23]. The equations of power plant components are linearised and suitably organised for inclusion in to the state-space matrix. Hence, the state variable matrix provides the complete description of the system dynamic behaviour. The method is very flexible, it allows the implementation of new elements into the state-space form with ease.

Eigen-value and eigen-vector analysis is the most popular tool for conducting small-signal stability studies in large power systems. The system stability characteristics are analysed by extracting valuable information contained in the eigen-properties of the system state-space matrix. They are obtained by solving the system characteristic equation. This technique is reported to work very well when second-order systems are analysed. For higher-order systems, this method is reported to

run into difficulties due to the widely differing magnitudes of the eigen-values involved [1]. The method used for the computation of eigen-values in large systems is the QR transformation method [1]. This method is numerically stable, robust and converges rapidly. It has been used for the small-signal stability studies of medium-size power systems. However, the QR method cannot take advantage of the sparse nature of power system networks. Instead, some powerful techniques such as iterations and a modified Arnoldi method have been developed to deal with this problem [26]. The AESOPS (Analysis of Essentially Spontaneous Oscillations in Power System) algorithm [27] has also been developed for a more efficient and reliable computation of eigen-values in very large power systems.

Alternatively, the multi-machine power system model equations can also be arranged in the form of a transfer-function representation. This leads to a physically-oriented block-diagram methodology that could be used very effectively to represent the system under study. This technique has in fact been used in [5, 28] where it has been found that the great advantage of this approach is the meaningful, physical-oriented explanation of how dynamic interactions take place between the various synchronous generators in the power system. The authors in [5, 28] developed the basic block-diagram model to represent a general n machine system, aiming at studying basic dynamic interactions between machines and between machines and their excitation control systems. In their work, the authors studied the behaviour of large scale-power systems by subdividing the system into subsystems. One of them includes a small number of synchronous machines, those of most concern. The other subsystems are external systems, which may contain a large number of machines and are of secondary concern. Each external system is then replaced by a dynamic equivalent [32-34]. This is reasonable because the attention is not focused on the dynamic behaviour of the external equivalent itself but on the dynamic interaction between synchronous generators in the internal subsystem and only the contribution from the external systems. Three main methods have been reported in the open literature for dynamic equivalencing for stability studies: the model approach [29, 30], the coherency approach [31-33] and the estimation approach [34].

The block-diagram model with application to dynamic equivalent estimation techniques [5, 34] yields a good explanation on dynamic interaction of multi-machine power systems. However, the system dynamic representation was not fully implemented because only the effects of the generator main field winding were included. In order to achieve a more realistic power system representation in a multi-machine environment, the generator model in the block-diagram framework requires further developments to include damper winding representation.

1.5 Small-signal stability of power systems including FACTS devices

With the advent of high-speed power electronics technology, a new generation of power system controllers has emerged [35-57]. These controllers can be grouped under the umbrella title of Flexible AC Transmission Systems (FACTS). The following plant components are examples of FACTS controllers: Static Var Compensators (SVC), Thyristor Control Series Compensators (TCSC), Thyristor Control Phase Shifters (TCPS), Unified Power Flow Controllers (UPFC). The main objectives of introducing FACTS devices into the power system is to increase the power transfer capability of transmission networks and to provide direct control of power flows over designated transmission routes [35]. The FACTS components achieve their objective by providing continuous control over one or more of the following power system parameters: voltage magnitude, line impedance, phase angle, active and reactive power flows. Owing to their rapid speed of response, FACTS devices perform a useful role during both steady-state and transient conditions [35, 36].

The study of the effects that FACTS devices have in enhancing power system stability has become a topic of great research importance. In the area of the small-signal stability analysis, the block-diagram approach has been used for studying the influence of FACTS controllers on power system stability. A unified model has recently been proposed by using the block-diagram approach [58-61]. These models are useful in describing some aspects of FACTS components that influence the generator's dynamic characteristic. However, the models exhibit serious short-comings since only the effect of the generator field winding is represented. In this situation, the all-important interactions between machines and between machines and FACTS devices through the d and q -axis damper windings are all but neglected. The models contain another major drawback, the dynamic interaction between FACTS controllers and the power system has not been fully implemented. For example, the feedback signal from the power network to the FACTS controller is not included for closed-loop control strategies [58-61]. Hence, further research activity is required to develop more accurate, reliable models of FACTS-upgraded power systems.

1.6 Main aims of the PhD research project

This research is primarily concerned with small-signal stability modelling of power systems containing electronically controlled shunt and series compensation. Since FACTS equipment has only been recently developed and installed in electrical power systems, it has become necessary to develop a new generation of power system tools to encompass models for all FACTS components, so that engineers can use the new tools for the planning and operation of power systems reliably and with satisfactory accuracy. The small-signal modelling of power systems including FACTS

devices is currently an area of great interest [58-61]. Very significant advances have been made with the incorporation of FACTS models within the state-space matrix oriented methodology. However, owing to the large amount of effort involved with developments in the block-diagram oriented methodology, heretofore a complete small-signal block-diagram framework, where the full aspects of dynamic interactions between synchronous generators and between generators and FACTS devices are accounted for, is not available. The inclusion of electronically controlled shunt and series compensation within a framework for conducting small-signal stability analysis is a contribution in that direction. The objectives of this research are as follows:

- To develop comprehensive power system models for single and multi-machine small-signal dynamic analysis. Models for SVC and TCSC devices are developed and seamlessly combined with models of other power system components. Synchronous generator models range from models with no damper windings to model where damper windings are included in the d and q -axes. The physical-oriented block-diagram methodology is employed to represent the system under study.
- To critically assess the dynamic performance of the various synchronous generator models covered in this research and to carry out an effective model comparison, in terms of their complexity and reliability of response, to identify a suitable number of damper windings required in small-signal stability studies using the block-diagram oriented methodology.
- To gain physical insight into the dynamic interactions taking place between synchronous generators and electronically controlled compensation, and to investigate the capabilities of these controllers to improve the generator's dynamic performance.

1.7 Main contributions

The main contributions of this research work are summarised below:

- Mathematical models of power systems containing electronically-controlled compensation are derived from first principles for small-signal stability analysis. SVC models have been developed for single-machine infinite-bus and for multi-machine frameworks. The graphical-oriented block-diagram methodology is applied to represent the power system model. Various generator models are realised which include a varying number of rotor windings.
- The various models are carefully evaluated by using the well-known frequency response methodology. Conclusions are reached as to what model yields the most satisfactory response, bearing in mind that this time the key interest lies on assessing the dynamic interactions

between synchronous generators and FACTS-type controllers, as opposed to only dynamic interactions between synchronous generators.

- The models were successfully applied to study the dynamic interactions between synchronous generators and SVCs. The influence of the SVC on the generator through the main flux linkage in the d and q -axes is investigated. The SVC's ability to improve the generator dynamic performance by contributing additional system damping, mainly through the d -axis, is demonstrated.
- The block-diagram methodology has been extended to encompass the TCSC with regards to the single-machine infinite-bus framework. Very timely investigations of the dynamic interactions between the synchronous generator and the TCSC are carried out. The TCSC's ability to improve system dynamic performance, as a function of compensation level, is demonstrated.

1.8 Transaction-grade publications

The following publications were generated during the course of the present research:

- P. Aree and E. Acha, "Block Diagram Model for Fundamental Studies of a Synchronous Generator-Static Var Compensator System", IEE Proceedings on Generation, Transmission and Distribution, Vol. 146, Part C, No. 5, September 1999, pp. 507-514.
- P. Aree and E. Acha, "A Generalised Block Diagram for Small-Signal Stability Analysis of Multi-machine, Multi-SVC Power System", Submitted to IEEE Transaction on Power System, 1999.

1.9 Outline of the thesis

This thesis is organised as follows:

Chapter 2 reviews key aspects of the mathematical modelling of power system plant components which are essential to the derivations carried out in Appendices A-C. Synchronous generator modelling and their excitation controls are briefly addressed. Also, an overview of FACTS technology with particular reference to SVC and TCSC modelling are presented.

Chapter 3 presents a comprehensive transfer-function block-diagram model for a single-machine infinite-bus power system, incorporating a SVC. The block-diagram model is employed to explain the dynamic interactions taking place between the synchronous generator and the SVC.

Chapter 4 deals with the overall assessment of the power system models developed in Chapter 3. The performance of the various orders of block-diagram models are evaluated using frequency response methods. The effects of damper windings on the level of reliability of the various system models are thoroughly investigated. Moreover, the system models are applied to investigate the SVC's ability to enhance the system dynamic performance, when the SVC is located at mid-point of tie line and when it is located at the generator's terminal bus.

Chapter 5 derives the transfer-function block-diagram models of the multi-machine, multi-SVC power system. The various degrees of system model representation are critically assessed, similarly to the case of the single-machine infinite-bus framework. The system dynamic performance is investigated when SVCs are applied in the multi-machine system.

Chapter 6 addresses the development of the transfer-function block-diagram models of a transmission system including a TCSC. This development is with regards to a single-machine infinite-bus system which resembles the very practical case of a long transmission line for which series compensation is essential. The block-diagram model is employed to explain the dynamic interactions taking place between the generator and the TCSC. For completeness, the capabilities of the TCSC and the SVC to improve the system dynamic performance are compared against each other.

Chapter 7 presents the major conclusions of the research project and discusses areas that require further research effort.

1.10 References

- [1] P. Kundur, "Power System Stability", McGraw-Hill Inc, 1993.
- [2] P. M. Anderson and A. A. Fouad, "Power System Control and Stability", The Iowa State University Press, 1986.
- [3] K. R. Padiyar, "Power System Dynamics Stability and Control", John Wiley & Sons Pte Ltd, 1995.
- [4] J. Machowski, J. W. Bialek and J. R. Bumby "Power System Dynamics and Stability", John Wiley & Sons, 1997.
- [5] Y. Yu, "Electric Power System Dynamic", Academic Press, 1983.
- [6] V. A. Venikov, "Transient Phenomena in Electrical Power System", Pergamon Press, Oxford, 1964.

- [7] IEEE Task Force on Term and Definitions, "Proposed Terms & Definitions for Power System Stability", IEEE Transactions on Power Apparatus and Systems, Vol. 101, No. 7, July 1982, pp. 1894-1898.
- [8] C. Concordia, "Steady-State Stability of Synchronous Machine as Affected by Voltage Regulator Characteristics", AIEE Transactions, Vol. 63, May 1944, pp. 215-220.
- [9] W. G. Heffron and R. A. Phillips, "Effect of Modern Amplidyne Voltage Regulator on Underexcited Operation of Large Turbine Generator" AIEE Transactions, Vol. 71, August 1952, pp. 692-697.
- [10] F. P. Demello and C. Concordia, "Concepts of Synchronous Machine Stability as Affected by Excitation Control", IEEE Transactions on Power Apparatus and Systems, Vol. 88, No. 4, April 1969, pp. 189-202.
- [11] D. P. SenGupta, N. G. Narahari and J. W. Lynn, "Damping and Synchronising Torques Contributed by a Voltage Regulator to a Synchronous Generator: A Quantitative Assessment", IEE Proceedings on Generation, Transmission and Distribution, Vol. 148, Part C, No. 8, August 1977, pp. 702-708.
- [12] A. A. Shaltout and T. H. Alden, "Analysis of Damping and Synchronising Torque", IEEE Transactions on Power Apparatus and Systems, Vol. 98, No. 5, September 1979, pp. 1701-1705.
- [13] K. L. Law, D. J. Hill and N. R. Godfrey, "Robust Co-Ordinate AVR-PSS Design" IEEE Transactions on Power Systems, Vol. 9, No. 3, August 1994, pp. 1281-1225.
- [14] M. Saidy and F. M. Hughes, "Block Diagram Transfer Function Model of a Generator Including Damper Windings", IEE Proceedings on Generation, Transmission and Distribution, Vol. 141, Part C, No. 6, November 1994, pp. 559-608.
- [15] M. Saidy and F. M. Hughes, "An Extended Block Diagram Transfer Function Model of a Synchronous Machine", International Journal of Electrical Power and Energy System, Vol. 18, No. 2, February 1996, pp. 139-142.
- [16] M. Saidy and F. M. Hughes, "Performance Improvement of a Conventional Power System Stabiliser", International Journal of Electrical Power and Energy System, Vol. 17, No. 5, October 1995, pp. 313-323.
- [17] IEEE Task Force on Definitions and Procedures, "Current Usage and Suggested Practices in Power System Stability Simulations for Synchronous Machines", IEEE Transactions on energy conversion, Vol. 1, No. 1, March 1986, pp. 77-93.

- [18] IEEE Standard 1110-1991, "IEEE Guide for Synchronous Generator Modelling Practices in Stability Analyses", 1991.
- [19] P. L. Dandeno and R. L. Hauth, "Effect of Synchronous Machine Modelling in Large Scale system Studies", IEEE Transactions on Power Apparatus and Systems, Vol. 92, No. 2, March 1973, pp. 574-852.
- [20] J. Arrillaga and C. P. Arnold, "Computer Analysis of Power System", John Wiley & Sons Pte Ltd, 1990.
- [21] W. E. Leithead, and J. O'Reilly, "m-Input m-Output feedback control by ICAD: Part 1 Structural issues", International Journal of Control, 1992, Vol. 56, pp. 1347-1397.
- [22] Z. Fadlalmoula, S. S. Robertson, J. O'Reilly and W. E. Leithead, "Individual Channel Analysis of the Turbo-generator With Power System Stabiliser", International Journal of Control, Vol. 69, No. 2, January 1998, pp. 175-202.
- [23] J. M. Undrill, "Dynamic Stability Calculation in an Arbitrary Number of Interconnected Synchronous Machines", IEEE Transactions on Power Apparatus and Systems, Vol. PAS-87, 1968, pp. 835-844.
- [24] P. Kundur, G. J. Rogers, D. Y. Wong, L. Wang and M. G. Lauby, "A Comprehensive Computer Program for Small Signal Stability Analysis of Power System", IEEE Transactions on Power Systems, Vol. 5, November 1990, pp. 1076-1083.
- [25] S. Arabi, G. J. Rogers, D. Y. Wong, P. Kundur and M. G. Lauby, "Small Signal Stability Program Analysis of SVC and HVDC in AC Power System", IEEE Transactions on Power Systems, Vol. 6, August 1991, pp. 1147-1153.
- [26] N. Uchida and T. Nagao, "A New Eigen-Analysis Method of Steady-state Stability Studies for Large Power System", IEEE Transactions on Power Systems, Vol. 3, No. 2, May 1988.
- [27] L. Wang and A. Semlyen, "Application of Sparse Eigenvalue Techniques to Small Signal Stability Analysis of Large Power System", IEEE Transactions on Power Systems, Vol. 5, No. 2, May 1990, pp. 635-642.
- [28] A. M. Moussa and Y. Yu, "Dynamic Interaction of Multi-Machine Power System and Excitation Control", IEEE Transactions on Power Apparatus and Systems, Vol. 93, No. 4, July 1974, pp. 1150-1158.
- [29] W. W. Price, D. N. Ewart, G. M. Gulanchenski and R. F. Silva, "Dynamic Equivalents from on-line Measurements", IEEE Transactions on Power Apparatus and Systems, Vol. 94, No. 4, July 1975, pp. 1349-1357.

- [30] J. M. Undrill, J. A. Casazza, E. M. Gulachenski and L. K. Kirchmayer, "Electromechanical Equivalents for Use in Power System Studies", IEEE Transactions on Power Apparatus and Systems, Vol. 90, No. 5, September 1971, pp. 2060-2071.
- [31] J. M. Undrill and A. E. Turner, "Construction of Power System Electromechanical Equivalents by Modal Analysis", IEEE Transactions on Power Apparatus and Systems, Vol. 90, No. 5, September 1971, pp. 2049-2059.
- [32] A. J. Germond, R. Podmore and K. N. Stanton, "Dynamic Aggregation of Generator Unit Models", IEEE Transactions on Power Apparatus and Systems, Vol. 97, No. 4, July 1978, pp. 1060-1069.
- [33] R. Podmore, "Identification of Coherent Generators for Dynamic Equivalent", IEEE Transactions on Power Apparatus and Systems, Vol. 97, No. 4, July 1978, pp. 1344-1354.
- [34] Y. Yu, M. A. El-Sharkawi and M. D. Wvong "Estimation of Unknown Large Power System", IEEE Transactions on Power Apparatus and Systems, Vol. 98, No. 1, January 1979, pp. 279-289.
- [35] IEEE/CIGRE, "FACTS Overview", Special Issue, 95-TP-108, IEEE Service Centre, Piscataway, N.J., 1995.
- [36] N. G. Hingorani, "Flexible AC Transmission System", IEEE Spectrum, Vol. 30, No. 4, April 1993, pp. 40-45.
- [37] E. V. Larsen, J. J. Sanchez-Gasca and J. H. Chow, "Concepts for Design of FACTS Controllers to Damp Power Swings", IEEE Transactions on Power Systems, Vol. 10, No. 2, May 1995, pp. 984-955.
- [38] L. Angquist, B. Lundin and J. Samuelsson, "Power Oscillation Damping Using Controlled Reactive Power Compensation: A Comparison between Series and Shunt Approaches", IEEE Transactions on Power Systems, Vol. 8, No. 2, May 1993, pp. 687-699.
- [39] R. M. Mathur and R. S. Basati, "A Thyristor Controlled Static Phase-Shifter for AC Power Transmission", IEEE Transactions on Power Systems, Vol. 100, No. 5, May 1981, pp. 2650-2655.
- [40] R. Mihalic and P. Zunko, "A Phase-Shifting Transformer with Fixed Phase Between Terminal Voltage and Voltage Boost: Tool for Transient Stability Margin Enhancement", IEE Proceedings on Generation, Transmission and Distribution, Vol. 142, Part C, No. 3, May 1995, pp. 257-262.
- [41] E. V. Larsen, K. Clark, S. S. Miske and J. Urbanek, "Characteristic and Rating Considerations

- of Thyristor Controlled Series Compensation”, IEEE Transactions on Power Delivery, Vol. 9, No. 2, April 1994, pp. 883-841.
- [42] S. G. Helbing and G. G. Karady, “Investigations of an Advanced Form of Series Compensation”, IEEE Transactions on Power Delivery, Vol. 9, No. 2, April 1994, pp. 939-947.
- [43] L. Gyugyi, C. D. Schauder, S. L. Williams, T. R. Rietman and A. Edris, “The Unified Power Controller: A New Approach to Power Transmission Control”, IEEE Transactions on Power Delivery, Vol. 10, No. 2, April 1995, pp. 1085-1097.
- [44] R. Mihalic, P. Zunko and D. Povh, “Improvement of Transient Stability Using Unified Power Flow Controller”, IEEE Transactions on Power Delivery, Vol. 11, No. 1, January 1996, pp. 485-490.
- [45] A. Nabavi-Niaki and M. R. Iravani, “Steady-State and Dynamic Models of Unified Power Flow Controller (UPFC) for Power System Studies”, IEEE Transactions on Power Systems, Vol. 11, No. 4, November 1996, pp. 1973-1943.
- [46] P. W. Lehn and M. R. Iravani, “Experimental Evaluation of STATCOM Closed Loop Dynamic”, IEEE Transactions on Power Delivery, Vol. 13, No. 4, October 1998, pp. 1378-1384.
- [47] J. Bian, D. G. Ramey, R. J. Nelson and A. Edris, “A Study of Equipment Size and Constraints for A Unified Power Flow Controller”, IEEE Transactions on Power Delivery, Vol. 12, No. 3, October 1997, pp. 1385-1391.
- [48] C. R. Fuerte-Esquivel, "Steady State Modelling and Analysis of Flexible AC Transmission System", PhD Thesis, University of Glasgow, Scotland, August 1997.
- [49] P. Pourbeik and M. J. Gibbard, “Damping and Synchronising Torques induced on Generator by FACTS Stabilisers in Multimachine Power Systems”, IEEE Transactions on Power Systems, Vol. 11, No. 4, November 1996, pp. 1920-1925.
- [50] IEEE Tutorial 87TH0187-5-PWR, “Application of Static Var System for System Dynamic Performance”
- [51] T. J. E. Miller, “Reactive Power Control in Electric System”, John Wiley & Sons, 1982.
- [52] S. Torseng, “Shunt-Connected Reactors and Capacitor Controlled by Thyristors”, IEE Proceedings, Vol. 128, No. 6, November 1981, pp. 366-373.
- [53] I. A. Erinmez, “Static Var Compensator” Work Group 38-01, Task Force No. 2, CIGRE, 1986.

- [54] A. E. Hammad, "Analysis of Power System Stability Enhancement by Static Var Compensator", IEEE Transactions on Power Systems, Vol. 1 No. 4, November 1986, pp. 222-227.
- [55] IEEE Special Stability Controls Working Group, "Static Var Compensator Models for Power Flow and Dynamic Performance Simulation", IEEE Transactions on Power Systems, February 1994, pp. 229-240.
- [56] E. Z. Zhou, "Application of Static Var Copensators to Increase Power System Damping", IEEE Transactions on Power Systems, Vol. 8, No. 2, May 1993, pp. 655-661.
- [57] M. Brucoli, F. Torelli and M. Trovato, "A Decentralised Control Strategy for Dynamic Shunt VAR Compensation in Interconnected Power System", IEE Proceedings on Generation, Transmission and Distribution, Vol. 132, Part C, No. 5, September 1985, pp. 229-236.
- [58] H. F. Wang and F. J. Swift, "A Unified Model for the Analysis of FACTS Devices in Damping Power System Oscillation Part I: Single-machine Infinite-bus Power System", IEEE Transactions on Power Delivery, Vol. 12, No. 2, Aprils 1997, pp. 941-946.
- [59] H. F. Wang, F. J. Swift and M. Li, "A Unified Model for the Analysis of FACTS Devices in Damping Power System Oscillation Part II: Multi-machine Power System", IEEE Transactions on Power Delivery, Vol. 13, No. 4, October 1998, pp. 1355-1360.
- [60] H. F. Wang and F. J. Swift, "Capability of the Static Var Compensator in Damping Power System Oscillations", IEE Proceedings on Generation, Transmission and Distribution, Vol. 143, Part C, No. 4, July 1996, pp. 353-358.
- [61] H. F. Wang and F. J. Swift, "Application of the Controllable Series Compensator in Damping Power System Oscillation", IEE Proceedings on Generation, Transmission and Distribution, Vol. 143, Part C, No. 4, July 1996, pp. 359-364.
- [62] Y. Tang and A. P. S. Meliopoulos, "Power System Small Signal Stability Analysis with FACTS Elements", IEEE Transactions on Power Delivery, Vol. 12, No. 3, July 1997, pp. 1353-1361.
- [63] R. M. Mathur, P. K. Dash and A. E. Hammad, "Transient and Small Signal Stability of a Supperconducting Turbogenerator Operating with Thyristor Controlled Static Compensator", IEEE Transactions on Power Apparatus and Systems, Vol. 98, No 6, November 1979, pp. 1937-1944.

Chapter 2

Power systems and Electronically-Controlled Compensation

2.1 Introduction

In conventional power systems, synchronous generators are the main source of electrical energy, which is exported to the points of consumption via high voltage transmission lines and low voltage distribution systems. From the operational control point of view, the quality of power supply should meet certain standards with regards to frequency and voltage levels, which should not deviate significantly from pre-specified operating values [1-2]; various levels of control are used to meet such requirements. For example, in the generating plant itself, there are prime-mover controls and excitation controls to regulate frequency and output voltage magnitude at the terminals of the generating plant, respectively. In the high-voltage transmission network, there are devices such as synchronous condensers, and tap-changing transformers which control voltage magnitude, and phase-shifting transformers which regulate active power flow. With the advent of modern high-power, high-current power electronics technology, a wide range of advanced power plant controllers is just becoming available. They are generically known as Flexible AC Transmission System (FACTS) devices. They have been developed to provide continuous power flow and voltage magnitude control at key points of the transmission network [3-5].

In order to carry out system level studies of modern power systems, accurate modelling of the newly emerging power plant components, alongside established power plant components, is a matter of fundamental importance. In this chapter, the mathematical models of power system components suitable for small-signal stability studies are reviewed. Emphasis is placed on the mathematical modelling of synchronous generators and electronically controlled shunt and series compensation. The chapter starts by reviewing the basic theory and classification of synchronous generator models, to be followed by a brief description of the turbine-governor control system and the excitation control system. The chapter ends with an overview of the main characteristics of FACTS devices with particular reference to electronically controlled shunt and series compensation.

2.2 Synchronous machine modelling

In system stability studies, the basic approach to generator modelling is to consider the generator as an arrangement of three stator windings, 120 electrical degrees apart, and a rotating structure with a field winding and one or more damper windings [6-12]. The schematic representation is shown in Fig. 2-1.

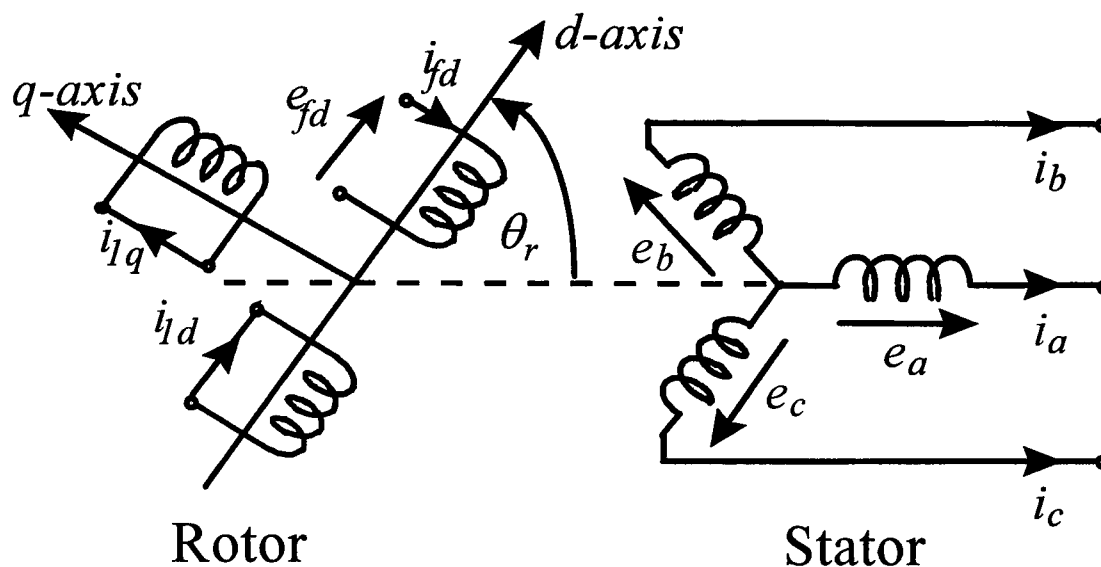


Figure 2-1 Modelling structure of a synchronous machine

In Fig. 2-1, the rotor circuits are located along the direct and quadrature axes, respectively. The d -axis coincides with the axis of the field winding and the q -axis leads the d -axis by 90 degrees in the direction of rotation.

The essential mathematical tool to study the synchronous machine is Park's transformation [6]. The idea is to mathematically transform all time varying three-phase stator voltages, currents and flux linkages into time invariant direct and quadrature axes quantities. In the transformed framework, deviations in speed of the rotor structure are easily accounted for as a function of the stator direct and quadrature axes flux linkages and voltage relationships. The circuit representation of the equivalent synchronous generator is shown in Fig. 2-2.

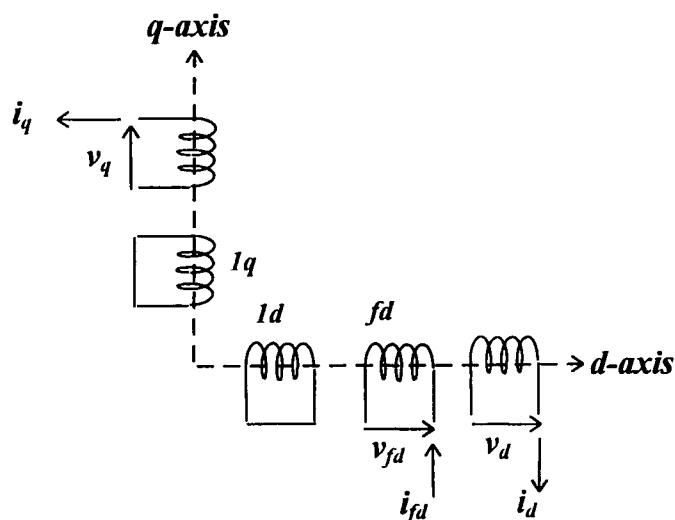


Figure 2-2 Machine equivalent circuit after applying Park's transformation

The two axes model in Fig. 2-2 is the best known configuration of the generator model. The order of the generator model may be defined as the number of rotor circuits in both the d and q -axes. Theoretically, rotor circuits may explicitly contain an arbitrary number of circuits. For the purpose of power system stability studies, however, the most complex model that has appeared in the open literature is the model $(3d.3q)$, which comprises the field winding, two damper windings in the d -axis and three damper windings in the q -axis. It should be mentioned that on-site non-standard test measurements were conducted to gather the data required to feed the model $(3d.3q)$ used in the study. Based on this model, twelve possible circuit combinations are indicated in Table 2-1 but according to some of the most authoritative material published in the field [12-13], it appears that only seven model structures are serious candidates for inclusion in large power system stability studies. Six of these model structures are drawn in Table 2-1, with the seventh model being the constant rotor flux linkage [2, 12]. Refer to the Abbreviations section for the notation used in the diagram of Table 2-1.

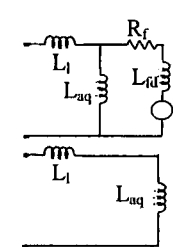
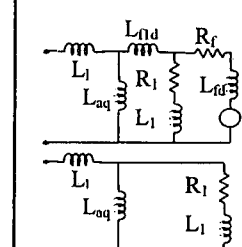
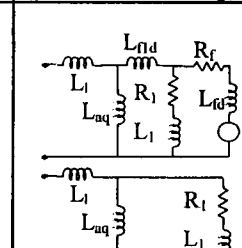
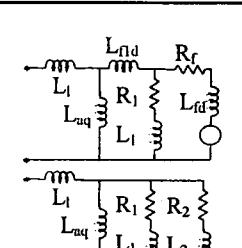
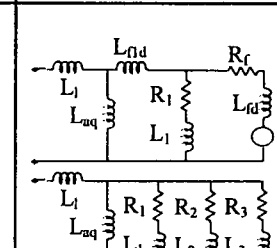
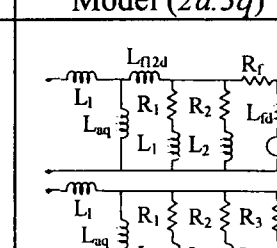
| Q-Axis ↗ ↘ D-Axis | No damper circuit | One damper circuit | Two damper circuits | Three damper circuits |
|--------------------------------|--|--|---|--|
| Field circuit only |  Model $(1d.0q)$ |  Model $(1d.1q)$ | Model $(1d.2q)$ | Model $(1d.3q)$ |
| Field plus one damper circuits | Model $(2d.0q)$ |  Model $(2d.1q)$ |  Model $(2d.2q)$ |  Model $(2d.3q)$ |
| Field plus two damper circuits | Model $(3d.0q)$ | Model $(3d.1q)$ | Model $(3d.2q)$ |  Model $(3d.3q)$ |

Table 2-1 Generator models for various d and q -axes combinations

It should be mentioned that in reality model choice might be more restricted than what is stated above. To conform with standard practices, it has been found necessary to limit the number of rotor circuits to a maximum of three or four circuits since lack of standard data inhibits the use of more elaborated rotor models except for very specialised studies [12].

For most practical purposes, Model (2d.2q) is the most elaborated structure used to represent synchronous machines in stability studies. The model considers two windings in each axis. Parameter values for this model are normally supplied by manufacturers of synchronous machines. Two time constants and two rotor reactances and resistances are employed to describe the response of the model in each of the d and q -axes. Model (2d.2q) is applicable to round rotor generators.

Model (2d.1q), with a single q -axis damper circuit, is used to represent salient pole structures such as hydro-generators. In this model, no distinction is made, in the q -axis, between transient and synchronous (steady-state) conditions and only one q -axis rotor circuit is used for representing the rapidly decaying subtransient effects.

Model (1d.1q) is a simplification of model (2d.2q), where only two rotor windings are considered, one in the d -axis and the other one in the q -axis. One time constant per axis is used to represent the generator's response.

Model (1d.0q) is a further simplified structure of model (2d.2q). Using this representation only changes in the field flux linkages can be determined. Model (1d.0q) has been widely used until very recently [15-23] but its limitations are far too many for the model to continue being used in small-signal stability studies.

The simplest generator model is the classical representation, which assumes a constant voltage behind a transient reactance. The rotor flux linkages are assumed to be constant and no transient saliency exists. Since the voltages and currents are not resolved into d and q -axis components, the model is not shown in Table 2-1. An advantage of this model is that the interfacing of the generator and network equations is carried out with ease during step-by-step calculations, and a minimum amount of data is required.

The mathematical representation of the model structures shown in Table 2-1 is presented below, following a decreasing order of model complexity.

2.2.1 Phasor and mathematical representation of a synchronous generator

Since the equations describing the electrical characteristics of a three-phase synchronous generator are well defined by a two-dimensional frame-of-reference, the electrical quantities can be expressed in terms of d and q -axis parameters. Because the synchronous machine's inertia prevents the flux linkages from changing instantly, machine models can be defined for steady-state, transient and subtransient conditions, depending on the speed of the external changes [2]. An example of a d - q phasor diagram for the transient model of the generator is shown in Fig. 2-3 [1].

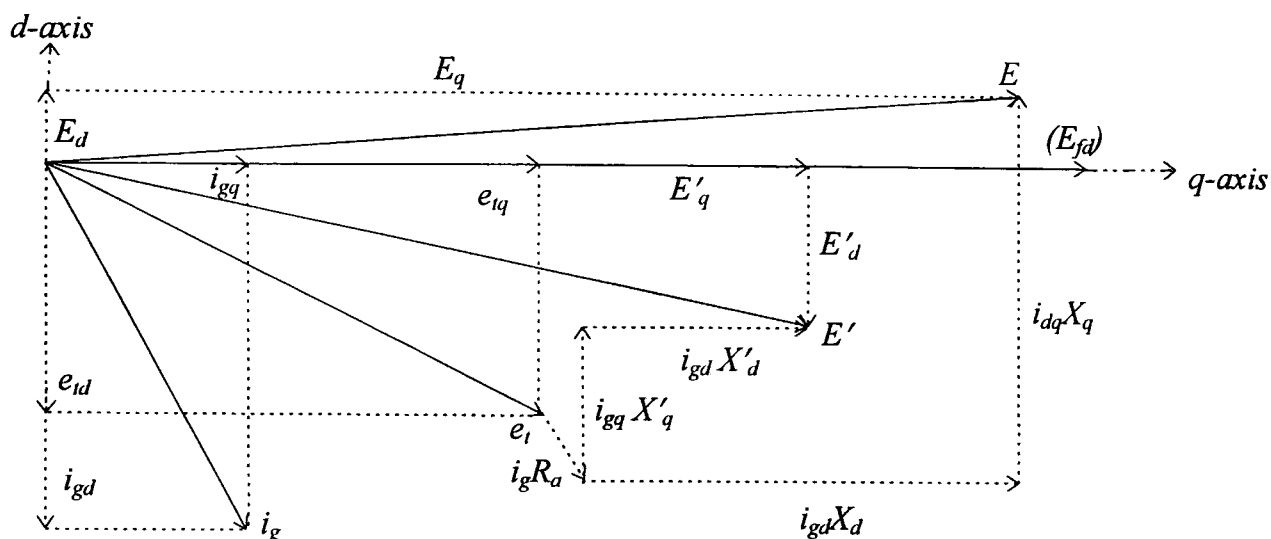


Figure 2-3 Phasor representation of the synchronous generator for transient operation

From Fig. 2-3, each phasor quantity can be represented in terms of its d and q -axis components,

$$\bar{i}_g = i_{gd} + j i_{gq} \quad (2-1)$$

$$\bar{e}_t = e_{td} + j e_{tq} \quad (2-2)$$

$$\bar{E} = E_d + j E_q \quad (2-3)$$

The algebraic equations for the synchronous machine transient model in Fig. 2-3 can be written as follows,

$$E'_d - e_{td} = R_a i_{gd} - X'_q i_{gq} \quad (2-4)$$

$$E'_q - e_{tq} = R_a i_{gq} + X'_d i_{gd} \quad (2-5)$$

These equations lead to the formulation of the following transient differential equations [14],

$$\frac{dE'_q}{dt} = \frac{1}{\tau'_{do}} [E_{fd} - i_{gd}(X_d - X'_d) - E'_q] \quad (2-6)$$

$$\frac{dE'_d}{dt} = \frac{1}{\tau'_{qo}} [i_{gd}(X_q - X'_q) - E'_d] \quad (2-7)$$

The subtransient equations are developed in a similar fashion than those for transient operation and are given as,

$$E''_d - e_{td} = R_a i_{gd} - X''_q i_{gq} \quad (2-8)$$

$$E''_q - e_{tq} = R_a i_{gq} + X''_d i_{gd} \quad (2-9)$$

$$\frac{dE''_q}{dt} = \frac{1}{\tau''_{do}} [E'_q - i_{gd}(X'_d - X''_d) - E''_q] + \frac{dE'_q}{dt} \quad (2-10)$$

$$\frac{dE''_d}{dt} = \frac{1}{\tau''_{qo}} [i_{gd}(X'_q - X''_q) - E''_d] \quad (2-11)$$

Suitable combination of equations (2-6), (2-7), (2-10) and (2-11) allows for five different generator models of varying complexity and accuracy.

Model (2d.2q)

In this model the generator is represented by the subtransient voltages E_q'' and E_d'' behind the subtransient reactances X_d'' and X_q'' , as defined by the modified armature voltage equations (2-8) and (2-9). The changes in E_q'' and E_d'' as the fluxes linking the rotor circuits decay are described by equations (2-6), (2-7), (2-10) and (2-11).

Model (2d.1q)

In this model the screening effects in the q -axis are neglected so that $X_q' = X_q$ and $E_d' = 0$. Hence, equation (2-7) is eliminated from the set of equations associated with model (2d.2q).

Model (1d.1q)

In this model the effects of the damper windings present in a round-rotor generator model (2d.2q) are neglected, and equations (2-10) and (2-11) are not used here. No damper winding is used in the d -axis and only on damper winding is used in the q -axis. The generator is now represented by the transient voltages E_q' and E_d' behind the transient reactances X_d' and X_q' as defined by equations (2-4) and (2-5). The changes in E_q' and E_d' are determined by equations (2-6) and (2-7).

Model (1d.0q)

In model (1d.0q), all damper winding effects are neglected. The d -axis transient voltage E_d' is assumed to remain constant, hence, $E_d' = 0$ and $X_q' = X_q$. The generator dynamics are only described by equation (2-6).

Classical Model

In this model, the generator is represented by a constant voltage E' behind the transient reactance X_d' . The existence of this model was justified in the past on the grounds that the time constant τ_{d0}' in equation (2-6) is relatively long. In this situation, E_q' can be assumed to remain constant because changes in E_f and i_d are small. The model may be used for simplified analysis of power system transient stability.

2.2.2 Synchronous generator frame-of-reference

The mathematical equations describing the synchronous machine are greatly simplified when they are formulated in the machine's d - q axes frame-of-reference [1-2]. Since each machine has its own reference, rotating independently from each other, studies of interactions between machines through the network are difficult. However, this problem can be resolved by changing the frame-of-reference of each individual machine to the network's frame-of-reference, which rotates at

synchronous speed. By way of example, the transformation of the machine's d - q voltages to the network's D - Q frame-of-reference is shown in Fig. 2-4.

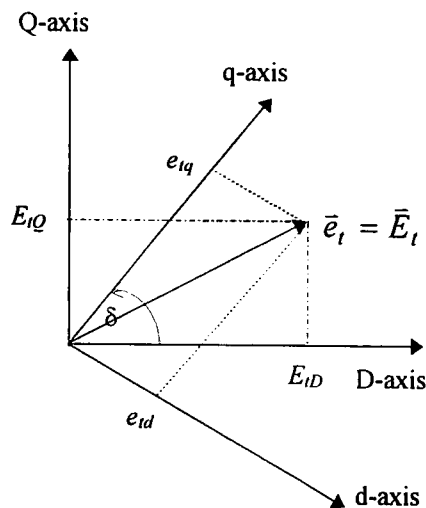


Figure 2-4 Machine and network frame-of-reference

The following transformation matrix is formed by inspection of Fig. 2-4,

$$\begin{bmatrix} E_{tD} \\ E_{tQ} \end{bmatrix} = \begin{bmatrix} \sin \delta & \cos \delta \\ -\cos \delta & \sin \delta \end{bmatrix} \begin{bmatrix} e_{td} \\ e_{tq} \end{bmatrix} \quad (2-12)$$

or, in compact form,

$$\bar{E}_t = e^{j(\delta - \pi/2)} \bar{e}_t \quad (2-13)$$

where

$$\bar{e}_t = e_{td} + je_{tq} \quad (2-14)$$

$$\bar{E}_t = E_{tD} + jE_{tQ} \quad (2-15)$$

Similarly, for the currents,

$$\bar{I}_g = e^{j(\delta - \pi/2)} \bar{i}_g \quad (2-16)$$

where

$$\bar{i}_g = i_{gd} + ji_{gq} \quad (2-17)$$

$$\bar{I}_g = I_{gD} + jI_{gQ} \quad (2-18)$$

2.2.3 Power relationships

With the aid of Park's transformation, the electrical power of the synchronous generator can be simply written in terms of d and q -axis quantities as follows,

$$S = P + jQ = \bar{e}_t \bar{i}_g^* \quad (2-19)$$

$$S = (e_{td}i_{gd} + e_{tq}i_{gq}) + j(e_{tq}i_{gd} - e_{td}i_{gq}) \quad (2-20)$$

2.2.4 Dynamic equations of motion

Power system stability may be assessed by looking at the rotational inertia equations which describe the electrical and mechanical power mismatches for each individual machine. These equations, shown in [1], are given by,

$$\frac{d\Delta\omega}{dt} = \frac{1}{2H} [P_m - P_e - D\Delta\omega] \quad (2-21)$$

$$\frac{d\delta}{dt} = \omega_0 \Delta\omega \quad (2-22)$$

2.3 Electrical network

The electrical equations of the synchronous machine are normally given in the form of a Thevenin voltage behind an impedance. For a nodal representation of the network equations, the machine's Thevenin equivalent is converted into a Norton equivalent [1]. The network current injection vector then includes the Norton equivalent current of each synchronous machine and the machine's admittance is added to the system admittance at the machine's busbar. The matrix form of the network including n machines and r loads can be written as,

$$\begin{bmatrix} \bar{I}_g \\ \dots \\ 0 \end{bmatrix} = \begin{bmatrix} \bar{Y}_{nn} & \dots & \bar{Y}_{nr} \\ \dots & \dots & \dots \\ \bar{Y}_{rn} & \dots & \bar{Y}_{rr} \end{bmatrix} \begin{bmatrix} \bar{E}_t \\ \dots \\ \bar{V}_r \end{bmatrix} \quad (2-23)$$

If loads can be assumed to be static then all load nodes have zero current injection. In this situation, the reduction of the system matrix can be achieved by matrix algebra as shown below,

$$[\bar{I}_g] = [\bar{Y}][\bar{E}_t] \quad (2-24)$$

where

$$[\bar{Y}] = [\bar{Y}_{nn}] - [\bar{Y}_{nr}][\bar{Y}_{rr}]^{-1}[\bar{Y}_{rn}] \quad (2-25)$$

2.4 Generating units

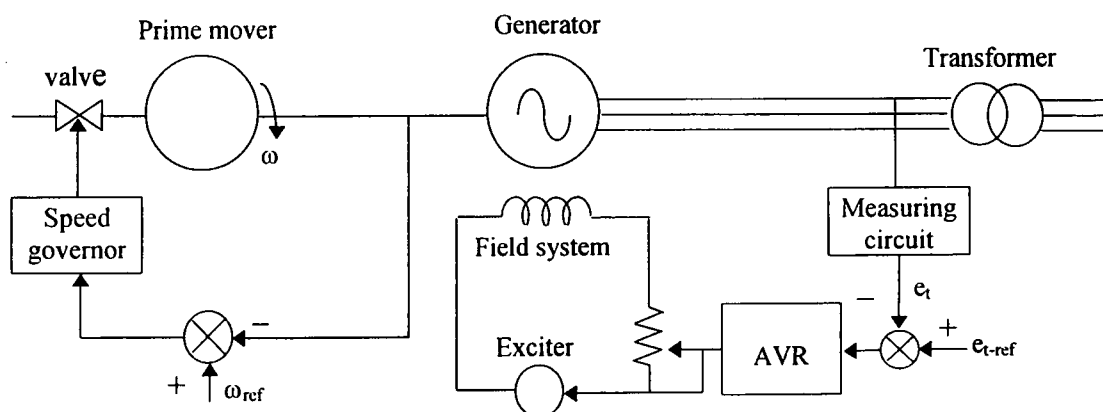


Figure 2-5 Generating unit

Fig. 2-5 shows the schematic diagram of a generating unit. Electrical energy is produced by the synchronous generator driven by a prime mover, such as a steam or a hydro turbine. The turbine is equipped with a governor to control the generator's speed according to a pre-set power-frequency

characteristic [24]. The generated power is fed into the transmission network via a step-up transformer. The DC excitation, required to produce the magnetic field inside the generator, is provided by the exciter. The generator output voltage is regulated by an Automatic Voltage Regulator (AVR) in the excitation control system. Brief descriptions of the turbine-governor and excitation systems are given below.

2.4.1 Turbine-governor system

In conventional power system, steam turbines, hydro turbines and diesel engines are normally used to drive the synchronous generators. Standard turbine configurations and their dynamic models can be found in [2, 24]. The generator speed is controlled by the governor, which adjusts the gate valve positions to increase or decrease the amount of mechanical power to the input turbine by using a servomotor mechanism. A simplified block diagram of the steam turbine governing system is shown in Fig. 2-6(a).

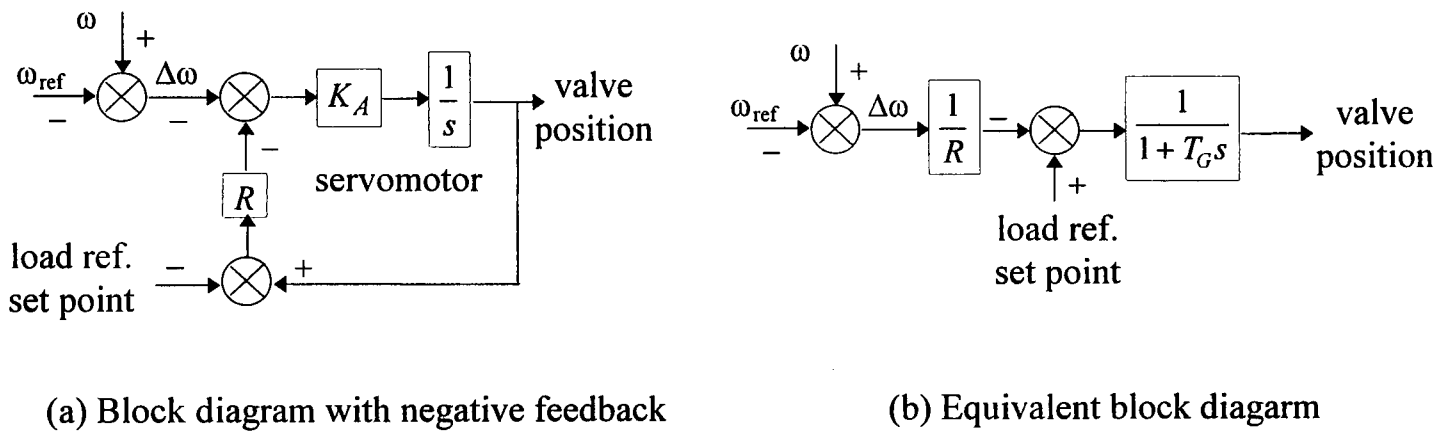


Figure 2-6 Simplified model of the steam turbine governor system

The coefficient K_A corresponds to the amplification gain of the servomotor while the coefficient R corresponds to the gain of the feedback loop. The block diagram in Fig 2-6(a) can be further simplified by moving the coefficient R from the feedback loop to the main loop with little loss of model fidelity. This is shown in Fig. 2-6(b), where $T_G=1/(K_A R)$ is the effective governor time constant. The block diagram in Fig. 2-6(b) can be used for reasonably accurate analysis of the static and dynamic properties of the turbine-governor system.

2.4.2 Excitation system

A generic structure of the excitation system is shown in Fig. 2-7. A comprehensive list of standard excitation system models can be found in [2, 25].

In Fig. 2-7, the excitation system consists of an exciter and an AVR. The AVR regulates the generator's terminal voltage by controlling the amount of current supplied to the generator field winding by the exciter. The measured generator's terminal voltage and the desired reference

voltage are compared to produce a voltage error. The error is then applied and used to alter the exciter's output. Generally speaking, exciters can be of either rotating type or static type.

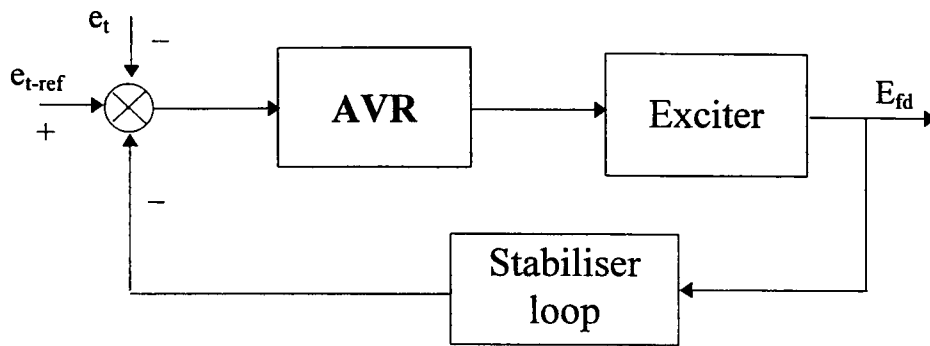


Figure 2-7 Structure of the excitation system

In rotating structures, the excitation current is supplied by either a *DC* generator or an *AC* generator fitted with a rectifier. Nowadays, all *DC* generators have almost been replaced by alternators, which are simpler in construction and more reliable. However, a disadvantage of the alternators is that slip rings are required to feed the rectified excitation current to the rotating field winding and also that the exciter itself is quite large. Therefore, static exciters have been introduced to overcome these difficulties. In static exciters, the thyristor rectifiers are controlled directly by the AVR to adjust the field current, so that the voltage error is eliminated. The transfer functions of the excitation control components are given below [2]:

AVR transfer function

$$g_{avr}(s) = \frac{K_a}{1 + \tau_a s} \quad (2-26)$$

Exciter transfer function

$$g_e(s) = \frac{1}{1 + \tau_e s} \quad (2-27)$$

Stabiliser loop

$$g_s(s) = K_f \frac{\tau_f s}{1 + \tau_f s} \quad (2-28)$$

2.5 FACTS devices

The Flexible AC Transmission System (FACTS) technology is a new application area in electrical power systems. FACTS devices, utilising modern power electronics technology, are deployed at key locations of the high-voltage transmission system in order to control and adjust one or more of the main parameters in the transmission system [3-5, 26-62]. It has been proposed more recently to incorporate similar devices in low-voltage distribution systems to solve power quality problems. The ensuing technology comes under the umbrella title of Custom Power. By introducing flexible and rapid control of key *AC* transmission parameters, FACTS enhances the power transfer capacity

of existing transmission corridors. They decrease line losses and generation costs, and improve the stability and security of the power system. Due to the great many advances of modern power electronics technology, a wide range of FACTS devices has emerged in recent years. A summary of the most promising devices is presented below:

Static Var compensator (SVC) [26-30]

The SVC belongs to the first generation of FACTS devices, it appeared in the market nearly twenty years ago. The SVC consists of fast thyristor switches controlling a Thyristor-Controlled Reactor (TCR) and paralleled with a capacitor bank (FC) as shown in Fig. 2-8. Its main task is to provide voltage support under periods of heavy load and, under certain circumstances, it may also contribute to system stability.

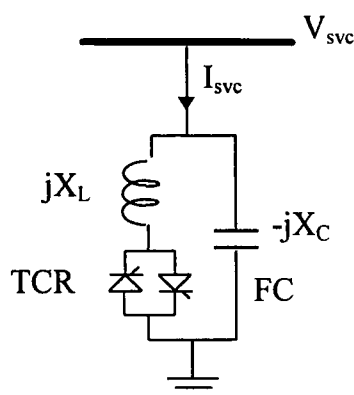


Figure 2-8 FC-TCR structure of the SVC

Thyristor controlled series capacitor (TCSC) [30-34]

The TCSC, shown in Fig 2-9, belongs to the second generation of FACTS devices. It is able to control the line impedance through the introduction of a controllable capacitor-inductor set in series with the transmission line. The major benefits of the TCSC are its ability to regulate power flows along the compensated line and to rapidly modulate the effective impedance of the line in response to dynamic events in the vicinity of the line.

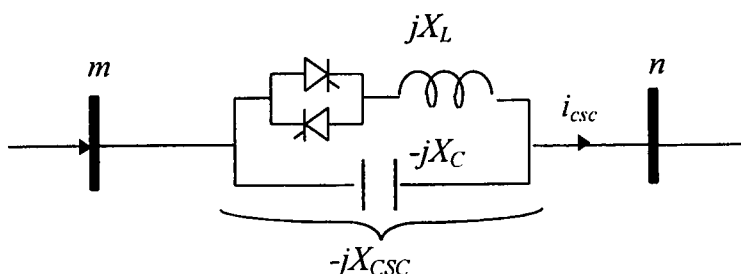


Figure 2-9 Configuration of the TCSC

Static phase shifter (SPS) [35-37]

The Static Phase Shifter is a FACTS device that helps to control the power flows between two nodes. Fig. 2-10 shows the configuration of the SPS, which comprises of a exciting transformer (ET), a boosting transformer (BT) and a converter circuit. The exciting transformer provides the input voltage to the phase shifter. The boosting transformer, inserted between the sending and receiving nodes, injects a controlled voltage in series with that of the system. The converter is used to adjust the magnitude and/or phase-angle of the injected voltage in order to control the voltage at the receiving node and the active power transfer across the transformer.

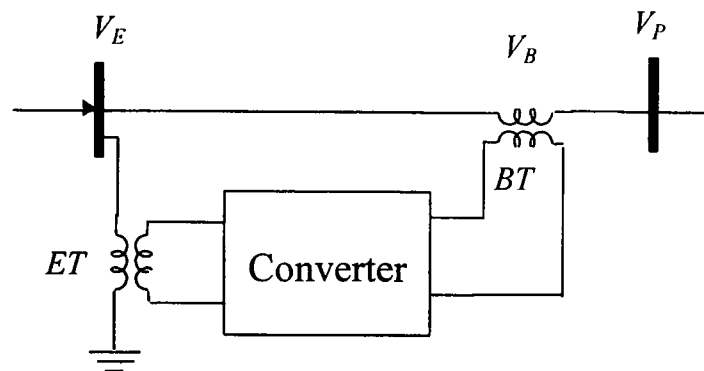


Figure 2-10 Configuration of the SPS

Static synchronous compensator (STATCOM) [38-40]

The STATCOM belongs to the latest generation of FACTS devices. Its configuration is shown in Fig. 2-11. It is a new reactive power compensator that overcomes the technical limitations and high cost of SVCs [5, 39]. The development of the STATCOM is based on the use of Gate-Turn-Off thyristors (GTO). The *DC* voltage source serving as an input voltage is converted into three-phase *AC* output voltages. STATCOMs can be made to either generate or absorb reactive power. It is superior to the SVC in providing voltage support and it can also respond more quickly to damp disturbances in the power system. STATCOMs exist for both high-voltage transmission applications and for low-voltage distribution systems.

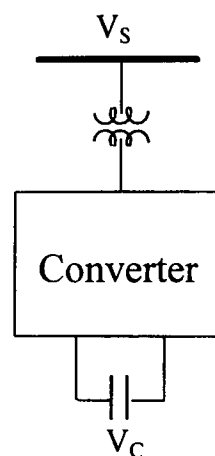


Figure 2-11 Configuration of the STATCOM

Static synchronous series compensator (SSSC)

The SSSC is similar to the STATCOM except that its output transformer is connected in series with the line as shown in Fig. 2-12. This is the high voltage counterpart of the Dynamic Voltage Restorer (DVR) that is used in low voltage distribution applications.

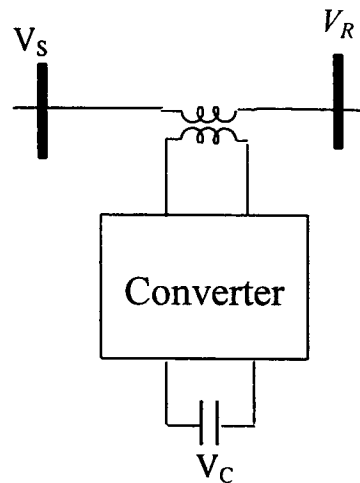


Figure 2-12 Configuration of the SSSC

Unified power flow controller (UPFC) [41-43]

The UPFC configuration is shown in Fig. 2-13. It consists of one STATCOM and one SSSC, connected by a common link that includes a storage capacitor. The UPFC has the ability to exert simultaneous control of active and reactive power flows, and nodal voltage magnitude. This combination of functions gives the UPFC unique advantages over other FACTS devices making it the most advanced FACTS controller currently under existence.

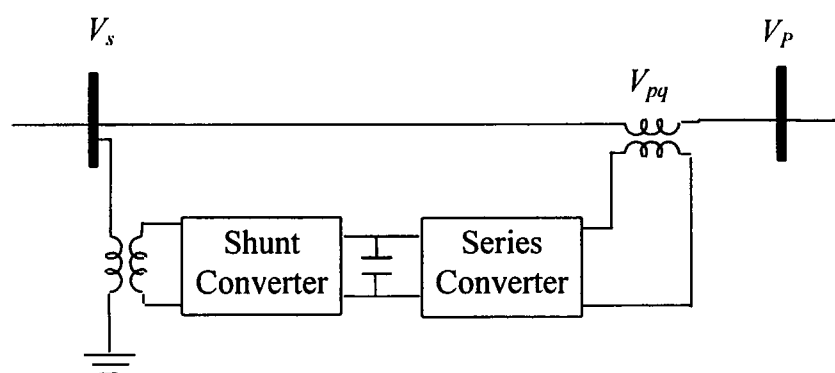


Figure 2-13 Configuration of the UPFC

Interphase power controller (IPC) [44-46]

Interphase Power Controllers belong to an alternative technology drive, which do not necessarily use power electronics. They have the potential for increasing very significantly the power transfer capability of phase shifting transformers [44]. Their ability to increase power transfer provides the economic justification surrounding the development of this new technology. IPC applications are ideally suited for cases where power transfer is thermally limited by the phase-shifting transformer [45]. The IPC consists of two parallel reactive branches, one inductive and one capacitive as shown in Fig. 2-14. Each branch is subjected to separately phase-shifted voltages [46].

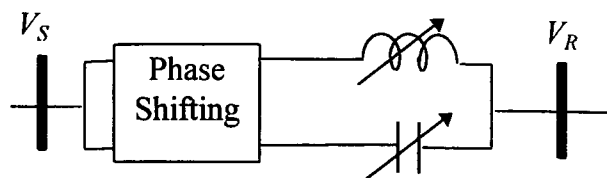


Figure 2-14 Configuration of the IPC

2.5.1 Static var compensators

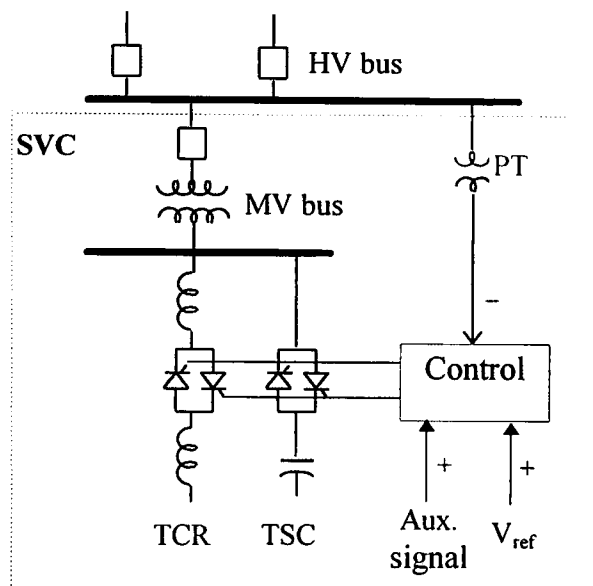


Figure 2-15 Typical Configuration of a SVC system

SVCs started being used in power systems in the late 1970s, long before the concept of FACTS was formulated. The role of SVCs is to adjust the amount of reactive power compensation at the point of connection. Before SVCs became widely available for controlling voltage at weak points of the network, voltage adjustment in specific locations of the transmission system was only possible by using mechanically controlled shunt elements or by using expensive synchronous compensators. The switching in and out of shunt reactors and capacitors lead to abrupt voltage changes along with voltage and current transients. SVCs on the other hand provide a rapid and fine voltage control, with no moving parts involved. SVCs have been used in various forms but the basic schematic diagram, in one-line diagram form, is shown Fig. 2-15 [2, 26].

Each phase of the Thyristor Controlled Reactor (TCR) consists of two bi-directional valves in series with a shunt reactor and the three phases are usually connected in a delta configuration to cancel out the third harmonic currents. These thyristors may be switched on at any point of the voltage wave (from 90 to 180 electrical degrees) to provide fully adjustable control over the range of rated reactive power absorption.

The Thyristor Switched Capacitor (TSC) also has bi-directional thyristor valves connected in series with the capacitor. The TSC switches on by firing 90 degrees ahead of the voltage wave to generate reactive power. A power transformer typically connects the SVC to the high-voltage busbar.

Another popular form of SVC is the combination of a Fixed Capacitor and a Thyristor Controlled Reactor (FC-TCR), as shown in Fig. 2-8. The fixed capacitor provides a permanently connected source of reactive power.

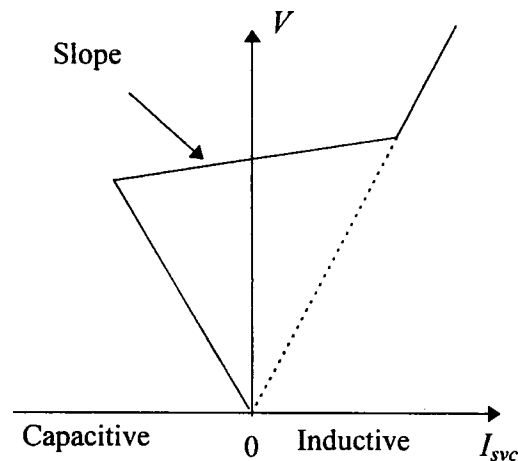


Figure 2-16 Voltage-current composite characteristic of the SVC

Referring to the SVC configuration in Fig. 2-8, the variable shunt reactance is adjusted in order to control voltage magnitude at the network point of connection. The SVC voltage-current (V/I) characteristic for the FC-TCR structure is shown in Fig. 2-16 [26].

Depending on the SVC's equivalent reactance, i.e. capacitive or inductive, Fig. 2-16 indicates that the SVCs is capable of drawing capacitive or inductive current from the power system. Suitable control of the equivalent reactance allows continuous voltage regulation at the node where the SVC is connected. The slope is determined by the capacitive and inductive susceptance limits. These susceptances represent the total SVC susceptance required to maintain the voltage magnitude at the specified value. The expression for the total susceptance value is given by [26],

$$B_{svc} = B_C - B_L(\alpha) \quad (2-29)$$

where

$$B_C = 2\pi fC \quad (2-30)$$

$$B_L(\alpha) = \frac{2}{\pi X_L} \{(\pi - \alpha) + 0.5 \sin(2\alpha)\} \quad (2-31)$$

2.5.1.1 SVC control scheme

SVC systems are usually configured to meet individual system requirements. Since application requirements may differ and the control techniques offered by different equipment vendors may vary [47-51], very detailed models of SVCs may not be necessary. Basic models for general purpose studies have been recommended by CIGRE [2, 47]. In stability studies, the general SVC control scheme shown in Fig. 2-17 is normally used [2].

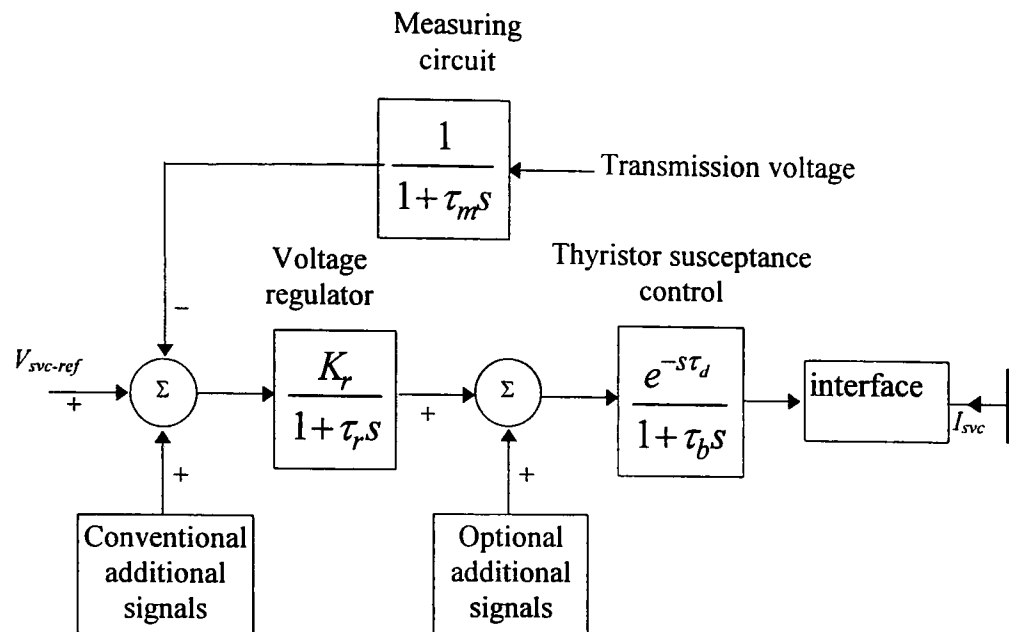


Figure 2-17 SVC block diagram model

The control block of the SVC voltage regulator consists of the gain K_r and time constant τ_r . The next block in line is the thyristor susceptance control block, that represents the variation of reactor susceptance as a function of firing angle. The parameter τ_d is a gating transport delay and, typically, it has values of around 1 ms, and it is normally neglected. Similarly, τ_b associated with the thyristor firing sequence control has a values of around 5 ms and can also be neglected in most studies. Moreover, the nonlinear relationship between the firing angle α and B_L is assumed to be compensated, thus, making the use of τ_d and τ_b all but redundant, except for very specialised studies where the control itself is the study subject. Thus, this block may be represented by a unity gain with no time delay. The SVC control system takes the feedback voltage from the high-voltage side of the connecting node. The time delay, τ_m , represents the lagging time constant of the measuring circuit. Conventional and optional additional signals, such as the speed signal, can also be injected at the summing points to improve the overall system dynamic performance.

2.5.2 Thyristor-controlled series compensators

Active power transfers between areas may be substantially increased and adjusted very effectively by varying the net series impedance of the tie-line. An established method of increasing transmission line capability is to install series banks of capacitors, whose effect is to reduce the electrical length of the line. Conventional series compensation schemes switch capacitors in and out of operation to vary the level of compensation, by using mechanical devices such as circuit breakers [3]. The limitations of using mechanical devices to switch series banks of capacitors are their relatively slow response due to the large number of capacitors in of the bank. The Thyristor-Controlled Series Compensator is the electronically-controlled counterpart of the conventional series banks of capacitors. It is able to rapidly control the line compensation over a continuous range resulting in increased flexibility. Active power across the compensated transmission line can

be maintained at a specified level under a wide range of operating conditions. A schematic diagram of the TCSC is shown in Fig. 2-9. TCSC controllers consist of a capacitor bank in parallel with a TCR, whose controlling elements are two anti-parallel thyristors, connected in series with a linear reactor. In practise, the TCSC comprises of a large number of series connected TCSC modules, which may be connected in tandem. This configuration is termed the Advanced Series Compensator (ASC) and it is very effective in exerting control with minimum losses and minimum harmonic distortion [52].

2.5.2.1 Basic characteristics of TCSCs

The main operational advantage of the TCSC is that it allows a smooth control of transmission line compensation levels. Series capacitive compensation is bypassed during minimum loading in order to avoid transmission line over-voltages resulting from excessive capacitive effects in the system. Conversely, series capacitive compensation is fully utilised during maximum loading. The purpose of this operating strategy is to increase the power transfer capability from generating sites to load centres, without over-loading compensated transmission lines. Basically, there are three fundamental modes of operation: thyristor-blocked mode, thyristor-bypassed mode, and thyristor operating in phase controlled mode [53].

In the thyristor-blocked mode, the thyristor current is zero and, consequently, the TCSC functions as a capacitive reactance. This operating mode is illustrated in Fig. 2-18. The arrow thickness represents the amount of electric current flowing across each component.

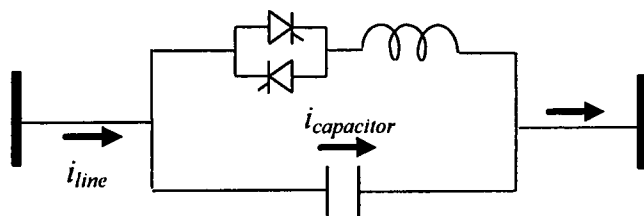


Figure 2-18 Configuration of the TCSC in thyristor-blocked mode

In the thyristor-bypassed mode, the thyristor is fired with no delay, i.e. the TCR is fully conducting. The TCSC behaves like a parallel connection of the series capacitor bank with the inductor. Fig. 2-19 shows this mode of operation.

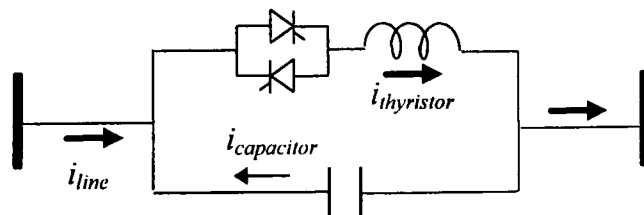


Figure 2-19 Configuration of the TCSC in thyristor-bypassed mode

The TCSC can work as either a capacitive or an inductive reactance, when the thyristor operates in phase-controlled mode, the thyristor operation is driven by the firing angle to vary the amount of effective capacitance, as shown in Fig. 2-20.

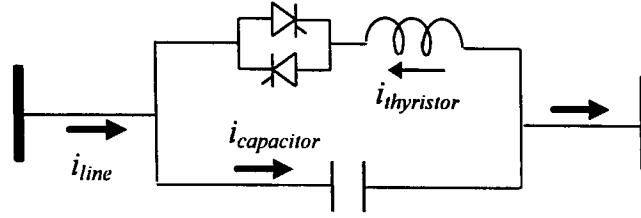
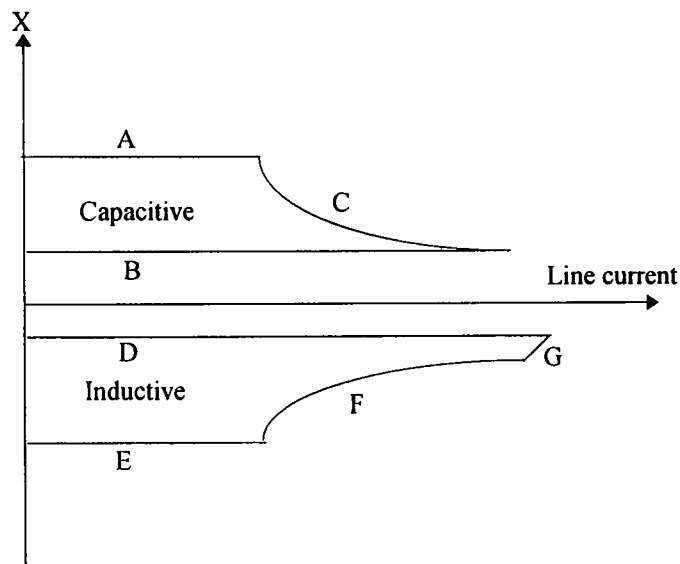


Figure 2-20 Configuration of the TCSC in phase-controlled mode

The TCSC operating range is limited by the firing angle range of the thyristors, and the current carrying limits of the capacitors. In actual operation, these limits may affect the performance of the control scheme. Fig 2-21 shows curves of the TCSC operating range versus line currents [54].



- | | |
|-----------------------------|----------------------------|
| A = Firing angle limit | B = Thyristor blocked |
| C = Maximum voltage limit | D = full thyristor |
| E = Firing angle limit | F = harmonic heating limit |
| G = thyristor current limit | |

Figure 2-21 Operating range of the TCSC

The expression for the fundamental frequency of the TCSC impedance, as a function of the thyristor's firing angle is given as [32],

$$\begin{aligned}
 -jX_{csc} = -j \left\{ X_c - C_1 \left[2(\pi - \alpha) + \sin(2(\pi - \alpha)) \right] \right. \\
 \left. + C_2 \cos^2(\pi - \alpha) \left[\lambda \tan(\lambda(\pi - \alpha)) - \tan(\pi - \alpha) \right] \right\}
 \end{aligned}
 \tag{2-32}$$

where

$$C_1 = \frac{X_C + X_{LC}}{\pi}
 \tag{2-33}$$

$$C_2 = \frac{4X_{LC}^2}{\pi X_L}
 \tag{2-34}$$

$$\lambda = \frac{\omega_o}{\omega} \quad (2-35)$$

$$X_{LC} = \frac{X_C X_L}{X_C - X_L} \quad (2-36)$$

$$\omega_o^2 = \frac{1}{LC} \quad (2-37)$$

2.5.2.2 TCSC control scheme

In power system operation and control, the TCSC has two key roles to play: to schedule active power flow and to enhance dynamic performance. In the latter application area, the control system becomes a matter of great importance, and a distinction is drawn between the transient stability control loop and the power damping control loop [55-61]. The former is a pre-programmed open-loop control used to improve first swing stability. The control allows for maximum compensation level just after the occurrence of a fault in the power network and it remains so for a pre-specified period of time. The control is then transferred to the damping control loop to mitigate the ensuing power oscillations [54]. For small-signal stability purposes, only the damping control loop is of practical relevance. Fig 2-22 shows a generic block diagram of the TCSC control which is well suited for small-signal stability studies [62].

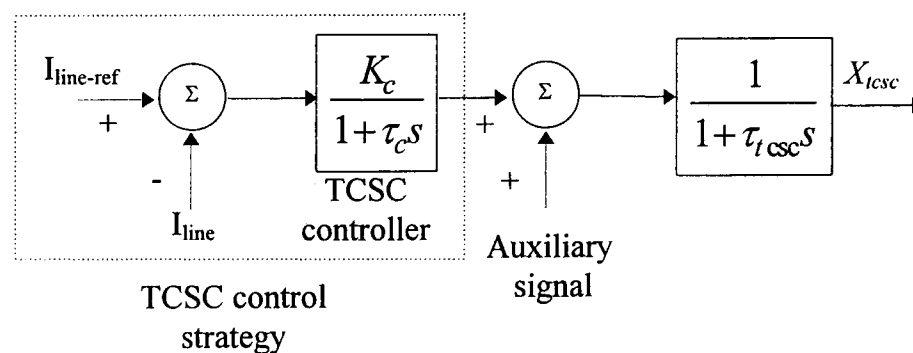


Figure 2-22 TCSC block diagram control

The TCSC block diagram control shown in Fig. 2-17 consists of TCSC control strategy, enclosed by the dotted block, and the first-order lag transfer function representing the time delay τ_{tcsc} associated with the thyristor's firing angle control. The value of τ_{tcsc} varies from 15 to 30 ms and it can be neglected in small-signal stability studies [62]. For the TCSC control strategy block, a simple control schemes such as PI controller can be used to schedule power flow. In Fig. 2-7, the TCSC controller is represented by the gain K_c and the lagging time constant τ_c , which is fully equivalent to the one used in Chapter 6. The current signal derived from the network (I_{line}) is compared with the reference signal ($I_{line-ref}$) in order to control active power flow, which is achieved by adjusting the TCSC reactance (X_{tcsc}). The auxiliary signal can be used for the purpose of damping system oscillations when the input comes from an additional damping control loop.

2.6 Conclusions

This chapter has touched on generic aspects of power system models, with emphasis on the new generation of power electronics based plant components currently emerging under the FACTS initiative. The basic theory and modelling of synchronous generators is addressed in some detail. The mathematical representation of synchronous generators with decreasing order of model complexity is presented, as well as the turbine-governor and excitation control systems. The many benefits that the application of FACTS controllers will bring to power systems operation are highlighted. Against this background, the main characteristics and key modelling aspects of electronically-controlled shunt and series compensation are addressed. These two FACTS devices together with the synchronous generator form the main power system plant components that are to be modelled as part of the research efforts on small-signal transient stability undertaken in this investigation. The aim is to provide readers with a working understanding of the mathematical modelling associated with such power plant components. It is the author's view that this basic knowledge should lead to a good understanding of the small-signal stability models developed in Appendices A-C.

2.7 References

- [1] P. M. Anderson and A. A. Fouad, "Power System Control and Stability", The Iowa State University Press, 1986.
- [2] P. Kundur, "Power System Stability", McGraw-Hill Inc, 1993.
- [3] IEEE/CIGRE, "FACTS Overview", Special Issue, 95-TP-108, IEEE Service Centre, Piscataway, N.J., 1995.
- [4] N. G. Hingorani, "Flexible AC Transmission System", IEEE Spectrum, Vol. 30, No. 4, April 1993, pp. 40-45.
- [5] E. V. Larsen, J. J. Sanchez-Gasca, J. H. Chow, "Concepts for Design of FACTS Controllers to Damp Power Swings", IEEE Transactions on Power Systems, Vol. 10, No. 2, May 1995, pp. 984-955.
- [6] R. H. Park, "Two-Reaction Theory of Synchronous Machines", AIEE Transactions, Part 1, Vol. 48, 1929, pp. 716-730 ; Part 2, Vol. 52, 1933, pp. 352-355
- [7] B. Adkins, "The General Theory of Electric Machines", Chapman and Hall, 1957.
- [8] C. Concordia, "Synchronous Machine: Theory and Performance", John Wiley, 1951
- [9] R. D. Dunlop and A. C. Parikh, "Verification of Synchronous Machine Modelling in Stability Studies: Comparative Test of Digital and Physical Scale Model Power System Simulation",

- IEEE Transactions on Power Apparatus and Systems, Vol. 98, No. 2, March 1979, pp. 369-378.
- [10] P. L. Dandeno, P. Kundur, A. T. Poray and M. E. Coultres, "Validation of Turbo-generator Stability Models by Comparison with Power System Tests", IEEE Transactions on Power Apparatus and Systems, Vol. 100, No. 4, April 1981, pp. 1637-1645.
- [11] E. L. Busby, J. D. Hurley, F. W. Keay and C. Raczkowski, "Dynamic Stability Improvement at Monticello Station-Analytical Study and Field Tests", IEEE Transactions on Power Apparatus and Systemx, Vol. 98, No. 3, May 1979, pp. 889-897.
- [12] IEEE Standard 1110-1991, "IEEE Guide for Synchronous Generator Modelling Practices in Stability Analyses", 1991.
- [13] IEEE Task Force on Definitions and Procedures, "Current Usage and Suggested Practices in Power System Stability Simulations for Synchronous Machines", IEEE Transactions on Energy Conversion, Vol. 1, No. 1, March 1986, pp. 77-93.
- [14] T. J. Hammons and D. J. Winning, "Comparison of Synchronous Machine Models in the Study of Transient Behaviour of Electrical System ", Proceeding of IEE, Vol. 118, No. 10, October 1971, pp. 1142-1458.
- [15] H. F. Wang, F. J. Swift and M. Li, "Selection of Installing Locations and Feedback Signals of FACTS-based Stabiliser in Multi-machine Power System by Reduced-Order Model Analysis", IEE Proceedings on Generation, Transmission and Distribution, Vol. 144, Part C, No. 3, May 1997, pp. 263-269.
- [16] H. F. Wang and F. J. Swift, "FACTS-based Stabiliser Designed by the Phase Compensation Method: Part I: Single-machine", IEE Conference Publication, No. 450, November 1997, Part I, pp. 644-649.
- [17] H. F. Wang and F. J. Swift, "FACTS-based Stabiliser Designed by the Phase Compensation Method: Part II: Multi-machine", IEE Conference Publication, No. 450, November 1997, Part II, pp. 638-643.
- [18] C. J. Wu and Y.S. Lee, "Damping of Synchronous Generator by Static Reactive Power Compensator with Digital Controller", IEE Proceedings on Generation, Transmission and Distribution, Vol. 138, Part C, No. 5, September 1991, pp. 427-431.
- [19] C. H. Cheng and Y. H. Hsu, "Damping of Generator Oscillation Using an Adaptive Static Var Compensator", IEEE Transactions on Power Systems, Vol. 7, No. 2, May 1992, pp. 718-725.
- [20] P. K. Dash, S. Mishra and A. C. Liew, "Fuzzy-Logic Based VAR Stabiliser for Power System

- Control”, IEE Proceedings on Generation, Transmission and Distribution, Vol. 142, Part C, No. 6, November 1995, pp. 618-624.
- [21] H. M. A. Rahim and S. G. A. Nassimi, “Synchronous Generator Damping Enhancement through Co-ordinated Control of Exciter and SVC”, IEE Proceedings on Generation, Transmission and Distribution, Vol. 143, Part C, No. 2, March 1996, pp. 211-217.
- [22] A. C. H. Cheng and Y.Y. Hsu, “Application of a Power System Stabiliser and a Static VAR Controller to a Multimachine Power System”, IEE Proceedings on Generation, Transmission and Distribution, Vol. 137, Part C, No. 1, January 1990, pp. 8-12.
- [23] H. F. Wang, “The Indexes for Selecting the best Location of PSS or FACTS-based Stabiliser in Multi-machine power system: A Comparison Study”, IEE Proceedings on Generation, Transmission and Distribution, Vol. 144, No. 2, Part C, May 1997, pp. 155-159.
- [24] IEEE Committee Report, “Dynamic Models for Steam and Hydro-turbine in Power System Studies”, IEEE Transactions on Power Apparatus and Systems, Vol. 92, No. 6, November 1973, pp. 1904-1915.
- [25] IEEE Committee Report, “Excitation System Models for Power System Stability Studies”, IEEE Transactions on Power Apparatus and Systems, Vol. 100, No. 2, February 1981, pp. 497-509.
- [26] T. J. E. Miller, “Reactive Power control in Electric System”, John Wiley & Sons, 1982.
- [27] S. Torseng, “Shunt-Connected Reactors and Capacitor Controlled by Thyristors”, IEE Proceedings, Vol. 128, No. 6, November 1981, pp. 366-373.
- [28] I. A. Erinmez, “Static Var Compensator”, Work Group 38-01, Task Force No. 2, CIGRE, 1986.
- [29] A. E. Hammad, “Analysis of Power System Stability Enhancement by Static Var Compensator”, IEEE Transactions on Power Systems”, Vol. 1 No. 4, November 1986, pp. 222-227.
- [30] L. Angquist, B. Lundin and J. Samuelsson, “Power Oscillation Damping Using Controlled Reactive Power Compensation: A Comparison between Series and Shunt Approaches”, IEEE Transactions on Power Systems. Vol. 8, No. 2, May 1993, pp. 687-699.
- [31] X. R. Chen, N. C. Pahalawaththa, U. D. Annakkage and C. S. Kumble, “Output Feedback TCSC Controllers to Improve Damping of Meshed Multi-machine Power Systems”, IEE Proceedings on Generation, Transmission and Distribution, Vol. 144, Part C, No. 3, May 1997, pp. 243-248.

- [32] S. G. Helbing and G. G. Karady, "Investigations of an Advanced Form of Series Compensation", IEEE Transactions on Power Delivery, Vol. 9, No. 2, April 1994, pp. 939-947.
- [33] M. Noroozian and G. Andersson, "Power Flow control by use of Controllable Series Components", IEEE Transactions on Power Delivery, Vol. 8, No. 3, July 1993, pp. 12-18.
- [34] A. Olwegard, "Improvement of System Stability by Switched Series Capacitors", IEEE Transactions on Power Apparatus and Systems", Vol. 85, No. 2, February 1981, pp. 3933-3939.
- [35] R. Baker, G. Guth, W. Egli and P. Eglin, "Control Algorithm for a Static Phase Shifting Transformer to Enhance Transient and Dynamic Stability of Large Power System", IEEE Transactions on Power Apparatus and Systems, Vol. 101, No. 9, September 1982, pp. 3532-3542.
- [36] M. R. Iravani and D. Maratukulam, "Review of Semiconductor-controlled (Static) Phase Shifter for Power System Application", IEEE Transactions on Power Systems, Vol. 9, No. 4, November 1994. pp. 1833-1839.
- [37] B. T. Ooi, S. Z. Dai and F. D. Galiana, "A Solid-state PWM Phase Shifter", IEEE Transactions on Power Delivery, Vol. 8, No. 2, April 1993, pp. 573-579.
- [38] P. W. Lehn and M. R. Iravani, "Experimental Evaluation of STATCOM Closed Loop Dynamic", IEEE Transactions on Power Delivery, Vol. 13, No. 4, October 1998, pp. 1378-1384.
- [39] C. D. Schauder, "Development of a 100 MAVR Static Condensor for Voltage Control of Transmission System", IEEE Transactions on Power Delivery, Vol. 10, No. 3, October 1995, pp. 1486-1493.
- [40] L. Gyugyi, "Dynamic Compensation of AC Transmission lines by Solid-state Synchronous Voltage Sources", IEEE Transactions on Power Delivery, Vol. 9, No. 2, April 1995, pp. 904-911.
- [41] L. Gyugyi, C. D. Schauder, S. L. Williams, T. R. Rietman and A. Edris, "The Unified Power Controller: A New Approach to Power Transmission Control", IEEE Transactions on Power Delivery, Vol. 10, No. 2, April 1995, pp. 1085-1097.
- [42] R. Mihalic, P. Zunko and D. Povh, "Improvement of Transient Stability Using Unified Power Flow Controller", IEEE Transactions on Power Delivery, Vol. 11, No. 1, January 1996, pp. 485-490.

- [43] A. Nabavi-Niaki and M. R. Iravani, "Steady-State and Dynamic Models of Unified Power Flow Controller (UPFC) for Power System Studies", IEEE Transactions on Power Systems, Vol. 11, No. 4, November 1996, pp. 1973-1943.
- [44] J. Lemay, F. Beaugard, J. Brochu and P. Pelletier, "Increasing the Capabilities of Phase-Shifting Transformers with the Interphase Power Flow Controller Technology", EPRI Conference on the Future of Power Delivery in the 21th Century, Session 2: Grid Operation and Planning, November 1997, La Jolla California.
- [45] J. Brochu, P. Pelletier, F. Beaugard and G. Morin, "Interphase Power Controller, A New Concep for Managing Power Flow Within AC Networks", IEEE Transactions on Power Delivery, Vol. 9, No. 2, April 1994, pp. 833-841.
- [46] F. Beaugard, J. Brochu, G. Morin and P. Pelletier, "Interphase Power Controller with Voltage Injection", IEEE Transactions on Power Delivery, Vol. 9, No. 4, October 1994, pp. 1956-1962.
- [47] IEEE Committee Report, "Static VAR Compensator Models for Power Flow and Dynamic Simulation", IEEE Transactions on Power Systems, Vol. 9, No. 1, January 1994, pp. 229-240.
- [48] C. H. Cheng and Y. H. Hsu, "Damping of Generator Oscillation Using an Adaptive Static Var Compensator", IEEE Transactions on Power Systems, Vol. 7, No 2, May 1992, pp. 718-725.
- [49] C. J. Wu and Y. S. Lee. "Damping of Synchronous Generator by Static Reactive Power Compensator with Digital Controller", IEE Proceedings on Generation, Transmission and Distribution, Vol. 138, Part C, No. 5, September 1991, pp. 427-431.
- [50] A. A. EI-Emary, "Formula For the Effect of Static VAr Compensator on Synchronising Torque Coefficients", IEE Proceedings on Generation, Transmission and Distribution, Vol. 143, Part C, No. 6, November 1996, pp. 582-586.
- [51] H. F. Wang and F. J. Swift, "Capability of the Static Var Compensator in Damping Power System Oscillations", IEE Proceedings on Generation, Transmission and Distribution, Vol. 143, Part C, No. 4, July 1996, pp. 353-358.
- [52] N. Christl, R. Hedin, R. Johnson, P. Krause and A. Montoya, "Power System Studies and Modelling for the Kayenta 230 KV Substation Advanced Series Compensator", Proceeding of the IEE 5th International Conference on AC and DC Power Transmission, London, 1991, pp. 33-37.
- [53] E. V. Larsen, K. Clark, S. S. Miske and J. Urbanek, "Characteristic and Rating Considerations of Thristor Controlled Series Compensation", IEEE Transactions Power Delivery, Vol. 9, No. 2, April 1994, pp. 883-841.

- [54] X. Zhou and J. Liang, "Overview of Control Schemes for TCSC to Enhance the Stability of Power System", IEE Proceedings on Generation, Transmission and Distribution, Vol. 146, Part C, No. 2, March 1999, pp. 125-130.
- [55] L. Clark and B. Fardanesh, "Thyristor Controlled Series Compensation Application Study-control Interaction Considerations", IEEE Transactions on Power Delivery, Vol. 10, No. 2, April 1995, pp. 1031-1037.
- [56] G. N. Taranto and D. M. Falcao, "Robust Decentralised Control Design Using Genetic Algorithms in Power System Damping Control", IEE Proceedings on Generation, Transmission and Distribution, Vol. 145, Part C, No. 1, January 1998, pp. 1-6.
- [57] L. Rouco and F. L. Pagola, "An Eigenvalue Sensitivity Approach to Location and Controller Design of Controllable Series Capacitor for Damping the Power System Oscillation", IEEE Transactions on Power Systems, Vol. 12, No. 4, November 1997, pp. 1660-1666.
- [58] M. Noroozian and G. Andersson, "Damping the Power Oscillation by Use of Controllable Components", IEEE Transactions on Power Delivery, Vol. 9, No. 4, October 1994, pp. 2046-2054.
- [59] H. F. Wang F. J. Swift, "A Unified Model for the Analysis of FACTS Devices in Damping Power System Oscillation Part I: Single-machine Infinite-bus Power System", IEEE Transactions on Power Delivery, Vol. 12, No. 2, April 1997, pp. 941-946.
- [60] H. F. Wang, F. J. Swift and M. Li, "A Unified Model for the Analysis of FACTS Devices in Damping Power System Oscillation Part II: Multi-machine Power System", IEEE Transactions on Power Delivery, Vol. 13, No. 4, October 1998, pp. 1355-1360.
- [61] H. F. Wang and F. J. Swift, "Application of the Controllable Series Compensator in Damping Power System Oscillation", IEE Proceedings on Generation, Transmission and Distribution, Vol. 143, Part C, No. 4, July 1996, pp. 359-364.
- [62] K. R. Padiyar, "Analysis of Subsynchronous Resonance in Power System", Kluwer Academic Publisher, 1999.

Chapter 3

Small-Signal Modelling of a Synchronous Generator-SVC System in a Single-Machine Environment

3.1 Introduction

In small-signal stability studies, a transfer-function block-diagram model of single-machine infinite-bus system has been used extensively in the past [1-7]. It has been used for explaining and assessing the synchronous generator's dynamic behaviour [8, 9], and for the analysis and design of power system controllers such as AVRs and PSSs [7, 10].

Major break-throughs in high-current, high-power solid-state technology have seen the widespread use of power electronic controllers in the high-voltage side of the network to provide fast-acting control. The new generation of power plant components is collectively known as FACTS devices [11-13]; with the SVC being the older and better known of these devices. The SVC main uses are to provide fast reactive power support and to damp power system oscillations. Accordingly, studies of dynamic interactions between synchronous generators and SVCs have become a matter of paramount importance.

In this chapter the block-diagram model is extended to include the full SVC dynamic effects and a comprehensive synchronous generator representation, to bring the synchronous generator model in line with what is known to be the most complete, yet realistic representation in small-signal stability studies [8, 9]. The overall block-diagram model includes, in addition to the main field winding in the d -axis, one damper winding in the d -axis and one damper winding in the q -axis. The synchronous generator excitation system and the turbine-governor control system form an integral part of the block-diagram model. The SVC plant caters for an explicit representation of the damping control loop in addition to the standard voltage control loop. Indeed, it is this ability to incorporate in a unified frame-of-reference the fuller representation of both plant components that makes the new block-diagram model a more advanced analysis tool than a contemporary, less rigorous block-diagram model [14, 15].

The new transfer-function block-diagram model is used to study and to elucidate the dynamic interactions taking place between the synchronous generator and the SVC plant. The model yields physical insight into the dynamic interactions taking place between the various rotor windings, between the generator windings and the excitation control system, between the electrical and the mechanical parts of the generating plant, etc. This is in contrast to eigenvalue and eigenvector-based techniques, which rely exclusively on mathematical abstraction to produce an aggregated

system result from which system stability is assessed. Arguably, the block-diagram approach is the most attractive way of conducting fundamental analysis of dynamic interactions between generating plants and between generating plants and FACTS controllers, e.g. SVCs, TCSCs.

3.2 System under study

The test system in Fig. 3-1 is used to study the influence that the SVC exerts on the generator dynamic characteristic. The test system consists of a synchronous generator feeding into an infinite bus via a tie-line system, which includes a shunt compensator in the form of a SVC system. In order to conduct a more general study of dynamic interactions between the generator and a SVC, the SVC is located at an arbitrary point along the tie-line system, between the reactance X_{t1} and X_{t2} . The two extreme cases are when the SVC is connected at the generator terminals, i.e., $X_{t1}=0$ and when it is connected at the infinite bus, i.e., $X_{t2}=0$.

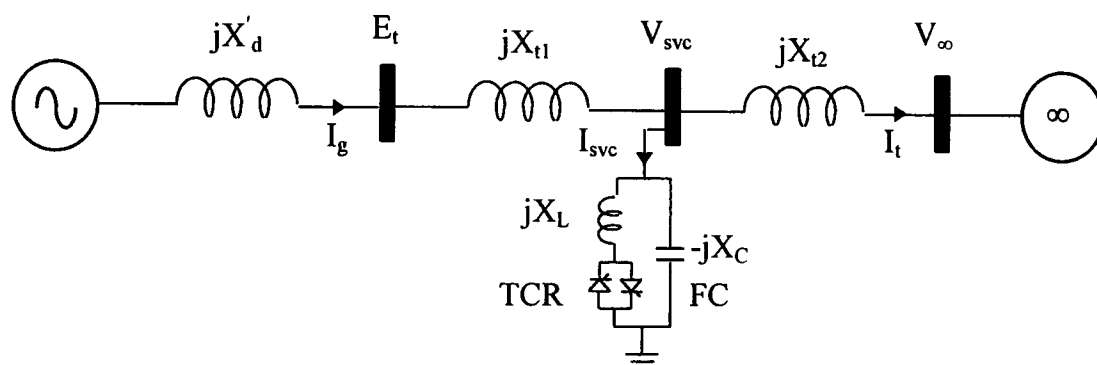


Figure 3-1 System under study

3.3 Mathematical representation of the system under study

The small-signal model that represents the system under study is developed from first principles, by using the non-linear differential and algebraic equations that represent the synchronous generator and the SVC. The dynamic equations of the generator [16-18] and SVC [19-21] system are well documented in the open literature, respectively. Several transfer function models, with decreasing order of complexity and accuracy, are established by using salient-pole synchronous generator models with varying degrees of rotor winding representation. They are as follows:

Model 1

The model accounts for the effects of the generator main field winding plus one damper winding in the d -axis and one in the q -axis.

Model 2

In this model, the damper winding in the d -axis rotor circuit is removed from Model 1. Hence, $\Delta E_q''$ and X_d'' are replaced by $\Delta E_q'$ and X_d' , respectively.

Model 3

All damper windings in Model 1 and 2 are neglected. Hence, only the effect of the field winding exists, i.e., $\Delta E_q'' = \Delta E_d'' = X_d'' = X_q'' = 0$.

The main differential and algebraic equations required for establishing Models 1-3 are summarised in Table 3-1.

| | | Model 1 | Model 2 | Model 3 |
|------------------------------|-------------------------------|---|--|--|
| Synchronous Generator | <i>Field Equation</i> | $\tau'_{do} \dot{E}'_q = E_{fd} - E'_q - (X_d - X'_d)I_{gd}$ | $\tau'_{do} \dot{E}'_q = E_{fd} - E'_q - (X_d - X'_d)I_{gd}$ | $\tau'_{do} \dot{E}'_q = E_{fd} - E'_q - (X_d - X'_d)I_{gd}$ |
| | <i>D-axis Damper Equation</i> | $\tau''_{do} \dot{E}''_q = E'_q - E''_q + \tau''_{do} \dot{E}'_q - (X_d - X''_d)I_{gd}$ | ----- | ----- |
| | <i>Q-axis Damper Equation</i> | $\tau''_{qo} \dot{E}''_d = -E''_d + (X_q - X''_q)I_{gq}$ | $\tau''_{qo} \dot{E}''_d = -E''_d + (X_q - X''_q)I_{gq}$ | ----- |
| | <i>Stator Equation</i> | $E_{tq} = E''_q - X''_d I_{gd}$ $E_{td} = E''_d + X''_q I_{gq}$ | $E_{tq} = E'_q - X'_d I_{gd}$ $E_{td} = E''_d + X''_q I_{gq}$ | $E_{tq} = E'_q - X'_d I_{gd}$ $E_{td} = X_q I_{gq}$ |
| SVC | <i>Current Equation</i> | $\bar{i}_{svc} = jB_{svc} \bar{v}_{svc}$ where $B_{svc} = B_C - B_L(\alpha)$ | | |
| | <i>Susceptance Equation</i> | $B_L(\alpha) = [2(\pi - \alpha) + \sin(2\alpha)] / \pi X_L$ $B_C = 2\pi fC$ | | |

Table 3-1 Summary of synchronous generator and SVC equations required for small-signal stability analysis

3.4 Representation of system model

A straightforward but cumbersome linearisation exercise of the dynamic equations shown in Table 3-1 (refer to Appendix A for details) produces the following transfer-function expressions, in S domain:

Model 1

Active power equation

$$\Delta P_e = \Delta P_{syn} + \Delta P_{ed} - \Delta P_{eq} + \Delta P_{svc} \quad (3-1)$$

or

$$\Delta P_e = K_1 \Delta \delta + K_2 \Delta E''_q - K_{2d} \Delta E''_d + K_{svc1} \Delta \alpha \quad (3-2)$$

Generator terminal voltage equation

$$\Delta e_t = K_5 \Delta \delta + K_6 \Delta E_q'' + K_{6d} \Delta E_d'' + K_{svc3} \Delta \alpha \quad (3-3)$$

SVC Terminal voltage equation

$$\Delta v_{svc} = K_{5n} \Delta \delta + K_{6n} \Delta E_q'' + K_{6dn} \Delta E_d'' + K_{svc3n} \Delta \alpha \quad (3-4)$$

d and q-axis flux linkages equations

$$\Delta E_q'' = g_3(s) \Delta E_{fd} - g_4(s) \Delta \delta + g_{svc2}(s) \Delta \alpha \quad (3-5)$$

$$\Delta E_d'' = g_{4d}(s) \Delta \delta + g_{svc2d}(s) \Delta \alpha \quad (3-6)$$

Model 2

$$\Delta P_e = K_1 \Delta \delta + K_2 \Delta E_q' - K_{2d} \Delta E_d'' + K_{svc1} \Delta \alpha \quad (3-7)$$

$$\Delta e_t = K_5 \Delta \delta + K_6 \Delta E_q' + K_{6d} \Delta E_d'' + K_{svc3} \Delta \alpha \quad (3-8)$$

$$\Delta v_{svc} = K_{5n} \Delta \delta + K_{6n} \Delta E_q' + K_{6dn} \Delta E_d'' + K_{svc3n} \Delta \alpha \quad (3-9)$$

where

$$\Delta E_q' = g_3(s) \Delta E_{fd} - g_4(s) \Delta \delta + g_{svc2}(s) \Delta \alpha \quad (3-10)$$

$$\Delta E_d'' = g_{4d}(s) \Delta \delta + g_{svc2d}(s) \Delta \alpha \quad (3-11)$$

Model 3

$$\Delta P_e = K_1 \Delta \delta + K_2 \Delta E_q' + K_{svc1} \Delta \alpha \quad (3-12)$$

$$\Delta e_t = K_5 \Delta \delta + K_6 \Delta E_q' + K_{svc3} \Delta \alpha \quad (3-13)$$

$$\Delta v_{svc} = K_{5n} \Delta \delta + K_{6n} \Delta E_q' + K_{svc3n} \Delta \alpha \quad (3-14)$$

where

$$\Delta E_q' = g_3(s) \Delta E_{fd} - g_4(s) \Delta \delta + g_{svc2}(s) \Delta \alpha \quad (3-15)$$

The system coefficients and transfer functions for representing Models 1-3 are given in Appendix A. The generic block diagram of Models 1-3 is shown in Fig. 3-2.

Fig. 3-2 shows the overall structure of the system, which can be represented by three single-input single-output feedback subsystems, i.e. excitation control, turbine-governor control, and SVC voltage and damping control loops. These are in addition to the generator-SVC system. The outputs of interest are: generator speed ($\Delta \omega$), generator output voltage (Δe_t) and SVC output voltage (Δv_{svc}). Since the response of the turbine-governor system is typically slow, i.e. 0-1 rad/sec, it is assumed here that no variation in electrical power (ΔP_m), due to the governor action, takes place during small perturbations. Hence, the system can be treated as a two single-input single-output systems. The second channel is the excitation control, which regulates the generator output voltage by controlling the generator field voltage (ΔE_{fd}). Throughout the thesis, a fast acting AVR is used.

In the third channel, the SVC voltage control loop is designed to control output voltage by changing the firing angle ($\Delta \alpha$). The feedback control voltage is directly taken from the SVC terminal voltage. The SVC voltage control loop can be represented by one simple lagging transfer

function of gain K_r , and time constant τ_r . The non-linear component in this control loop will be cancelled out by an ideal linearised block [21]. At the summing point of the SVC voltage control loop, the additional stabilising signal (Δv_{add}), due to the SVC damping control loop, can be injected to provide system damping capabilities [22-25].

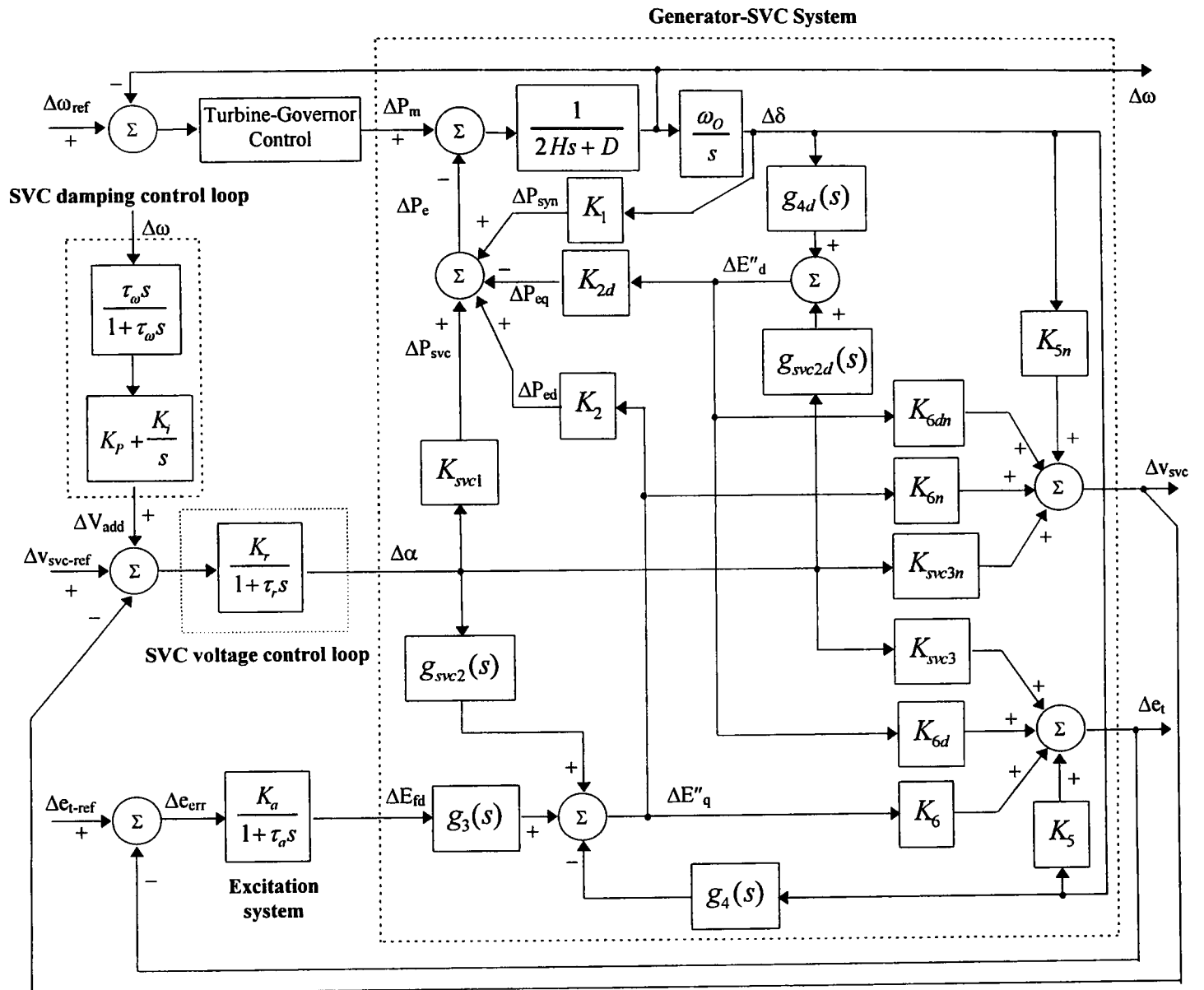


Figure 3-2 Detailed block diagram of the generator-SVC system

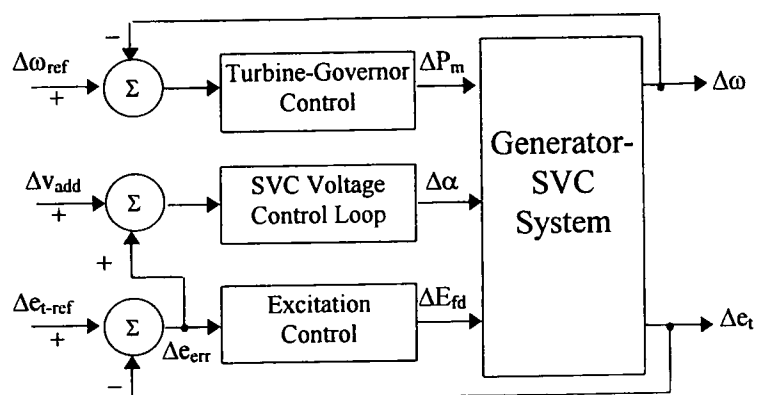


Figure 3-3 Block diagram of the generator-SVC system with the SVC is placed at generator's terminal bus

The block diagram in Fig. 3-2 represents the generator-SVC system, where the SVC is located at an arbitrary point along the tie-line system. For the case where the SVC is located at the generator's bus, the SVC voltage control loop is directly controlling the generator output voltage in parallel with the AVR. The voltage references Δe_{t-ref} and $\Delta v_{svc-ref}$ become one, as shown in Fig. 3-3. The complexity of the generator-SVC block diagram reduces because the SVC output voltage coefficients K_{5n} , K_{6n} , K_{6dn} and K_{svc3n} coalesce with those of the generator output voltage.

3.5 Analysis of the interaction between a synchronous generator and a SVC

In small signal stability studies, the incremental change in synchronous machine electrical power and terminal voltage (ΔP_e , Δe_t) are the key relations for describing power system dynamic characteristic. In this chapter, changes in ΔP_e is the main variable which is employed to study the interacting effects between the generator and the SVC.

The physically oriented block-diagram model of Fig. 3-2 gives a detailed account of the many dynamic interactions that may exist in the generator-SVC system. These effects can also be presented in terms of the generator output power loop, as shown by the block diagram in Fig. 3-4.

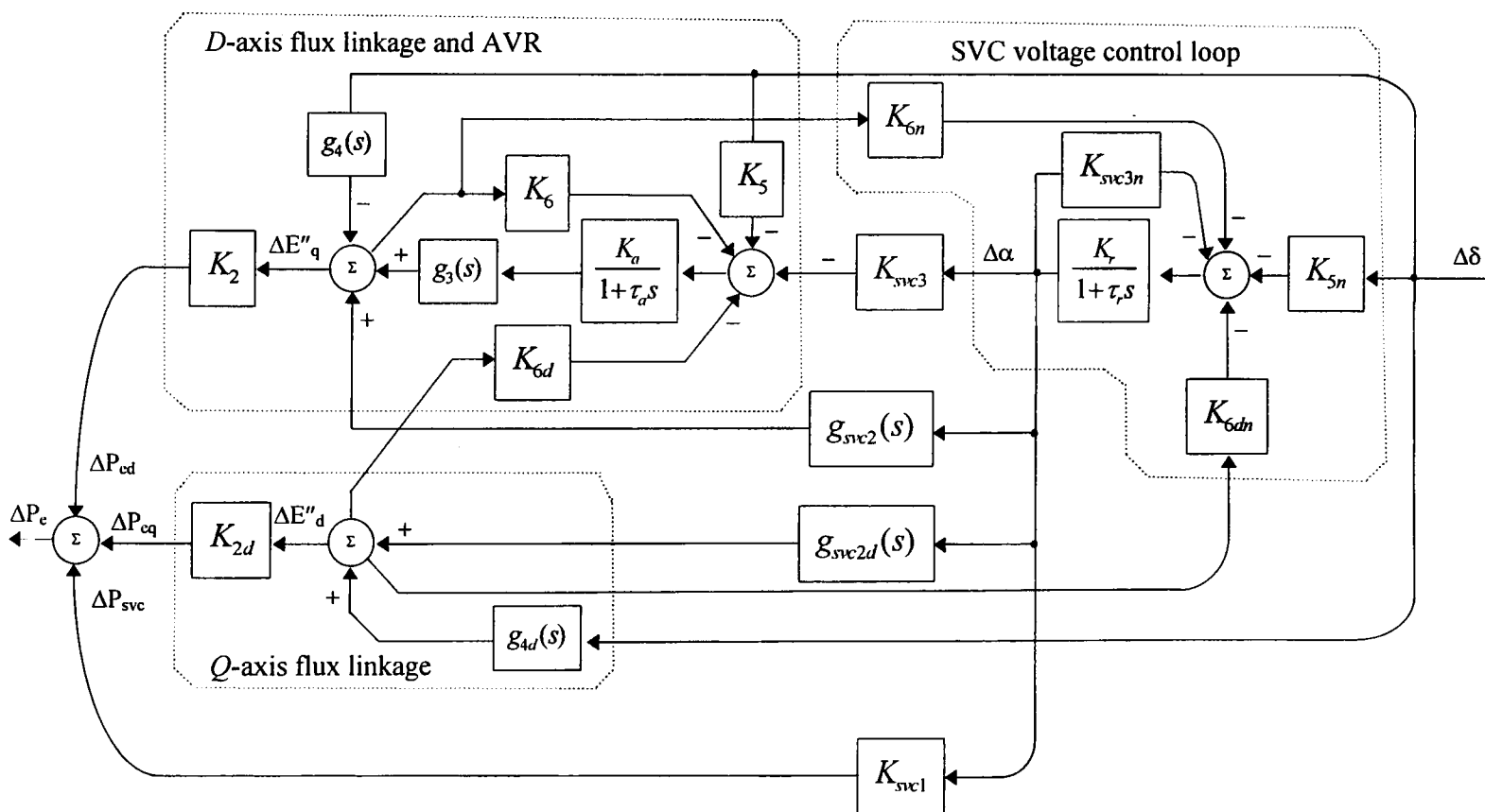


Figure 3-4 Electrical power loops of the synchronous generator-SVC system

Here, it can be seen that increment changes in the generator's electrical output power (ΔP_e) and the rotor angle ($\Delta \delta$) are taken to be as output and input signals, respectively, in the power loop. A change in $\Delta \delta$ is directly fed into the flux linkage in the direct axis via the transfer function $g_4(s)$, and into the flux linkage in the quadrature axis via the transfer functions $g_{4d}(s)$. Also, $\Delta \delta$ is passed

on into the SVC voltage control loop via the coefficient K_{5n} to make an increment change into the firing angle ($\Delta\alpha$). A variation in $\Delta\alpha$ may lead to change in voltage proportional to d -axis flux linkage ($\Delta E''_q$) directly through the transfer function $g_{svc2}(s)$ and indirectly through the coefficient K_{svc3} ; it will also induce a change in voltage proportional to q -axis flux linkage ($\Delta E''_d$) through the transfer function $g_{svc2d}(s)$; and a change in electrical power ΔP_{svc} through the coefficient K_{svc1} . ΔP_{svc} is a portion of generator's output power that is changed due to a change in SVC susceptance (ΔB_{svc}) induced by a change in the firing angle. Hence, it can be seen that the generator's electrical output power ΔP_e is influenced by the SVC directly through variation in ΔP_{svc} and indirectly through variations in ΔP_{ed} , and ΔP_{eq} , which are due to d and q -axis flux linkages, respectively.

3.6 Analysis of the SVC impact on the synchronous generator dynamic characteristic

When the SVC is incorporated into the system, it impacts the electrical performance of the generator in various ways. For one, the SVC susceptance (B_{svco}) and location along the tie line have a major impact on generator performance. All coefficients and transfer functions, making up the generator-SVC system in Fig. 3-2, are functions of B_{svco} and X_{t1} to X_{t2} . The generator performance is also greatly affected by the SVC firing angle. Once a small perturbation in firing angle takes place, its effect is delivered to the generator through the relevant coefficients and transfer functions, i.e., K_{svc1} , K_{svc3} , and $g_{svc2}(s)$, $g_{svc2d}(s)$. The two kinds of SVC contribution to generator are further elaborated below:

3.6.1 Effect of changes in initial operating conditions and SVC location

Firstly, let us consider the effect of SVC location. The coefficients and transfer functions, making up the generator-SVC system, are a function of the tie-line reactance X_{t1} and X_{t2} , subjected to $X_{t1}+X_{t2} = X_t$. Hence, dynamic interactions between the generator and SVC depend critically on the electrical distance between them. Furthermore, a situation which deserves special attention is when the SVC is located at the generator's terminal bus, i.e, the reactive tie-line X_{t1} becomes zero. The coefficients K_{5n} , K_{6n} , K_{6dn} and K_{svc3n} become equivalent to K_5 , K_6 , K_{6d} and K_{svc3} , respectively. Therefore, the terminal voltage magnitudes and angles of the generator and SVC coincide with each other.

Secondly, all the coefficients and transfer functions are also affected by the susceptance B_{svco} , which is determined by the initial firing angle, α_0 , as given by eqn. (A-12). There are three quite distinct conditions, which can be identified: (i) the SVC provides reactive power to the system $B_{svco}>0$ ($B_L(\alpha)<B_C$); (ii) the SVC absorbs reactive power from the system $B_{svco}<0$ ($B_L(\alpha)>B_C$); (iii) the SVC neither injects nor draws reactive power from the system, $B_{svco}=0$ ($B_L(\alpha)=B_C$). In this case, the coefficients K_{svc1} , K_{svc3} , K_{5n} , K_{6n} , K_{6dn} , K_{svc3n} , and transfer function $g_{svc2}(s)$, $g_{svc2d}(s)$ will still exist in the model.

3.6.2 Effect of changes in firing angle

Incremental changes in the SVC firing angle will impact on the generator dynamic characteristic. The extent of which can be assessed by examining the variation in electrical power in the power loop, i.e. ΔP_{ed} , ΔP_{eq} , and ΔP_{svc} .

3.6.2.1 Variation in electrical power ΔP_{ed}

From Fig. 3-4, it is easy to see that the output power (ΔP_e) of the generator can be changed due to a variation in ΔP_{ed} , resulting from a change in the d -axis flux linkage. There are two pathways through which the SVC can influence the d -axis flux linkage, when a small disturbance occurs. The first one is a direct pathway via the transfer function $g_{svc2}(s)$. The second one is an indirect pathway through which the SVC induces a variation in generator terminal voltage (Δe_t) via the coefficient K_{svc3} . In a regulated system, the AVR takes the generator terminal voltage as the feedback voltage, which is compared with the reference voltage (Δe_{t-ref}) and then amplified by its normal high gain in order to exert generator field voltage (ΔE_{fd}). Hence, the AVR with high gain plays a crucial role in substantially enhancing the SVC contribution to the d -axis flux linkage via the coefficient K_{svc3} . In general, the SVC's impact via made the K_{svc3} branch is greater than the impact through the $g_{svc2}(s)$ branch.

According to eqns. (A-60) and (A-78), the transfer function $g_{svc2}(s)$ and coefficient K_{svc3} are given by,

$$g_{svc2}(s) = \frac{2}{\pi X_L} \left[\frac{X_{t2} V_{svcqo} \left((X_d - X_d'') + \{ \tau'_{do} (X_d' - X_d'') + \tau''_{do} (X_d - X_d') \} s \right)}{\Delta_d + \{ \tau'_{do} \Delta_d' + \tau''_{do} (\Delta_d'' + (X_d - X_d')(1 - X_{t2} B_{svco}) \} s + \{ \tau'_{do} \tau''_{do} \Delta_d'' \} s^2} \right] \quad (3-16)$$

$$K_{svc3} = \frac{2}{\pi X_L} \left[\frac{E_{tdo}}{E_{to}} \cdot \frac{X_{t2} X_q'' V_{svcd0}}{\Delta_q''} + \frac{E_{tqo}}{E_{to}} \cdot \frac{X_{t2} X_d'' V_{svcqo}}{\Delta_d''} \right] \quad (3-17)$$

where

$$\Delta_d = X_{t2} + (X_d + X_{t1})(1 - X_{t2} B_{svco}) \quad (3-18)$$

$$\Delta_d' = X_{t2} + (X_d' + X_{t1})(1 - X_{t2} B_{svco}) \quad (3-19)$$

$$\Delta_d'' = X_{t2} + (X_d'' + X_{t1})(1 - X_{t2} B_{svco}) \quad (3-20)$$

$$\Delta_q'' = X_{t2} + (X_q'' + X_{t1})(1 - X_{t2} B_{svco}) \quad (3-21)$$

As seen from eqns. (3-16) and (3-17), the magnitude of the transfer function $g_{svc2}(s)$ and coefficient K_{svc3} is always positive. The maximum impact that the SVC can make to influence the d -axis flux linkage will take place when the magnitude of the transfer function $g_{svc2}(s)$ and the coefficient K_{svc3} are greatest, i.e., when the SVC is located at the generator's bus.

3.6.2.2 Variation in electrical power ΔP_{eq}

The SVC's impact on the q -axis flux linkage is mainly carried out through the transfer function $g_{svc2d}(s)$ as shown in Fig. 3-4. Hence, the generator's output power will be influenced by changes in the electrical power ΔP_{eq} , generated by the q -axis flux linkage, in response to change in SVC firing angle. From eqn. (A-65), $g_{svc2d}(s)$ is given as,

$$g_{svc2d}(s) = \left[\frac{K_{svc2d}}{(1 + \tau_q''s)} \right] \quad (3-22)$$

where

$$K_{svc2d} = \frac{2}{\pi X_L} \left[\frac{X_{t2}(X_q - X_q'')V_{svcd0}}{\Delta_q} \right] \quad (3-23)$$

$$\Delta_q = X_{t2} + (X_q + X_{t1})(1 - X_{t2}B_{svco}) \quad (3-24)$$

Similar to $g_{svc2}(s)$, the SVC located at the generator terminals will induce maximum effect on the q -axis flux linkage.

3.6.2.3 Variation in electrical power ΔP_{svc}

It can be seen from Fig. 3-4 that the generator's output power will also changed in response to variations in electrical power ΔP_{svc} , as a result of variations in SVC susceptance following change in firing angle $\Delta\alpha$.

Referring to eqn. (A-95), the coefficient K_{svc1} is given as,

$$K_{svc1} = \frac{2}{\pi X_L} \left[\frac{(X_{t1} + X_d'')V_{\infty d0}V_{svcq0}}{\Delta_d''} - \frac{(X_{t1} + X_q'')V_{\infty q0}V_{svcd0}}{\Delta_q''} \right] \quad (3-25)$$

Since the coefficient K_{svc1} can take either a positive or a negative value, depending on generator and SVC operating conditions, SVC location, generator and tie-line reactances, the SVC causes the generator to increase or decrease its electrical output power. The coefficient K_{svc1} will take a maximum positive value when the system is operating under heavy load since $V_{svcq0}V_{\infty d0} > V_{svcd0}V_{\infty q0}$.

3.7 Analysing the generator's impact on SVC

We have now established that the SVC interacts electrically with the generator through the coefficients K_{svc1} , K_{svc3} and transfer functions $g_{svc2}(s)$, $g_{svc2d}(s)$. On the other hand, any change from the generator rotor angle, d and q -axis flux linkages will affect the SVC through SVC terminal voltage (Δv_{svc}). These changes are induced through the coefficients K_{5n} , K_{6n} and K_{6dn} , respectively. Moreover, the SVC output voltage can be determined by the negative feedback making through the coefficient K_{svc3n} at the voltage control loop.

According to eqns. (A-82)-(A-85), K_{5n} , K_{6n} , K_{6dn} and K_{svc3n} are expressed as,

$$K_{5n} = \left[\frac{V_{svcd0}}{V_{svco}} \cdot \frac{(X_q'' + X_{t1})V_{\infty q0}}{\Delta_q''} - \frac{V_{svcq0}}{V_{svco}} \cdot \frac{(X_d'' + X_{t1})V_{\infty d0}}{\Delta_d''} \right] \quad (3-26)$$

$$K_{6n} = \left[\frac{V_{svcq0}}{V_{svco}} \cdot \frac{X_{t2}}{\Delta_d''} \right] \quad (3-27)$$

$$K_{6dn} = \left[\frac{V_{svcd0}}{V_{svco}} \cdot \frac{X_{t2}}{\Delta_q''} \right] \quad (3-28)$$

$$K_{svc3n} = \frac{2}{\pi X_L} \left[\frac{V_{svcd0}^2}{V_{svco}} \cdot \frac{X_{t2}(X_q'' + X_{t1})}{\Delta_q''} + \frac{V_{svcq0}^2}{V_{svco}} \cdot \frac{X_{t2}(X_d'' + X_{t1})}{\Delta_d''} \right] \quad (3-29)$$

As indicated in eqn. (3-26), K_{5n} can take either positive or negative values but it is usually negative. On the other hand, K_{6n} , K_{6dn} and K_{svc3n} in eqns. (3-27)-(3-29) are always positive. If the SVC is installed at the generator's bus, the coefficients K_{5n} , K_{6n} , K_{6dn} and K_{svc3n} have maximum magnitudes and, hence, the generator has maximum influence on the SVC output voltage.

3.8 Assessing the SVC's effects on the generator dynamic performance

In this section, the generator dynamic performance is assessed by measuring the synchronising and damping power components of the electrical powers ΔP_{ed} , ΔP_{eq} , and ΔP_{svc} due to oscillations in the rotor angle ($\Delta\delta$). The total power can be decomposed into two components: the first component in phase with $j\omega_n\Delta\delta$ or $\Delta\omega$ (imaginary axis co-ordinate) gives the damping power and the second component in phase with $\Delta\delta$ (real axis co-ordinate) gives the synchronising power [6]. The system becomes stable if both power components are contained in the first quadrant in the $\Delta\delta$ - $\Delta\omega$ plane. In this section, the frequency response method is used to investigate power components of $\Delta P_{ed}/\Delta\delta$, $\Delta P_{eq}/\Delta\delta$, and $\Delta P_{svc}/\Delta\delta$. Comparison of the power components of the tie-line system with the SVC and with no SVC are made in order to evaluate the system dynamic performance. The system operating condition is given in Table 3-2. It should be noted that the same amount of active powers delivered from the generator to the infinite bus is considered in both cases, i.e., when the system has a SVC and when it has not.

3.8.1 Electrical power ΔP_{ed}

The phase versus frequency in Fig. 3-5 shows that at frequencies around of 8-18 rad/sec, because the phase angle of $\Delta P_{ed}/\Delta\delta$ with no SVC is greater than 180° , there are undamped responses due to negative damping and synchronising power components in the d -axis flux linkage.

| | Without SVC | With SVC |
|----------------|--|--|
| P_g | 0.736 p.u. | 0.736 p.u. |
| Q_g | 0.752p.u. | 0.5514 p.u. |
| Q_{svc} | - | 0.378 p.u. |
| Q_t | 0.552 p.u. | 0.727 p.u. |
| X_t | 0.2 p.u. | 0.2 p.u. |
| X_{t1} | - | 0.1 p.u. |
| v_∞ | 0.92 p.u. | 0.92 p.u. |
| e_t | 1.0522 p.u. | 1.0522 p.u. |
| V_{mid} | 0.9832 p.u. | 1.0022 p.u. |
| I_t | 1 p.u. | 1.1246 p.u. |
| α | - | 150° |
| δ_o | 29.85 | 35.92 |
| E_{fdo} | 2.3087 p.u. | 2.0618 p.u. |
| | Model 1 | Model 1 |
| $g_3(s)$ | $\frac{6.789 + 0.19s}{29.47 + 49.38s + s^2}$ | $\frac{6.789 + 0.19s}{29.24 + 49.24s + s^2}$ |
| $g_4(s)$ | $\frac{10.39 + 6.17s}{29.47 + 49.38s + s^2}$ | $\frac{11.346 + 6.74s}{29.24 + 49.24s + s^2}$ |
| $g_{svc2}(s)$ | - | $\frac{0.5288 + 0.314s}{29.24 + 49.24s + s^2}$ |
| $g_{4d}(s)$ | $\frac{11.048}{20.136 + s}$ | $\frac{11.116}{19.987 + s}$ |
| $g_{svc2d}(s)$ | - | $\frac{11.116}{19.987 + s}$ |
| K_1 | 2.8639 | 2.86248 |
| K_2 | 1.2085 | 1.32003 |
| K_{2d} | 2.2041 | 2.21768 |
| K_5 | -0.07319 | -0.07463 |
| K_6 | 0.49228 | 0.48896 |
| K_{6d} | 0.19899 | 0.22076 |
| K_{svc1} | - | 0.01538 |
| K_{svc3} | - | 0.01225 |
| K_{5n} | - | -0.06031 |
| K_{6n} | - | 0.24106 |
| K_{6dn} | - | 0.13042 |
| K_{svc3n} | - | 0.01925 |

Table 3-2 System operating conditions

When the SVC is used, the phase angle drops down below 180° for all the frequency ranges considered. Hence, at frequency ranges of 8-18 rad/sec, the SVC improves the system stability by supplying positive damping power component to the d -axis flux linkage. Moreover, the gain versus frequency plot indicates that the electrical power contributed from the flux linkage is significantly enhanced when the SVC is used. From the stability point of view, however, since the phase of $\Delta P_{ed}/\Delta\delta$ is greater than 90° , the synchronising power component of the d -axis flux linkage is negative throughout the oscillation frequency range.

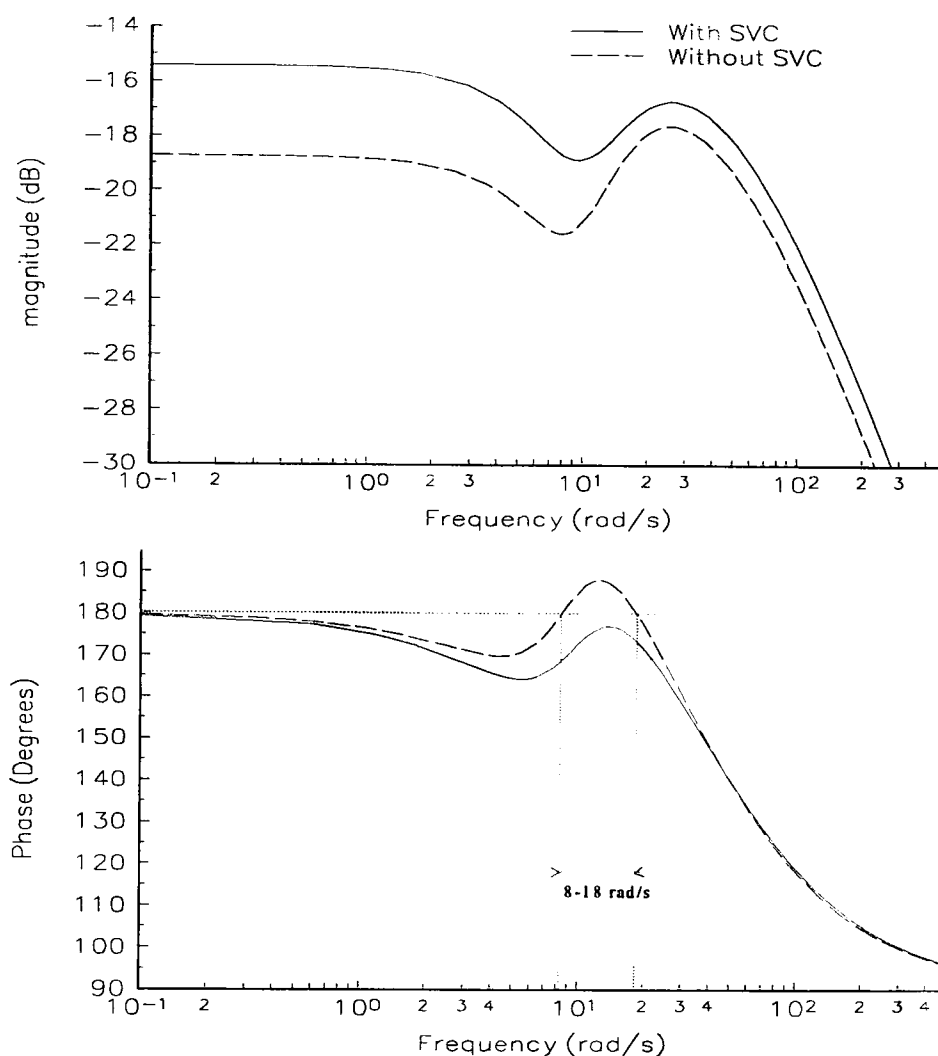


Figure 3-5 Frequency response of $\Delta P_{ed}/\Delta\delta$ with and with no SVC

It is well known that the power system exhibits undamped responses at local oscillation modes, i.e., 6-10 rad/sec. An interesting point is to assess by how much the SVC can increase the damping power generated from the d -axis flux linkage when an undamped frequency is considered, e.g., 7.5 rad/sec as calculated from operating conditions in Table 3-2. It can be appreciated from Fig. 3-5 that the SVC shifts down the phase angle of $\Delta P_{ed}/\Delta\delta$ from 177° to 167° at 7.5 rad/sec. The system dynamic performance can be also assessed from the synchronising and damping power components of ΔP_{ed} in the $\Delta\delta-j\Delta\delta$ plane, as shown by Fig. 3-6.

Fig. 3-6 shows that the SVC increases the damping power component of the d -axis flux linkage but at the expense of a deteriorating synchronising power component over a range of AVR operating gain. In other words, the SVC counteracts the AVR action. The block diagram in Fig. 3-4 can also

be used to explain why the AVR action is reduced. It should be noted that signal $\Delta\delta$ supplied through the coefficient K_{5n} opposes the signal supplied through the coefficient K_5 , before being passed on to influence the d -axis flux linkage. Moreover, Fig. 3-6 shows that the damping improvement due to the SVC is quite small.

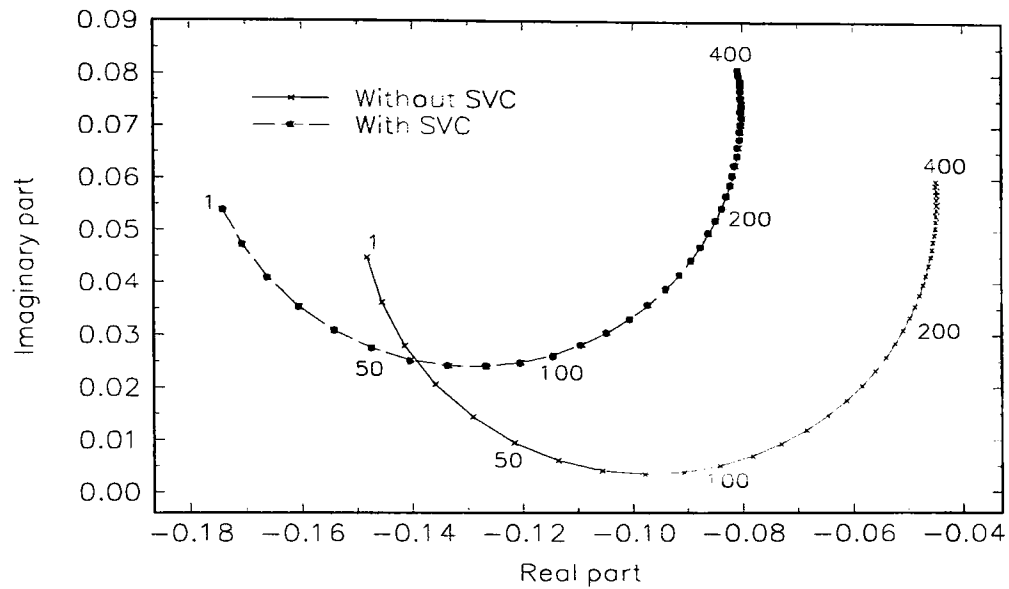


Figure 3-6 Plot of electrical power generated by the d -axis flux linkage with various AVR gains

3.8.2 Electrical power ΔP_{eq}

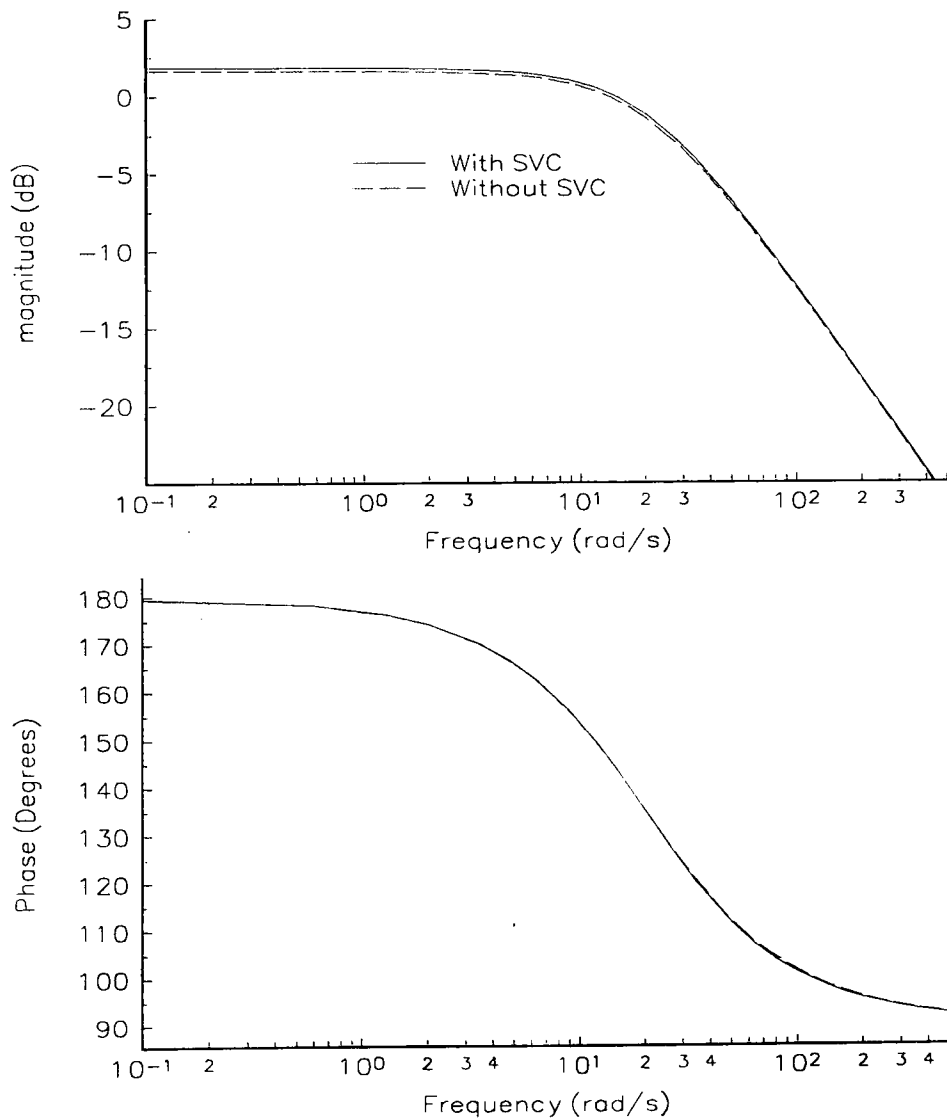


Figure 3-7 Frequency response of $\Delta P_{eq}/\Delta\delta$ with and with no SVC

The plot of $\Delta P_{eq}/\Delta\delta$ in Fig 3-7 shows the power characteristic of the q -axis flux linkage over a wide frequency range. The phase angle is a gradual decrease towards 90° , as the oscillation frequency increases. Therefore, it can be said that the damper windings always provide positive damping power, hence, suppressing oscillations. According to the result in Fig 3-7, the SVC only provides a slight increase in frequency gain and no change in phase, compared to the case when no SVC is used.

3.8.3 Electrical power ΔP_{svc}

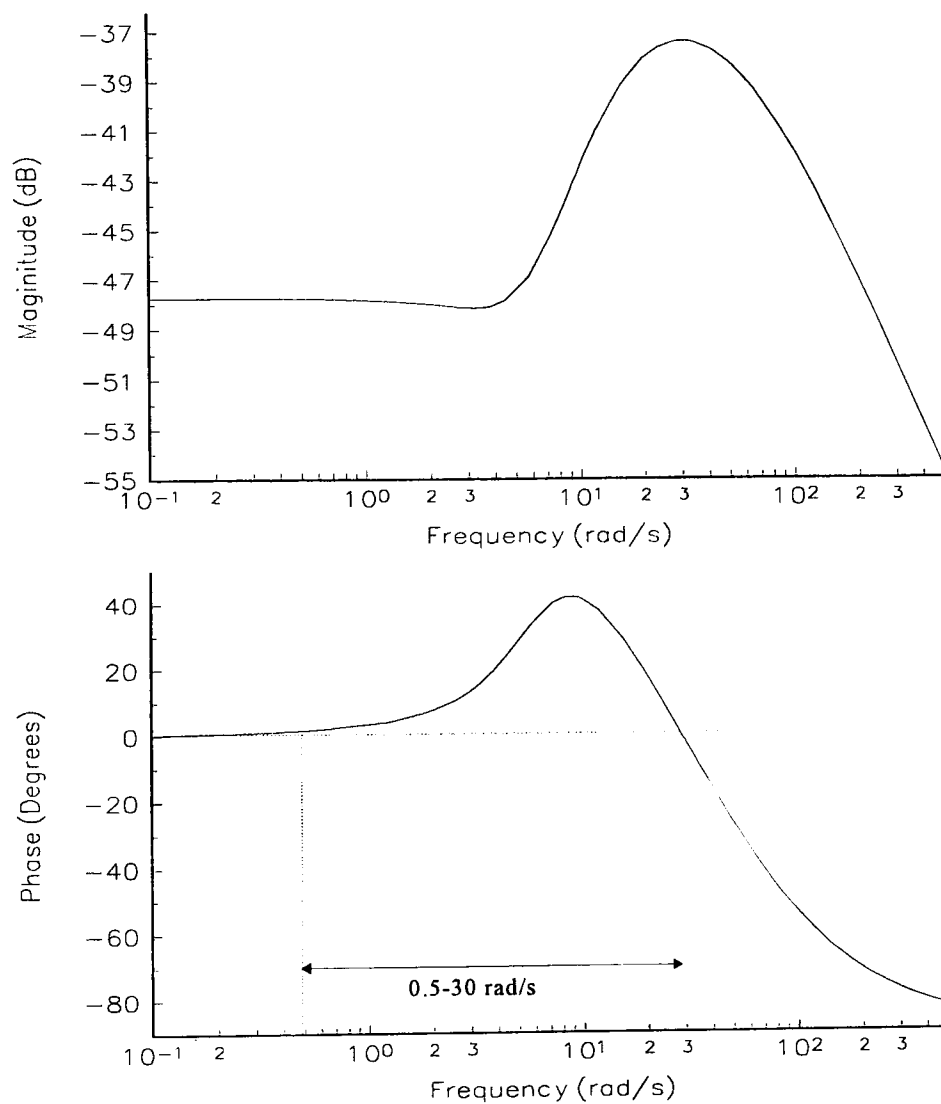


Figure 3-8 Frequency response of $\Delta P_{svc}/\Delta\delta$ with SVC

Fig. 3-8 shows the frequency response characteristic of $\Delta P_{svc}/\Delta\delta$. In the frequency range of 0.5-30 rad/sec, where phase is greater than zero, the positive synchronising and damping power components of ΔP_{svc} due to a variation in the firing angle, is obtained. Hence, the SVC improves system stability. After that frequency range the phase decreases downwards trend -90° . The damping power component is changed from the positive to the negative direction, and system stability is reduced.

3.9 Conclusions

A new and more comprehensive transfer-function block-diagram model of a synchronous generator with a SVC system has been derived from first principles and presented in this chapter. It provides a fundamental basis for the analysis and elucidation of the dynamic interactions between synchronous generators and SVCs. The block-diagram model confirms that the generator dynamic characteristics are significantly influenced by a change in SVC firing angle as well as by the SVC location along the tie-line system and the base operating point. The generator's dynamic performance has been assessed by analysing the synchronising and damping electrical power components produced by the generator's flux linkages. The SVC increases the damping power contributed from the d -axis flux linkage of the generator's main field winding by counteracting the negative AVR effects. Due to the high AVR operating gains, the SVC has a greater effect on the power characteristic of the d -axis flux linkage than on the power characteristic of the q -axis flux linkage. It should be noted that the SVC is not able to increase significantly the system damping contributed from the q -axis flux linkages. These more detailed observations than what has been possible heretofore, advance the understanding of the role played by SVC plant in power system dynamics. They have been made possible by the more comprehensive approach to plant modelling undertaken in this research.

3.10 References

- [1] W.G. Heffron and R. A. Phillips, "Effect of Modern Amplidyne Voltage Regulator on Underexcited Operation of Large Turbine Henerator", AIEE Transactions, Vol. 71, August 1952, pp. 692-697.
- [2] F.P. Demello and C. Concordia, "Concepts of Synchronous Machine Stability as Affected by Excitation Control", IEEE Transactions on Power Apparatus and Systems, Vol. 88, No. 4, April 1969, pp. 189-202.
- [3] D. P. SenGupta, N. G. Narahari and J. W. Lynn, "Damping and Synchronising Torques Contributed by a Voltage Regulator to a Synchronous Generator: A Quantitative Assessment", IEE Proceedings on Generation, Transmission and Distribution, Vol. 148, Part C, No. 8, August 1977, pp. 702-708.
- [4] A. A. Shaltout and T. H. Alden, "Analysis of Damping and Synchronising Torque", IEEE Transactions on Power Apparatus and Systems, Vol. 98, No. 5, September 1979, pp. 1701-1705.
- [5] P. M. Anderson and A. A. Fouad, "Power System Control and Stability", The Iowa State University Press, 1986.

- [6] P. Kundur, "Power System Stability", McGraw-Hill Inc, 1993.
- [7] K. L. Law, D. J. Hill and N. R. Godfrey, "Robust Co-ordinate AVR-PSS Design", IEEE Transactions on Power Systems, Vol. 9, No. 3, August 1994, pp. 1281-1225.
- [8] M. Saidy and F. M. Hughes, "Block Diagram Transfer Function Model of a Generator Including Damper Windings", IEE Proceedings on Generation, Transmission and Distribution, Vol. 141, Part C, No. 6, November 1994, pp. 559-608.
- [9] M. Saidy and F. M. Hughes, "An Extended Block Diagram Transfer Function Model of a Synchronous Machine", International Journal of Electrical Power and Energy System, Vol. 18, No. 2, February 1996, pp. 139-142.
- [10] M. Saidy and F. M. Hughes. "Performance Improvement of a Conventional Power System Stabiliser", International Journal of Electrical Power and Energy System, Vol. 17, No. 5, October 1995, pp. 313-323.
- [11] IEEE/CIGRE, "FACTS Overview", Special Issue, 95-TP-108, IEEE Service Centre, Piscataway, N.J., 1995.
- [12] N. G. Hingorani, "Flexible AC Transmission System", IEEE Spectrum, Vol. 30, No. 4, April 1993, pp. 40-45.
- [13] E. V. Larsen, J. J. Sanchez-Gasca and J. H. Chow, "Concepts for Design of FACTS Controllers to Damp Power Swings", IEEE Transactions on Power Systems, Vol. 10, No. 2, May 1995, pp. 984-955.
- [14] H. F. Wang and F. J. Swift, "A Unified Model for the Analysis of FACTS Devices in Damping Power System Oscillation Part I: Single-machine Infinite-bus Power System" IEEE Transactions on Power Delivery, Vol. 12, No. 2, April 1997, pp. 941-946
- [15] H. F. Wang and F. J. Swift, "Capability of the Static Var Compensator in Damping Power System Oscillations", IEE Proceedings on Generation, Transmission and Distribution, Vol. 143, Part C, No. 4, July 1996, pp. 353-358.
- [16] IEEE Task Force on Definitions and Procedures, "Current Usage and Suggested Practices in Power System Stability Simulations for Synchronous Machines", IEEE Transactions on Energy Conversion, Vol. 1, No. 1, March 1986, pp. 77-93.
- [17] IEEE Standard 1110-1991, "IEEE Guide for Synchronous Generator Modelling Practices in Stability Analyses", 1991.
- [18] T. J. Hammons and D. J. Winning, "Comparisons of Synchronous Machine Models in the Study of the Transient Behaviour of Electrical Power System", Proceeding of IEE, 118, No.

10, October 1971, pp. 1422-1458.

- [19] T. J. E. Miller, "Reactive Power control in Electric System", John Wiley & Sons, 1982.
- [20] P. Kundur, "Power System Stability", McGraw-Hill Inc, 1993.
- [21] S. Arabi, G. J. Rogers, D. Y. Wong, P. Kundur and M. G. Lauby, "Small Signal Stability Program Analysis of SVC and HVDC in AC Power System", IEEE Transactions on Power Systems, Vol. 6, August 1991, pp. 1147-1153.
- [22] P. K. Dash, P. C. Panda, A. M. Sharaf and E. F. Hill, "Adaptive Controller for Static Reactive-Power Compensators in Power System", IEE Proceedings on Generation, Transmission and Distribution, Vol. 134, Part C, No. 3, May 1987, pp. 256-262.
- [23] N. Martins, A. T. Poray and M. E. Coultres, "Determination of Suitable Locations For Power System Stabilisers and Static Var Compensators for Damping Electromechanical Oscillation in Large Scale Power System", IEEE Transactions on Power Systems, Vol. 5, No. 4, November 1990, pp. 1455-1469.
- [24] S. C. Kapoor, "Dynamic Stability of Static Compensator-Synchronous Generator Combination", IEEE Transactions on Power Apparatus and Systems, Vol. 100, No 4, April 1981, pp. 1694-1720.
- [25] R. J. Koessler, "Dynamic Simulation of Static Var Compensators in Distribution System", IEEE Transactions on Power Systems, Vol. 7, No 3, August 1992, pp. 1285-1291.

Chapter 4

Evaluation and Application of the Small-Signal Block-Diagram Models

4.1 Introduction

In power system dynamic studies, the order of the synchronous generator model affects significantly the reliability of the result and the computational time required for the analysis [1-5]. A comprehensive transfer-function block-diagram model of a synchronous generator-SVC system was introduced in Chapter 3, where a different number of damper windings has been catered for, i.e. Models 1-3. The selection of the simplest system model that still yields a high level of reliability while minimising the computational time required in the study of the power system behaviour is of critical concern.

The main aims of this chapter are:

- (i) To evaluate the various modelling possibilities with a view to identify and recommend a suitable model of the synchronous generator-SVC plant for small-signal stability studies, for the purpose of single-machine infinite-bus framework. The overall dynamic performance of the three system models is investigated, i.e. Models 1-3, with the SVC influence on the dynamic characteristics of the flux linkages in the d and q -axes being compared. The end result is a critical assessment of the impact of damper winding representation on the study of synchronous generator-SVC systems.
- (ii) To apply the newly developed dynamic model to investigate the role played by the SVC voltage control loop and damping control loop in the enhancement of the generator dynamic performance. Two different network conditions are considered: when the SVC is placed at the generator's terminal bus and when the SVC is placed at mid-point of the tie-line system.

It should be mentioned that the well-established frequency response, i.e. bode analysis, and time response are used to carry out all the fundamental analyses presented in this chapter.

4.2 Fundamental evaluation of small-signal system models

With various classes of Models 1-3, the influence of the SVC generator dynamic performance is investigated by examining the frequency response characteristics of the additional transfer functions and coefficients, which bring the SVC effects to the flux linkages in the d and q -axes.

The characteristic of the electrical power generated by the flux linkages is then compared. The overall dynamic responses of various system models are finally assessed.

4.2.1 Characteristics of the additional transfer functions and coefficients

Referring to the general block-diagram model in Fig. 3-2, $\Delta E''_q$ and $\Delta E''_d$ represent the variation in the subtransient voltages proportional to total flux linkage of the d -axis field plus damper windings and q -axis damper winding, respectively. The output power of the generator can be influenced by the SVC contributions to $\Delta E''_q$ and $\Delta E''_d$. The SVC affects $\Delta E''_q$ directly via the $g_{svc2}(s)$ branch and indirectly via the K_{svc3} branch of the generator terminal voltage. In a regulated system, the AVR can enhance the SVC contribution through the K_{svc3} branch, to influence $\Delta E''_q$ by controlling the field voltage (ΔE_{fd}). Therefore, a change in $\Delta E''_q$ due to a change in the SVC fringe angle $\Delta\alpha$ is given by the total transfer function $-K_{svc3}g_3(s)g_{avr}(s)$, where $g_{avr}(s)$ represents the AVR system. The negative sign is introduced because of the negative voltage feedback nature of the AVR system. The $g_{svc2}(s)$ and K_{svc3} branches bring about a change in the electrical power ΔP_{ed} in the d -axis flux linkage. Moreover, $\Delta E''_d$ is influenced by $\Delta\alpha$ through the $g_{svc2d}(s)$ branch, which is amenable to a SVC contribution to the electrical power ΔP_{eq} of the q -axis flux linkage.

In this section, the characteristics of the transfer functions $g_{svc2}(s)$, $-K_{svc3}g_3(s)g_{avr}(s)$ and $g_{svc2d}(s)$ with Models 1-3 are investigated via frequency response analysis to show how the flux linkage characteristic changes with the number of damper windings included in the model. The system operating conditions are given in columns 2 and 3 of Table 4-1, which shows that the SVC is used to increase the voltage at mid tie-line point (V_{mid}) from 0.9832 to 1.002 p.u. and to increase the reactive power exported to the infinite bus from 0.522 to 0.727 p.u., while the active power is kept constant. The system parameters are given in Appendix D.

Characteristics of the transfer function $g_{svc2}(s)$

Fig. 4-1 shows the direct SVC effects on the d -axis flux linkage due to changes in $\Delta\alpha$ via the $g_{svc2}(s)$ branch, with constant ΔE_{fd} and $\Delta\delta$. The gain and phase versus frequency of $g_{svc2}(s)$ corresponding to Model 1 differ substantially from those of Models 2 and 3. In Model 1, the SVC gives a higher frequency gain and a higher phase lead to $\Delta E''_q$ to improve system performance over the frequency range of concern. For Models 2 and 3, a lower gain and phase lead are given to $\Delta E''_q$ because the d -axis damper winding is neglected. Fig. 4-1 also indicates that the steady-state gains obtained for the three models are quite low (approximately 35 dB). It is noted that the gain and phase of Models 2 and 3 are identical because they only consider the effect of the main field winding.

| | With no SVC | With SVC | | |
|----------------|--|--|------------------------------|------------------------------|
| P_g | 0.736 p.u. | 0.736 p.u. | | |
| Q_g | 0.752 p.u. | 0.5514 p.u. | | |
| Q_{svc} | - | 0.378 p.u. | | |
| Q_t | 0.552 p.u. | 0.727 p.u. | | |
| X_t | 0.2 p.u. | 0.2 p.u. | | |
| X_{t1} | - | 0.1 p.u. | | |
| v_∞ | 0.92 p.u. | 0.92 p.u. | | |
| e_t | 1.0522 p.u. | 1.0522 p.u. | | |
| V_{mid} | 0.9832 p.u. | 1.0022 p.u. | | |
| I_t | 1 p.u. | 1.1246 p.u. | | |
| α | - | 150° | | |
| δ_o | 29.85 | 35.92 | | |
| E_{fd0} | 2.3087 p.u. | 2.0618 p.u. | | |
| | Model 1 | Model 1 | Model 2 | Model 3 |
| $g_3(s)$ | $\frac{6.789 + 0.19s}{29.47 + 49.38s + s^2}$ | $\frac{6.789 + 0.19s}{29.24 + 49.24s + s^2}$ | $\frac{0.19}{0.6029 + s}$ | $\frac{0.19}{0.6029 + s}$ |
| $g_4(s)$ | $\frac{10.39 + 6.17s}{29.47 + 49.38s + s^2}$ | $\frac{11.346 + 6.74s}{29.24 + 49.24s + s^2}$ | $\frac{0.2086}{0.6029 + s}$ | $\frac{0.2086}{0.6029 + s}$ |
| $g_{svc2}(s)$ | - | $\frac{0.5288 + 0.314s}{29.24 + 49.24s + s^2}$ | $\frac{0.00972}{0.6029 + s}$ | $\frac{0.00972}{0.6029 + s}$ |
| $g_{4d}(s)$ | $\frac{11.048}{20.136 + s}$ | $\frac{11.116}{19.987 + s}$ | $\frac{11.116}{19.987 + s}$ | - |
| $g_{svc2d}(s)$ | - | $\frac{11.116}{19.987 + s}$ | $\frac{11.116}{19.987 + s}$ | - |
| K_1 | 2.8639 | 2.86248 | 2.6866 | 1.45331 |
| K_2 | 1.2085 | 1.32003 | 0.9722 | 0.97220 |
| K_{2d} | 2.2041 | 2.21768 | 2.21768 | - |
| K_3 | - | - | 0.31531 | 0.31531 |
| K_4 | - | - | 1.09761 | 1.09761 |
| K_{4d} | - | - | 0.55615 | - |
| K_5 | -0.07319 | -0.07463 | -0.13975 | -0.01697 |
| K_6 | 0.49228 | 0.48896 | 0.36012 | 0.36012 |
| K_{6d} | 0.19899 | 0.22076 | 0.22076 | - |
| K_{svc1} | - | 0.01538 | 0.02358 | 0.00507 |
| K_{svc2} | - | - | 0.05116 | 0.05116 |
| K_{svc2d} | - | - | 0.00835 | - |
| K_{svc3} | - | 0.01225 | 0.01528 | 0.017126 |
| K_{5n} | - | -0.06031 | -0.09241 | -0.01987 |
| K_{6n} | - | 0.24106 | 0.17754 | 0.17754 |
| K_{6dn} | - | 0.13042 | 0.13042 | - |
| K_{svc3n} | - | 0.01925 | 0.02075 | 0.021838 |

Table 4-1 System operating conditions (Section 4.2)

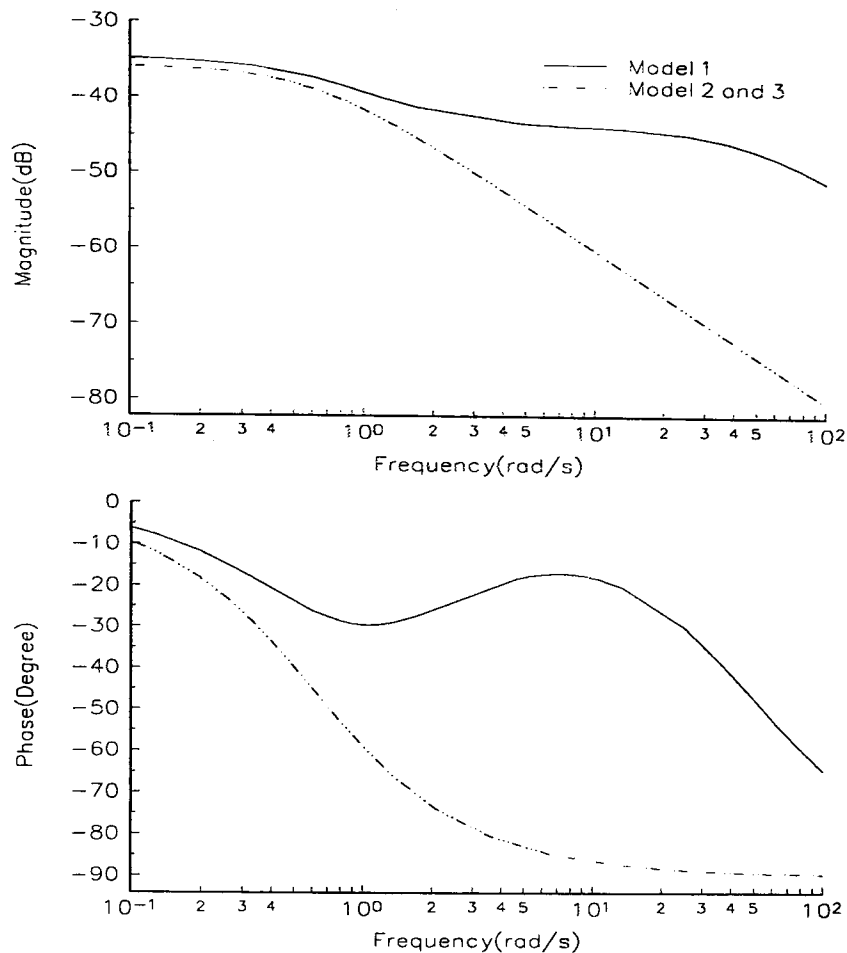


Figure 4-1 Frequency response characteristic of the transfer function $\Delta E''_q/\Delta\alpha$ through the $g_{svc2}(s)$ branch

Characteristics of transfer function $-K_{svc3}g_3(s)g_{avr}(s)$

The bode plot of the transfer function $-K_{svc3}g_3(s)g_{avr}(s)$ in Fig. 4-2 shows the indirect SVC effects on the d -axis flux linkage via the generator terminal voltage in a regulated system. In this result a change in $\Delta\delta$ and $\Delta\alpha$, given via the $g_4(s)$ and $g_{svc2}(s)$ branch, respectively, are kept constant. This plot shows that a phase lead is given to the d -axis flux linkage by all three models, owing to the negative voltage feedback effect produced by the AVR system. The plot of gain versus frequency shows that Models 2 and 3 have a higher gain at lower frequencies, up to about 100 rad/sec. However, Model 1 provides better phase lead, obtained from the numerator of $g_3(s)$, which improves the system dynamic performance during high frequency oscillations.

The frequency responses of Models 1-3 in Fig. 4-2 correspond to a $g_{avr}(s)$ gain of 100. It can be observed that the AVR enhances the SVC contributions via the K_{svc3} branch, with a higher steady-state gain of 9-11 dB. By comparing Figs. 4-1 and 4-2, it is not difficult to see that the SVC contributions via the K_{svc3} branch are greater than the contribution via the $g_{svc2}(s)$ branch, owing to the important role played by the AVR.

Characteristics of the transfer function $g_{svc2d}(s)$

The frequency response in Fig. 4-3 indicates that the SVC effects on the q -axis flux linkage through the $g_{svc2d}(s)$ branch, with constant $\Delta\delta$, has a low steady-state gain of 41.5 dB. This gain remains almost constant over a medium range of oscillation frequencies, i.e. 10 rad/sec.

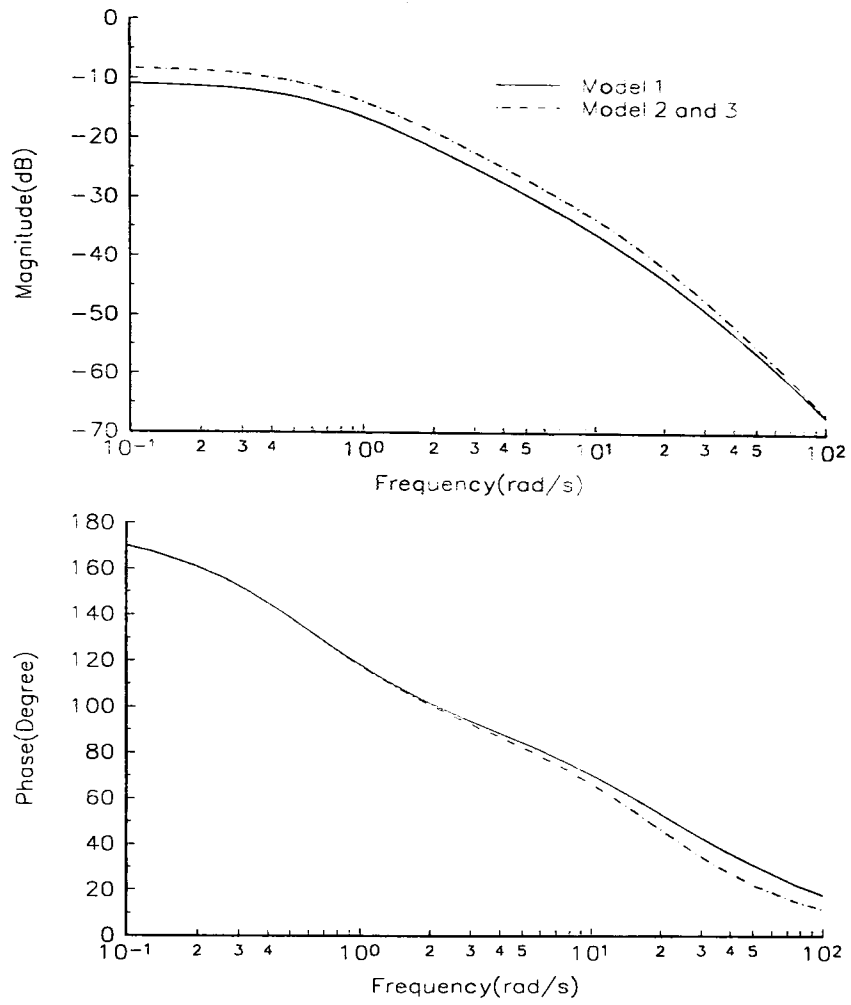


Figure 4-2 Frequency response characteristic of the transfer function $\Delta E''_q/\Delta\alpha$ through the K_{svc3} branch and AVR

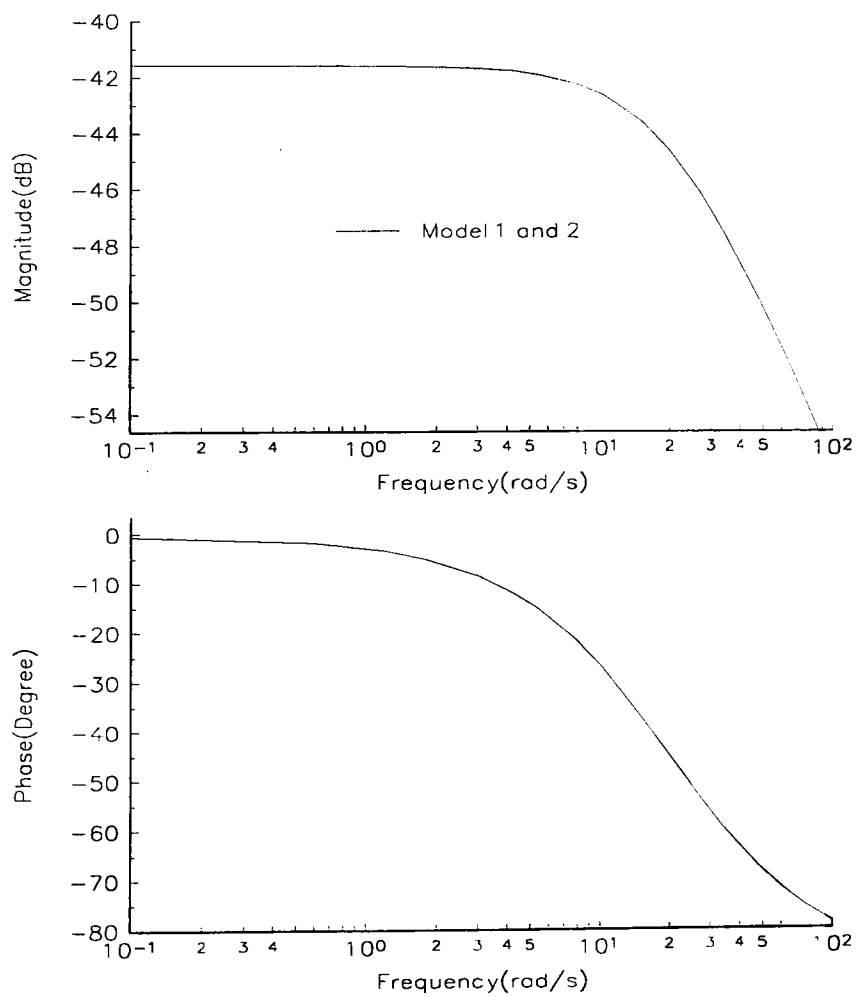


Figure 4-3 Frequency response characteristic of the transfer function $\Delta E''_d/\Delta\alpha$ through the $g_{svc2d}(s)$ branch

The gains and phases of Model 1 and 2 are identical, since $g_{\text{svc}2d}(s)$ is the same for both models. It is noted that $g_{\text{svc}2d}(s)$ does not exist in Model 3 because the q -axis damper winding does not exist in this model.

It can be said that the number of damper windings influences significantly the SVC contribution to the d and q -axis flux linkages of the generator. A close observation of the SVC contributing branches reveals that the $K_{\text{svc}3}$ branch plays a significant role when the generator output voltage is regulated, since the AVR enhances significantly the SVC contribution, which is passed on to influence the d -axis flux linkage.

4.2.2 An investigation of the power characteristics of the flux linkages in d - and q -axes

The flux linkages of the d and q -axes are among the most significant factors which determine the generator dynamic characteristics. Hence, variations in the electrical powers generated by these flux linkages can be meaningfully used to describe how the system dynamic response changes with respect to various orders of system models. Hence, in this section, the frequency response characteristics of $\Delta P_{ed}/\Delta\delta$ and $\Delta P_{eq}/\Delta\delta$ in Models 1-3 are plotted, so that the synchronising and damping power components can be investigated and compared. The system operating conditions are given in columns 3-5 of Table 4-1.

The frequency response in Fig. 4-4 indicates the phase characteristics of the electrical power generated by the d -axis flux linkages. The phase versus frequency of Model 1 is greater than 90° throughout the frequency range of concern. This means that Model 1 has positive damping and negative synchronising power components. For Model 2, the positive synchronising and damping powers can only be obtained during the following frequency ranges 0.1 and 8 rad/sec, where the phase angle is greater than 0° and less than 90° . Then, during the high frequency range, Model 2 has a poor performance due to a very significant negative damping power component, which is shown by a gradual decrease of the phase angle from 0° to -180° . The frequency response also shows that Model 3 has negative damping power components since its phase angle is always less than 0° .

The frequency response in Fig. 4-5 gives the power characteristics of the q -axis flux linkage, where it is observed that the flux linkages produce positive damping power components at all frequencies. The response characteristics of Model 1 and 2 are identical since there is one q -axis damper winding in these models. In contrast, Model 3 contains no damper circuits.

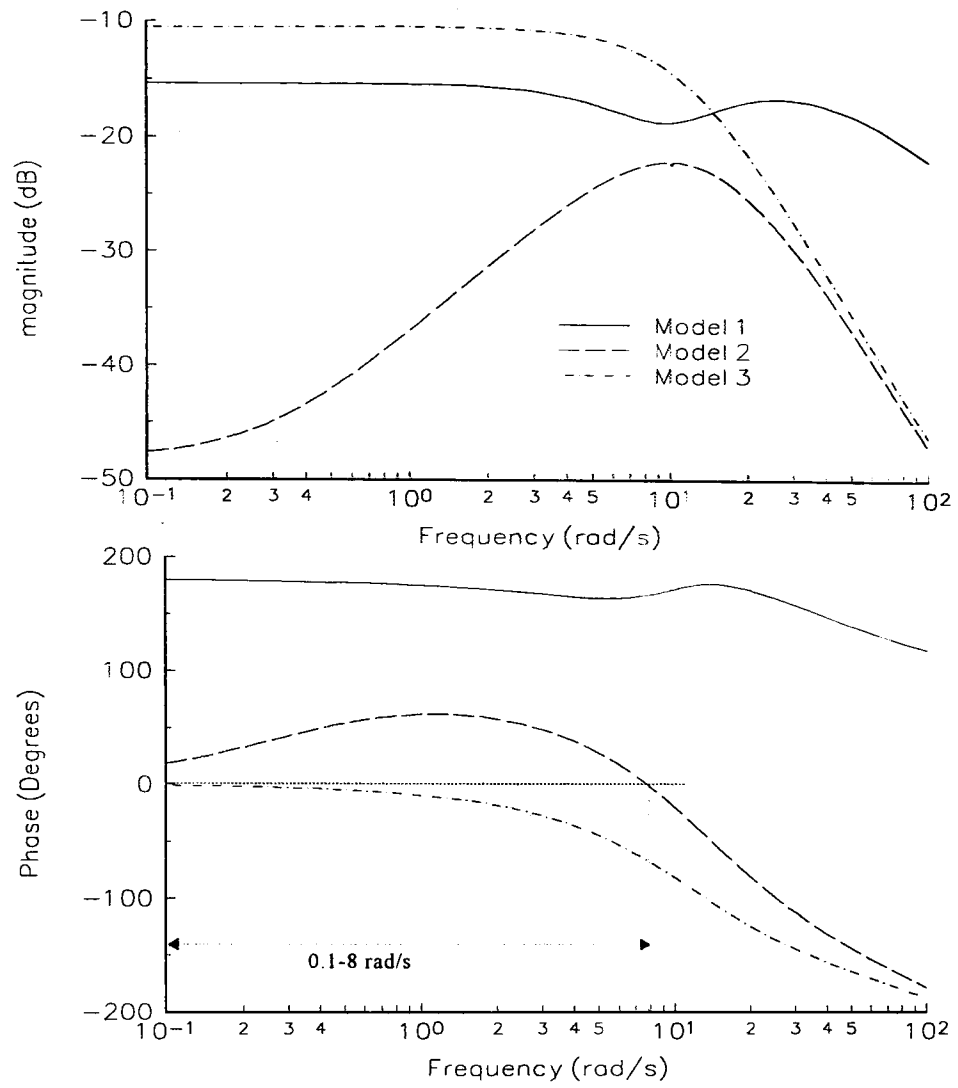


Figure 4-4 Frequency response of $\Delta P_{ed}/\Delta\delta$ with Model 1-3

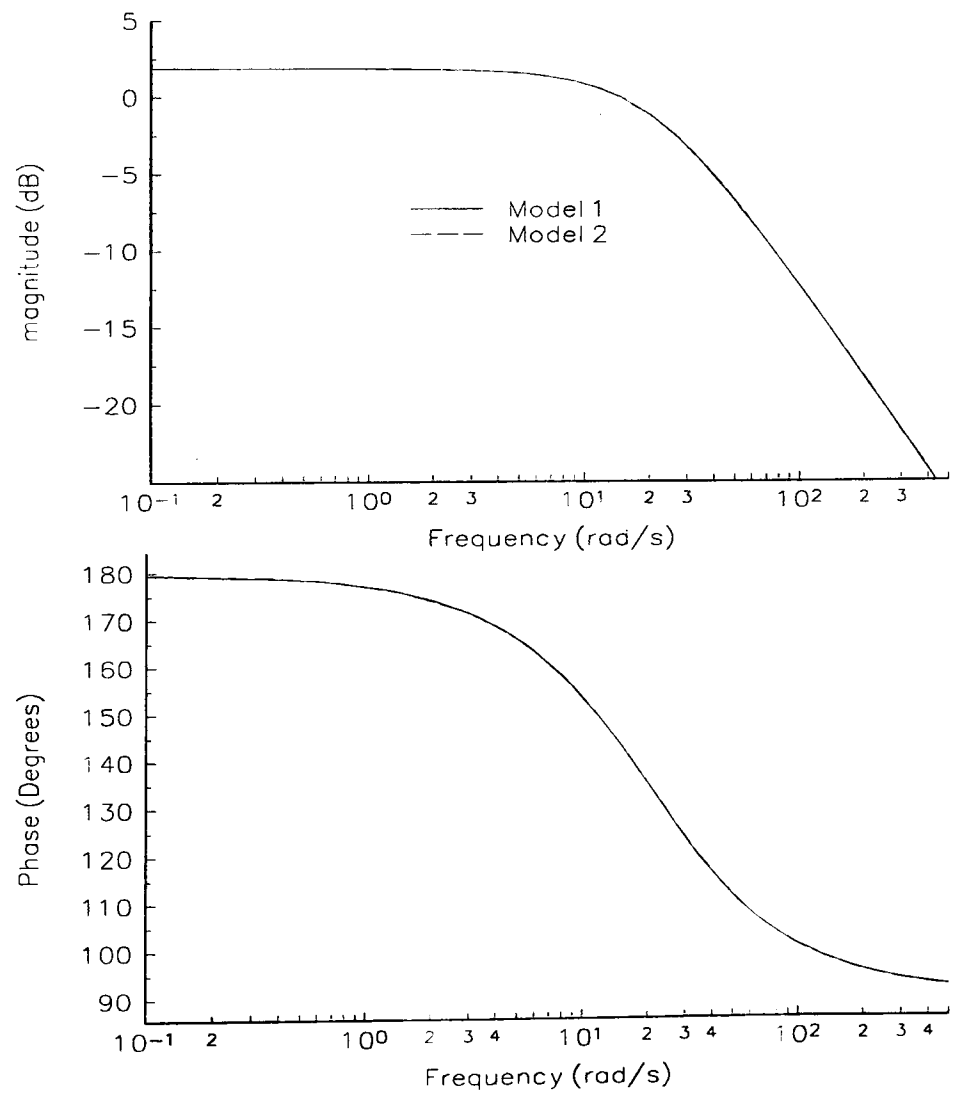


Figure 4-5 Frequency response of $\Delta P_{eq}/\Delta\delta$ with Model 1-2

4.2.3 Assessment of the overall system models

This section assesses overall system dynamic performances, as given by Models 1-3, in order to identify a suitable block-diagram model for small-signal stability studies. This is in relation to the synchronous generator-SVC system shown in Fig. 3-2. The open-loop frequency responses relating to $\Delta e_f/\Delta e_{err}$ and time responses are used. The SVC with a voltage control loop gain of 2.5 is used. The excitation control system consists of a fast-acting AVR with no stabiliser. The AVR gain is tuned at 100. The system operating conditions are given in columns 3-5 of Table 4-1. It is noted that a zero mechanical damping term D is used.

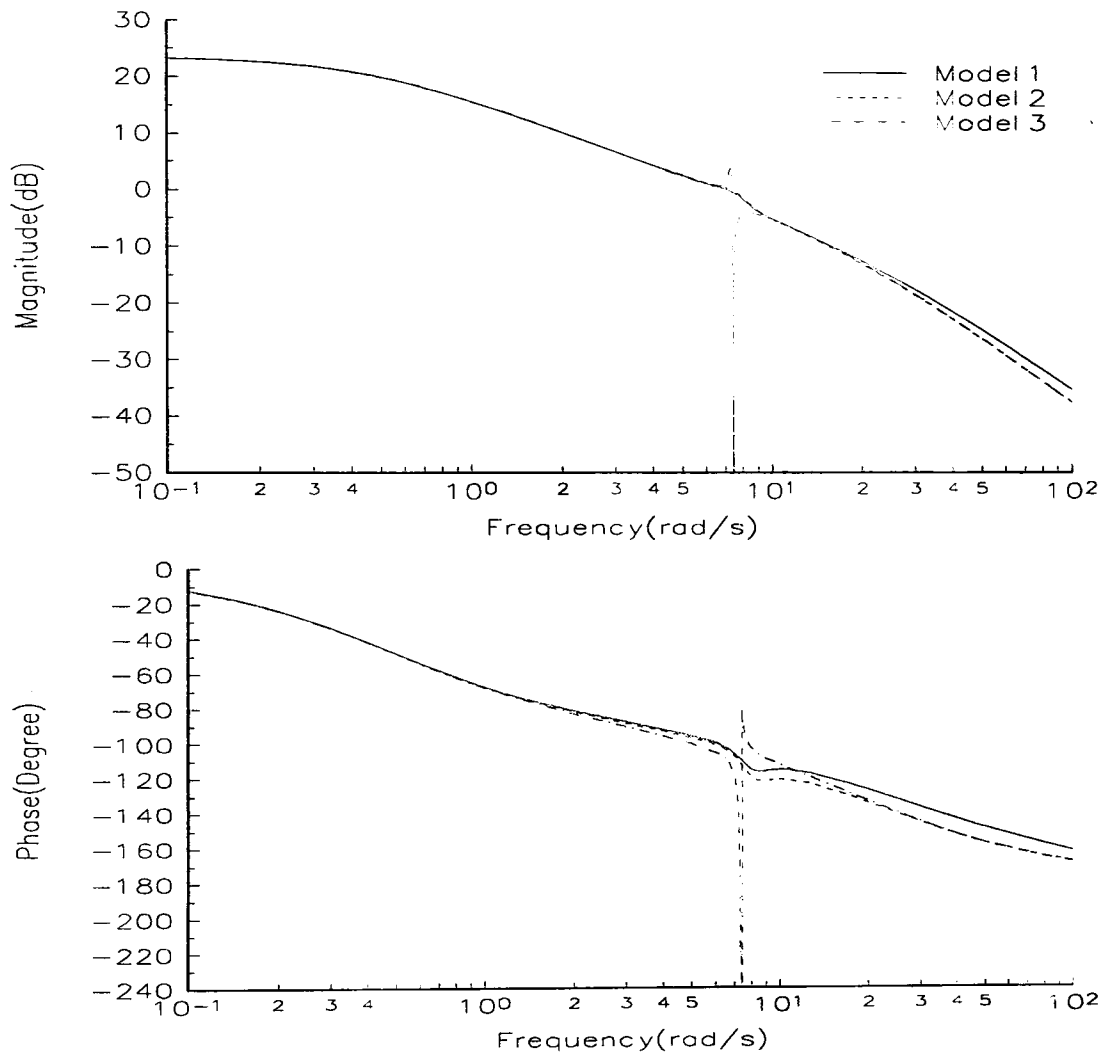
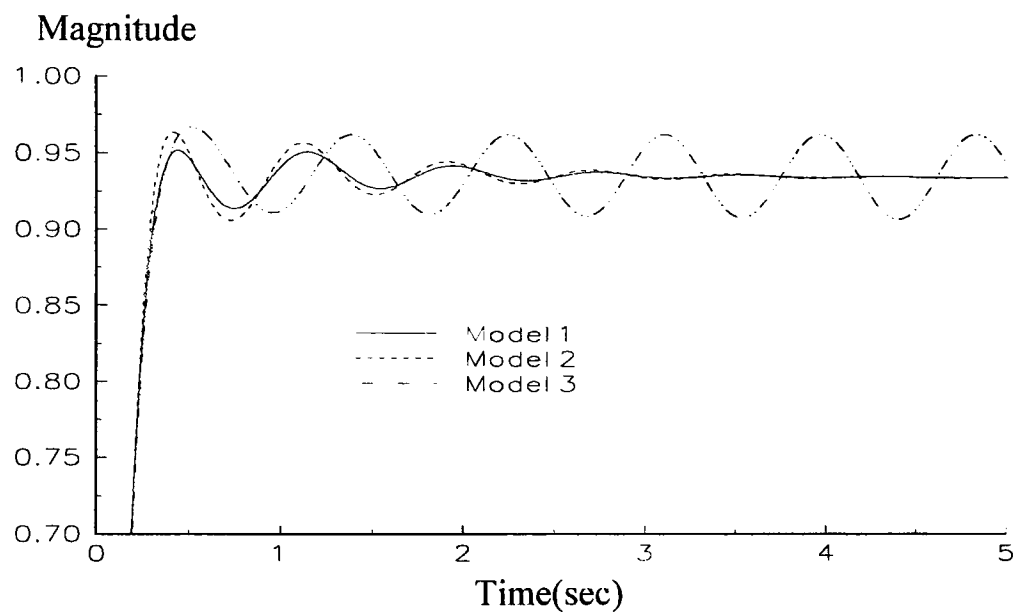


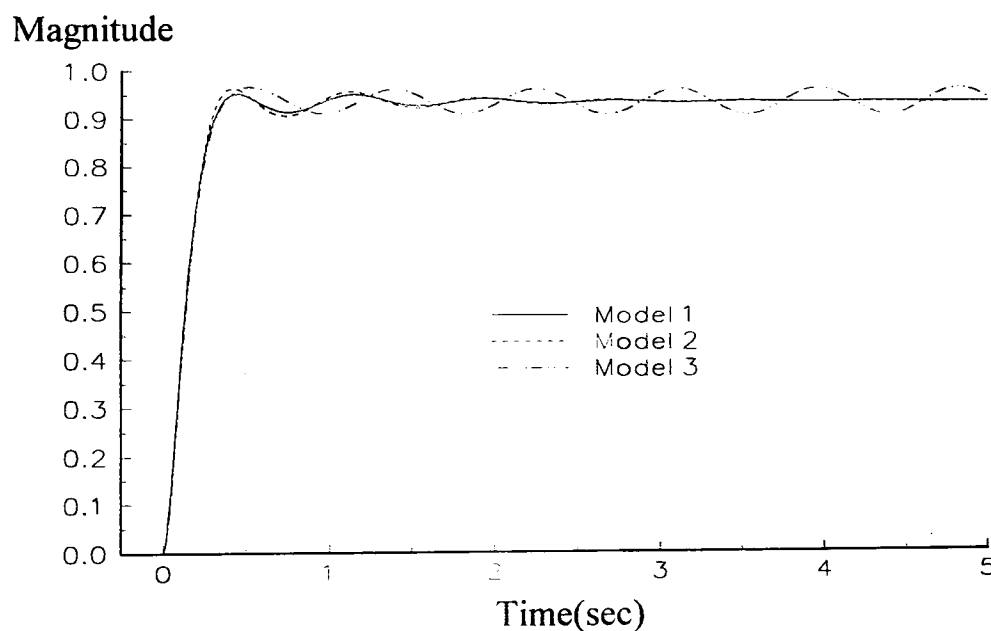
Figure 4-6 Frequency response characteristic of $\Delta e_f/\Delta e_{err}$

The stability of Models 1-3 can be investigated by looking at the phase margin angle, which should not drop beyond -180° at the gain-crossover point [1, 2]. In Fig. 4-6, the plots of phase versus frequency shown clearly demonstrate that Model 3 is undamped at the natural oscillation frequency, with a high switch-back characteristic due to the lack of realistic damping. By incorporating the q -axis damper winding in Model 2, system damping is introduced over the frequency range of concern. However, Model 2 has an appreciable lower phase lead at the high frequency range compared to that of Model 1. Therefore, during high frequency oscillations, Model 1 provides a better dynamic performance because of the phase lead, which is supplied by the d -axis damper winding. It should be mentioned that the frequency response of Models 1 and 2 resemble quite well the measured responses presented in [8].

The time responses obtained from the three models can also be employed to further demonstrate how the damping windings influence system dynamic performance. The transient responses of the generator output Δe_t are obtained by applying a step change to Δe_{t-ref} with no time delay while $\Delta v_{svc-ref}$ remains constant. It should be noted that the step size of 0.001 is used in the integration process to obtain the output Δe_t . The voltage profile of Model 3 is undamped, as shown in Fig. 4-7, while those of Model 1 and 2 are better damped. Although a higher overshoot in the step response of Δe_t is observed in Model 2, its magnitude settles down to a steady-state value similar to that of Model 1.



(a)



(b)

Figure 4-7 Step response of generator output voltage Δe_t resulting from applying a step change to Δe_{t-ref}

It can be said that Model 3, including only the effect of the d -axis main field winding, does not yield sufficient system damping. An approach that has been used in the past to compensate for the undamped response in Model 3 is to introduce artificial damping, D , into the mechanical system equations [1, 2, 6-7]. From Fig. 4-8, it can be seen that the undamped response is compensated by

including a damping term D greater than zero. It requires a high value of D , e.g. 12.5, which is exceptionally high. Hence, the application of Model 3, as a block-diagram tool for small-signal stability studies, may lead to inaccurate analysis. Due to the vast improvement observed in system damping, Model 2 may be the best model to use for small-signal stability analysis, because it minimises complexity and computational time. However, Model 1 exhibits a higher level of reliability and it may be used instead if better dynamic performances over the high frequency range are required.

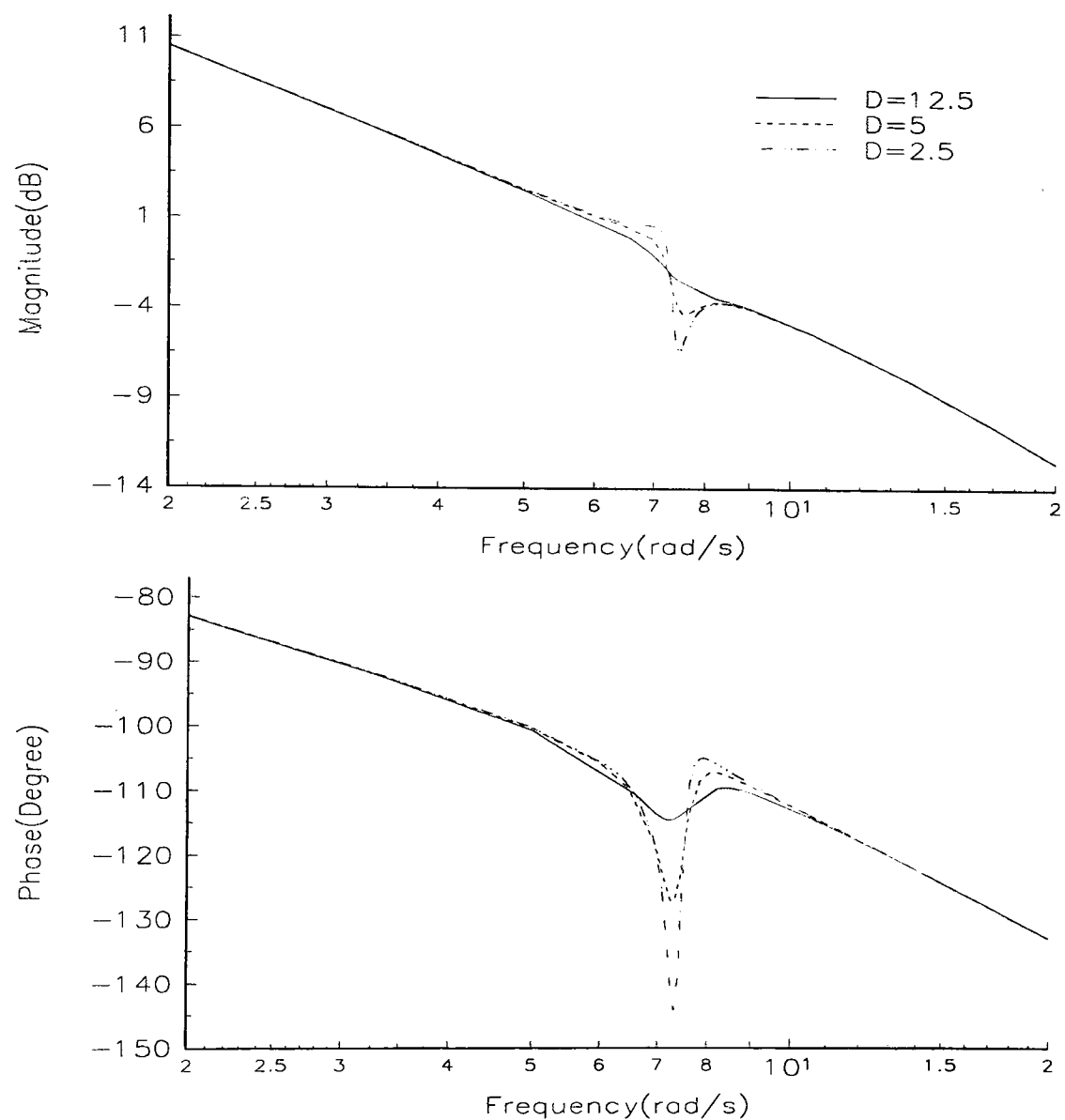


Figure. 4-8 Frequency response characteristic of $\Delta e_t/\Delta e_{err}$

4.3 An investigation of the generator dynamic performance

In this section, the overall dynamic performance of the generator is assessed. The performance is evaluated with the aid of open-loop frequency responses of the transfer function $\Delta e_t/\Delta e_{err}$, corresponding to Model 2. The system operating conditions are given in Table 4-2 and the system parameters are given in Appendix D. Three different kinds of studies are carried out below: (i) system with no SVC, (ii) system with SVC placed at mid point of the tie-line system and (iii) system with SVC placed at the generator's terminal bus.

4.3.1 Generator performance with no SVC

Before assessing the generator dynamic performance with the SVC being applied, let us consider the inherent dynamic characteristic of the system when no SVC is present. The static excitation control with a gain of 100 is applied to maintain constant generator terminal voltage. Under lagging power factor, the generator dynamic performance with different operating conditions are assessed: Firstly, the effects of changing the tie-line reactance values from 0.2 to 0.8 p.u. are investigated. The former corresponds to a strong connection while the latter corresponds to a weak connections. Secondly, generator output powers of 0.5 and 1 p.u. are considered. The system operating conditions are given in columns 2-4 of Table 4-2.

The open-loop frequency response in Fig. 4-9 shows the generator dynamic performance as the reactance of the tie line is increased from 0.2 to 0.8 per units. The high switch-back characteristic occurs at the natural frequency of oscillation because the damping power contributed from the flux linkages is greatly reduced when the tie-line reactance becomes larger. Similarly, the frequency response in Fig. 4-10 illustrates the generator dynamic performance with respect to different output powers. The switch-back characteristic at a frequency of around 8 rad/sec indicates that the system damping is reduced as the demanded power increases from 0.5 to 1 per unit. The resulting switch-back characteristic indicates a poor generator voltage output profile and introduces difficulties in controlling the system at this frequency range.

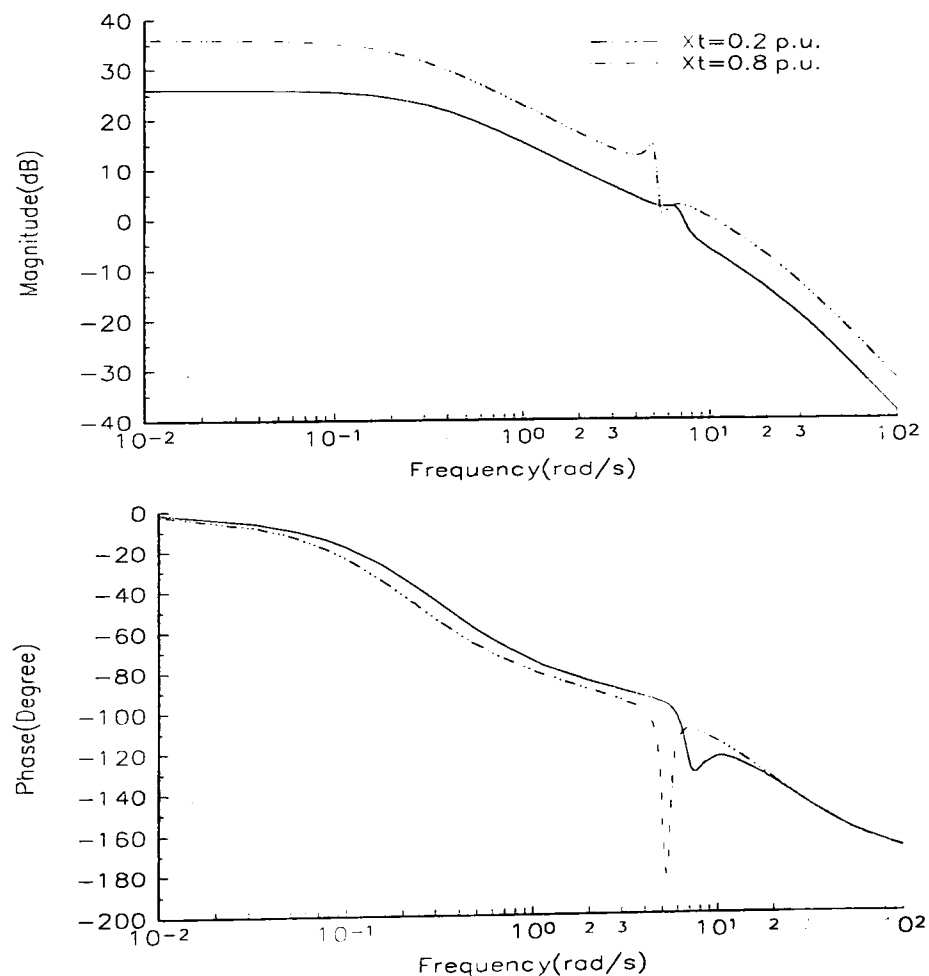


Figure 4-9 Open-loop frequency response between $\Delta e_t/\Delta e_{err}$ for two tie-line reactance values

| | Without SVC | | | With SVC | |
|-------------|-------------|-------------|-------------|-------------|-------------|
| | | | | Case I | Case II |
| α | - | - | - | 150° | 150° |
| P_g | 0.736 p.u. | 0.736 p.u. | 1.00 p.u. | 0.736 p.u. | 0.736 p.u. |
| Q_g | 0.127 p.u. | 0.512 p.u. | 0.80 p.u. | 0.258 p.u. | 0.04 p.u. |
| Q_{svc} | - | - | - | 0.425 p.u. | 0.473 p.u. |
| Q_t | 0.0 p.u. | 0.0 p.u. | 0.19 p.u. | 0.212 p.u. | 0.0 p.u. |
| X_t | 0.2 p.u. | 0.8 p.u. | 0.2 p.u. | 0.8 p.u. | 0.8 p.u. |
| X_{t1} | - | - | - | 0.4 p.u. | 0.0 p.u. |
| X_{trans} | 0.2 p.u. | 0.8 p.u. | 0.2 p.u. | 0.734 p.u. | 0.8 p.u. |
| v_∞ | 0.92 p.u. | 0.92 p.u. | 0.92 p.u. | 0.92 p.u. | 0.92 p.u. |
| e_t | 0.9339 p.u. | 1.1207 p.u. | 1.0522 p.u. | 1.1207 p.u. | 1.1207 p.u. |
| v_{mid} | 0.923 p.u. | 0.974 p.u. | 0.98 p.u. | 1.062 p.u. | 0.974 p.u. |
| I_t | 0.8 p.u. | 0.8 p.u. | 1.23 p.u. | 0.832 p.u. | 0.8 p.u. |
| δ_o | 29.85 | 32.62 | 39.02 | 35.92 | 63.45 |
| E_{fdo} | 2.3087 | 2.0095 | 2.54 | 1.7388 | 1.48 |
| K_1 | 1.98643 | 0.79475 | 2.8002 | 0.86871 | 0.75836 |
| K_2 | 1.26576 | 0.69000 | 1.5283 | 0.76557 | 0.80632 |
| K_{2d} | 1.78999 | 0.52331 | 1.9744 | 0.57089 | 0.45025 |
| K_3 | 0.31367 | 0.49710 | 0.3136 | 0.51252 | 0.56416 |
| K_4 | 1.42894 | 0.77901 | 1.2660 | 0.86433 | 0.91303 |
| K_{4d} | 0.44558 | 0.22809 | 0.7165 | 0.25468 | 0.22294 |
| K_5 | -0.1836 | -0.17041 | -0.09784 | -0.17969 | -0.18869 |
| K_6 | 0.31610 | 0.66464 | 0.46978 | 0.66424 | 0.68793 |
| K_{6d} | 0.31973 | 0.25396 | 0.25165 | 0.35829 | 0.41978 |
| K_{svc1} | - | - | - | 0.05923 | 0.05384 |
| K_{svc2} | - | - | - | 0.09348 | 0.22165 |
| K_{svc2d} | - | - | - | 0.03525 | 0.05932 |
| K_{svc3} | - | - | - | 0.07376 | 0.06375 |
| K_{5n} | - | - | - | -0.21916 | - |
| K_{6n} | - | - | - | 0.30630 | - |
| K_{6dn} | - | - | - | 0.28986 | - |
| K_{svc3n} | - | - | - | 0.07376 | - |

Table 4-2 System operating conditions (Section 4.3)

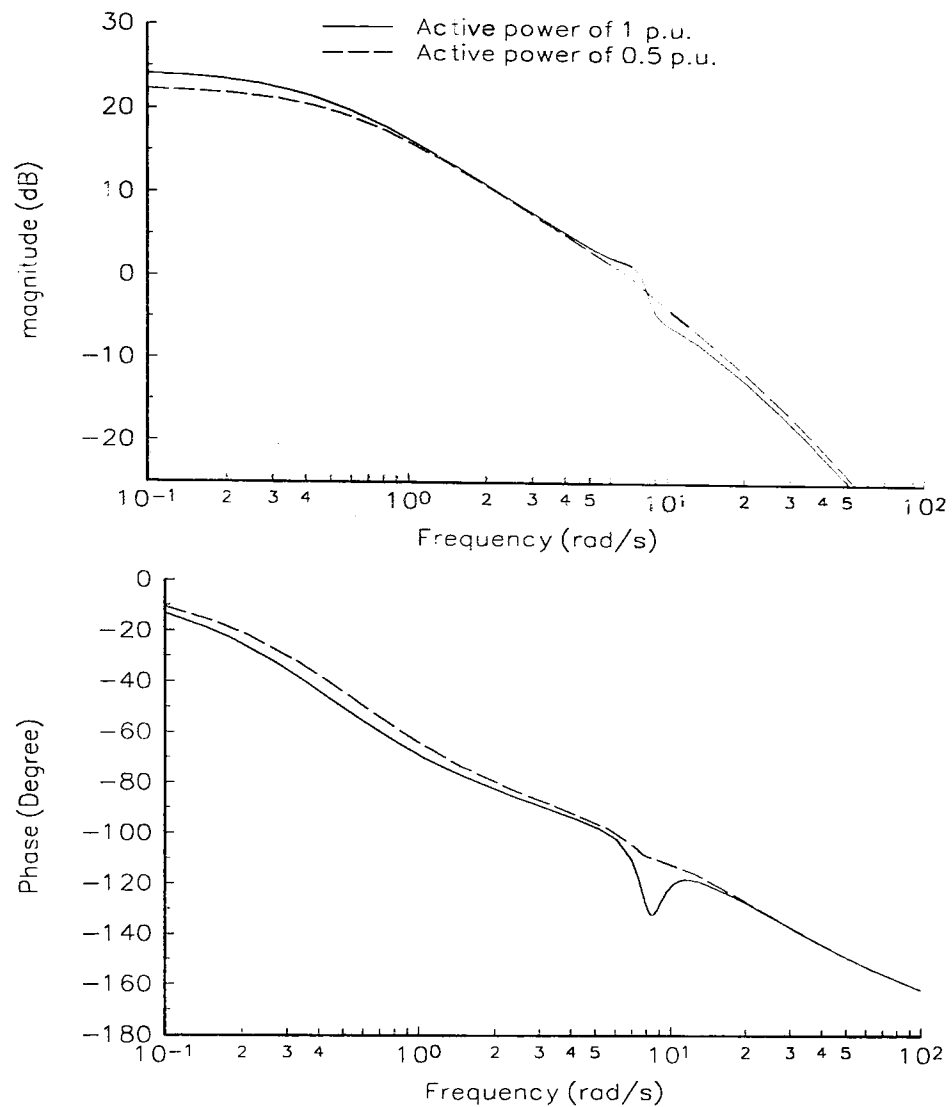


Figure 4-10 Open loop frequency response between $\Delta e_t/\Delta e_{err}$ for two electrical output powers

Fig. 4-9 also shows that the system phase surpasses the threshold of -180 degrees at approximately 5.3 rad/sec. Hence, the system becomes susceptible to instabilities with closed-loop control. Also, the frequency response indicates that increasing the tie-line reactance from 0.2 to 0.8 p.u. reduces the natural oscillation frequency from 7.5 to 5.3 rad/sec. Since the synchronising power is proportional to the natural oscillation frequency, increasing the tie-line reactance value results in decreasing system synchronising power.

4.3.2 Generator performance with SVC voltage control loop

Let us now introduce the SVC with only voltage control loop capabilities, to compensate the undamped system. The SVC is applied at two locations of the weak tie-line system, i.e. reactance value of 0.8 p.u. (i) at the mid-point of the tie-line reactance and (ii) at the generator's terminal bus.

Case I SVC placed at mid-point of the tie-line system

We first consider the SVC located at mid-point of the tie-line system ($X_{t1}=X_{t2}=0.4$ p.u.), which maximises active power transfer. The SVC firing angle is adjusted to 150 degrees which results in the SVC injecting 0.425 p.u. reactive power, increasing the voltage at mid-point of the tie-line system from 0.974 to 1.062 p.u., i.e. 9% voltage increase. An active power of 0.736 p.u. flows

from the generator to the infinite bus. It should be noted that this power flow is the same for both cases, the system with SVC and with no SVC. The equivalent reactance (X_{trans}) of the network, as seen from the generator terminals, reduces from 0.8 to 0.734 per units. The reactive power injected to the infinite bus increases to 0.212 p.u., from a previous value of zero (see Table 4-2).

Fig. 4-11 shows the frequency response when the SVC is placed at the mid-point of the tie-line system with a voltage controller gain of 2.5, the system phase increases from -182 to -160 degrees. It should be noted that the SVC voltage control loop provides phase lead to compensate the undamped response at the natural oscillation frequency. The SVC also increases the system synchronising power, as observed by the slight shift of the switch-back characteristic towards the higher region of the frequency scale, hence, enhancing system stability.

The generator performance is further investigated by increasing the SVC voltage controller gain in the range 2.5 to 40. The frequency response characteristics in Fig. 4-12 show that increasing the SVC voltage control loop gain, up to a value of 20, brings about an improved damped system response, owing to the SVC giving a higher phase lead to reduce the system switch-back characteristic. The trade off is a reduction of system steady-state gain from 35 to 31 dB.

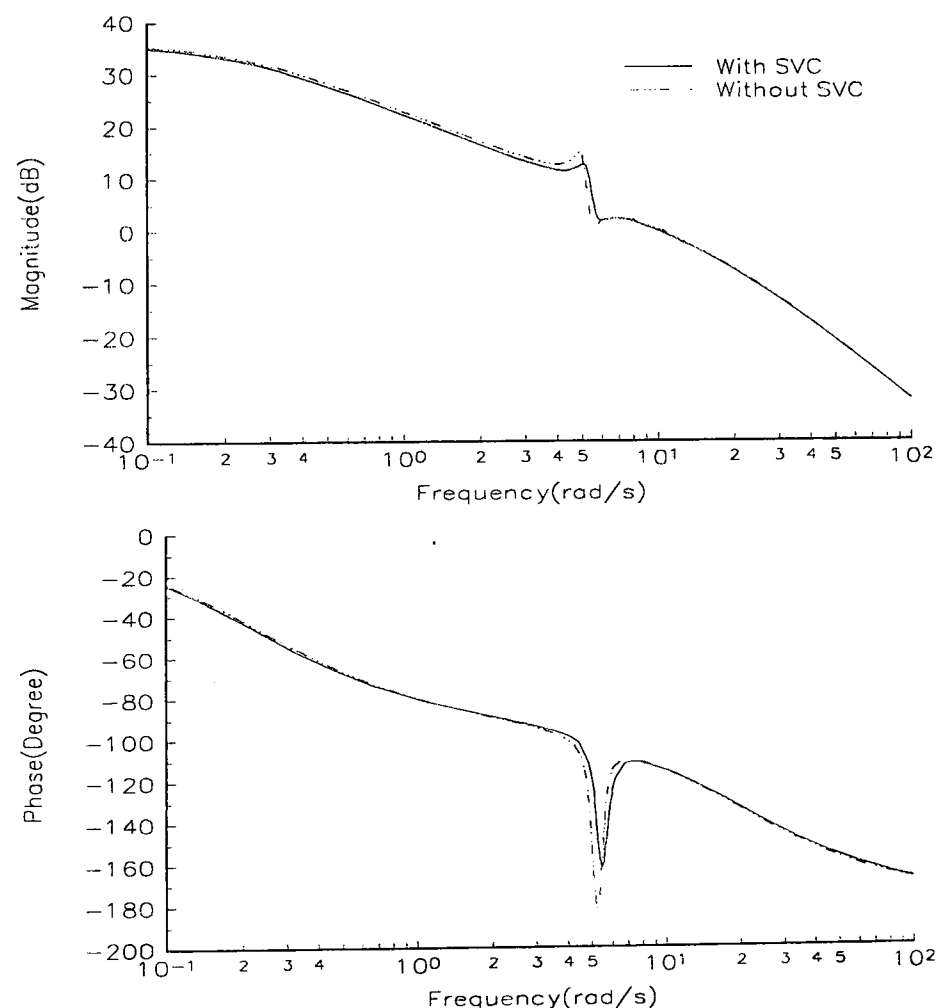


Figure 4-11 Open-loop frequency response between $\Delta e_t/\Delta e_{err}$ for cases with SVC and with no SVC

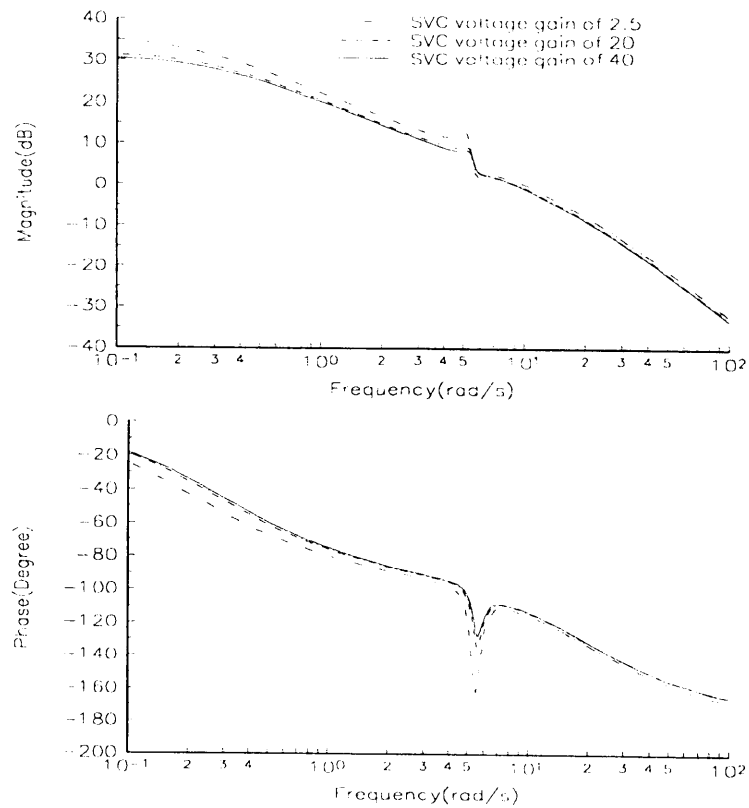


Figure 4-12 Open-loop frequency response between $\Delta e_t/\Delta e_{err}$ for different SVC voltage control loop gains

Referring to Fig. 4-12, it was found that the use of the SVC voltage gain of 2.5 does not affect adversely the system steady-state gain. It was also found that increasing the SVC voltage gain above 40 does not yield any significant improvement in the reduction of the switch-back characteristic.

Case II SVC placed at the generator's terminal bus

This section considers the case when the SVC is located at the generator's terminal bus ($X_{t1}=0$). The SVC firing angle is kept at 150 degrees. The SVC aids the generator by exporting 0.473 p.u. reactive power to the tie-line (see column 6 of Table 4-2). The active power delivered to the infinite bus is kept at the same level as in the previous study. The generator dynamic performance with the SVC located at the generator's terminal is investigated below.

It can be seen from Fig. 4-13 that when the SVC, with a voltage controller gain of 2.5, is applied at the generator's terminal bus, it provides phase lead to improve the generator dynamic performance across the full frequency range, except at the natural oscillation frequency. In particular, the SVC provides extra damping at the high oscillation frequencies as observed by the marked increase in system phase, which tends towards -90 degrees instead of -180 degrees. However, with the voltage gain of 2.5, the SVC voltage control loop does not yield any significant smoothing of the system switch-back characteristic.

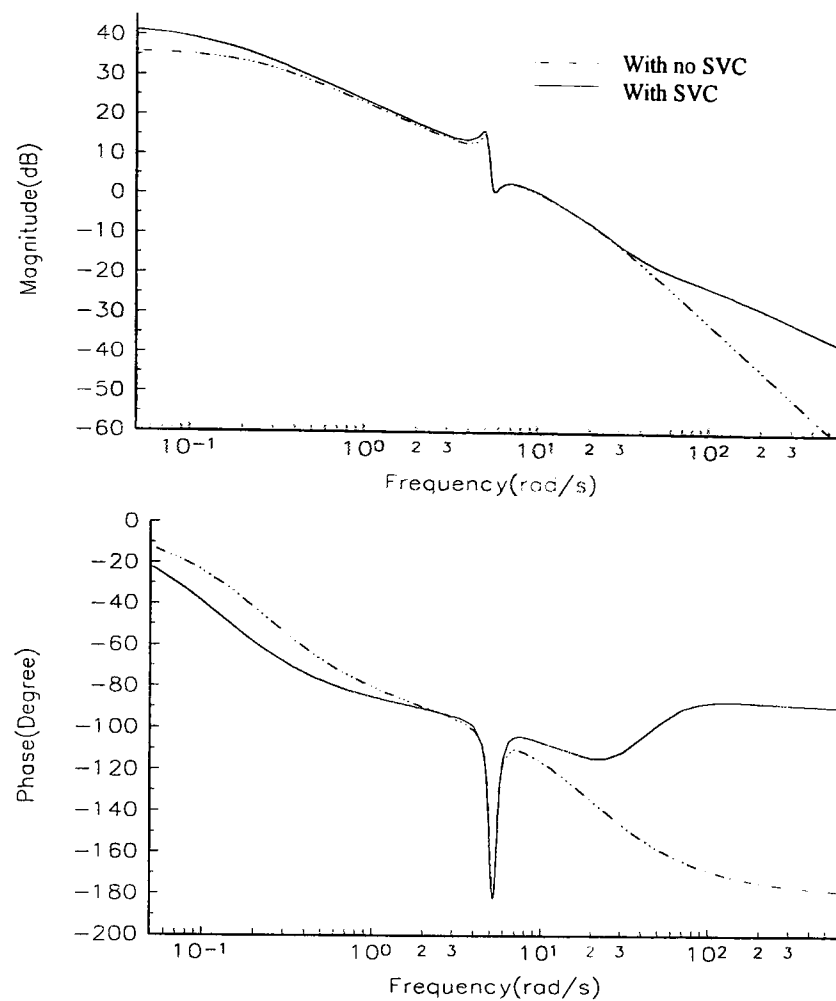


Figure 4-13 Open-loop frequency response between $\Delta e_t/\Delta e_{err}$ for cases with SVC and with no SVC

The generator dynamic performance as a function of SVC voltage controller gain is shown in Fig. 4-14. Increasing the SVC voltage gain from 2.5 to 100 is a very effective way of providing a higher phase lead over the entire frequency range considered. This also results in a reduction of the switch-back characteristic, hence, system damping is very much improved. However, the switch-back characteristic cannot be completely overcome, even when voltage gains as high as 150 are used.

By comparing the frequency responses between Figs. 4-12 and 4-14, it can be seen that when the SVC is placed at mid-point, increases in the voltage control loop gain provides a phase lead at only the frequency where the switch-back frequency occurs. On the other hand, when the SVC is placed at the generator's terminal bus, the phase lead is given over the full frequency range.

However, as seen from these results, increasing the SVC voltage controller gain is not the most effective method of overcoming the switch-back characteristic. Moreover, high SVC voltage gains deteriorate system performance at the low frequency range when the SVC is located at mid-point of the tie-line system.

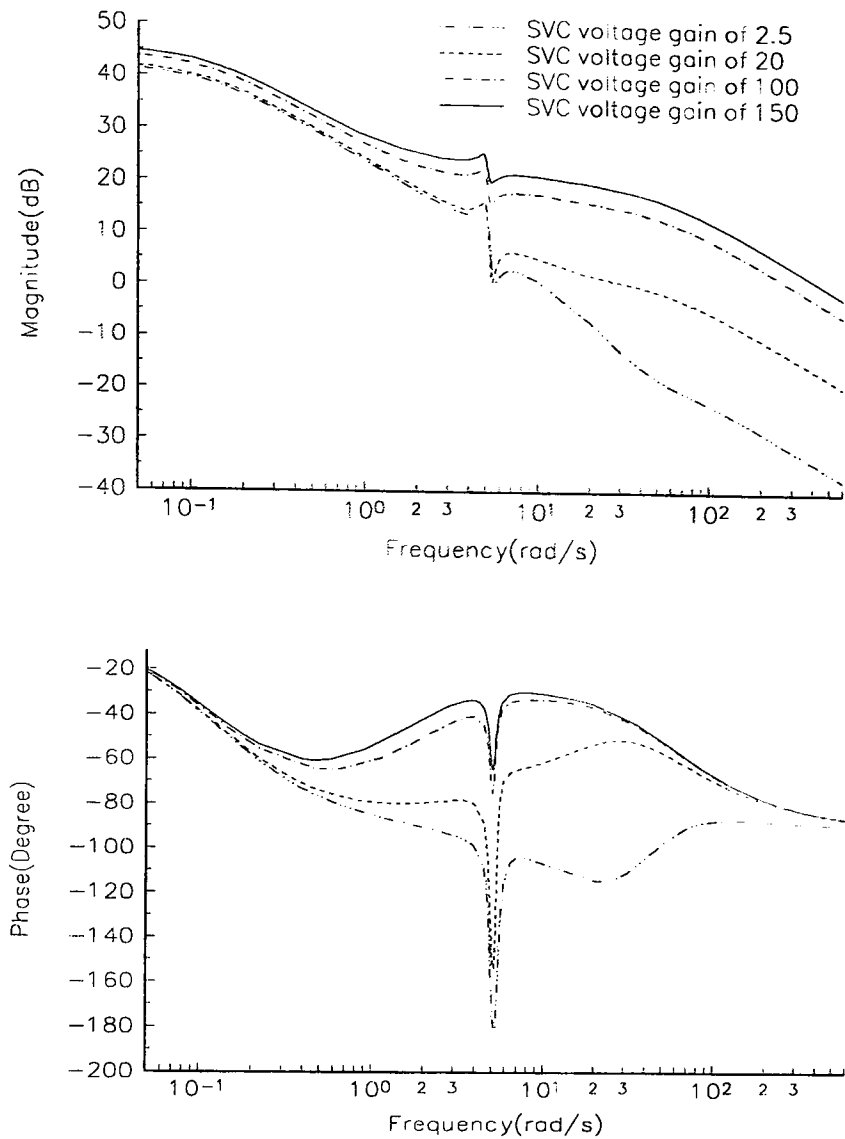


Figure 4-14 Open-loop frequency response between $\Delta e_v/\Delta e_{err}$ for different SVC voltage control loop gains

4.3.3 Generator performance with SVC voltage and damping control loops

From the discussion above, it is clear that the SVC voltage control loop does not yield an effective means of eliminating the switch-back characteristic. We now turn our attention to the SVC damping control loop, which supplies an additional stabilising signal (ΔV_{add}) at the summing point of the SVC voltage controller as shown in Fig. 3-2 of Chapter 3. The SVC damping controller is a PI controller. The generator speed deviation, $\Delta\omega$, is the input signal, which is passed through the wash-out element before being fed to the PI controller. Two locations of the SVC are considered, i.e, at mid-point of the tie-line system, and at the generator's terminal bus.

Case I SVC placed at mid-point of the tie-line system

In this location, the PI damping controller gain and wash-out time constant are suitably tuned to gains of $K_p=27$ and $K_i=335$, and $\tau_w=10$, respectively. The SVC voltage controller gain is kept at 2.5, with a firing angle of 150 degrees.

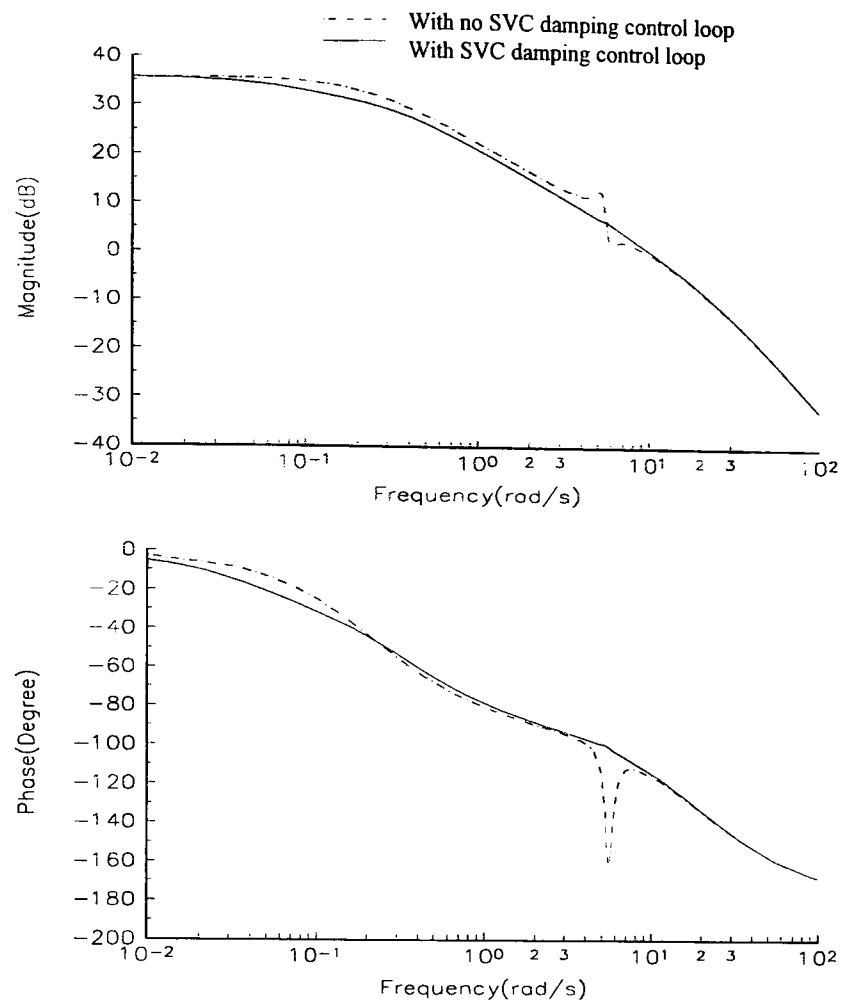


Figure 4-15 Open-loop frequency response between $\Delta e_i/\Delta e_{err}$ with and with no SVC damping control loop

Fig. 4-15 shows the open-loop frequency response of the system with no damping controller and with damping controller being applied to the SVC voltage control loop. It can be seen that the PI damping controller is capable of eliminating the switch-back characteristic very effectively. A well-damped system is obtained, resulting in an easily controllable system across the entire frequency range, including the frequency range where the switch-back characteristic lies. Moreover, it can be seen from Fig. 4-15 that applying the SVC damping control loop does not affect adversely the system performance at low frequencies.

Case II SVC placed at the generator's terminal bus

Let us now apply the PI damping controller to the SVC when it is installed at the generator's terminal bus. Two cases are presented below, which correspond to two different SVC voltage and damping controller parameter sets.

Case 1: $K_r=2.5$, $K_p=13$, $K_i=155$, $\tau_\omega=10$.

Case 2: $K_r=20$, $K_p=1.7$, $K_i=19.5$, $\tau_\omega=10$.

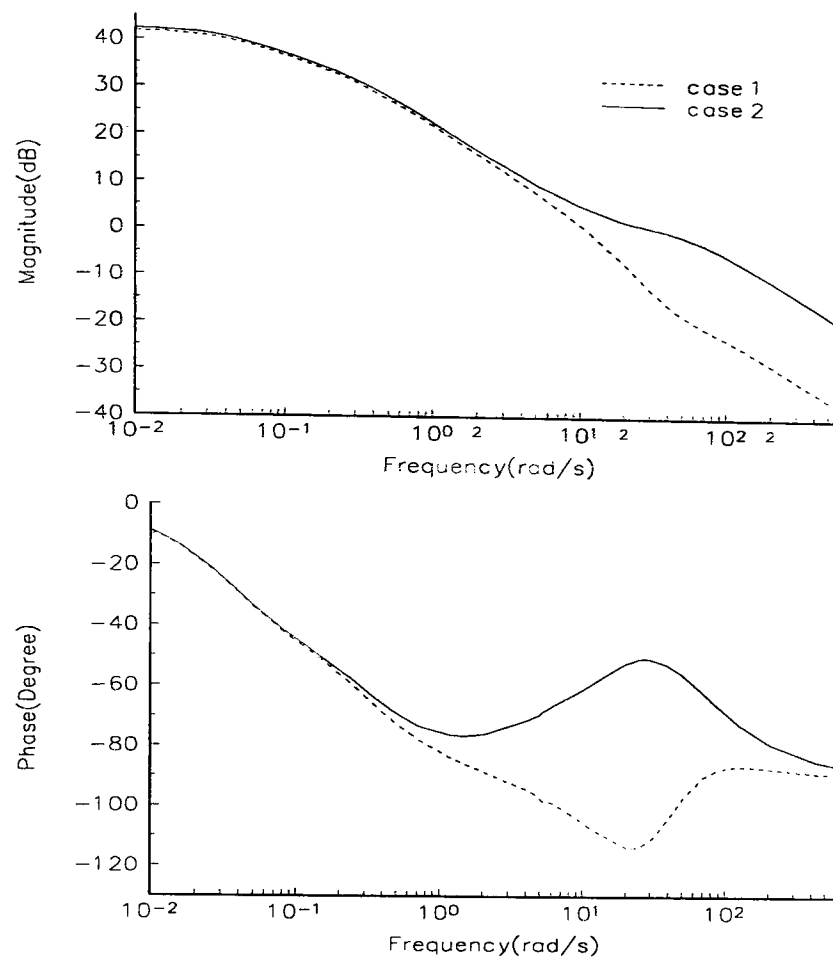


Figure 4-16 Open-loop frequency response between $\Delta e_t/\Delta e_{err}$ with SVC damping control loop

Fig. 4-16 shows the absence of switch-back characteristic. The system in case 2, with a SVC voltage controller gain of 20, exhibits a better dynamic performance than the system in case 1, with a SVC voltage controller gain of 2.5. Applying the SVC voltage control and the SVC damping control loop is an effective way to improve the system dynamic performance, particularly when connected at the generator terminals. It should be stressed that SVC control parameters must be tuned correctly to ensure the complete elimination of the switch-back characteristic. In this case, the parameters were obtained by performing an extensive range of simulations, i.e. 10 simulations.

4.4 Conclusions

The overall transfer-function block-diagram model, Models 1-3, has shown to be an effective aid for acquiring fundamental knowledge of the dynamic interactions taking place between a synchronous generator and a SVC plant. It is evident from the investigations conducted that the dynamic performance of the system model is highly dependent upon the number of damper windings used in the study since they influence the dynamic interactions between the flux linkages in the d and q -axes and the SVC. Detailed studies of the dynamic responses of Models 1-3 have shown that system damping over a wide frequency range is significantly improved by taking account of the generator damper windings in both axes, i.e. d and q -axes, as given by Model 1. This indicates that in reality modern synchronous generators will exhibit a better dynamic

behaviour than what they are sometimes credited with, since they indeed have physical damper windings that, from the modelling viewpoint, would correspond to having damper windings in the d and q -axes. The full synchronous generator representation becomes all the most important as new power electronics-based damper controllers become more widespread. It is in this respect that the new small-signal block-diagram model brings about substantial new improvements over traditional block-diagram models [1-3,7], and even over contemporary block-diagram models [9-12]. Based on the new light shed by the comprehensive results presented in this chapter, it is recommended that Model 1, which exhibits the greatest level of reliability of response be adopted as the block-diagram tool for carrying out small-signal stability studies of synchronous generator-SVC infinite-bus system. Nowadays, with the inexpensive, massive computational resources available to engineers it seems that, at least for the purpose of small-signal stability studies, past anxieties concerning computation times are subsiding and the onus is on model fidelity.

4.5 References

- [1] M. Saidu and F. M. Hughes, "Block Diagram Transfer Function Model of a Generator Including Damper Windings", IEE Proceedings on Generation, Transmission and Distribution, Vol. 141, Part C, No. 6, November 1994, pp. 559-608.
- [2] M. Saidu and F. M. Hughes, "An Extended Block Diagram Transfer Function Model of a Synchronous Machine", International Journal of Electrical Power and Energy System, Vol. 18, No. 2, February 1996, pp. 139-142.
- [3] M. Saidu and F. M. Hughes, "Performance Improvement of a Conventional Power System Stabilizer", International Journal of Electrical Power and Energy System, Vol. 17, No. 5, October 1995, pp. 313-323.
- [4] IEEE Task Force on Definitions and Procedures, "Current Usage and Suggested Practices in Power System Stability Simulations for Synchronous Machines", IEEE Transaction on Energy Conversion, Vol. 1, No. 1, March 1986, pp. 77-93.
- [5] IEEE Standard 1110-1991, "IEEE Guide for Synchronous Generator Modelling Practices in Stability Analyses", 1991.
- [6] P. Kundur, "Power System Stability", McGraw-Hill Inc, 1993
- [7] W. G. Heffron and R. A. Phillips, "Effect of Modern Amplidyne Voltage Regulator on Underexcited Operation of Large Turbine Generator", AIEE Transactions, Vol. 71, August 1952, pp. 692-697.
- [8] P. L. Dandeno, P. Kundur, A. T. Poray and H. M. Zein Eldin, "Application and Validation of Turbo-generator Model Parameter through On-line Frequency Response Measurements", IEEE Transaction on Power Apparatus and Systems, Vol. 100, No. 4, April 1981, pp. 1656-1622.
- [9] H. F. Wang and F. J. Swift, "A Unified Model for the Analysis of FACTS Devices in Damping Power System Oscillation Part I: Single-machine Infinite-bus Power System", IEEE

- Transaction on Power Delivery, Vol. 12, No. 2, April 1997, pp. 941-946.
- [10] H. F. Wang and F. J. Swift, "Application of the Phillips-Heffron Model in the Analysis of the Damping Torque Contribution to Power systems by SVC Damping Control", International Journal of Electrical Power and Energy System, Vol. 18, No. 5, June 1996, pp. 307-313.
- [11] H. F. Wang and F. J. Swift, "Capability of the Static Var Compensator in Damping Power System Oscillations", IEE Proceedings on Generation, Transmission and Distribution, Vol. 143, Part C, No. 4, July 1996, pp. 353-358.
- [12] H. F. Wang, F. J. Swift and M. Li, "A Unified Model for the Analysis of FACTS Devices in Damping Power System Oscillation Part II: Multi-machine Power System", IEEE Transaction on Power Delivery, Vol. 13, No. 4, October 1998, pp. 1355-1360.

Chapter 5

Small-Signal Stability of the Synchronous Generator-SVC in Multi-Machine Environment

5.1 Introduction

In Chapters 3 and 4, a comprehensive transfer-function block-diagram model was used to study the dynamic behaviour of a SVC-upgraded transmission system. The long-time honoured infinite-bus concept served rather well, as a first approach, the research work carried out in this investigation. That block-diagram model proved very useful for studying the dynamic interactions taking place between the synchronous generator and the SVC plant. The great improvement brought about by the SVC plant on the generator's dynamic performance has been clearly demonstrated. It is realised, however, that modern power systems are hardly radial and that a more realistic transfer-function block-diagram model, suitable for multi-machine and multi-SVC plant, would need to be developed, with the potential to study the behaviour of large, practical power systems.

Small-signal stability studies of multi-machine power systems are normally carried out using eigen-analysis and eigenvectors based techniques. Indeed, for many years this has been the preferred route taken by power system researchers world-wide and numerically efficient, comprehensive algorithms have been developed to carry out these kind of studies. The drawback is the lack of physical insight afforded by this approach which relies, exclusively, on mathematical abstraction. A few researchers, encouraged by the success of the single-machine block-diagram system in providing physical insight, have conducted work on multi-machine block-diagram techniques but the outcome has been block-diagram models of limited value [1]. The reason is that only a very contrived representation of the synchronous generator has been used heretofore, i.e. no damper winding representation has been used [2-4]. This comes as a no surprise given the very arduous algebra associated with the derivation of the full model, as evidenced by the long derivations in Appendix B. The work of Wang is remarkable though [2, 5] in the sense that he has incorporated many of the most promising FACTS devices within his block-diagram framework. Nevertheless, the lack of damper winding representation in the synchronous generator model severely impairs the usefulness of his block-diagram model to conduct fundamental studies of dynamic interactions between synchronous generators and power system dampers, which may be electronically controlled, e.g. SVC, TCSC, UPFC.

In this chapter the small-signal stability model of the multi-machine, multi-SVC plant is developed from first principles. The transfer-function block-diagram model is designed to accommodate n synchronous generators and m SVC plants. Similarly to the 1 synchronous generator and 1 SVC plant model developed in Chapter 2, several orders of generator models are available enabling a variety of small-signal stability models of varying complexity and, consequently, of varying reliability of response. The various system models, with different number of damper windings, are critically assessed. The new simulation environment is used to conduct fundamental studies of dynamic interactions between synchronous generators and between synchronous generators and SVC plants. The test system used in these investigations is still a relatively simple transmission system consisting of only two synchronous generators, and two SVC plants. The study of more complex power systems was not deemed necessary in this investigation because the thrust is on understanding the dynamic interactions that exist between devices. It was felt then a network with a small number of dynamic elements was better place to aid to this fundamental objective than a network with a larger number of components. The multi-machine, multi-SVC plant model introduced here, however, is general enough to allow the solution of large power networks. Bode analysis and time response are used to carry out all the analyses presented in this chapter. It should be noted that the time responses are obtained with no time delay and with a step size of 0.001.

5.2 System under study

The system under study in the multi-machine environment is shown in Fig. 5-1. It consists of n synchronous machines and m SVCs linked together through the electrical network.

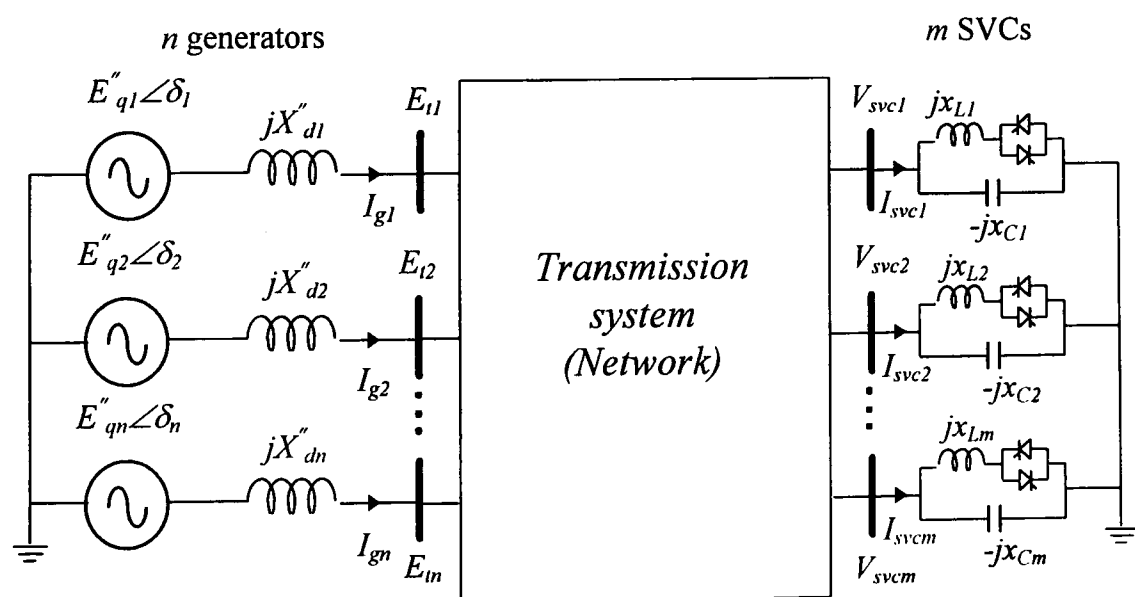


Figure 5-1 Representation of the system under study

5.3 Representation of system model

To study the dynamic interactions taking place between the many generators and SVCs, a linearised transfer-function which caters for n generators and m SVCs is developed. Full

derivations of the i^{th} machine and i^{th} SVC transfer functions are given in Appendix B. Three models with a varying degree of complexity, similar to those presented in Chapter 3 for the single-machine infinite-bus case, also exist for the multi-machine case.

Model 1: This model accounts for the effect of the generator main field winding plus one damper winding in the d -axis and one in the q -axis.

Active Power Equation

$$\begin{aligned} \Delta P_{ei} = & \left(K_{1ii} \Delta \delta_i + K_{2ii} \Delta E''_{qi} + K_{2dii} \Delta E''_{di} \right) + \sum_{j \neq i}^n \left(K_{1ij} \Delta \delta_j + K_{2ij} \Delta E''_{qj} + K_{2dij} \Delta E''_{dj} \right) + \\ & \left(K_{svclii} \Delta \alpha_i \right) + \sum_{j \neq i}^m \left(K_{svclij} \Delta \alpha_j \right) \end{aligned} \quad (5-1)$$

Generator Terminal Voltage Equation

$$\begin{aligned} \Delta e_{ti} = & \left(K_{5ii} \Delta \delta_i + K_{6ii} \Delta E''_{qi} + K_{6dii} \Delta E''_{di} \right) + \sum_{j \neq i}^n \left(K_{5ij} \Delta \delta_j + K_{6ij} \Delta E''_{qj} + K_{6dij} \Delta E''_{dj} \right) + \\ & \left(K_{svc3ii} \Delta \alpha_i \right) + \sum_{j \neq i}^m \left(K_{svc3ij} \Delta \alpha_j \right) \end{aligned} \quad (5-2)$$

d -axis Flux Linkage Equation

$$\begin{aligned} \Delta E''_{qi} = & \left(g_{3ii}(s) \Delta E_{fdi} - g_{4ii}(s) \Delta \delta_i - g_{7ii}(s) \Delta E''_{di} \right) - \\ & \sum_{j \neq i}^n \left(g_{4ij}(s) \Delta \delta_j + g_{3ij}(s) \Delta E''_{qj} + g_{7ij}(s) \Delta E''_{dj} \right) - \left(g_{svc2ii}(s) \Delta \alpha_i \right) - \sum_{j \neq i}^m \left(g_{svc2ij}(s) \Delta \alpha_j \right) \end{aligned} \quad (5-3)$$

q -axis Flux Linkage Equation

$$\begin{aligned} \Delta E''_{di} = & \left(g_{4dii}(s) \Delta \delta_i + g_{3dii}(s) \Delta E''_{qi} \right) + \sum_{j \neq i}^n \left(g_{4dij}(s) \Delta \delta_j + g_{3dij}(s) \Delta E''_{qj} + g_{7dij}(s) \Delta E''_{dj} \right) \\ & \left(g_{svc2dii}(s) \Delta \alpha_i \right) + \sum_{j \neq i}^m \left(g_{svc2dij}(s) \Delta \alpha_j \right) \end{aligned} \quad (5-4)$$

SVC Terminal Voltage Equation

$$\begin{aligned} \Delta V_{svci} = & \left(K_{5nii} \Delta \delta_i + K_{6nii} \Delta E''_{qi} + K_{6dnii} \Delta E''_{di} \right) + \sum_{j \neq i}^n \left(K_{5nij} \Delta \delta_j + K_{6nij} \Delta E''_{qj} + K_{6dnij} \Delta E''_{dj} \right) + \\ & \left(K_{svc3nii} \Delta \alpha_i \right) + \sum_{j \neq i}^m \left(K_{svc3nij} \Delta \alpha_j \right) \end{aligned} \quad (5-5)$$

The coefficients and transfer functions appearing in (5-1)-(5-5) are derived in Appendix B.

Model 2: In this model the damper winding in the d -axis rotor circuit is removed from Model 1. Hence, $\Delta E''_q$ and X''_d in (5-1)-(5-5) are replaced by $\Delta E'_q$ and X'_d , respectively.

Model 3: In this model both damper windings are neglected. Hence, only the effect of the field winding, $\Delta E'_q$, exists, i.e. $\Delta E''_q = \Delta E''_d = X''_d = X''_q = 0$.

Equations (5-1)-(5-4) represent the dynamic characteristic of the i^{th} generator and equation (5-5) represents the SVC dynamic voltage of the i^{th} SVC. These equations form the basis for drawing the

generic block-diagram model, which represents the i^{th} generator and the i^{th} SVC shown in Fig. 5-2. The i^{th} generator represents the characteristic of any one generator in the n multi-machine system. The dynamic behaviour of the i^{th} generator is represented by an incremental change in four main variables, namely output power (ΔP_{ei}), output voltage (Δe_{ti}), voltages proportional to the d and q -axis flux linkages ($\Delta E''_{qi}$) and ($\Delta E''_{di}$), respectively. As seen from Fig. 5-2, these variables will change in response to changes in $\Delta\delta$, $\Delta E''_q$ and $\Delta E''_d$ delivered from within the i^{th} generator itself, from the other $n-1$ generators and by changes in $\Delta\alpha$ delivered from the both i^{th} SVC and the other $m-1$ SVCs. The dotted lines enclose the coefficients and transfer functions corresponding to the internal change of the four main variables of the i^{th} generator. On the other hand, the external dynamic contributions consist of a summation of changes in $\Delta\delta_j$, $\Delta E''_{qj}$ and $\Delta E''_{dj}$ from the rest of the generators, i.e. $n-1$ generators, inputted to influence the i^{th} generator through the coupling coefficients with subscripts ij , where $j=1 \dots n$ and $j \neq i$. Conversely, the dynamic characteristic of the $n-1$ generators will be influenced by changes in $\Delta\delta_i$, $\Delta E''_{qi}$ and $\Delta E''_{di}$ from the i^{th} generator inputted through the coupling coefficients with subscripts ji , where $j=1 \dots n$ and $j \neq i$.

As shown in Fig. 5-2, the dot-dot-dashed lines enclose the i^{th} SVC system. It can be seen that the i^{th} SVC terminal voltage (Δv_{svci}) is made up of changes in $\Delta\delta$, $\Delta E''_q$ and $\Delta E''_d$ through the coefficients K_{5n} , K_{6n} and K_{6dn} . The changes contributed by the i^{th} and $n-1$ generators are combined and fed into the i^{th} SVC voltage controller. The terminal voltage of the i^{th} SVC is also determined by changes in its firing angle ($\Delta\alpha_i$) through the coefficient K_{svc3ni} and by a summation of changes in the $m-1$ SVC firing angle ($\Delta\alpha_j$) through the coupling coefficients $K_{svc3nij}$, where $j=1 \dots m$, and $j \neq i$. A change in $\Delta\alpha_j$ through the coupling coefficient $K_{svc3nij}$ reflects the contributions from the $m-1$ SVCs to the i^{th} SVC (block within dotted long-dashed lines in Fig. 5-2). Conversely, a change in $\Delta\alpha_i$ of the i^{th} SVC will induce a dynamic change in the $m-1$ SVCs through the coefficient $K_{svc3nji}$. The discussion indicates how the interaction between the m SVCs takes place. The combined impact of the i^{th} and $m-1$ SVCs (see block with long-dashed lines) is inputted at the summing points A, B, C and D. All contributions from the m SVCs will be delivered to change in variable Δe_t , $\Delta E''_q$, $\Delta E''_d$ and ΔP_e of the i^{th} machine and the $n-1$ generators through the existing connections between the generators and the SVCs at points A, B, C and D, respectively.

It can be seen from the i^{th} machine model that changes in Δe_{ti} and ΔP_{ei} are mainly determined by variations in the flux linkages $\Delta E''_q$ and $\Delta E''_d$ of all n generators. It should be noted that in this case, compared to the block-diagram model of a single-machine infinite-bus system, there is an additional dynamic loop formed by the flux linkages inside each machine, via the transfer functions $g_7(s)$ and $g_{3d}(s)$, since damper windings in both the d and q -axes are accounted for.

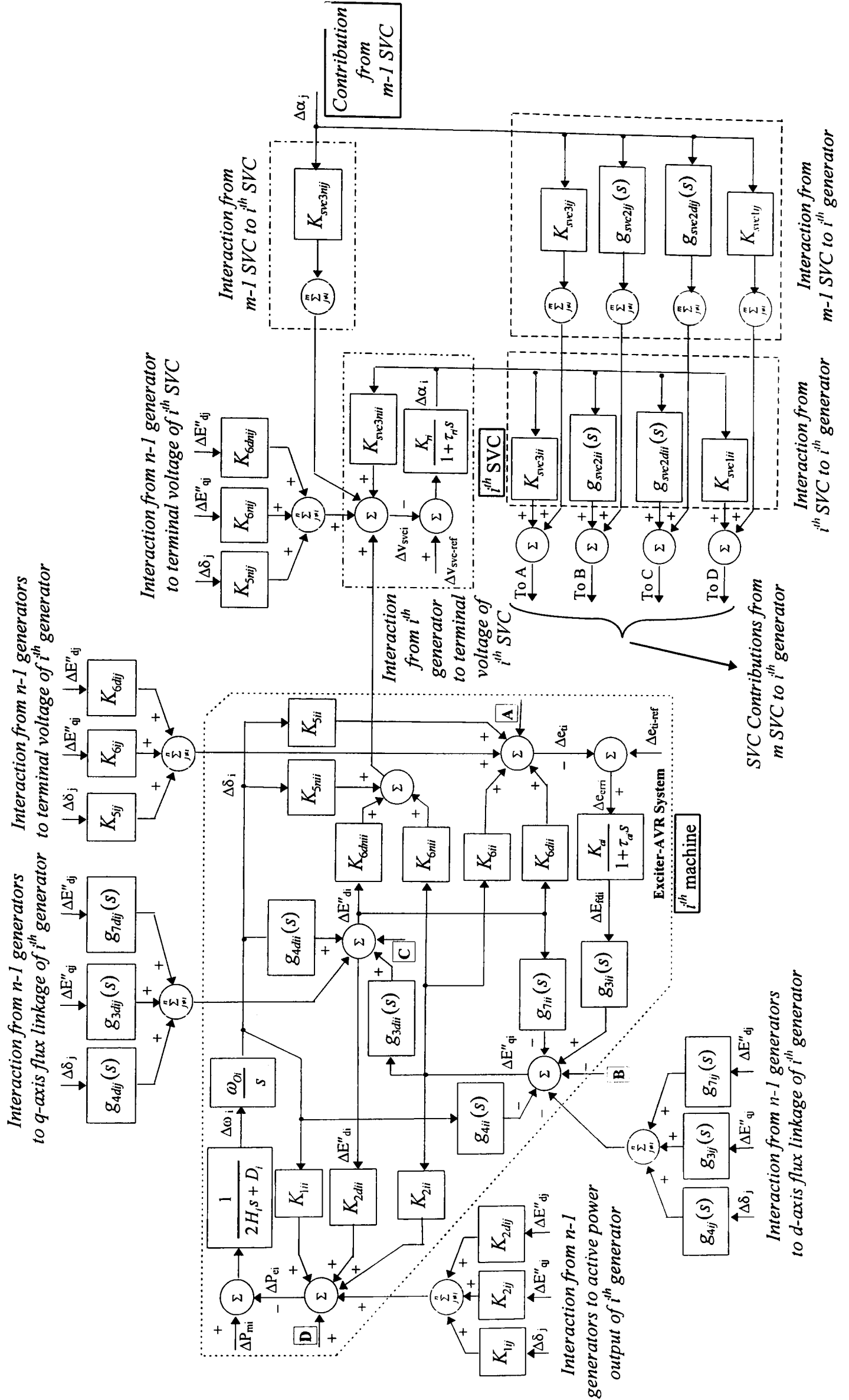


Figure 5-2 Block diagram of the i^{th} machine and the i^{th} SVC in a multi-machine system

The existence of $g_7(s)$ and $g_{3d}(s)$ is due to the more realistic conditions being considered in this analysis, such as the resistive part of transmission lines impedances and the explicit representation of PQ loads, represented as admittances. Also, subtransient saliency, i.e., $X''_d \neq X''_q$, plays an important part in the existence of these transfer functions. Referring to (5-3), it can also be seen that the various transfer functions making up $\Delta E''_{qi}$ have the same time constants, but different gains. A similar situation arises for $\Delta E''_{di}$ in (5-4).

In power system operation, the machine damper windings play a crucial role in providing system damping [6-9]. It can be seen from Fig. 5-2 that changes in $\Delta E''_{qi}$ and $\Delta E''_{di}$ will be influenced by the d and q -axis damper windings, respectively. Also, the flux linkage between the d and q -axes within the i^{th} machine will interact dynamically with those of other machines and with SVCs. Therefore, if the effects of the generator damper winding were to be neglected, it would lead to a system model with unrealistic system damping. In the section below, an assessment of the various system models, with decreasing order of machine damper modelling, is carried out.

5.4 Overall assessment of system models

In this section, Models 1-3 are assessed and recommendations are given for a suitable model to be used in small-signal stability studies of multi-machine power systems. The frequency response method is used to explore the dynamic characteristics.

5.4.1. Generator dynamic interactions

The adverse effects of neglecting machine damper windings on system model integrity is investigated. Firstly the two-machine system shown in Fig. 5-3 is used in this study. Machine 2 is represented by Models 1, 2 and 3 at the time whereas machine 1 is always represented by Model 1.

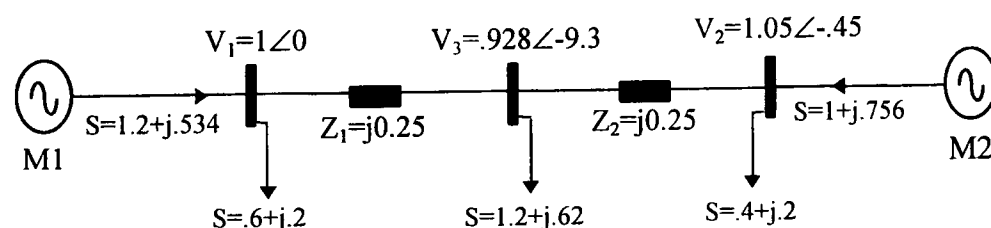


Figure 5-3 System under study (2-generator system)

The open-loop frequency responses between Δe_t and Δe_{err} of machines 1 and 2 are used in order to gain insight into the effect of neglecting damper winding representation. In this experiment, the open-loop frequency response of one of the machines is obtained while the other machine is kept in close-loop control with the fast-acting voltage regulator (AVR), whose gain is tuned at 100 and 120 for machines 1 and 2, respectively. The system operating conditions are shown in Fig. 5-3, and the machine parameters are given in Appendix D. It should be noted that machines 1 and 2 are identical.

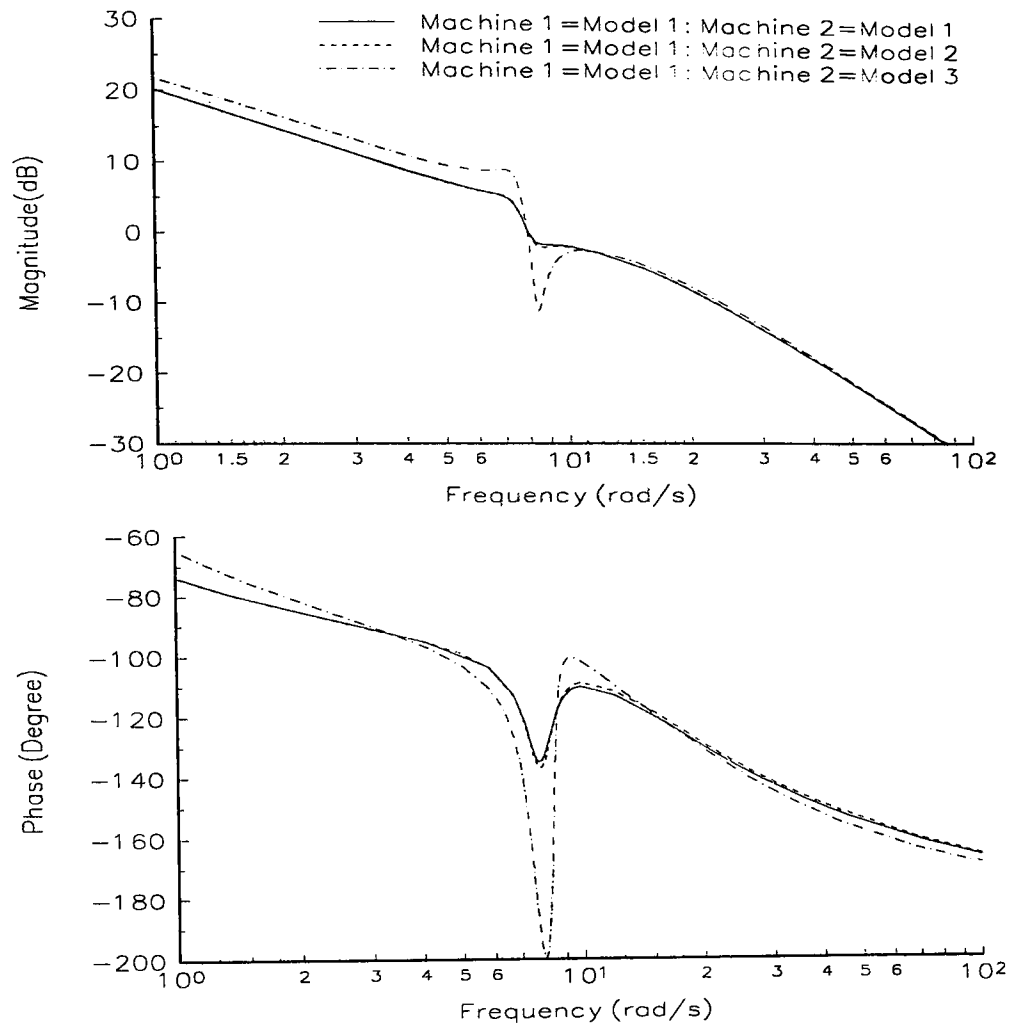


Figure 5-4 Open-loop frequency response between Δe_t and Δe_{err} of machine 1

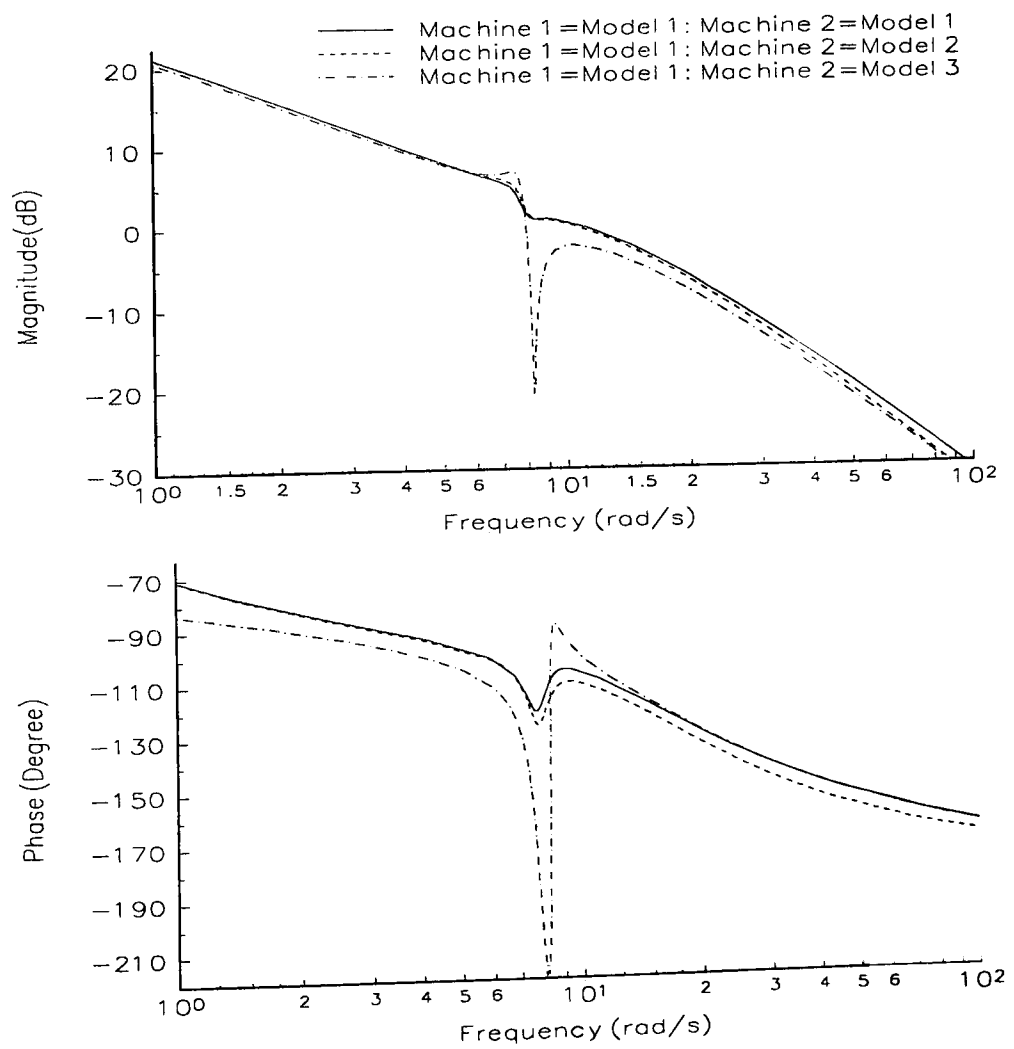


Figure 5-5 Open-loop frequency response between Δe_t and Δe_{err} of machine 2

Figs. 5-4 and 5-5 show the open-loop frequency responses of machines 1 and 2, respectively. It can be seen from Fig. 5-5 that when Model 2 is used to represent machine 2, its frequency response shows a reduction in phase lead with respect to the case when Model 1 is used to represent machine 2. The reduction starts at the natural oscillation frequency and results are shown up to 100 rad/sec. As expected, machine 2 represented by Model 1 exhibits better dynamic performances in these frequency ranges than those of machine 2 with Model 2.

The effect of using Model 2 for machine 2 is passed on to machine 1. It can be seen from Fig. 5-4 that this effect causes a slight change in machine 1's characteristic. When Model 3 is applied to represent machine 2, the frequency response in Fig. 5-5 shows that machine 2 is unstable, exhibiting a very pronounced switch-back characteristic due to the lack of realistic system damping. In this exercise, and for the sake of presenting results, a damping term $D=12.5$ was applied to the mechanical mode of machine 2. The effect of using Model 3 to represent machine 2 also introduces an undamped response, with a high switch-back characteristic, into the frequency response of machine 1, even though this machine is represented by Model 1. It can be concluded that neglecting the machine damping windings may have a very significant degrading effect on the generator dynamic response in multi-machine small-signal stability studies.

5.4.2 Generator-SVC dynamic interactions

In order to assess the overall dynamic characteristics of Models 1-3, including the SVC, the test system in Fig. 5-6 is used. The SVC with the voltage control loop is applied at node 3 to supply 0.357 p.u. reactive power with a voltage gain of 20 and as a present of this, the voltage magnitude increases from 0.928 to 0.98 per unit. The system operating conditions are shown in Figs. 5-6, respectively. Three different cases are analysed below: Model 1 is used to represent machines 1 and 2, then Model 2 is used to represent both machines and, finally Model 3 is used. It should be noted that for the first two cases the mechanical damping term D of both machines is set to zero whereas for the third case is $D=9.75$.

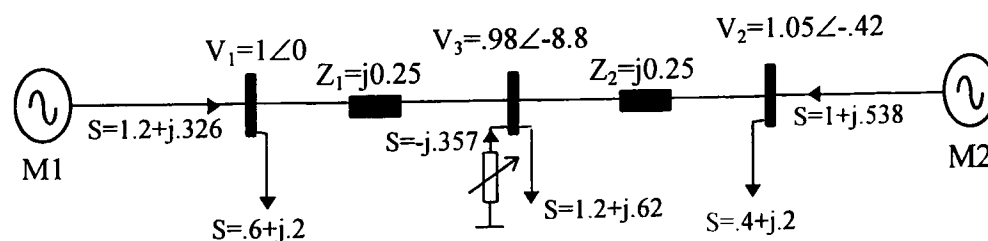


Figure 5-6 System under study (2-generators, 1-SVC system)

Fig. 5-7 shows plots of gain and phase versus frequency for machine 1. In this case, a high value of mechanical damping, $D=9.75$, is applied to Model 3 in order to provide a similar amount of phase than Model 1, at the switch-back frequency point. It should be noted that a severely undamped

response would take place if a zero mechanical damping were to be used in Model 3. When Model 2 is employed the system damping is significantly improved over the frequency range of concern, without having to resort to artificially high levels of mechanical damping. Nevertheless, when compared to Model 1, Model 2 has approximately a 10° lower phase lead at the natural oscillation frequency. This indicates that Model 2 has indeed a lower damping. The phase of Model 2 is also lower than that of Model 1, starting at the natural oscillation frequency. Therefore, Model 1 with generator damper windings in the d and q -axes provides a better frequency performance than Models 2 and 3, particularly during the high frequency range.

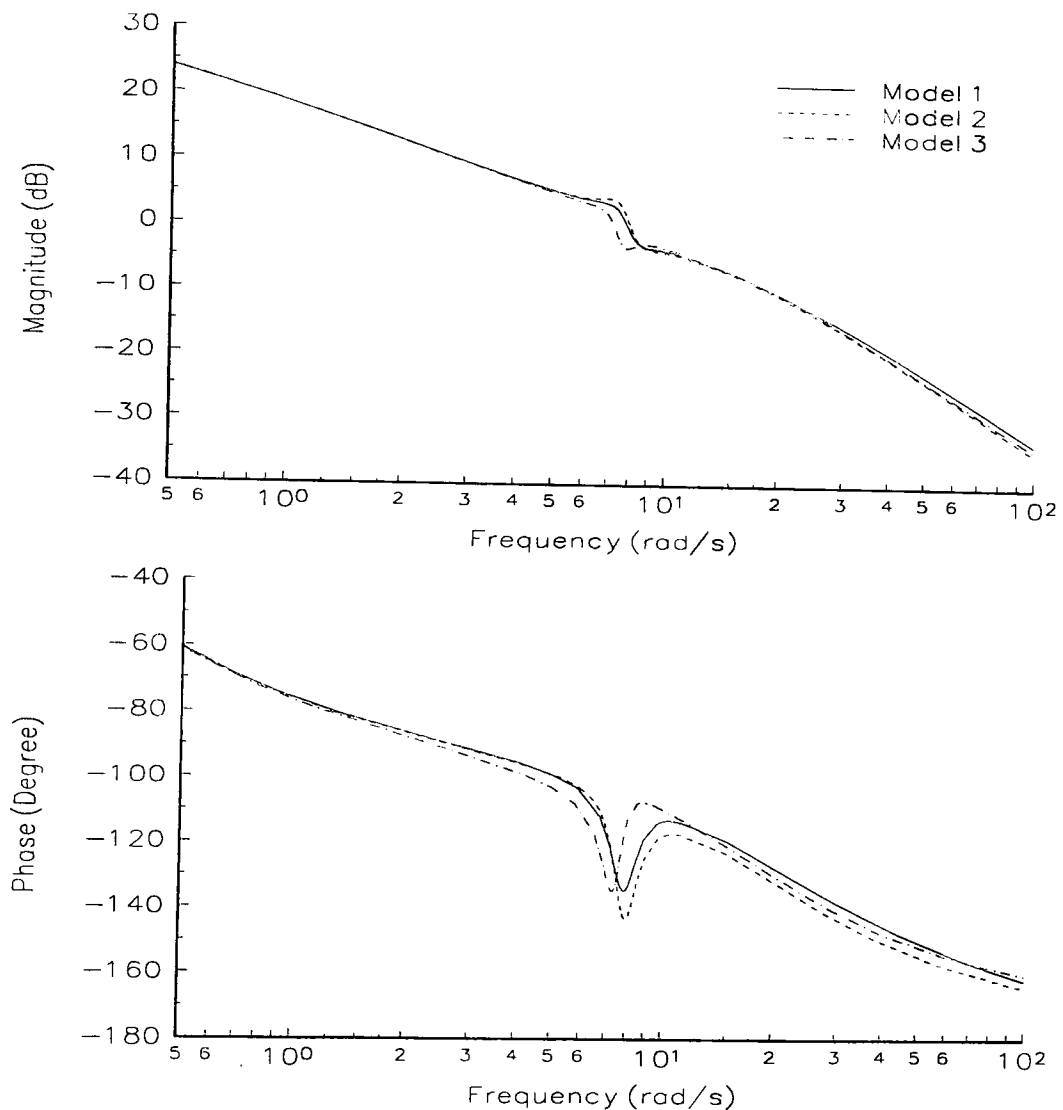
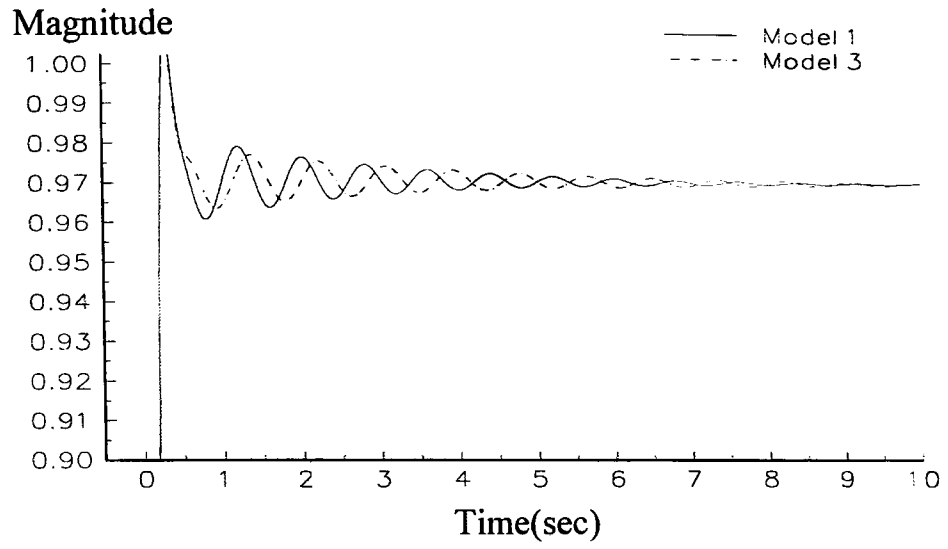
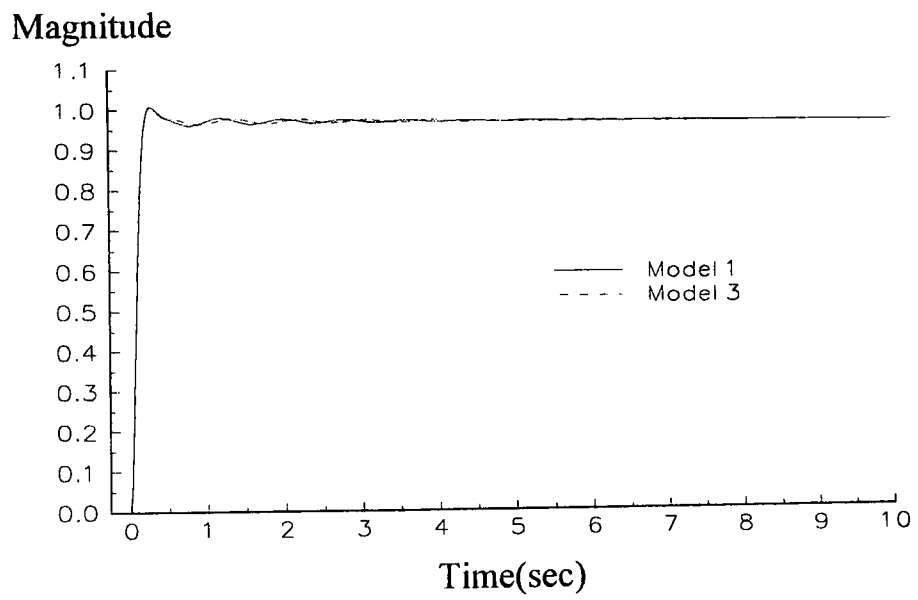


Figure 5-7 Open-loop frequency response between Δe_t and Δe_{err} of machine 1 with Model 1-3

Step responses of the machine output voltages (Δe_t) can also be used to assess the impact of damper winding representation in system model. They are obtained by giving a step change to the voltage reference (Δe_{t-ref}). In this study, lack of inherent damping in Model 3 is compensated by adding artificial mechanical damping, i.e. $D=9.75$. However, Fig. 5-8 reveals that the voltage time response obtained from Model 3 has a different frequency of oscillation than that of Model 1. On the other hand, Fig. 5-9 shows that the oscillation frequency in the voltage time response of Model 2 is very close to the response of Model 1. However, it has a higher oscillatory magnitude and it also reaches the steady state at a slightly later time.

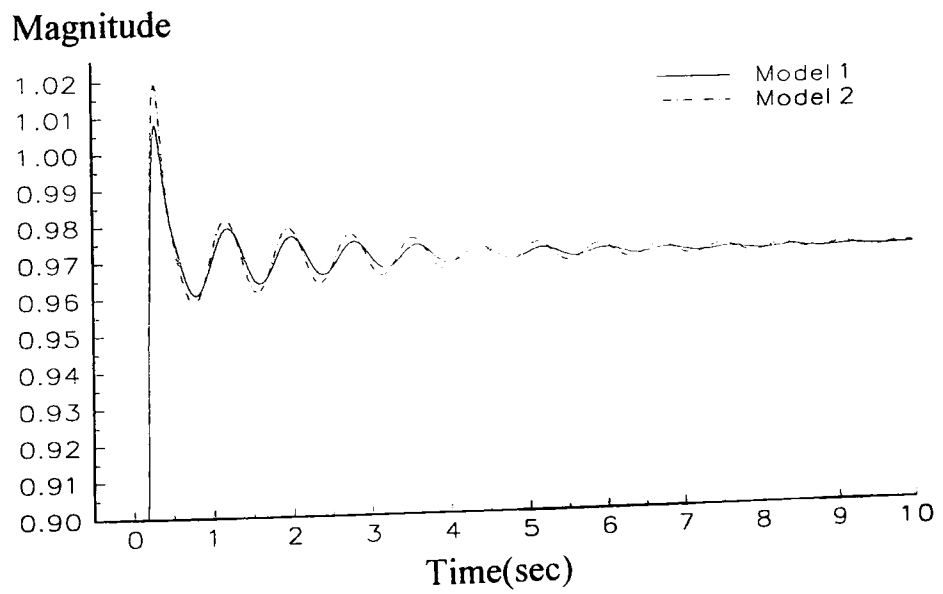


(a)

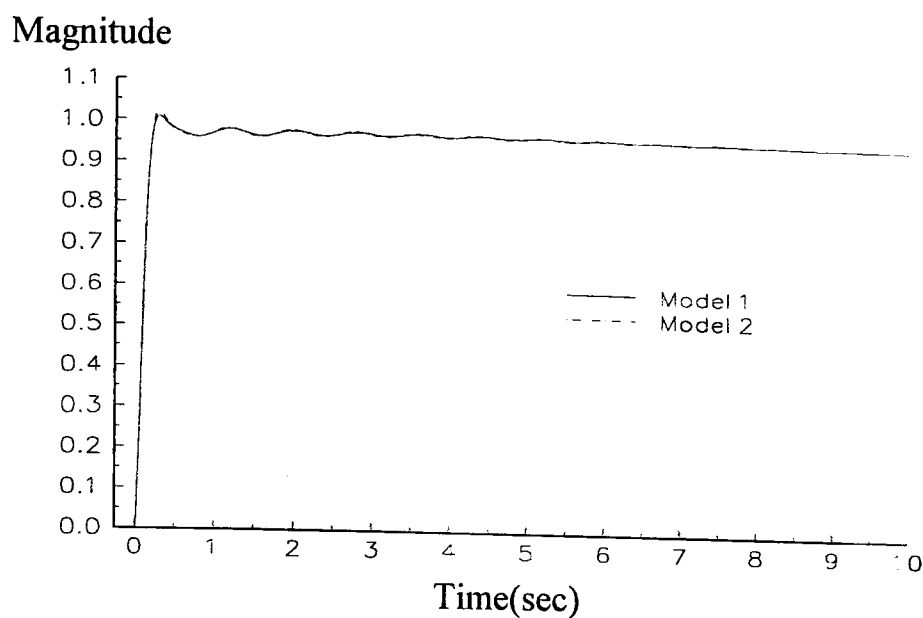


(b)

Figure 5-8 Step responses of machine 1's output voltage (Δe_t) with Models 1 and 3



(a)



(b)

Figure 5-9 Step responses of machine 1's output voltage (Δe_t) with Models 1 and 2

It is clear that neglecting both machine damper windings, i.e. Model 3, is not a suitable option for carrying out small-signal stability analysis. Adding the q -axis damper winding, i.e. Model 2, improves significantly the reliability of system model response. However, including damper windings in both the d and q -axes leads to an even better reliability of system model response.

5.5 Multi-machine case study

In this section, the generator dynamic performance in a multi-machine system is further investigated. The effect of changing system operating conditions due to changes in the interconnecting tie-line impedance between two machines is explored. First for the case with no SVC and then for the case with two SVCs are included, using various voltage control loop gains.

5.5.1 System dynamic performance with various operating conditions

This aspect of system dynamic performance with changes in interconnection tie-line impedance values is investigated by using the system shown in Fig. 5-10. The system consists of two machines linked by the series impedances Z_1 and Z_2 . The studies involve changing the values of Z_1 and Z_2 from $0+j0.25$ to $0.05+j0.25$ per unit, and then from $0+j0.25$ to $0+j0.1$ per unit. The system operating conditions are shown in Figs. 5-10 (a), (b), (c). Model 1 is used in the study. The two machines are identical and their parameters are given in Appendix D.

Figs. 5-11 and 5-12 show the open-loop frequency response characteristics between Δe_t and Δe_{err} of machines 1 and 2, respectively. The damping of both machines increase as the resistive parts of Z_1 and Z_2 increase from 0 to 0.05 p.u., as indicated by a reduction of the switch-back characteristic at the natural oscillation frequency. The frequency responses also show that machine 2 achieves greater damping than machine 1. The reason is that increases of output power in a generator degrades its damping, and in this study, machine 1 is responsible for supplying the active power losses, i.e. generator 1 is the slack node, the resistive parts of Z_1 and Z_2 .

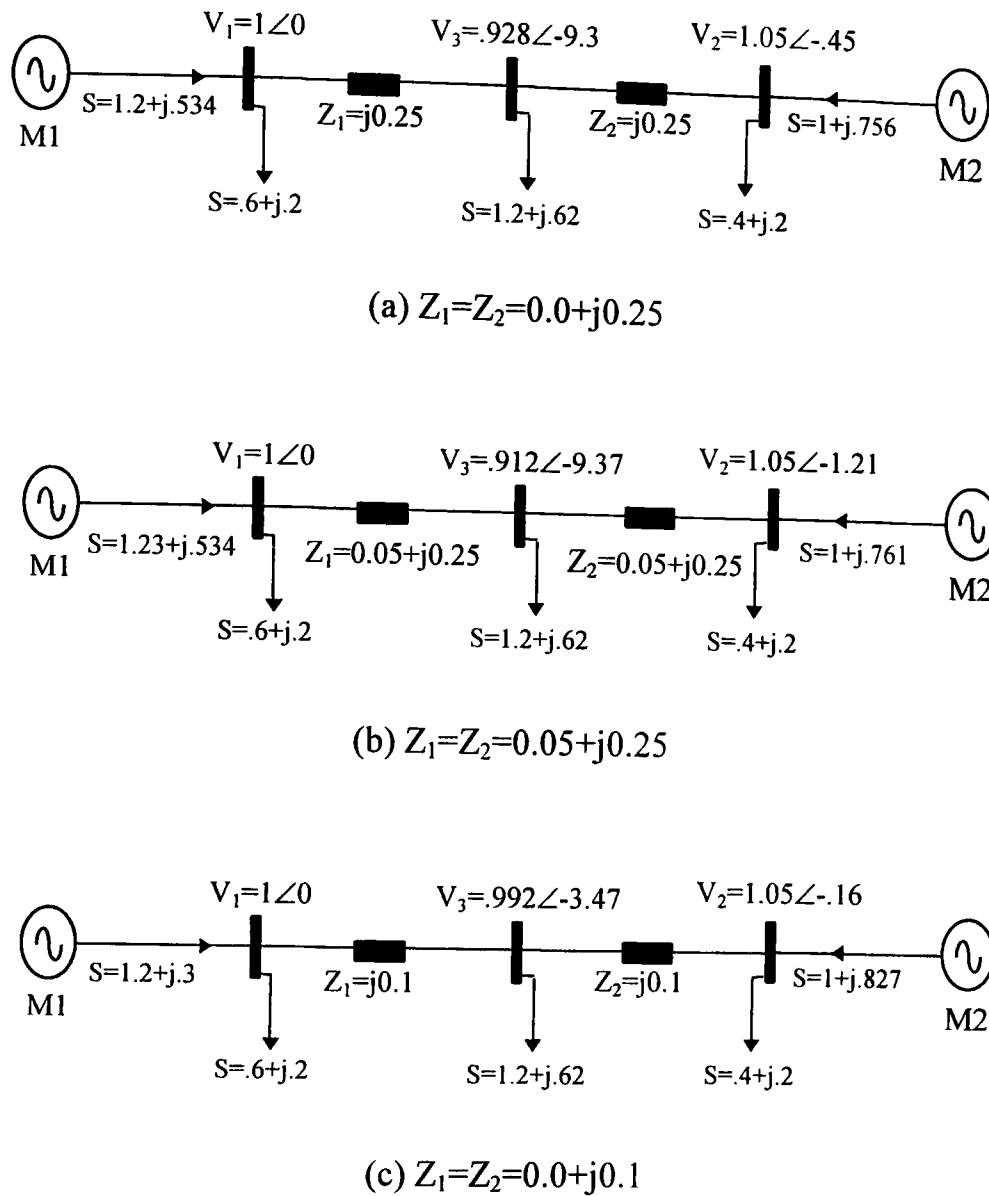


Figure 5-10 System with various operating conditions

Figs. 5-13 and 5-14 show the frequency response characteristics of machines 1 and 2, corresponding to the case when the reactive parts of Z_1 and Z_2 are increased from 0.1 to 0.25 per unit. The system operating conditions are given in Figs. 5-10(a), (b), (c). It can be seen that significant reductions in the damping of both machines is accompanied by an increase in the switch-back characteristic. As expected, the dynamic performance of both machines becomes severely impaired when the interconnecting tie weakens, i.e. the reactance value increases [8-10].

It is generally agreed that the network impedance plays a significant role in determining the system dynamic performance. Increasing the resistive part of the system impedance introduces extra damping but at the expense of increasing losses. Hence, reducing the inductive reactance of the network is the preferred method of improving power system damping [11-14]. This issue will be addressed in greater detail in Chapter 6.

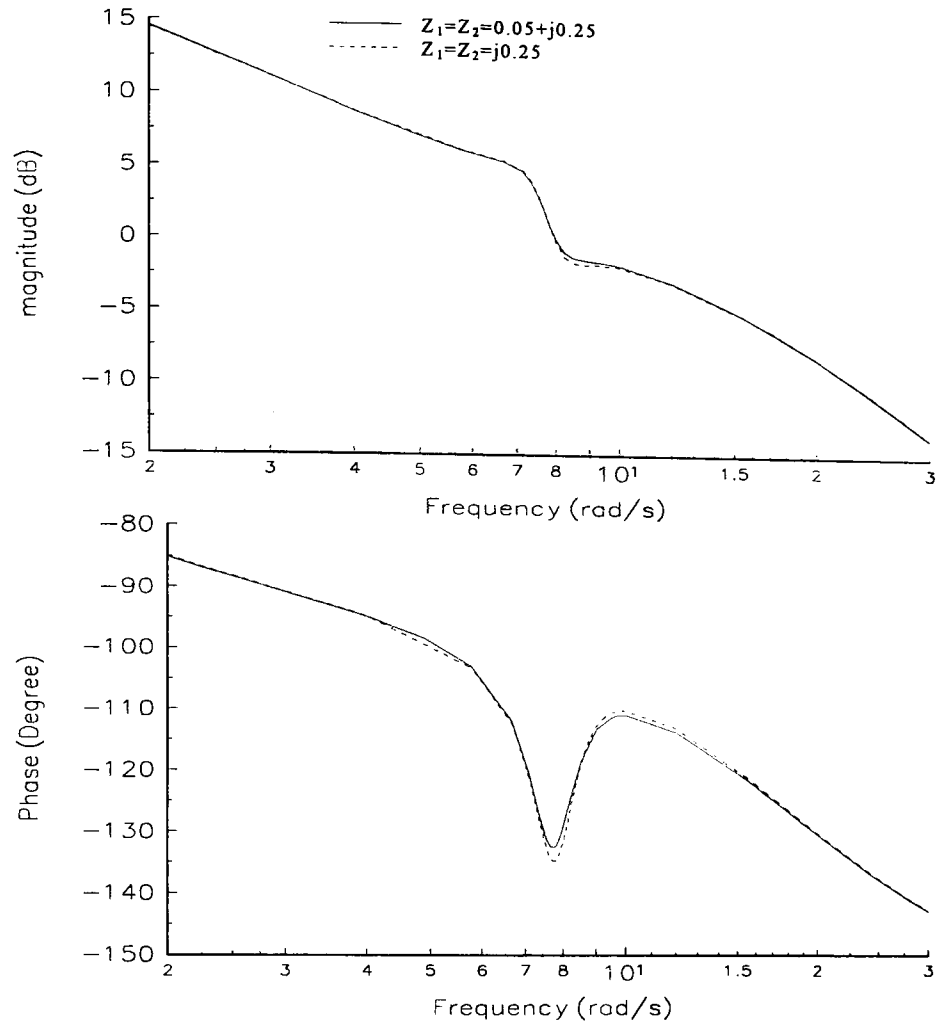


Figure 5-11 Open-loop frequency response between Δe_t and Δe_{err} of machine 1 with Z_1 and Z_2 changing from $0+j0.25$ to $0.05+j0.25$ p.u.

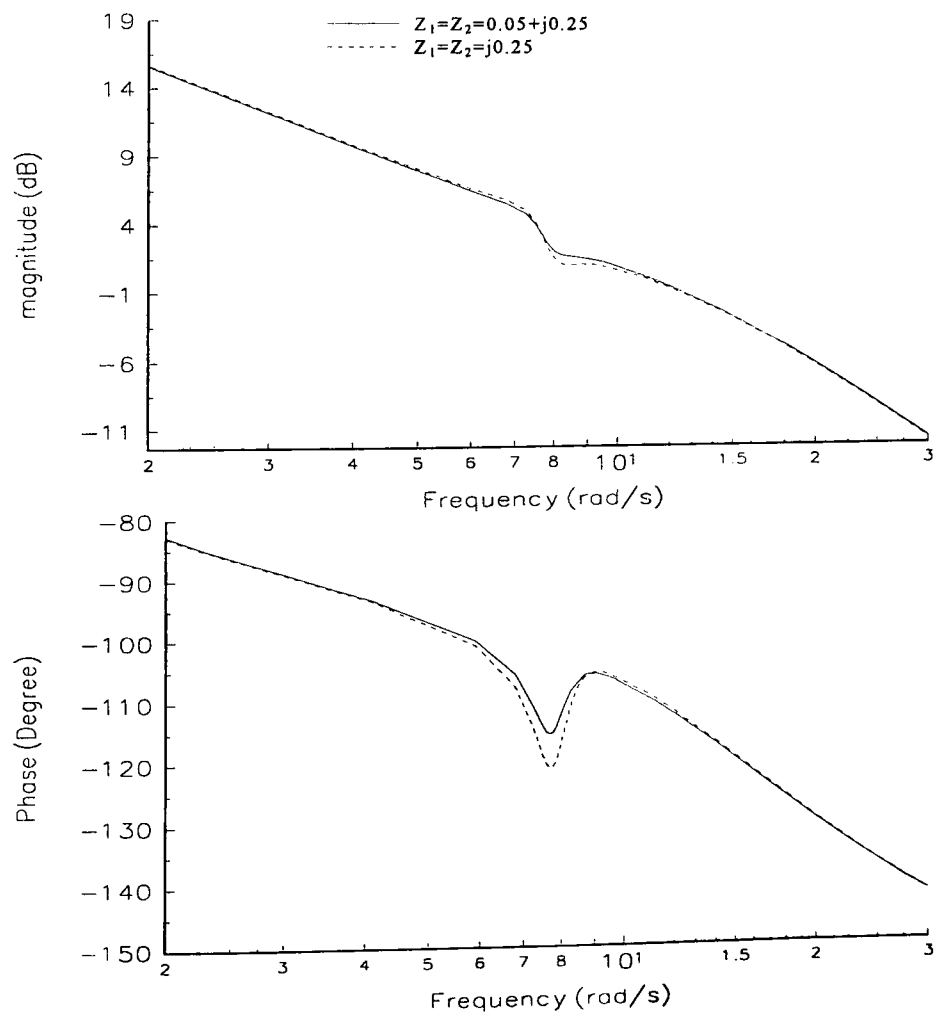


Figure 5-12 Open-loop frequency response between Δe_t and Δe_{err} of machine 2 with Z_1 and Z_2 changing from $0+j0.25$ to $0.05+j0.25$ p.u.

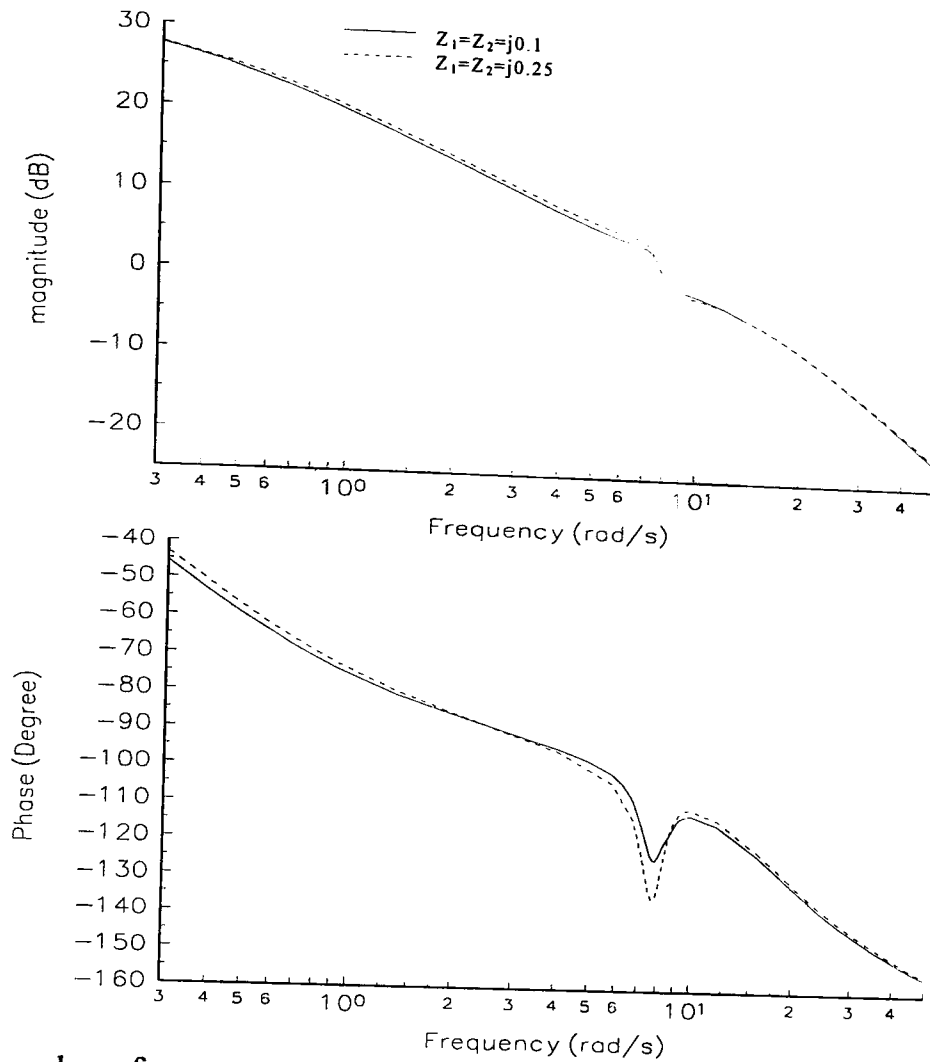


Figure 5-13 Open-loop frequency response between Δe_t and Δe_{err} of machine 1 with Z_1 and Z_2 changing from $0+j0.1$ to $0+j0.25$ p.u.

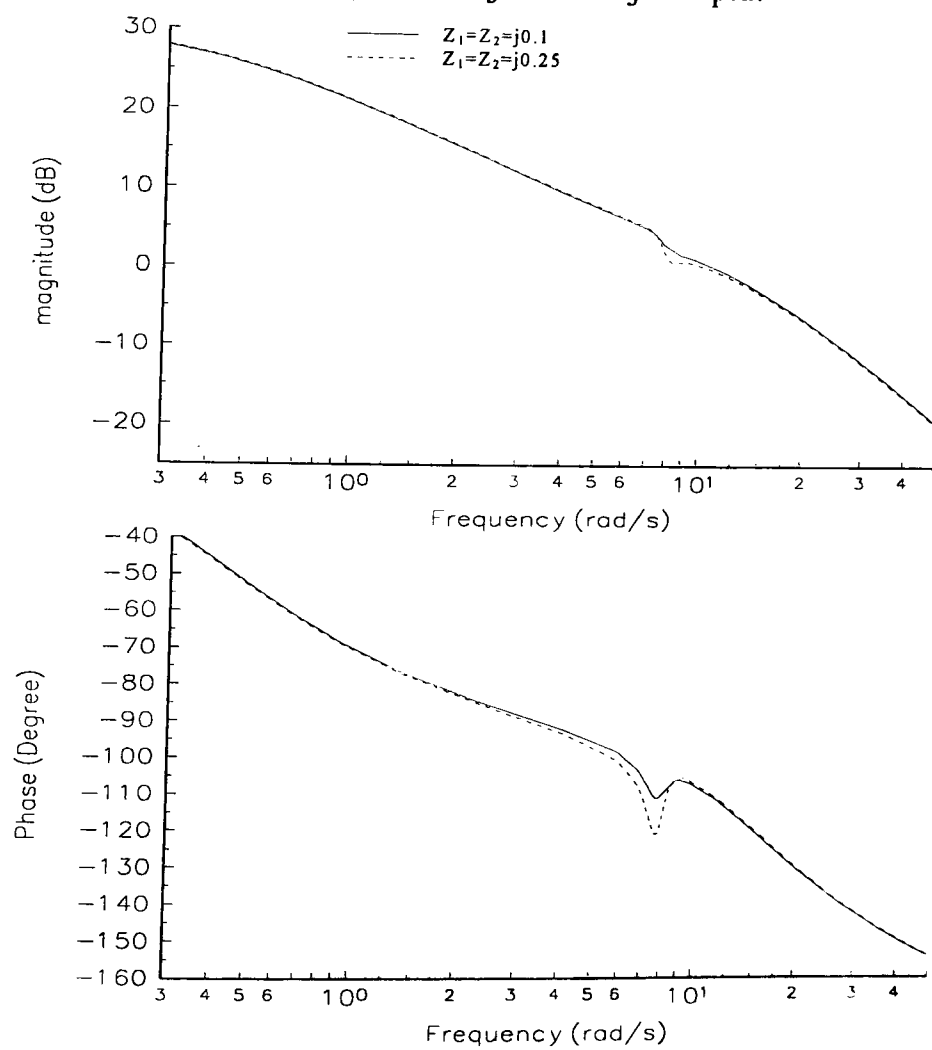


Figure 5-14 Open-loop frequency response between Δe_t and Δe_{err} of machine 2 with Z_1 and Z_2 changing from $0+j0.1$ to $0+j0.25$ p.u.

5.5.2 System dynamic performance with SVCs

Continuing from the previous section, further investigations are carried out for the two-machine system but now two SVCs are included. Before applying SVCs, the system is operated as shown in Fig. 5-15a.

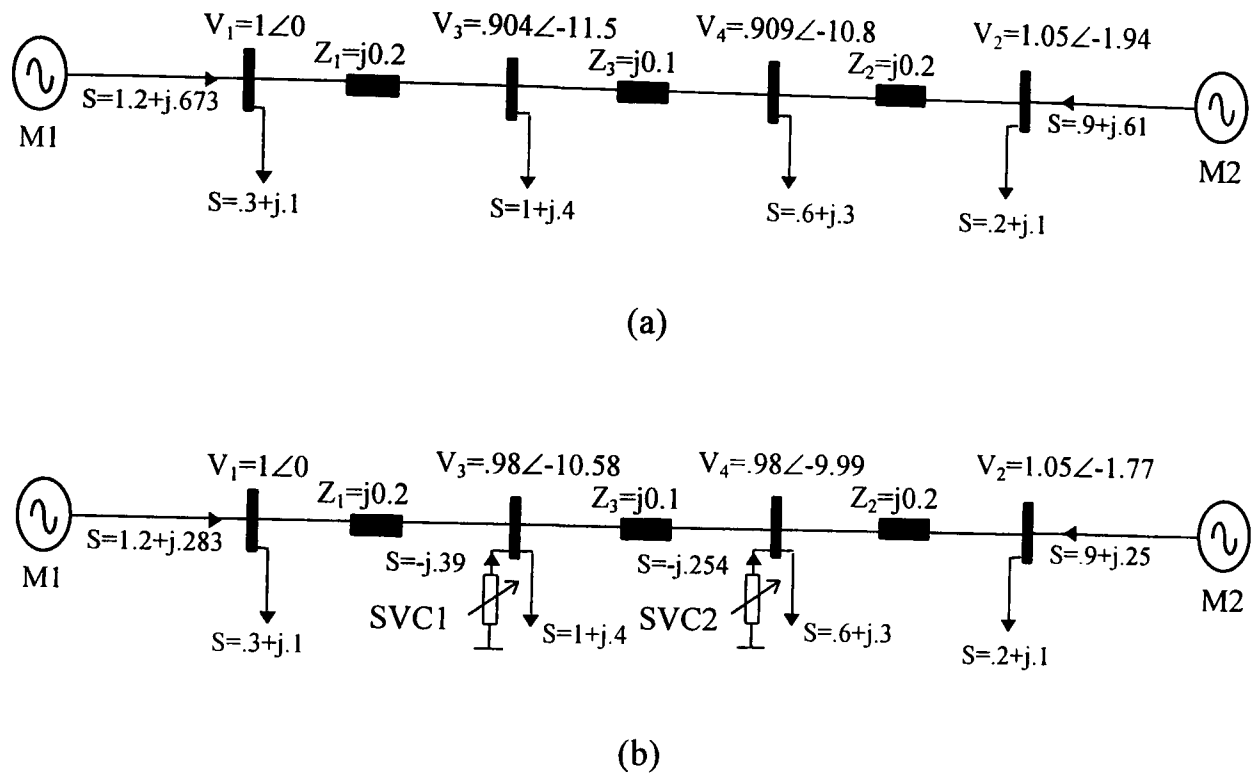


Figure 5-15 System under study (2-generator, 2-SVC systems)

The voltage magnitudes at nodes 3 and 4 with SVCs installed at both nodes, increase from 0.904 to 0.98 and from 0.909 to 0.98, respectively. The SVCs operate with only voltage control loops whose gains are both adjusted at 15. The AVR gains of machines 1 and 2 are tuned at 100 and 120 respectively. In the simulation, Model 1 is used to represent the machines.

The plots of gain and phase versus frequency for both machines are shown in Figs. 5-16 and 5-17. After applying SVCs in nodes 3 and 4, the switch-back characteristics clearly show that machine 1 has a lower damping response at the natural oscillation frequency than machine 2. This is an expected result since machine 1 supplies a heavier active load than machine 2, as seen by the power flows in Fig. 5-15b. The frequency responses also show that the SVCs only provide a slight damping improvement to machine 1 at the natural oscillation frequency. However, the SVCs enhance the high frequency performance of both machines, where higher phase leads can be observed at frequencies above 11 rad/sec.

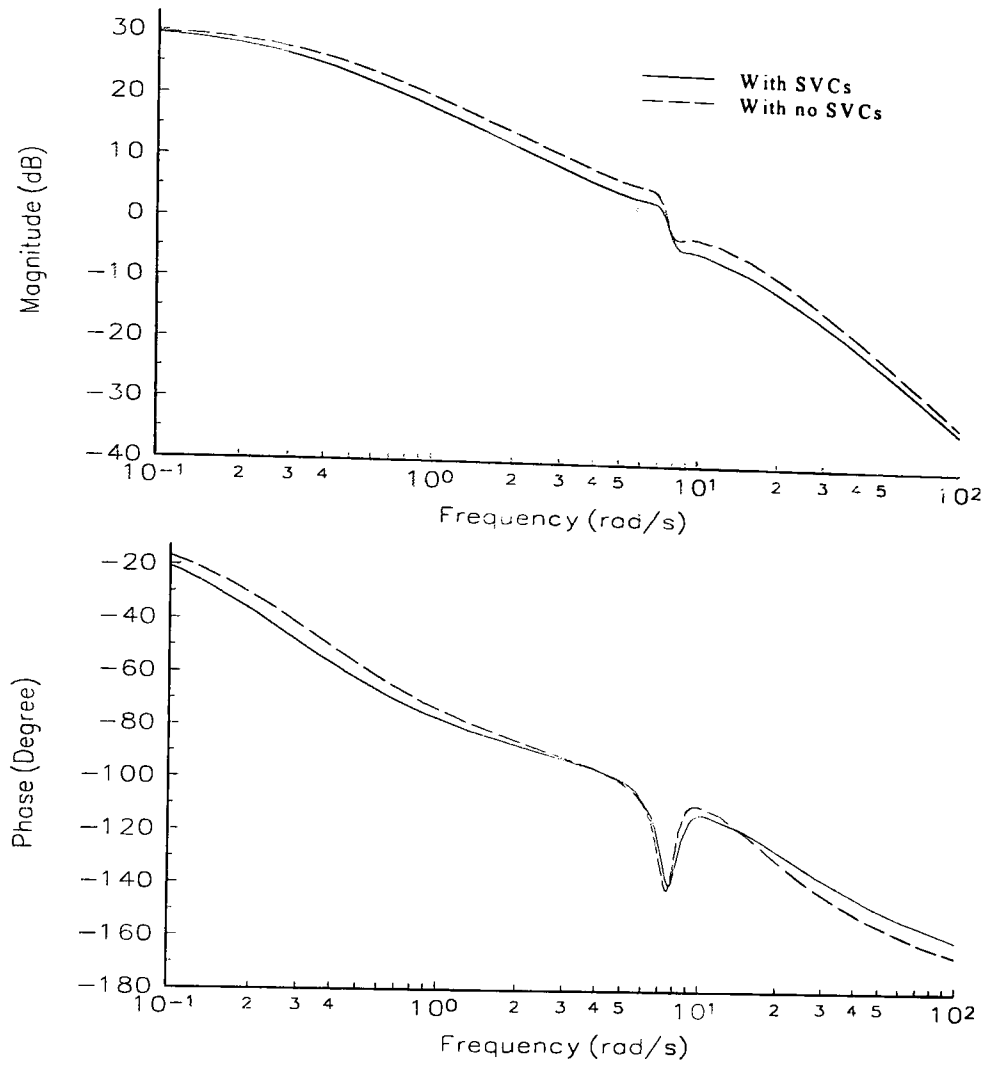


Figure 5-16 Open-loop frequency response between Δe_t and Δe_{err} of machine 1

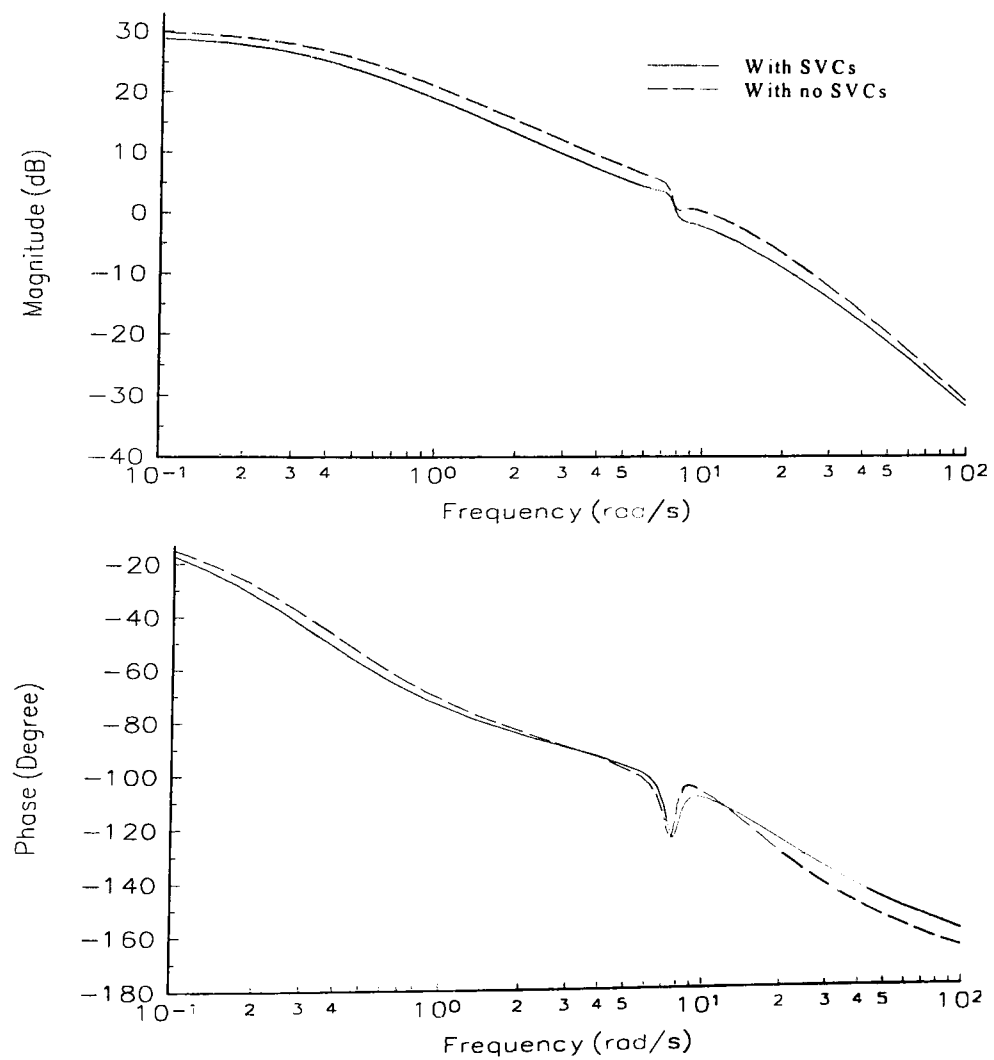
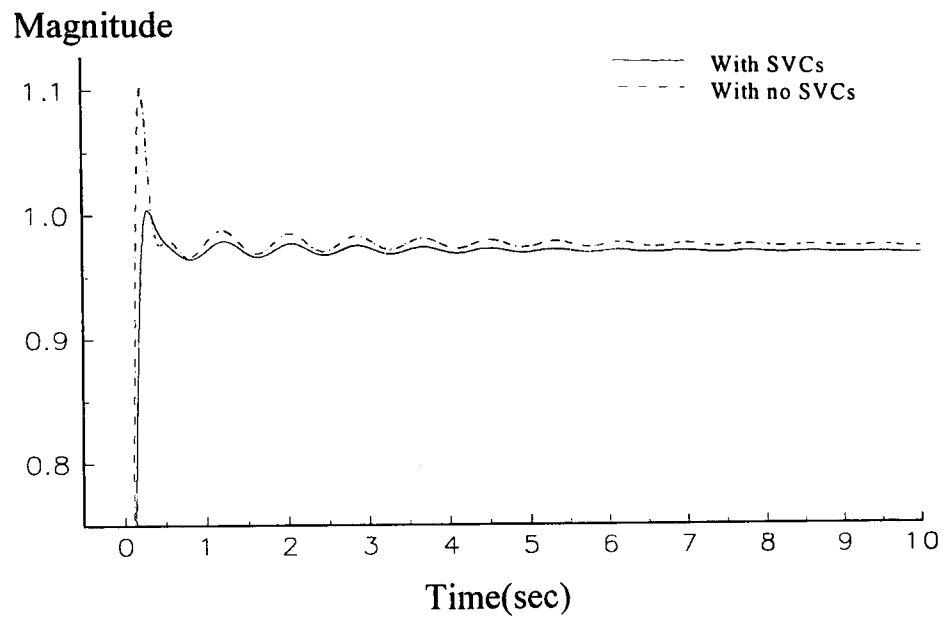
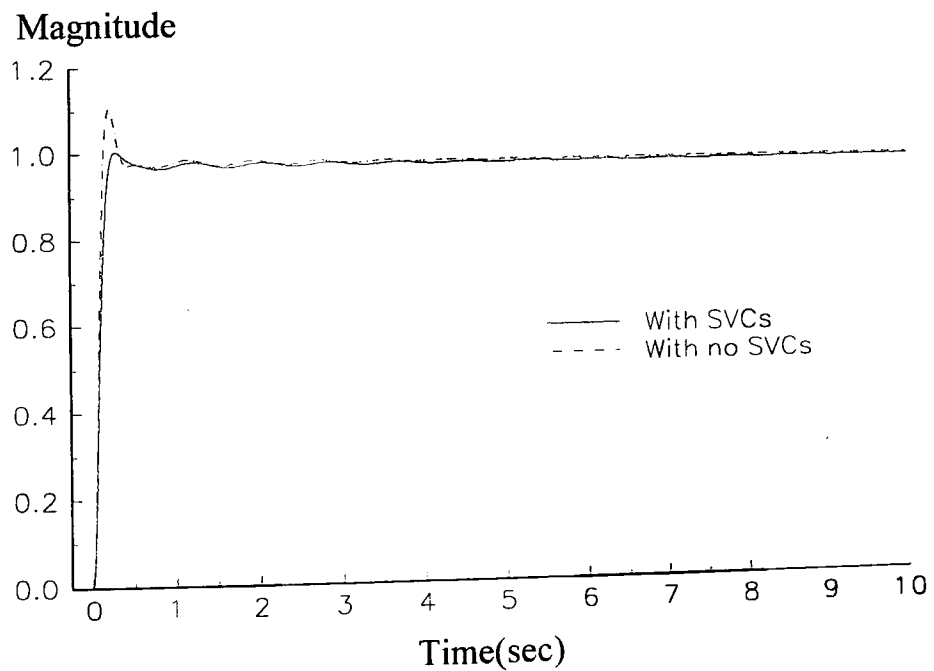


Figure 5-17 Open-loop frequency response between Δe_t and Δe_{err} of machine 2

Also, the time voltage responses in Figs. 5-18 and 5-19 show that the SVCs reduce the first peak of Δe_t when a step change in the AVR reference voltage ($\Delta e_{t\text{-ref}}$) is applied. However, the frequency responses illustrate that the SVCs are responsible for a slight reduction in the steady-state gains of the system, causing the output Δe_t to reach slightly lower steady-state levels. It should be noticed from Figs. 5-15(a) and (b) that the same amount of loading is considered for both cases, when the system contains SVCs and no SVCs.

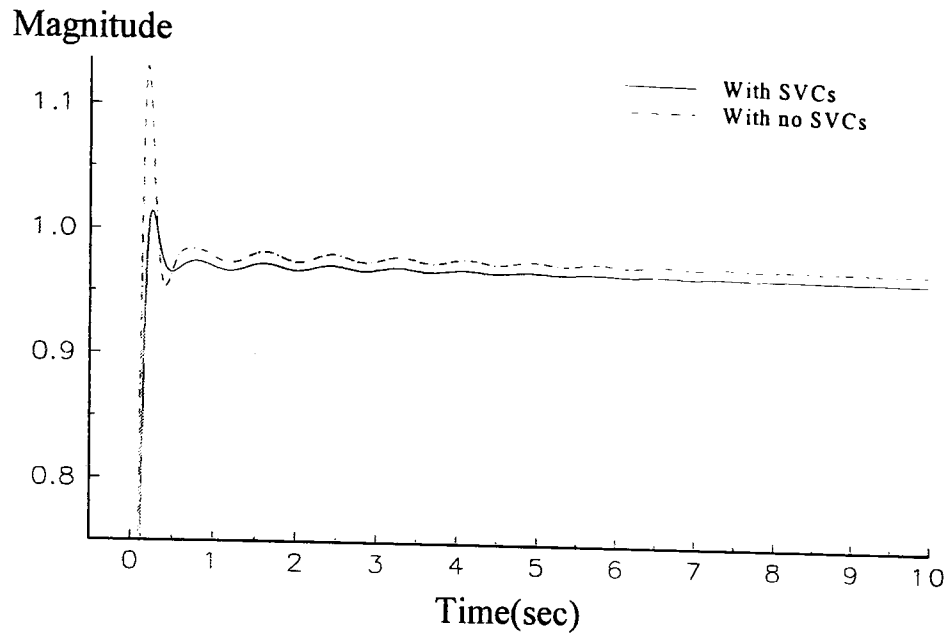


(a)

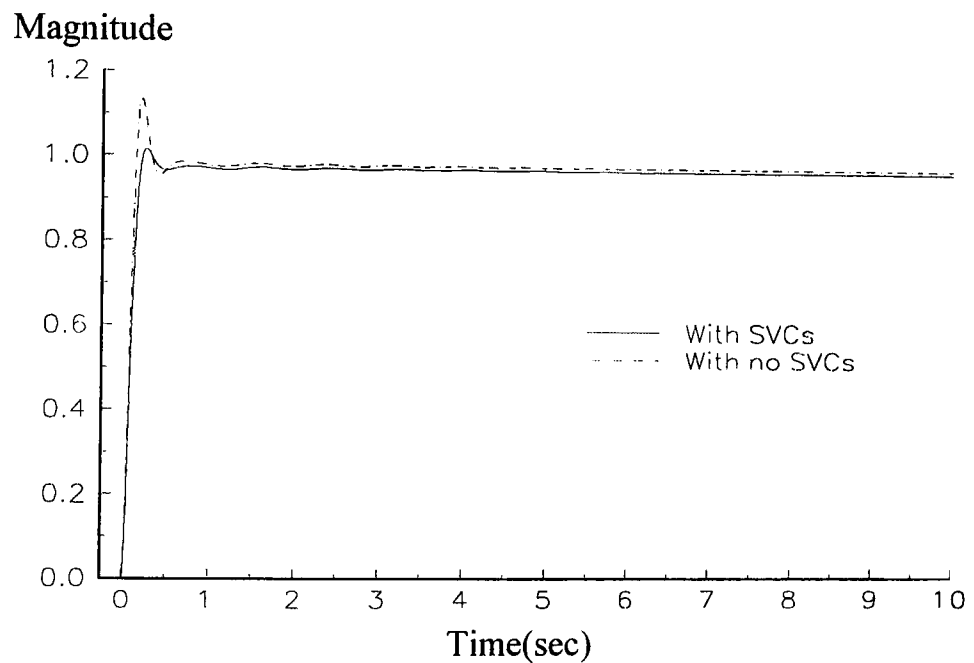


(b)

Figure 5-18 Step response of output voltage Δe_t of machine 1



(a)



(b)

Figure 5-19 Step response of output voltage Δe_t of machine 2

System damping with various SVC voltage control loop gains is explored below. The open-loop frequency response in Fig. 5-20 shows that machine 1's damping improves slightly together with a small reduction of the switch-back characteristic at the natural oscillation frequency when the voltage control loop gains of both SVCs increase from 15 to 30. Moreover, Figs. 5-20 and 5-21, indicate that the damping of both machines is improved in the high frequency range, above 40 rad/sec, where phase lead is obtained as the SVC voltage gain is increased. Time responses in Figs. 5-22 and 5-23 also show that the SVC gain of 30 provides a important reduction in the magnitudes of the first oscillatory peaks of output voltage Δe_t , when step changes are applied to Δe_{t-ref} , hence, improving the system dynamic performance.

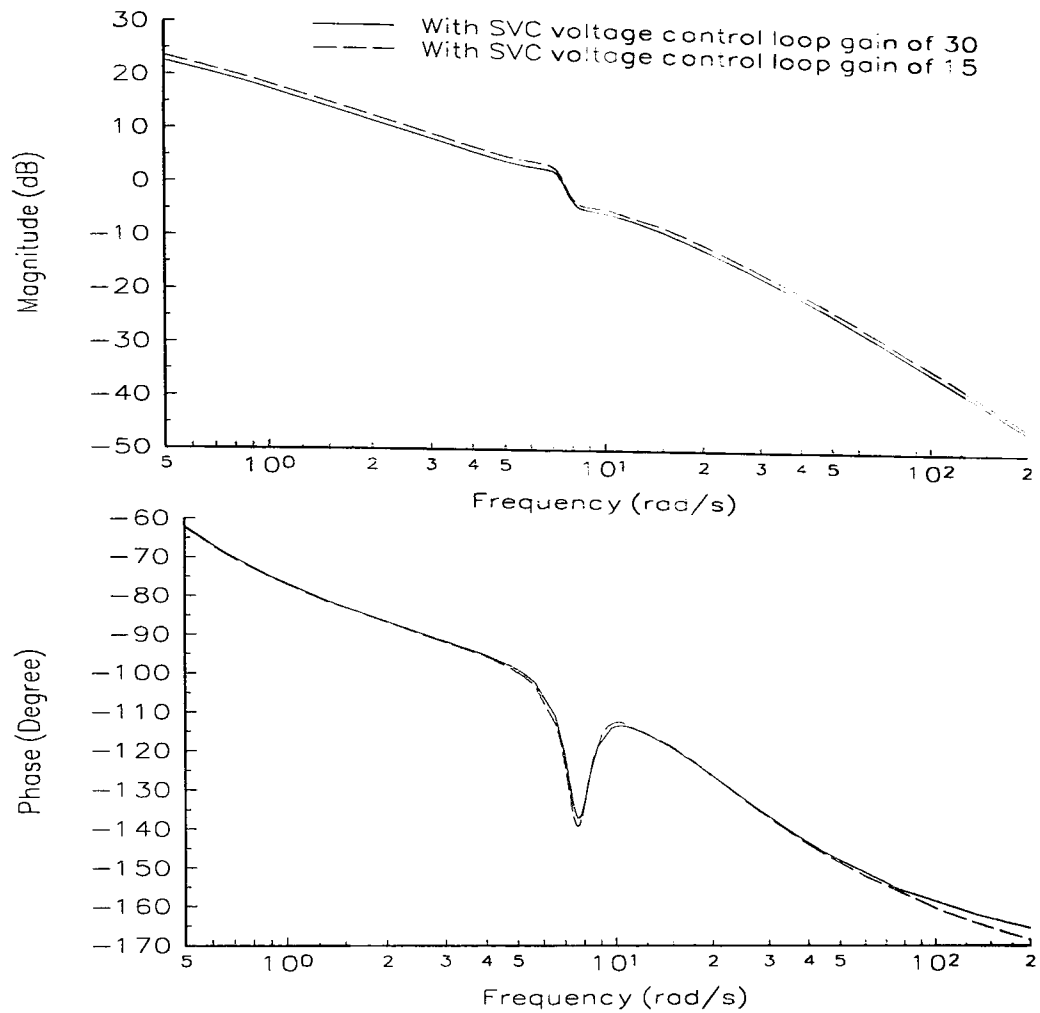


Figure 5-20 Open-loop frequency response between Δe_t and Δe_{err} of machine 1 with two different gains of SVC voltage control loop

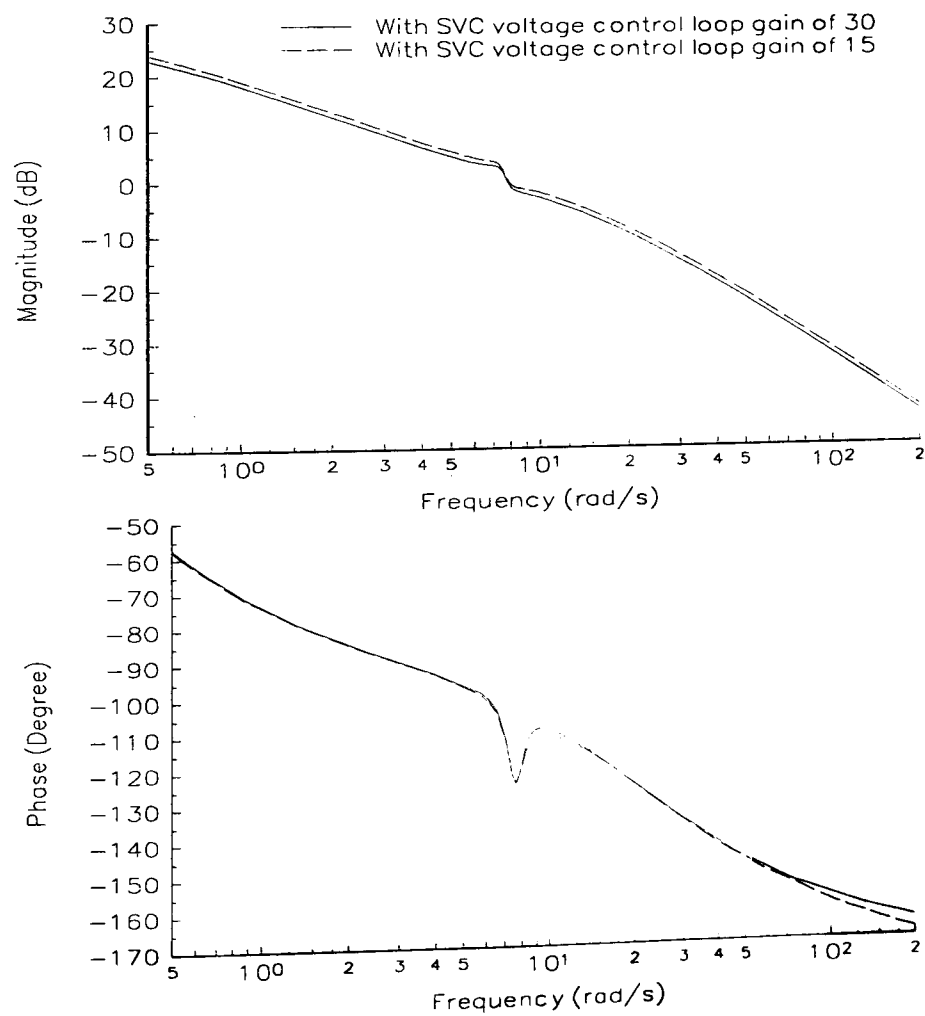
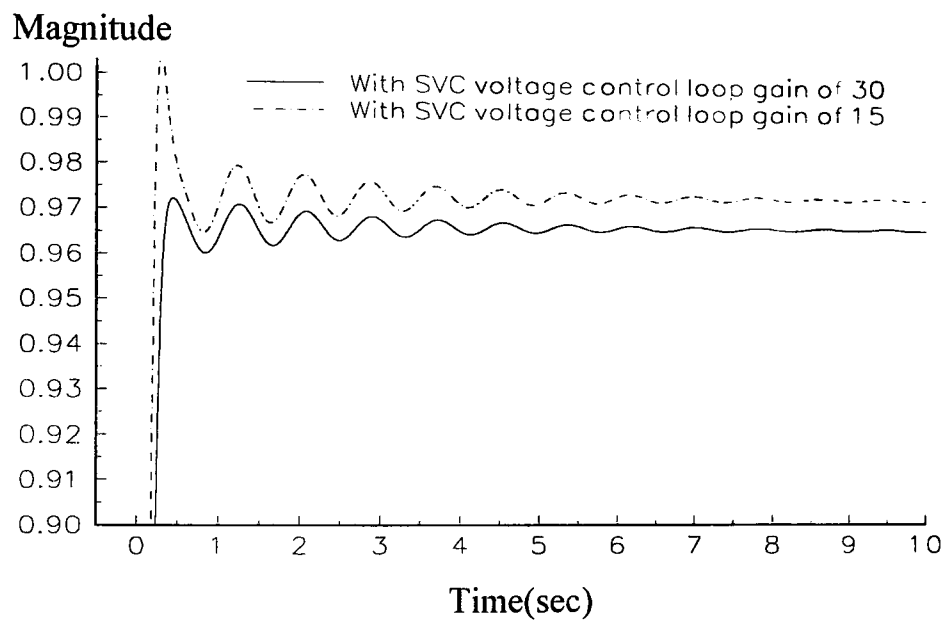
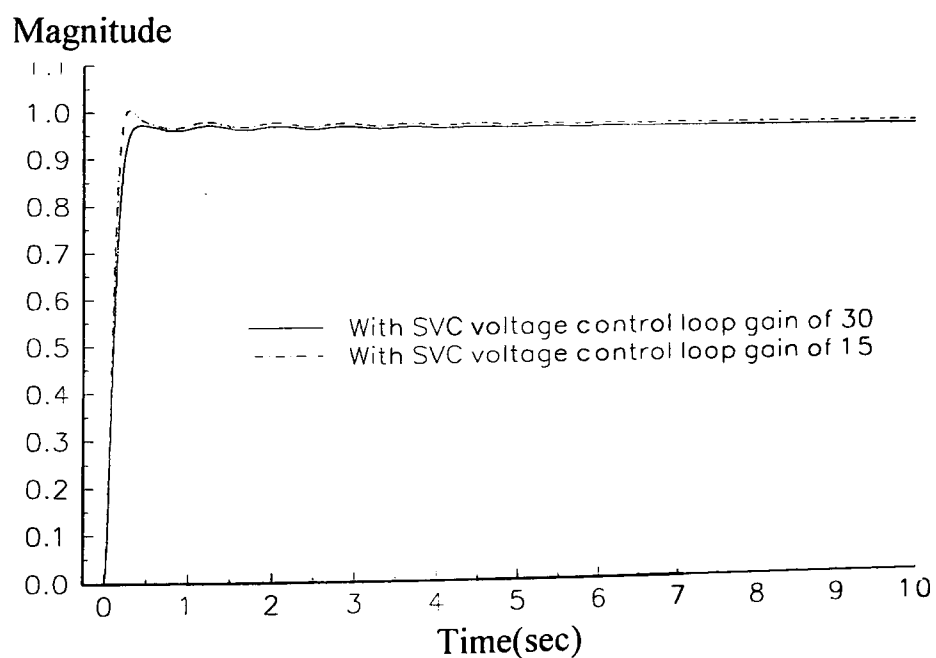


Figure 5-21 Open-loop frequency response between Δe_t and Δe_{err} of machine 2 with two different gains of SVC voltage control loop

System damping with various SVC voltage control loop gains is explored below. The open-loop frequency response in Fig. 5-20 shows that machine 1's damping improves slightly together with a small reduction of the switch-back characteristic at the natural oscillation frequency when the voltage control loop gains of both SVCs increase from 15 to 30. Moreover, Figs. 5-20 and 5-21, indicate that the damping of both machines is improved in the high frequency range, above 40 rad/sec, where phase lead is obtained as the SVC voltage gain is increased. Time responses in Figs. 5-22 and 5-23 also show that the SVC gain of 30 provides a important reduction in the magnitudes of the first oscillatory peaks of output voltage Δe_t , when step changes are applied to Δe_{t-ref} , hence, improving the system dynamic performance.

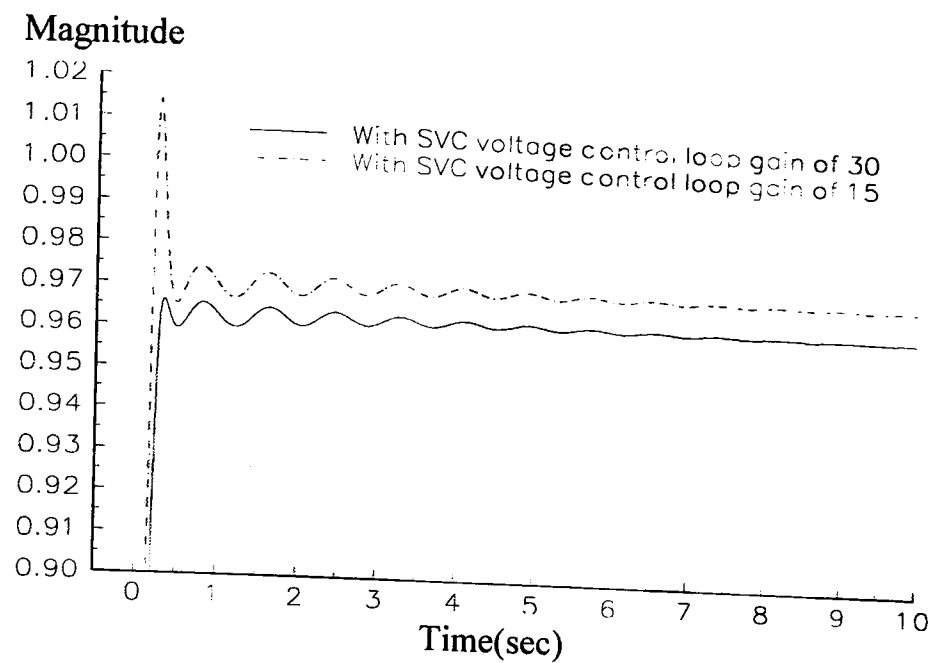


(a)

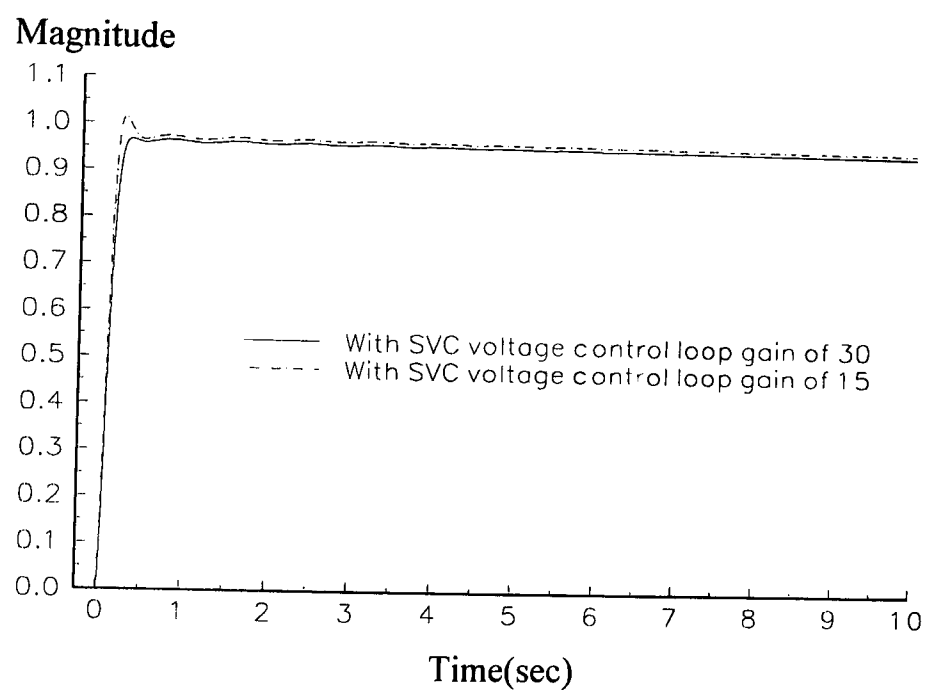


(b)

Figure 5-22 Step response of output voltage Δe_t of machine 1 with two different gains of SVC voltage control loop



(a)



(b)

Figure 5-23 Step response of output voltage Δe_i of machine 2 with two different gains of SVC voltage control loop

5.6 Conclusions

The block-diagram model of multi-machine and multi-SVC plant has been developed from first principles and presented in this chapter. In this simulation environment full dynamic interactions between generators and between generators and SVCs are comprehensively accounted for. The models have been used to enable a good explanation of how, in the multi-machine environment, SVCs impact on the generator dynamic characteristics. The assessment of various system models indicates that their dynamic characteristics are severely impaired if the generator damper winding effects are neglected in the study. The results presented demonstrate that the reliability of system model response critically depends on including at least one damper winding in the q -axis but the inclusion of two damper windings adds enhanced fidelity to the representation. Hence, it is

recommended that Model 1, including one damper winding in the d -axis and one in the q -axis should become the standard machine model in small-signal stability studies. This representation will ensure a high level of system model reliability in multi-machine small-signal stability studies, with the full dynamic representation of the other power system components, such as the generator's excitation control and FACTS devices, also included.

From the stability viewpoint, the dynamic performance of the synchronous machines is strongly influenced by network impedance. The machine's ability to damp system oscillations is severely degraded if the network's equivalent impedance is large. The results presented show that the deployment of SVC plant, with only the voltage control loop, does not reduce by much the total reactance of the network's equivalent impedance but, instead, it yields effective voltage support. Hence, the SVC plant with voltage control loop is only capable of increasing slightly the system damping. However, the SVC voltage control loop, particularly when it operates with high gain, has the ability to improve the high-frequency performance of the system. It should be noted that the study is based on the small-signal stability analysis by considering the SVCs ability to provide voltage support at the heavy-load node. For large signal-stability studies, the location of the SVCs should be changed, i.e. to the mid-point of tie line. The multi-machine test system used in these investigations is a relatively simple power network which has helped in understanding further the dynamic interactions that exist between devices and to establish more clearly the level of synchronous generator model complexity to be used in small-signal stability studies.

5.8 References

- [1] P. Kundur, "Power System Stability", McGraw-Hill Inc, 1993.
- [2] H. F. Wang, F. J. Swift and M. Li, "A Unified Model for the Analysis of FACTS Devices in Damping Power System Oscillation Part II: Multi-machine Power System", IEEE Transaction on Power Delivery, Vol. 13, No. 4, October 1998, pp. 1355-1360.
- [3] H. F. Wang, "Selection of Robust Installing Locations and Feedback Signals of FACTS-based Stabilizers in Multi-machine Power System", IEEE Transaction on Power Systems, Vol. 14, No. 2, April 1999. pp. 569-574.
- [4] H. F. Wang, F. J. Swift and M. Li, "Selection of Installing Locations and Feedback Signals of FACTS-based Stabilisers in Multimachine Power Systems by Reduced-Order Modal Analysis", IEE Proceedings on Generation, Transmission and Distribution, Vol. 144, Part C, No. 3, May 1997, pp. 263-269.
- [5] H. F. Wang, "Applications of Modelling UPFC into Multi-machine Power Systems", IEE Proceedings on Generation, Transmission and Distribution, Vol. 146, Part C, No. 3, May 1999, pp. 306-312.
- [6] Task Force on Definitions and Procedures, "Current Usage and Suggested Practices in Power

- System Stability Simulations for Synchronous Machines”, IEEE Transaction on Energy conversion, Vol. 1, No. 1, March 1986, pp. 77-93.
- [7] IEEE Standard 1110-1991, “IEEE Guide for Synchronous Generator Modelling Practices in Stability Analyses” 1991.
- [8] M. Saidy and F. M. Hughes, “Block Diagram Transfer Function Model of a Generator Including Damper Windings”, IEE Proceedings on Generation, Transmission and Distribution, Vol. 141, Part C, No. 6, November 1994, pp. 559-608.
- [9] M. Saidy and F. M. Hughes, “An Extended Block Diagram Transfer Function Model of a Synchronous Machine”, International Journal of Electrical Power and Energy System, Vol. 18, No. 2, February 1996, pp. 139-142.
- [10] M. Saidy and F. M. Hughes, “Performance Improvement of a Conventional Power System Stabilizer”, International Journal of Electrical Power and Energy System, Vol. 17, No. 5, October 1995, pp. 313-323.
- [11] L. Angquist, B. Lundin and J. Samuelsson, “Power Oscillation Damping Using Controlled Reactive Power Compensation: A Comparison between Series and Shunt Approaches”, IEEE Transaction on Power Systems, Vol. 8, No. 2, May 1993, pp. 687-699.
- [12] R. M. Mathur and R. S. Basati, “A Thyristor Controlled Static Phase-Shifter for AC Power Transmission”, IEEE Transaction on Power Apparatus and Systems, Vol. 100, No. 5, May 1981, pp. 2650-2655.
- [13] E. V. Larsen, K. Clark, S. S. Miske and J. Urbanek, “Characteristic and Rating Considerations of Thristor Controlled Series Compensation”, IEEE Transaction on Power Delivery, Vol. 9, No. 2, April 1994, pp. 883-841.
- [14] S. G. Helbing and G. G. Karady, “Investigations of an Advanced Form of Series Compensation”, IEEE Transaction on Power Delivery, Vol. 9, No. 2, April 1994, pp. 939-947.

Chapter 6

Small-Signal Modelling of Synchronous Generator-TCSC System in a Single-Machine Environment

6.1 Introduction

The use of series capacitors in high-voltage transmission systems to reduce the electrical length of the transmission corridor in order to increase its power transfer capabilities with enhanced transient stability performance, has been a very popular resource among power utility planners world-wide [1-5]. Very recently, great many efforts have been directed to researching into the use of power electronics to enable the fast switching of series compensation. This has resulted in a Thyristor-Controlled Series Compensator (TCSC) capable of: (i) introducing very substantial improvements on system stability performance and (ii) increasing power flows by a substantial margin, (iii) scheduling active power flows across the compensated transmission line [6-10]. It is well-known among power engineers that instability problems arise in systems exhibiting poor damping conditions and in transmission systems with long electrical distances. Recent experience with the operation of experimental TCSC facilities indicates that the TCSC will become a new powerful tool in the quest for providing better control in the high-voltage side of the power network. TCSCs are designed to modulate line reactance on a cycle-by-cycle basis.

This has provided the motivation to carry out fundamental studies of the dynamic behaviour of transmission systems including TCSC representation. Hence, the transfer-function block-diagram model of the synchronous generator-TCSC system is developed in this chapter. The development is based on the single-machine infinite-bus concept on two counts: (i) the 1 synchronous generator, 1 TCSC block-diagram model is conceptually simpler than the n synchronous generator, m TCSC block-diagram model, (ii) in most practical situations, compensated transmission systems will resemble a transmission system based on the infinite-bus concept. Arguably, this system model represents the best system to gain fundamental knowledge of the dynamic interactions between a synchronous generator and a TCSC. Similarly to the investigations carried out in Chapter 3, the dynamic interactions between the TCSC and the generator d and q -axis flux linkages are studied in a decoupled fashion.

6.2 System under study

The system under study is shown in Fig. 6-1. The system consists of one synchronous generator feeding into an infinite-bus system via a TCSC compensated tie line. The role of the TCSC is to

control the transmission system in order to control the impedance of the tie line on a cycle-by-cycle basis.

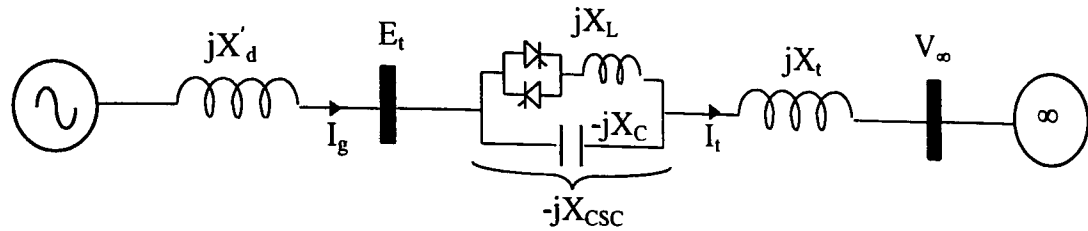


Figure 6-1 System under study

6.3 Representation of system model

In order to study the small-signal stability of TCSC-upgraded transmission systems, the linearisation of the system dynamic equations is carried out as shown in Appendix C. It should be noted that in order to study the dynamic interaction between the synchronous generator and the TCSC, the effects of the field winding and damping windings in the d and q -axes should be included. After manipulating the relevant transfer-function expressions, in the s domain, the following linearised equation are arrived at:

$$\Delta P_e = K_1 \Delta \delta + K_2 \Delta E_q'' - K_{2d} \Delta E_d'' + K_{csc1} \Delta \alpha \quad (6-1)$$

$$\Delta e_t = K_5 \Delta \delta + K_6 \Delta E_q'' + K_{6d} \Delta E_d'' + K_{csc3} \Delta \alpha \quad (6-2)$$

$$\Delta i_{csc} = K_{5n} \Delta \delta + K_{6n} \Delta E_q'' - K_{6dn} \Delta E_d'' + K_{csc3n} \Delta \alpha \quad (6-3)$$

where

$$\Delta E_q'' = g_3(s) \Delta E_{fd} - g_4(s) \Delta \delta - g_{csc2}(s) \Delta \alpha \quad (6-4)$$

$$\Delta E_d'' = g_{4d}(s) \Delta \delta + g_{csc2d}(s) \Delta \alpha \quad (6-5)$$

From (6-1)-(6-5), the block-diagram model shown in Fig. 6-2 of the generator-TCSC system is realised. The system coefficients and transfer functions are given in Appendix C.

There are three input-output feedback subsystems in the generator-TCSC block diagram, i.e. excitation control, turbine-governor control and TCSC impedance control loops. These are in addition to the generator-TCSC system, whose outputs of interest are: generator speed ($\Delta \omega$), generator output voltage (Δe_t) and TCSC current (Δi_{csc}) flowing through the tie line.

The main function of the impedance control loop of the TCSC is to schedule an amount of electrical power to be delivered through the tie line. The impedance control loop may be represented by the lagging transfer function with gain K_c and the time constant τ_c [12]. The feedback control signal is directly taken from the current (Δi_{csc}) flowing through the TCSC component. Hence, Δi_{csc} brings a change from the generator's flux linkages in the d and q -axes and rotor angle via the coefficients K_{6n} , K_{6dn} , and K_{5n} , which is compared with the reference ($\Delta i_{csc-ref}$) in order to adjust the firing angle at the desired power flows level.

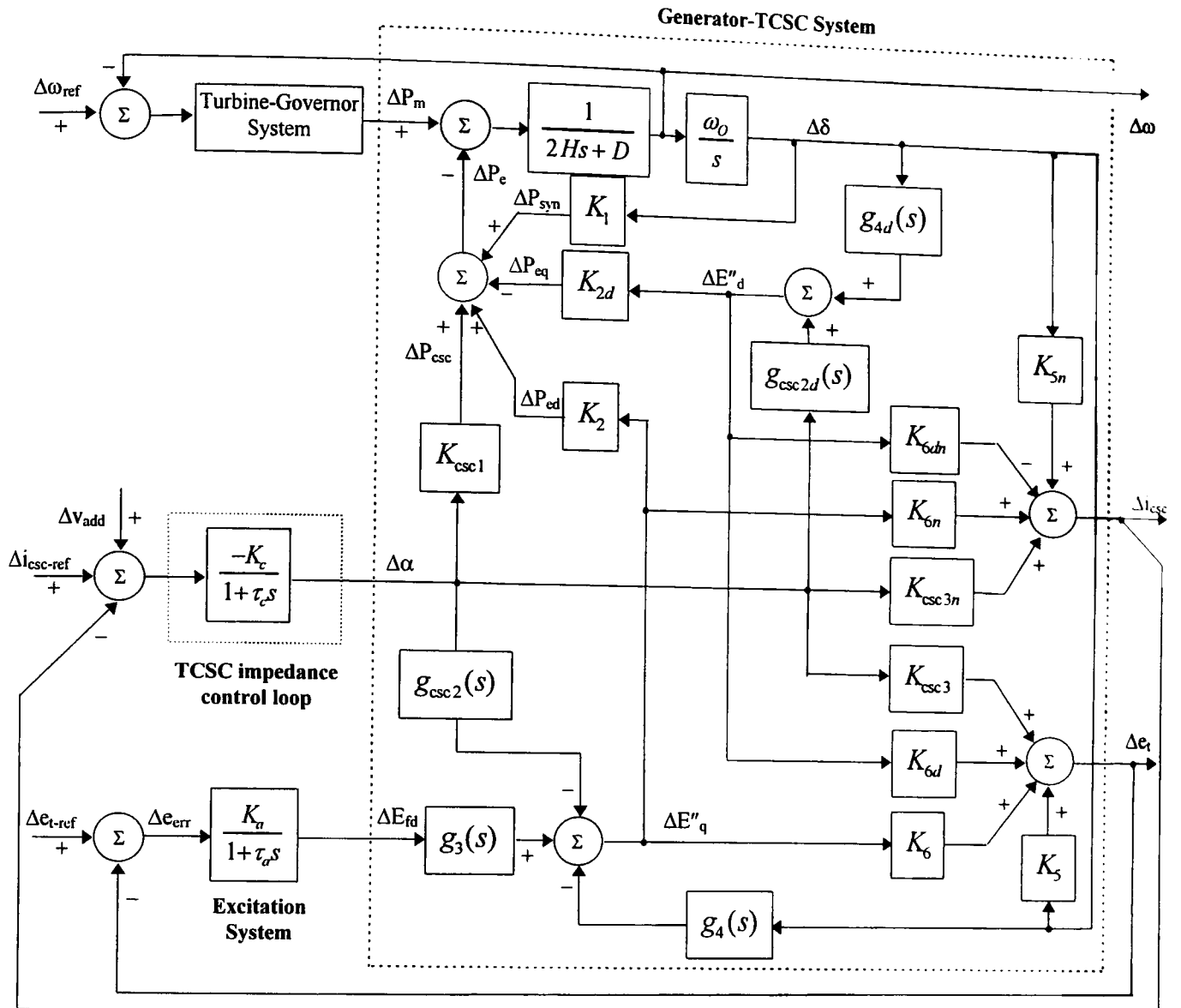


Figure 6-2 Detailed block-diagram model of the generator-TCSC system

6.4 TCSC characteristic and control scheme

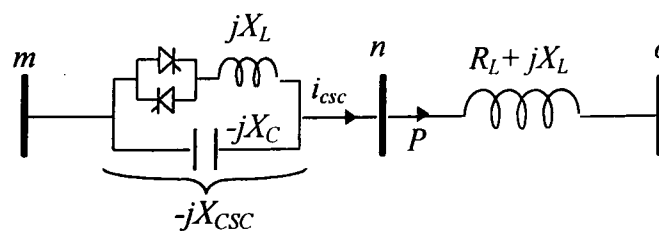


Figure 6.3 TCSC configuration

The TCSC is connected in series with the tie line, as shown in Fig. 6-3. The active power flow leaving node n can be adjusted by controlling the TCSC impedance (X_{csc}). This is achieved by suitably changing the thyristor's firing angle. The TCSC impedance characteristic as a function of firing angle can be calculated by using equation C-3 of Appendix C. The characteristic shown in Fig. 6-4 corresponds to the case when the inductive and capacitive reactances are 0.025 and 0.05 p.u., respectively.

It can be observed that the impedance characteristic has two distinctive regions of operation, one inductive and one capacitive, as the TCSC firing angle increases from 90° to 180° . The capacitive region starts at a firing angle of approximately 116° . For firing angle values near the resonant point, i.e. 116° , the variations of X_{csc} with respect to the firing angle are quite large even for a small variation in the controlling firing angle. It should be noted that the curve follows a similar pattern in both the inductive and capacitive regions. If an increase of TCSC impedance in the capacitive mode is required then the firing angle value should move towards the resonant point. Hence, the impedance control loop has a negative gain ($-K_c$) when the TCSC operates in the capacitive mode, as seen in Fig. 6-2.

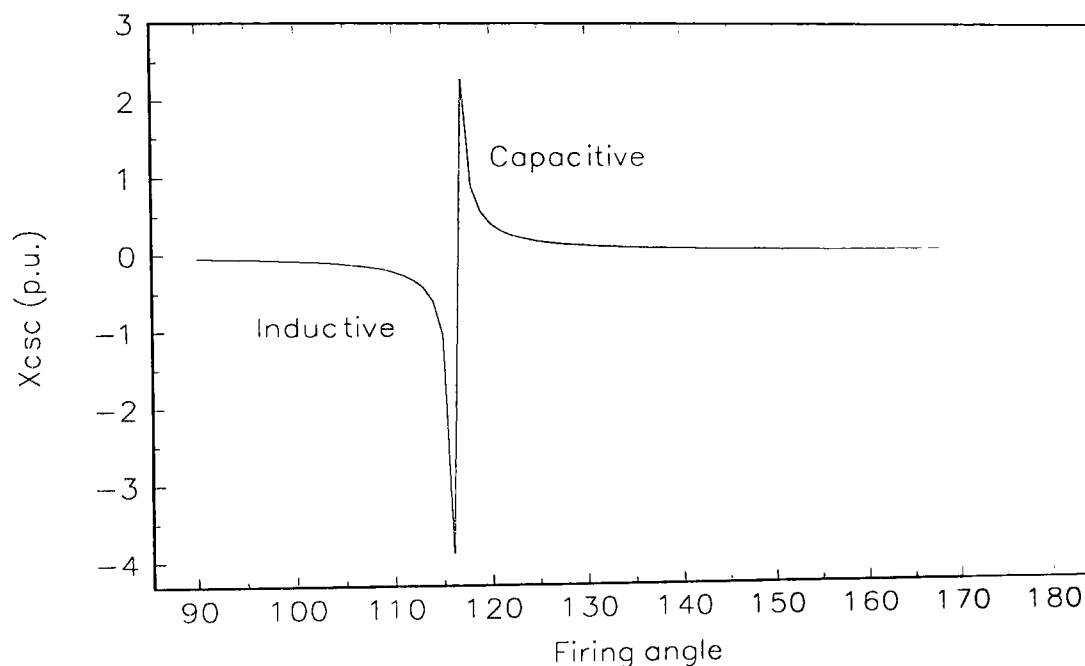


Figure 6-4 TCSC Impedance characteristic (X_{csc})

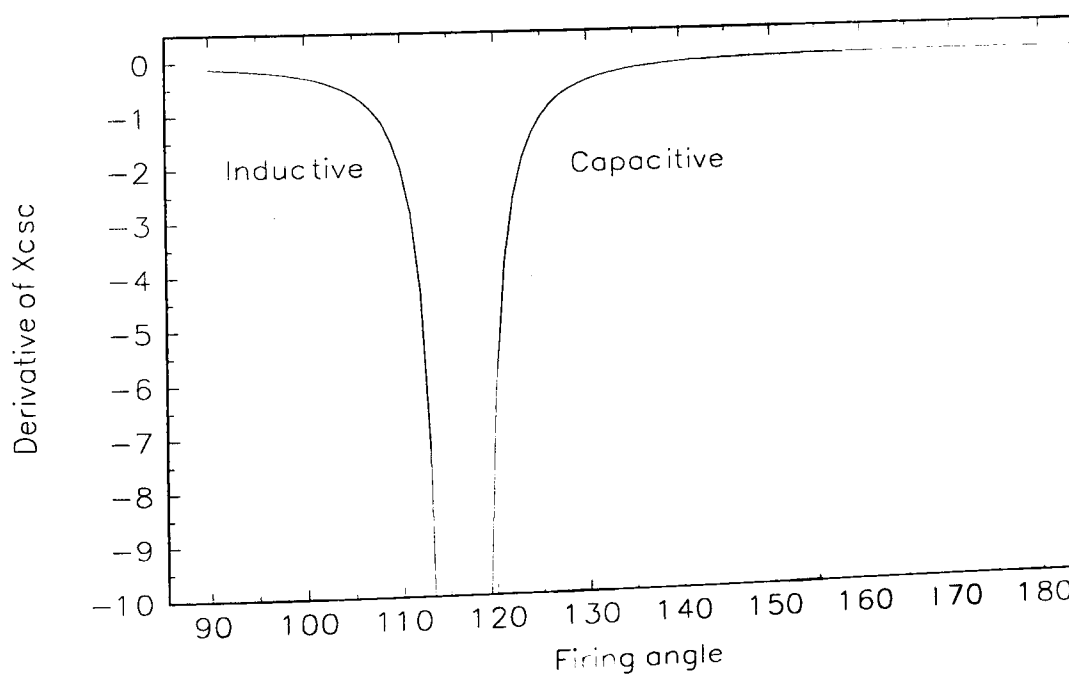


Figure 6-5 Derivative of the TCSC impedance characteristic (X_{csc})

For a small variation, the derivative value ($F(\alpha)$) of the TCSC impedance characteristic can be calculated from equation C-10 in Appendix C. The plot of $F(\alpha)$ with respect to the firing angle is

shown in Fig 6-5. $F(\alpha)$ has always negative values in the TCSC firing angle range. The effect of $F(\alpha)$ appears in many of the system coefficients and transfer functions of the block-diagram model, i.e. K_{csc1} , K_{csc3} , $g_{csc2}(S)$, $g_{csc2d}(S)$, as seen in the equations in Appendix C.

6.5 Analysis of the dynamic interactions between the synchronous generator and TCSC

Similarly to the study of the SVC conducted in Chapter 3, an incremental change in the electrical output power of the generator is also employed here to investigate the dynamic interactions between the generator and the TCSC system. The block diagram of the generator-TCSC system in Fig 6-2 yields unique physical insight as to how the TCSC interacts dynamically with the generator. The TCSC branches influencing the generator's behaviour are similar to those of the SVC. An incremental change in the TCSC firing angle leads to a direct change in the output power of the generator, which is made up of three individual electrical power loops, namely ΔP_{csc} , ΔP_{ed} and ΔP_{eq} . ΔP_{csc} is the component of the generator's output power that is directly channelled through the coefficient K_{csc1} and it is due to a change in TCSC impedance (ΔX_{csc}). ΔP_{ed} and ΔP_{eq} are portions of the output power produced by the d and q -axis flux linkages, respectively. The TCSC may influence the power produced by the flux linkages through the coefficient K_{csc3} and the transfer function $g_{csc2}(S)$ and $g_{csc2d}(S)$, respectively. Once the firing angle is changed to increase the TCSC contribution, in the capacitive mode, all the coefficients and transfer functions making up the entire system will be effected due to a reduction of the tie-line's impedance. How much the characteristic of the generator's output power is influenced by the three individual loops is investigated in the sections below.

6.6 Assessing the generator dynamic performance with the TCSC effects included

An assessment of the generator dynamic performance is carried out in this section, where the TCSC is applied to control the tie line's reactance linking the generator and the infinite bus. The synchronising and damping power method is used for investigating the stability of the electrical powers, i.e. $\Delta P_{ed}/\Delta\delta$, $\Delta P_{eq}/\Delta\delta$ and $\Delta P_{csc}/\Delta\delta$. The operating conditions of the system under study in are given in Table 6-1. It is noted that the same amount of the active power delivered to the infinite bus is used when the TCSC is used and when it is not used.

6.6.1 Electrical power ΔP_{ed}

Fig. 6-6 shows the frequency response of $\Delta P_{ed}/\Delta\delta$ with TCSC and with no TCSC in operation. As seen from the result in dotted lines, the phase of $\Delta P_{ed}/\Delta\delta$ is greater than 180° in the oscillatory frequency range of approximately 8-20 rad/sec. It shows that an inherent damping characteristic of the field plus damper windings in the d -axis is negative.

| With no FACTS device | | With TCSC | | With SVC | |
|----------------------|--|----------------|--|----------------|--|
| P_g | 0.736 p.u. | P_g | 0.736 p.u. | P_g | 0.736 p.u. |
| Q_g | 0.752 p.u. | Q_g | 0.763 p.u. | Q_g | 0.5514 p.u. |
| Q_{svc} | - | | | Q_{svc} | 0.378 p.u. |
| X_t | 0.2 p.u. | X_t | 0.2 p.u. | X_t | 0.2 p.u. |
| X_{t1} | - | | | X_{t1} | 0.1 p.u. |
| X_{total} | 0.2 p.u. | X_{total} | 0.196 p.u. | X_{total} | 0.196 p.u. |
| V_∞ | 0.92 p.u. | V_∞ | 0.92 p.u. | V_∞ | 0.92 p.u. |
| e_t | 1.0522 p.u. | e_t | 1.0522 p.u. | e_t | 1.0522 p.u. |
| V_{mid} | 0.9832 p.u. | | | V_{mid} | 1.0022 p.u. |
| I_t | 1 p.u. | I_t | 1.005 p.u. | I_t | 1.1246 p.u. |
| α | - | α | 152° | α | 150° |
| δ_o | 29.85 | δ_o | 29.43 | δ_o | 35.92 |
| E_{fdo} | 2.3087 p.u. | E_{fdo} | 2.3205 p.u. | E_{fdo} | 2.0618 p.u. |
| $g_3(s)$ | $\frac{6.789 + 0.19S}{29.47 + 49.38S + S^2}$ | $g_3(s)$ | $\frac{6.789 + 0.19S}{29.68 + 49.51S + S^2}$ | $g_3(s)$ | $\frac{6.789 + 0.19S}{29.24 + 49.24S + S^2}$ |
| $g_4(s)$ | $\frac{10.39 + 6.17S}{29.47 + 49.38S + S^2}$ | $g_4(s)$ | $\frac{10.35 + 6.15S}{29.68 + 49.51S + S^2}$ | $g_4(s)$ | $\frac{11.346 + 6.74S}{29.24 + 49.24S + S^2}$ |
| | - | $g_{csc2}(s)$ | $\frac{-0.235 - 0.139S}{29.68 + 49.51S + S^2}$ | $g_{svc2}(s)$ | $\frac{0.5288 + 0.314S}{29.24 + 49.24S + S^2}$ |
| $g_{4d}(s)$ | $\frac{11.048}{20.136 + S}$ | $g_{4d}(s)$ | $\frac{11.207}{20.276 + S}$ | $g_{4d}(s)$ | $\frac{11.116}{19.987 + S}$ |
| | - | $g_{csc2d}(s)$ | $\frac{-0.0607}{20.276 + S}$ | $g_{svc2d}(s)$ | $\frac{11.116}{19.987 + S}$ |
| K_1 | 2.8639 | K_1 | 2.9007 | K_1 | 2.86248 |
| K_2 | 1.2085 | K_2 | 1.2044 | K_2 | 1.32003 |
| K_{2d} | 2.2041 | K_{2d} | 2.2358 | K_{2d} | 2.21768 |
| K_5 | -0.07319 | K_5 | -0.07463 | K_5 | -0.07463 |
| K_6 | 0.49228 | K_6 | 0.48896 | K_6 | 0.48896 |
| K_{6d} | 0.19899 | K_{6d} | 0.22076 | K_{6d} | 0.22076 |
| | - | K_{csc1} | -0.02209 | K_{svc1} | 0.01538 |
| | - | K_{csc3} | 0.03878 | K_{svc3} | 0.01225 |
| | - | K_{5n} | 1.9799 | K_{5n} | -0.06031 |
| | - | K_{6n} | 2.4538 | K_{6n} | 0.24106 |
| | - | K_{6dn} | 1.0865 | K_{6dn} | 0.13042 |
| | - | K_{csc3n} | -0.02993 | K_{svc3n} | 0.01925 |

Table 6-1 System operating conditions

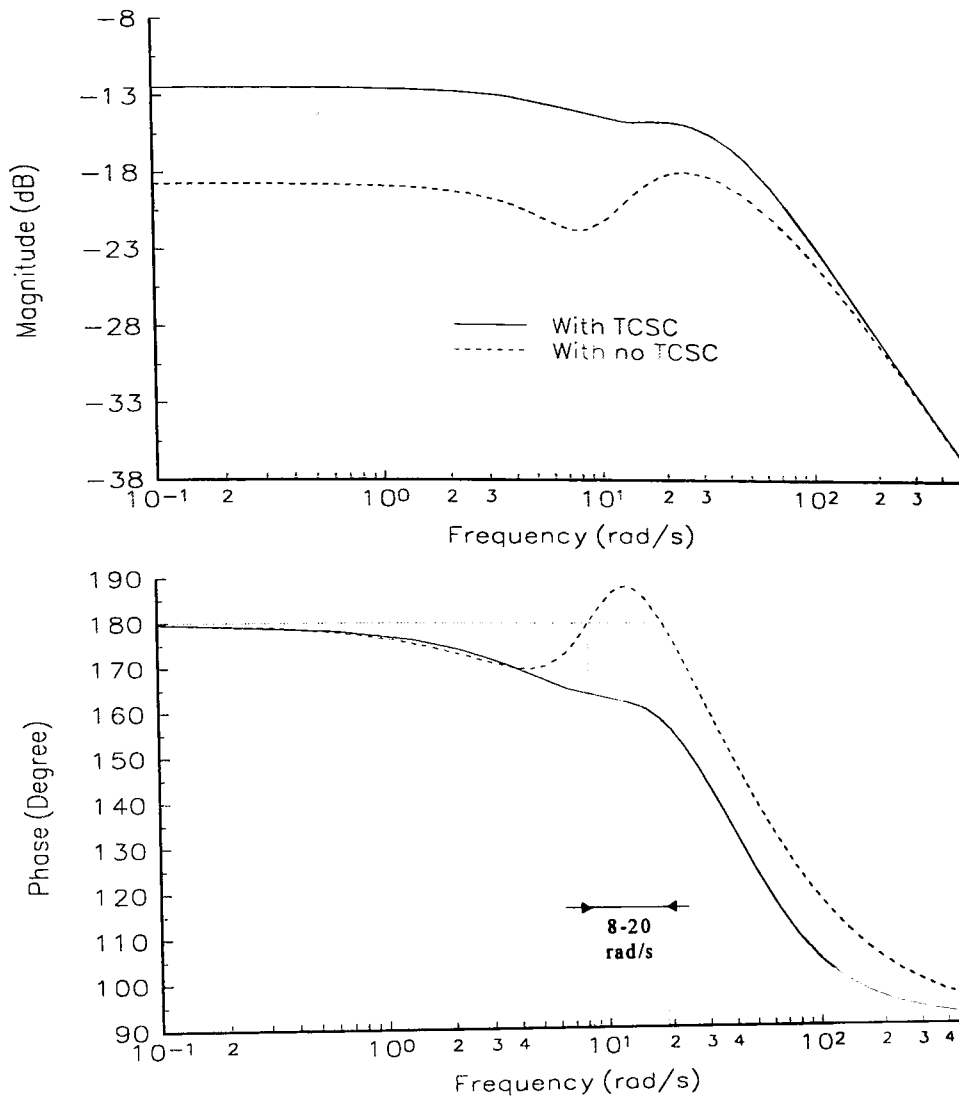


Figure 6-6 Frequency response of $\Delta P_{cd}/\Delta\delta$ with and with no TCSC

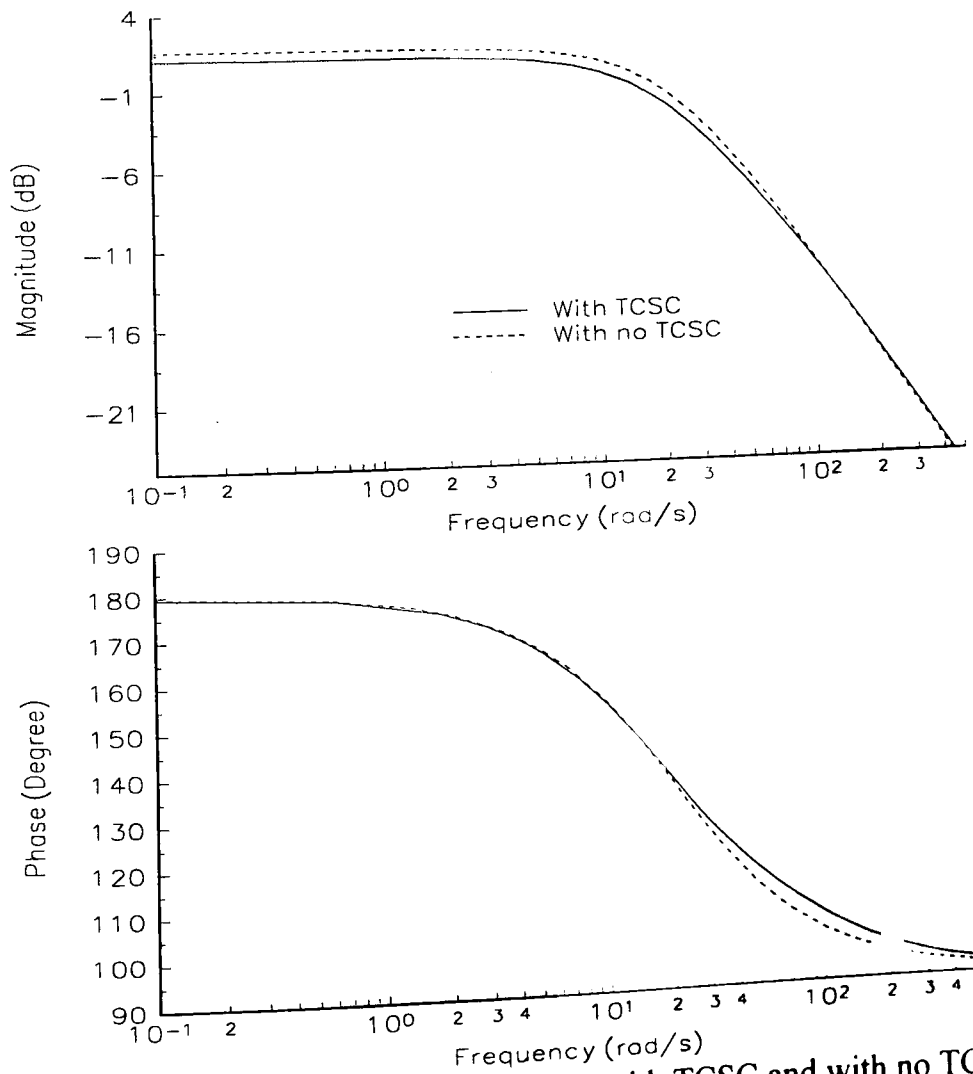


Figure 6-7 Frequency response of $\Delta P_{eq}/\Delta\delta$ with TCSC and with no TCSC

In this situation, the potential of the system to damp oscillations is weak. By including the TCSC, the phase in this frequency range is compensated, dropping below 180° by a considerable margin. This indicates that the TCSC is capable of increasing the damping power generated by the d -axis flux linkage. Moreover, the gain of $\Delta P_{ed}/\Delta\delta$ clearly shows a significant increase in electrical power over a wide range of oscillation frequencies. This results in a higher amount of damping power available to suppress oscillations.

Using the block-diagram representation, one can clearly appreciate the great capability that the TCSC counteract the AVR action by increasing the damping power component of $\Delta P_{ed}/\Delta\delta$. As seen from the given system operating conditions given Table 6-1, the coefficient K_{csc3} is positive because $\{e_{tq0} \times i_{gdo}\}$ is greater than $\{e_{td0} \times i_{gq0}\}$. Hence, the positive rotor angle signal delivered through the coefficient K_{csc3} counteracts the AVR action to improve system damping.

6.6.2 Electrical power ΔP_{eq}

The frequency response in Fig. 6-7 shows the q -axis flux linkage power characteristic with TCSC and with no TCSC. Over a wide range of frequencies, the incorporation of the TCSC leads to a small reduction of gain and a small increment of phase lead, particularly at high frequencies. Therefore, the TCSC does not introduce any significant change into the power characteristic of the q -axis damper winding. The contribution is through the transfer function $g_{csc2d}(S)$. Fig. 6-7 also shows that the q -axis flux linkage always supplies a positive damping power component.

6.6.3 Electrical power ΔP_{csc}

The frequency response in Fig. 6-8 shows that the power characteristic of ΔP_{csc} has a negative synchronising and damping power component in the frequency range 0.1-14 rad/sec, where the phase angle is lower than -180° , i.e. greater than 180° . At the frequency above 14 rad/sec, the phase of ΔP_{csc} tends to increase from -180° to -270° , i.e. it tends to reduce from 180° to 90° in absolute terms. Hence, this result again shows that system stability improvement is obtained.

6.7 Comparison of the damping capabilities of SVCs and TCSCs

In high voltage applications, SVCs are usually installed at mid-point of tie-line system to provide fast-acting voltage support. TCSCs, on the other hand, are used to control the tie-line's impedance to vastly improve active power transfers. Both FACTS devices control different variables of the power system. Nevertheless, in this section, notwithstanding their differences in control schemes, both devices are compared in their ability to damp local oscillations. Basically, the characteristics of the electrical powers generated by the main flux linkages in the d and q -axes are compared, as well as the overall dynamic response between the generator output Δe_t and input Δe_{err} .

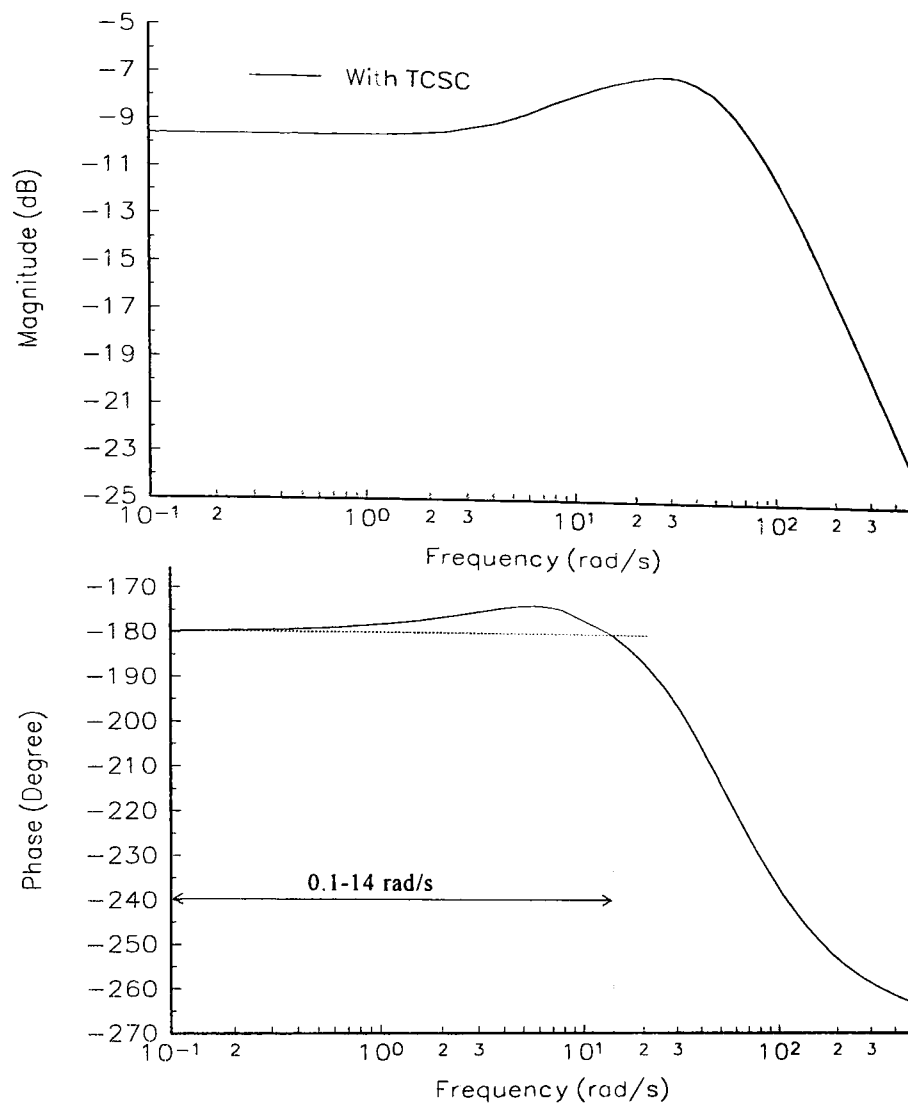


Figure 6-8 Frequency response of $\Delta P_{csc}/\Delta\delta$ with TCSC

In order to compare meaningfully the capability of both plant components to damp system oscillations, the system needs to be operated at the same operating point in both case. Hence, the same amount of active power that is delivered to the infinite bus and the total impedance of the tie line (between generator and infinite bus) are kept when either the SVC or the TCSC are used. Moreover, the gain and time constant of both the SVC and the TCSC controllers are adjusted identically. The system operating conditions are shown in Table 6-1.

Since the generator's damping characteristic is primarily determined by its d - and q -axis flux linkages, the effect of the SVC and TCSC on these flux linkages are a matter of great interest. The power of the d -axis flux linkage is plotted in Fig. 6-9 for three cases: (i) with SVC, (ii) with TCSC, (iii) with no FACTS controller. It can be seen that the damping characteristic of the generator, including no FACTS device, becomes negative at the frequency range of 8-20 rad/sec. The frequency response shows that the TCSC has a better capability to increase system damping in this frequency range than the SVC. It pushes down the phase characteristic of $\Delta P_{ed}/\Delta\delta$ back towards 90° . Furthermore, the TCSC provides a higher magnitude level of electrical power produced by the d -axis flux linkage over a wide range of oscillatory frequencies. Hence, impedance control of the tie line yields a greater damping improvement than the nodal voltage magnitude control.

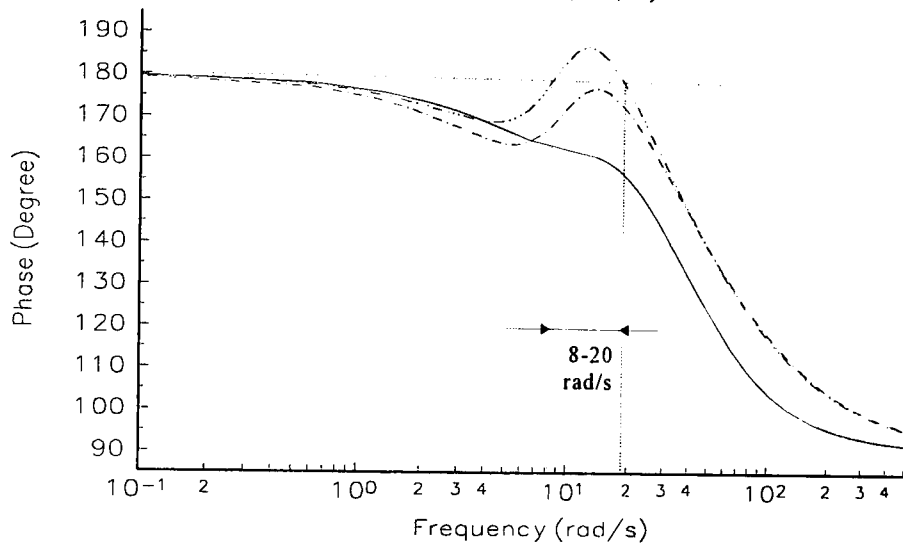
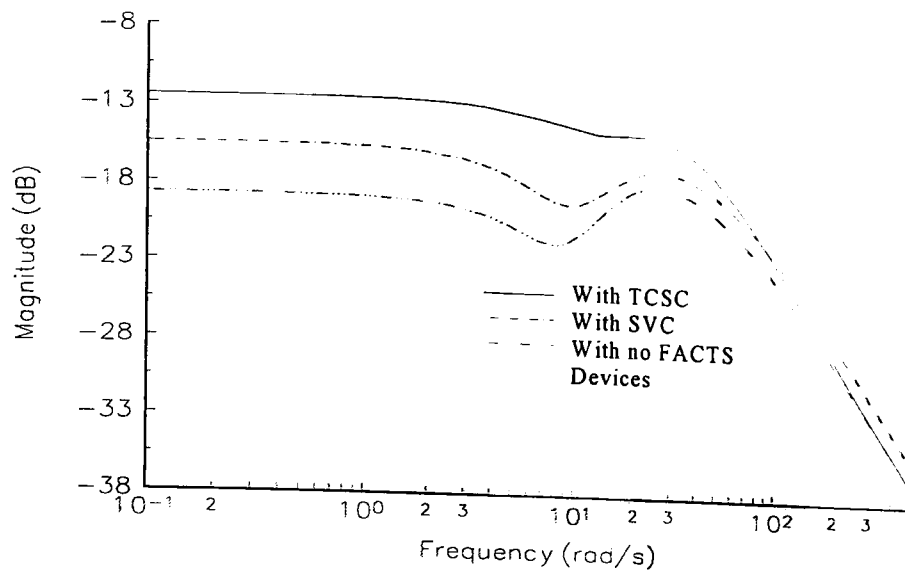


Figure 6-9 Frequency response of $\Delta P_{ed}/\Delta\delta$

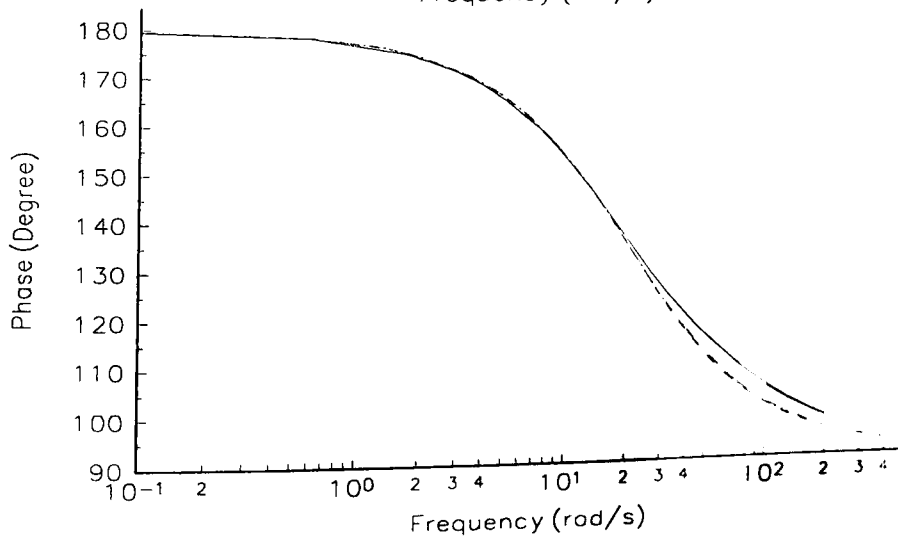
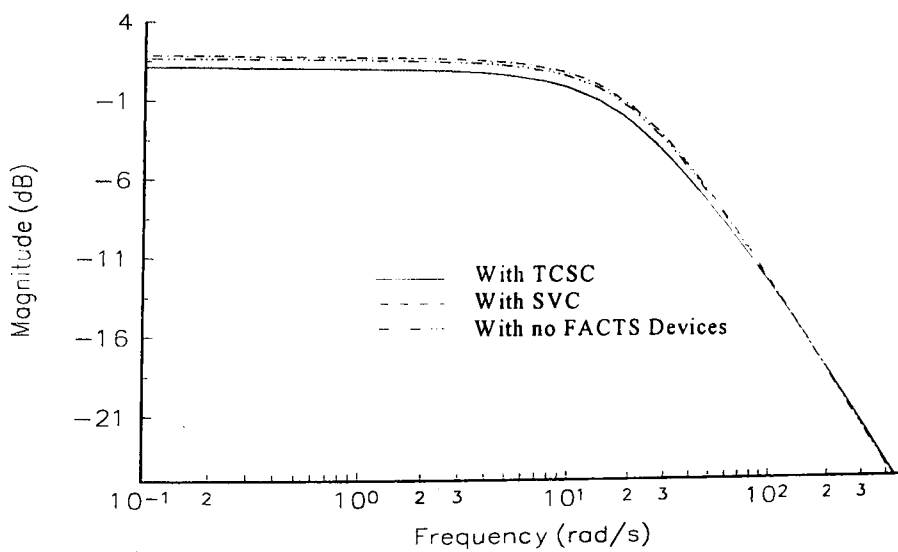


Figure 6-10 Frequency response of $\Delta P_{eq}/\Delta\delta$

The TCSC and SVC play an important role in increasing the power generated by the d -axis flux linkages due to the field plus damper windings. On the other hand, Fig. 6-10 shows that there is no significant change in the electrical power characteristic generated by the q -axis damper winding when either a TCSC or a SVC is used. We can conclude then the effect of the TCSCs and SVCs on the q -axis flux linkage is of little consequence compared to those on the d -axis flux linkages in regulated systems.

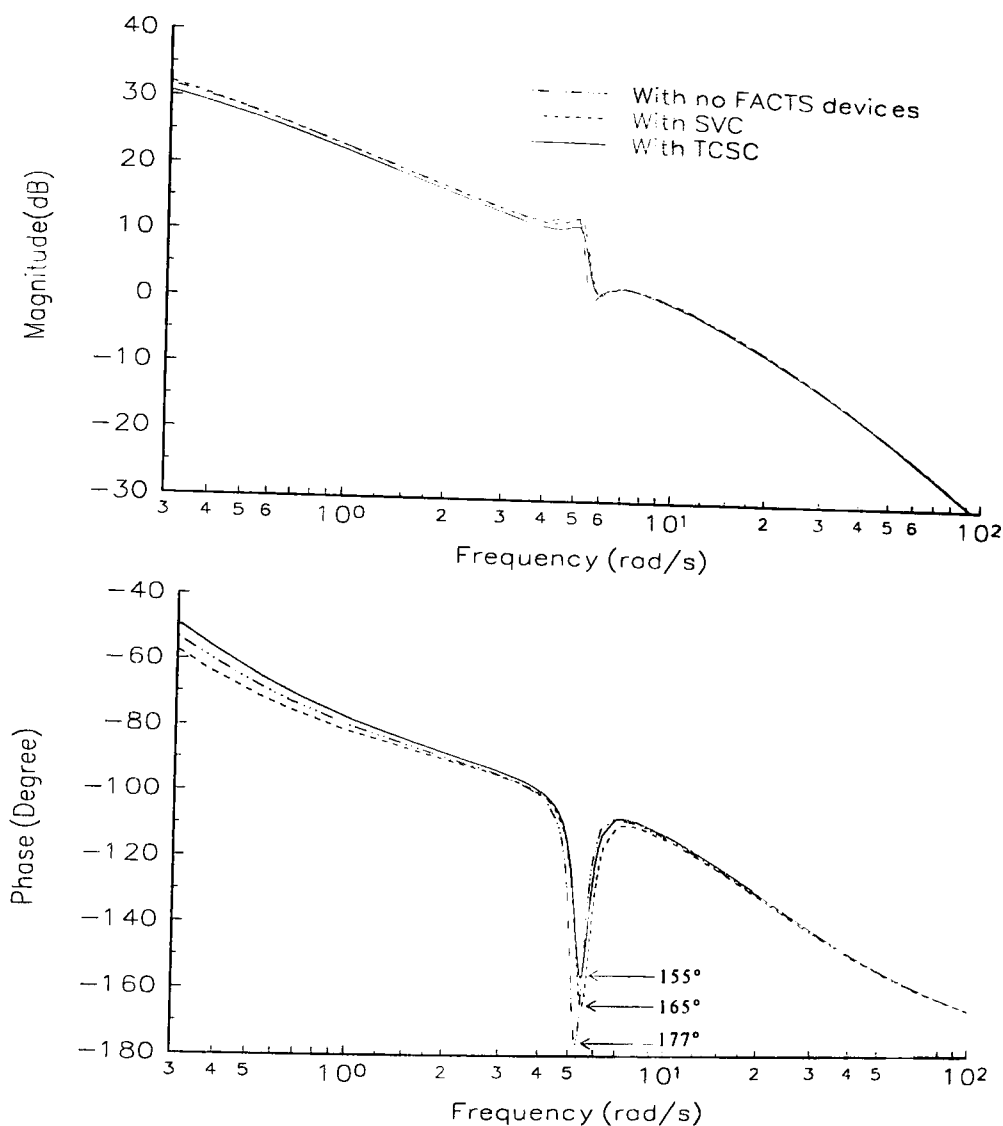


Figure 6-11 Open-loop frequency response between Δe_t and Δe_{err}

After having compared the characteristic of the electrical power generated by the flux linkages in the d and q -axis, the overall dynamic performance of the system is assessed by comparing the open-loop frequency responses between the output Δe_t and the input Δe_{err} . Three different cases are considered, when the transmission system contains a TCSC, a SVC and when no compensating devices is used. In this study, the system is assumed to contain a weak tie line (0.8 p.u.) connecting the generator and the infinite bus. In order to make a meaningful comparison of system damping enhancement, all factors affecting system stability are kept equal between studies, e.g. compensated tie-line reactance and the active power exported to the infinite bus. As seen from the system operating condition in Table 6-2, the percentage of tie-line reactance is 7.5, i.e. reactance is 0.74 per unit. Also, the active power is 0.736 per unit in cases when the SVC is used and when the TCSC is used. Moreover, the controller gains of both devices are tuned at 10.

| With no FACTS device | | With TCSC | | With SVC | |
|----------------------|--|----------------|---|----------------|--|
| P_g | 0.736 p.u. | P_g | 0.736 p.u. | P_g | 0.736 p.u. |
| Q_g | 0.512 p.u. | Q_g | 0.50 p.u. | Q_g | 0.258 p.u. |
| Q_{svc} | - | | | Q_{svc} | 0.427 p.u. |
| X_t | 0.8 p.u. | X_t | 0.8 p.u. | X_t | 0.8 p.u. |
| X_{t1} | - | | | X_{t1} | 0.4 p.u. |
| X_{total} | 0.8 p.u. | X_{total} | 0.74 p.u. | X_{total} | 0.74 p.u. |
| V_∞ | 0.92 p.u. | V_∞ | 0.92 p.u. | V_∞ | 0.92 p.u. |
| e_t | 1.1207 p.u. | e_t | 1.1207 p.u. | e_t | 1.1207 p.u. |
| V_{mid} | 0.974 p.u. | | | V_{mid} | 1.06 p.u. |
| I_t | 0.8 p.u. | I_t | 0.79 p.u. | I_t | 0.83 p.u. |
| α | - | α | 165° | α | 150° |
| δ_o | 56.8 | δ_o | 53.7 | δ_o | 57.92 |
| E_{fdo} | 2.0 p.u. | E_{fdo} | 2.003 p.u. | E_{fdo} | 1.72 p.u. |
| $g_3(s)$ | $\frac{6.789 + 0.19S}{15.57 + 41.12S + S^2}$ | $g_3(s)$ | $\frac{6.789 + 0.19S}{16.11 + 41.44S + S^2}$ | $g_3(s)$ | $\frac{6.789 + 0.19S}{14.97 + 40.76S + S^2}$ |
| $g_4(s)$ | $\frac{6.761 + 4.01S}{15.57 + 41.12S + S^2}$ | $g_4(s)$ | $\frac{6.91 + 4.1S}{16.11 + 41.44S + S^2}$ | $g_4(s)$ | $\frac{7.43 + 4.4S}{14.97 + 40.76S + S^2}$ |
| | - | $g_{csc2}(s)$ | $\frac{-0.304 - 0.18S}{16.11 + 41.44S + S^2}$ | $g_{svc2}(s)$ | $\frac{0.84 + 0.47S}{14.97 + 40.76S + S^2}$ |
| $g_{4d}(s)$ | $\frac{2.623}{11.5 + S}$ | $g_{4d}(s)$ | $\frac{3.01}{11.83 + S}$ | $g_{4d}(s)$ | $\frac{2.86}{11.14 + S}$ |
| | - | $g_{csc2d}(s)$ | $\frac{-0.18}{11.83 + S}$ | $g_{svc2d}(s)$ | $\frac{0.392}{11.14 + S}$ |
| K_1 | 0.869 | K_1 | 0.964 | K_1 | 0.959 |
| K_2 | 0.786 | K_2 | 0.804 | K_2 | 0.865 |
| K_{2d} | 0.523 | K_{2d} | 0.601 | K_{2d} | 0.570 |
| K_5 | -0.0987 | K_5 | -0.0973 | K_5 | -0.1 |
| K_6 | 0.757 | K_6 | 0.747 | K_6 | 0.759 |
| K_{6d} | 0.3115 | K_{6d} | 0.306 | K_{6d} | 0.358 |
| | - | K_{csc1} | -0.039 | K_{svc1} | 0.0492 |
| | - | K_{csc3} | 0.00445 | K_{svc3} | 0.0205 |
| | - | K_{5n} | 1.003 | K_{5n} | -0.182 |
| | - | K_{6n} | 0.908 | K_{6n} | 0.346 |
| | - | K_{6dn} | 0.604 | K_{6dn} | 0.289 |
| | - | K_{csc3n} | -0.0424 | K_{svc3n} | 0.0698 |

Table 6-2 System operating conditions

The ability of the SVC and TCSC to improve system damping is shown in Fig. 6-11. The well-known undamped response at the local oscillation frequency of 5.3 rad/sec is clearly shown. The plot of phase versus frequency shows that the SVC provides phase lead to compensate the undamped response. A phase lead of 12° is obtained at 5.3 rad/sec. For the case when the TCSC is used, the frequency response illustrates that the TCSC is more effective than the SVC in overcoming the undamped response because it supplies a larger amount of phase lead, i.e. 22° , to reduce the switch-back characteristic.

From these results, it can be observed that controlling the tie-line impedance yields better damping than by exerting voltage control. System damping of course depends on the amount of tie-line compensation. In order to assess this point, the system dynamic performance with a varying amount of tie-line compensation is shown in Fig. 6-12.

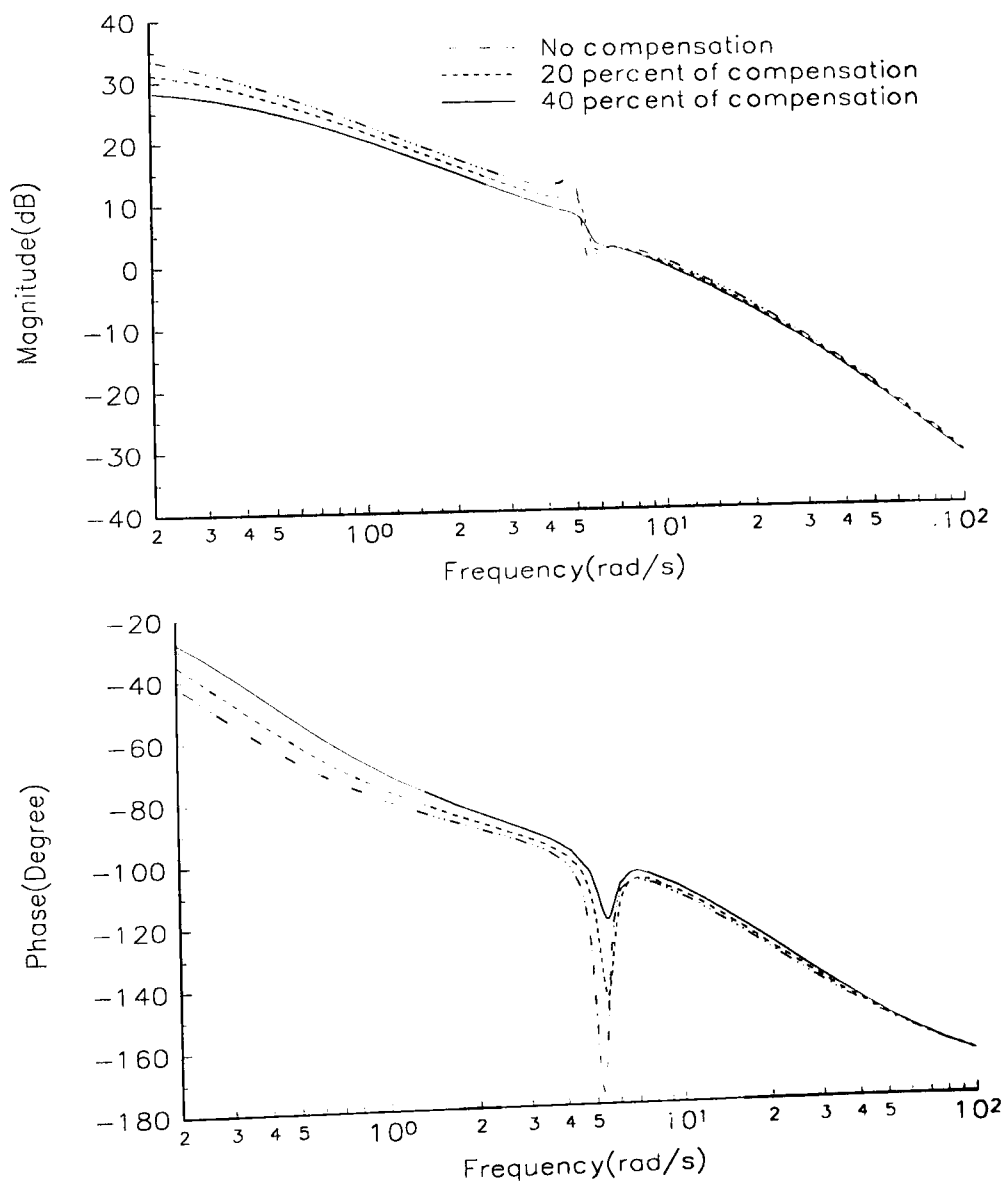


Figure 6-12 Open-loop frequency response between Δe_t and Δe_{err}

Fig. 6-12 shows the poor system damping that exists with no compensation of the tie-line. The use of the TCSC is shown to be very effective in improving the system dynamic performance which, as expected, its effectiveness increases with the compensation level, i.e. from 20 to 40 percent.

6.8 Conclusions

A comprehensive transfer-function block-diagram model of a synchronous generator with a TCSC has been developed in this chapter. This has enabled fundamental studies of dynamic interactions between the TCSC and the synchronous generator to be conducted. These investigations show that the generator dynamic characteristic is significantly influenced by the TCSC's contribution to the d -axis flux linkages. The TCSC yields a very significant improvement to system damping by increasing the damping power component produced, mainly, by the generator's d -axis flux linkages.

Although it is realised that the sphere of application of TCSCs and the SVCs lies on different application areas, for completeness, the system damping capabilities of the TCSC have been compared against those of the SVC with only voltage control loop. As expected, the TCSC's ability to damp system oscillation exceeded that of the SVC. Compensation level studies were also carried out to gain first hand knowledge of the impact that TCSC-based compensation has on damping system oscillations. The results obtained conform with the expectation that the higher the compensation level the more effective the TCSC is in contributing to system damping.

6.9 References

- [1] IEEE/CIGRE, "FACTS Overview", Special Issue, 95-TP-108, IEEE Service Centre, Piscataway, N.J., 1995.
- [2] G. Jancke, N. Fahlen and O. Nerf, "Series Capacitor in Power System", IEEE Transactions on Power Apparatus and Systems, Vol. 94, May 1975, pp. 915-925.
- [3] F. Iliceto and E. Cinieri, "Comparative Analysis of Series and Shunt Compensation Control Schemes for AC Transmission System", IEEE Transactions on Power Apparatus and Systems, Vol. 96, No. 1, November 1977, pp. 1819-1830.
- [4] L. Angquist, B. Lundin and J. Samuelsson, "Power Oscillation Damping Using Controlled Reactive Power Compensation: A Comparison between Series and Shunt Approaches", IEEE Transactions on Power Systems, Vol. 8, No. 2, May 1993, pp. 687-699.
- [5] A. Olwegard, "Improvement of System Stability by Switched Series Capacitors", IEEE Transactions on Power Apparatus and Systems, Vol. 85, No. 2, February 1981, pp. 3933-3939.
- [6] E. V. Larsen, K. Clark, S. S. Miske and J. Urbanek, "Characteristic and Rating Considerations of Thyristor Controlled Series Compensation", IEEE Transactions on Power Delivery, Vol. 9, No. 2, April 1994, pp. 883-841.
- [7] X. R. Chen, N. C. Pahalawaththa, U. D. Annakkage and C. S. Kumble, "Output Feedback TCSC Controllers to Improve Damping of Meshed Multi-machine Power Systems", IEE

- Proceedings on Generation, Transmission and Distribution, Vol. 144, Part C, No. 3, May 1997, pp. 243-248.
- [8] S. G. Helbing and G. G. Karady, "Investigations of an Advanced Form of Series Compensation", IEEE Transactions on Power Delivery, Vol. 9, No. 2, April 1994, pp. 939-947.
- [9] M. Noroozian and G. Andersson, "Power Flow control by use of Controllable Series Components", IEEE Transactions on Power Delivery, Vol. 8, No. 3, July 1993, pp. 12-18.
- [10] P. S. Dolan, J. R. Smith and W. A. Mittelstadt, "A Study of TCSC Optimum Damping Control Parameter for Different Operating Conditions", IEEE Transactions on Power Systems, Vol. 10, No. 4, November 1995, pp. 1972-1978.
- [11] E. V. Larsen, K. Clark, S. S. Miske and J. Urbanek "Characteristic and Rating Considerations of Thyristor Controlled Series Compensation", IEEE Transactions on Power Delivery, Vol. 9, No. 2, April 1994, pp. 883-841.
- [12] X. Zhou and J. Liang, "Overview of Control Schemes for TCSC to Enhance the Stability of Power System", IEE Proceedings on Generation, Transmission and Distribution, Vol. 146, Part C, No. 2, March 1999, pp. 125-130.
- [13] L. Clark and B. Fardanesh, "Thyristor Controlled Series Compensation Application Study-Control Interaction Considerations", IEEE Transactions on Power Delivery, Vol. 10, No. 2, April 1995, pp. 1031-1037.
- [14] G. N. Taranto and D. M. Falcao, "Robust Decentralised Control Design Using Genetic Algorithms in Power System Damping Control", IEE Proceedings on Generation, Transmission and Distribution, Vol. 145, Part C, No. 1, January 1998, pp. 1-6.
- [15] L. Rouco and F. L. Pagola, "An Eigenvalue Sensitivity Approach to Location and Controller Design of Controllable Series Capacitor for Damping the Power System Oscillation", IEEE Transactions on Power Systems, Vol. 12, No. 4, November 1997, pp. 1660-1666.
- [16] M. Noroozian and G. Andersson, "Damping the Power Oscillation by Use of Controllable Components", IEEE Transactions on Power Delivery, Vol. 9, No. 4, October 1994, pp. 2046-2054.
- [17] H. F. Wang and F. J. Swift, "A Unified Model for the Analysis of FACTS Devices in Damping Power System Oscillation Part I: Single-machine Infinite-bus Power System", IEEE Transactions on Power Delivery, Vol. 12, No. 2, April 1997, pp. 491-496.

Chapter 7

Conclusions and Suggestions for Further Work

7.1 General

The FACTS technology is a recent development in power system engineering. FACTS devices have been designed for controlling the main variables of the power system, such as active and reactive powers, voltage magnitude and transmission line impedance [1-3]. Due to their fast speed of operation they also have a crucial role to play in improving the dynamic performance of the power system. This has prompted the urgent need to upgrade most of the power system analysis tools to encompass all plant components of the FACTS family, so that they are made available to power system planning and operation engineers.

This author has been motivated by this challenging task and has carried out research work to provide improved power system models and tools within the context of small-signal stability analysis. The new analytical tools include a subset of the FACTS devices available today, namely SVCs and TCSCs. The main aim was to develop comprehensive models of power systems that fall within the realm of electronically controlled compensation. The resulting SVC and TCSC models have been incorporated into a transfer-function block-diagram framework. This methodology was selected to represent the power system model to gain a fundamental understanding and elucidation of the dynamic interactions taking place between the various power system components. System models have been successfully accomplished for single-machine infinite-bus and multi-machine frameworks, with varying degrees of synchronous generator representation.

The small-signal transfer function of a power system model emanates from the fundamental set of non-linear differential and algebraic equations that describe the behaviour of synchronous generators and FACTS devices. Various orders of generator models are available and they are well documented in the open literature [4-9] but there is still some debate as to what model order is best suited for conducting small-signal stability studies. With the recent need to cater for the inclusion of FACTS-type controllers within the framework for small-signal stability studies, the question of model complexity versus reliability of response has resurfaced. Bearing this in mind, three power system models were developed in this research work, where SVC and TCSC plant components were included. They cater for synchronous generator representation of varying order of complexity. The resulting models are useful for comparing their dynamic responses. These models are useful analytical tools to study the fundamental behaviour of the power system with FACTS devices.

In Chapters 4 and 5, the dynamic responses of the various system models are captured with ease by the well-established frequency response methods. The results clearly reveal the inadequacy of synchronous generator models when only the effect of the generator's main field winding is used, owing to a lack of inherent damping, leading to unreliable system responses. This observation is valid for both single-machine and multi-machine studies. The inclusion of the damper winding in the q -axis substantially improves system damping over the natural frequency range. Moreover, the inclusion of the d -axis damper winding greatly enhances the dynamic performance of the system model over the high frequency range. Therefore, the inclusion of generator damper windings in both the d and q -axis is strongly recommended because it leads to more reliable dynamic responses over a wide frequency range. The end result, when a system model with an adequate level of reliability is used, is more realistic and meaningful small-signal stability analyses .

Referring to Chapters 3 and 6, the block-diagram model has shown to be a physical-oriented, comprehensive way of conducting fundamental studies of the dynamic interactions taking place between synchronous generators and between synchronous generators and FACTS-type devices. Both the SVC and TCSC interact dynamically with the synchronous generator by delivering direct and indirect changes to its output power characteristic. An incremental change in the thyristor's firing angle causes an incremental change in SVC susceptance and TCSC impedance, leading to a direct change in the output power and in flux linkages in the d and q -axis of the generator. A change in flux linkages is amenable to subsequent changes in the generator's output power. In regulated power systems, the influence of both SVCs and TCSCs in the d -axis flux linkages is far greater than in the q -axis flux linkages because AVRs are normally designed with quite high operating gains. The SVC and TCSC contributions to a change in the generator's terminal voltage is enhanced by the AVR, which controls the field voltage to influence the d -axis flux linkages. Consequently, both FACTS devices play an important role in increasing the damping power component generated by the d -axis flux linkage. From the system stability viewpoint, the capability of the TCSC to increase the damping power component of the d -axis flux linkage is far superior to that of the SVC. The reason is that the TCSC is capable of compensating very effectively the tie-line reactance.

Power system models for conducting small-signal stability studies have been used to in Chapters 4 and 5 investigate the generator dynamic performance when enhanced by SVCs. They have been applied to a power system where the effects of poor damping are clearly exhibited at the natural frequency of oscillation, and are due to a weak tie line. The system dynamic performance is clearly improved by incorporating the SVC, increasing damping power. This corresponds to a reduction of the switch-back characteristic. Furthermore, the SVCs yields a very significant improvement of system damping in the high frequency range. Further studies were conducted to assess the benefits

on system damping using various values of gain in the SVC voltage control loop. In agreement with current knowledge, it was observed that the dynamic performance of the system improves as the gain increases. However, it was observed that beyond a certain level, further gain increases did not translate into improved performances.

From the stability viewpoint, SVC voltage control loops on their own were not able to overcome the poor system damping introduced by the electromechanical mode. The voltage control loop was, however, successful in providing dynamic voltage support. Moreover, ways in which SVCs can also contribute to system damping were investigated in Chapter 4, e.g. the use of a PI controller as damping control loop. The additional stabilising signal is derived from the generator speed [10-14]. The damping control loop introduces substantial improvement to system damping by overcoming the switchback characteristic that exists at the natural oscillatory frequency. Consequently, the SVC with damping control loop represents an interesting possibility for providing system damping.

7.2 Suggestions for Further Research Work

Promising developments in the development of comprehensive power system models for FACTS devices have been presented in this thesis. The block-diagram models give rise to the availability of a small-signal stability analysis tool, which should generate further research work in the following areas:

- (I) System models have been evaluated and carefully selected for small-signal stability studies and they should provide a powerful, reliable tool to investigate all the important aspects of dynamic interactions taking place between synchronous generators and electronically controlled compensation. However, parameter tuning for SVC and TCSC was not addressed in this research. It is suggested that in order to improve the system dynamic performance several methodologies should be looked at to address this issue, such as sliding mode [15], reduced-order model analysis [16-17], phase compensation technique [18-19], pole placement technique [20-21], eigen-value assignment [22].
- (II) The multi-machine block-diagram model is a tool that is suitable for the study of power systems of any size. It is a physical-oriented methodology that could be used in conjunction with a variety of techniques currently used in small-signal stability analysis. The conventional eigen-value approach could be used with the state-space equations, from which the block-diagram model is derived, to explore the stability characteristics of the system. Moreover, one very interesting approach that the author would like to propose is the application of the Individual Channel Analysis and Design (ICAD) methodology to the block-diagram model itself. The ICAD methodology has recently been developed in [27-28] to overcome difficulties

in the analysis of multivariable systems (multi-input, multi-output). Since the multi-machine block-diagram representation can be seen as a multi-input, multi-output system then the new application oriented framework, ICAD methodology, should provide an excellent method to enable the application of classical Bode/Nyquist analysis and the application of other multivariable system tools.

(III) A wide range of FACTS and Custom Power devices have been designed for use in the power system. Because these devices provide fast control of many key system parameters, improving the reliability of system operation, further models of FACTS devices should be developed for inclusion in the transfer-function block-diagram framework. The author suggests that the following FACTS components should be modelled as a matter of some priority: the STATCOM and the UPFC.

7.3 References

- [1] IEEE/CIGRE, "FACTS Overview", Special Issue, 95-TP-108, IEEE Service Centre, Piscataway, N.J., 1995.
- [2] N. G. Hingorani, "Flexible AC Transmission System", IEEE Spectrum, Vol. 30 No. 4, April 1993, pp.40-45.
- [3] E. V. Larsen, J. J. Sanchez-Gasca and J. H. Chow, "Concepts for Design of FACTS Controllers to Damp Power Swings", IEEE Transactions on Power Systems, Vol. 10, No. 2, May 1995, pp. 984-955.
- [4] P. M. Anderson, A. A. Fouad, "Power System Control and Stability", The Iowa State University Press, 1986.
- [5] P. Kundur, "Power System Stability", McGraw-Hill Inc, 1993.
- [6] P. Kundur and P. L. Dandeno, "Implementation of Advanced Generator Models into Power System Stability Programs", IEEE Transactions on Power Apparatus and Systems, Vol. PAS-102, No. 7, July 1983, pp. 2047-2054.
- [7] R. D. Dunlop and A. C. Parikh, "Verification of Synchronous Machine Modelling in Stability Studies: Comparative Test of Digital and Physical Scale Model Power System Simulation", IEEE Transactions on Power Apparatus and Systems, Vol. 98, No. 2, March 1979, pp. 369-378.
- [8] IEEE Standard 1110-1991, "IEEE Guide for Synchronous Generator Modelling Practices in Stability Analyses", 1991.
- [9] IEEE Task Force on Definitions and Procedures, "Current Usage and Suggested Practices in

- Power System Stability Simulations for Synchronous Machines”, IEEE Transactions on Energy Conversion, Vol. 1, No. 1, March 1986, pp. 77-93.
- [10] C. H. Cheng and Y. H. Hsu, “Damping of Generator Oscillation Using an Adaptive Static Var Compensator”, IEEE Transactions on Power Systems. Vol. 7, No 2, May 1992, pp. 718-725.
- [11] P. K. Dash, P. C. Panda, A. M. Sharaf and E. F. Hill, “Adaptive Controller for Static Reactive-Power Compensators in Power System”, IEE Proceedings on Generation, Transmission and Distribution, Vol. 134, Part C, No. 3, May 1987, pp. 256-262.
- [12] N. Martins, A. T. Poray and M. E. Coultres, “Determination of Suitable Locations For Power System Stabilisers and Static Var Compensators for Damping Electromechanical Oscillation in Large Scale Power System ”, IEEE Transactions on Power Systems, Vol. 5, No. 4, November 1990, pp. 1455-1469.
- [13] S. C. Kapoor, “Dynamic Stability of Static Compensator: Synchronous Generator Combination”, IEEE Transactions on Power Apparatus and Systems, Vol. 100, No. 4, April 1981, pp. 1694-1720.
- [14] R. J. Koessler, “Dynamic Simulation of Static Var Compensators in Distribution System”, IEEE Transactions on Power Systems, Vol. 7, No 3, August 1992, pp. 1285-1291.
- [15] P. K. Dash, N. C. Sahoo, S. Elangovan and A. C. Liew, “Sliding Mode Control of a Static Var Controller for Synchronous Generator Stabilisation”, International Journal of Electrical Power and Energy System, Vol. 18. No. 1, January 1996, pp. 55-64.
- [16] H. F. Wang, F. J. Swift and M. Li, “Selection of Installing Locations and Feedback Signals of FACTS-based Stabiliser in Multi-machine Power System by Reduced-Order Model Analysis”, IEE Proceedings on Generation, Transmission and Distribution, Vol. 144, Part C, No. 3, May 1997, pp. 263-269.
- [17] H. F. Wang, “Eigen-solution Free Method of Reduced-order Modal Analysis to Select the Installing Locations and Feedback Signals of FACTS-based Stabilisers”, International Journal of Electrical Power and Energy System, Vol. 21, No. 8, May 1999, pp. 547-554.
- [18] H. F. Wang and F. J. Swift, “FACTS-based Stabiliser Designed by the Phase Compensation Method: Part I: Single-machine”, IEE Conference Publication, No. 450, November 1997, Part I, pp. 644-649.
- [19] H. F. Wang and F. J. Swift, “FACTS-based Stabiliser Designed by the Phase Compensation Method: Part II: Multi-machine”, IEE Conference Publication, No. 450, November 1997, Part II, pp. 638-643.

- [20] C. J. Wu and Y.S. Lee, "Damping of Synchronous Generator by Static Reactive Power Compensator with Digital Controller", IEE Proceedings on Generation, Transmission and Distribution, Vol. 138, Part C, No. 5, September 1991, pp. 427-431.
- [21] X. R. Chen, N. C. Pahalawaththa, U. D. Annakkage and C. S. Kumble, "Enhancement of Power System Stability by Using Controlled Series Compensator", International Journal of Electrical Power and Energy System, Vol. 18, No. 7, October 1996, pp. 475-481.
- [22] K. Liou and Y. Hsu, "Damping of Generator Oscillations Using Static VAR Compensator", IEEE Transactions on Aerospace and Electronic Systems, Vol. 22, No. 5, September 1986, pp. 605-617.
- [23] C. H. Cheng, Y. H. Hsu, "Damping of Generator Oscillation Using an Adaptive Static Var Compensator", IEEE Transactions on Power Systems", Vol. 7, No 2, May 1992, pp. 718-725.
- [24] P. K. Dash, S. Mishra and A. C. Liew, "Fuzzy-Logic Based VAR Stabiliser for Power System Control", IEE Proceedings on Generation, Transmission and Distribution, Vol. 142, Part C, No. 6, November 1995, pp. 618-624.
- [25] H. M. A. Rahim and S. G. A. Nassimi, "Synchronous Generator Damping Enhancement through Co-ordinated Control of Exciter and SVC", IEE Proceedings on Generation, Transmission and Distribution, Vol. 143, Part C, No. 2, March 1996, pp. 211-217.
- [26] A. C. H. Cheng and Y.Y. Hsu, "Application of a Power System Stabiliser and a Static VAR Controller to a Multimachine Power System", IEE Proceedings on Generation, Transmission and Distribution, Vol. 137, Part C, No. 1, January 1990, pp. 8-12.
- [27] W. E. Leithead and J. O'Reilly, " m -Input m -Output feedback control by ICAD: part 1: Structural issues", International Journal of Control, 1992, Vol. 56, pp. 1347-1397.
- [28] Z. Fadlalmoula, S. S. Robertson, J. O'Reilly and W. E. Leithead, "Individual Channel Analysis of the Turbo-generator With Power System Stabiliser" International Journal of Control, Vol. 69, No. 2, January 1998, pp. 175-202.

Appendix A

Derivation of the Small-Signal Transfer-Function Block Diagram Models of the Synchronous Generator- SVC System

This appendix derives the transfer function block diagram models of the synchronous generator-SVC system shown in Fig. 3-1 of Chapter 3. With reference to Table 3-1, various orders of salient-pole generator models are used to establish the block diagram models for Models 1-3. The linearisation process for each model, in decreasing order of complexity, is presented below:

A-1 Model 1

The phasor diagram of the system under study may be drawn as shown in Fig. A-1.

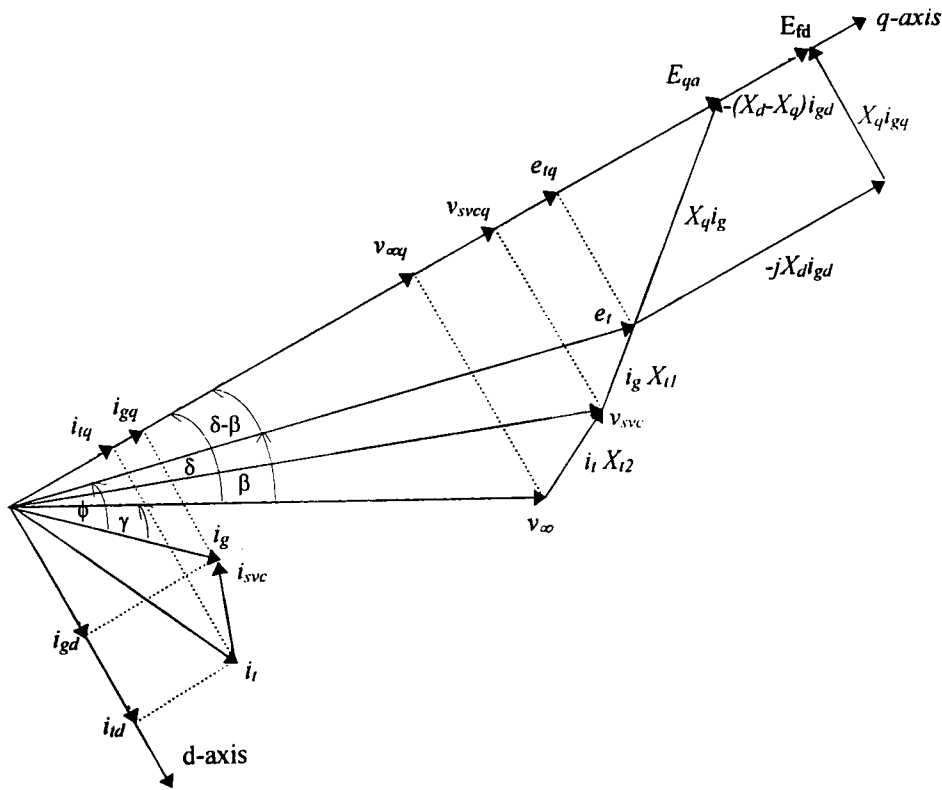


Figure A-1 Vector diagram of the synchronous generator-SVC system

From the vector diagram, the generator rotor position is taken as the reference vector, hence,

$$\Delta v_{\infty q} = v_{\infty} \cos \delta \quad (\text{A-1})$$

$$\Delta v_{\infty d} = v_{\infty} \sin \delta \quad (\text{A-2})$$

For small variations,

$$\Delta v_{\infty q} = -v_{\infty o} \sin \delta_o \Delta \delta = -v_{\infty do} \Delta \delta \quad (\text{A-3})$$

$$\Delta v_{\infty d} = v_{\infty o} \cos \delta_o \Delta \delta = v_{\infty qo} \Delta \delta \quad (\text{A-4})$$

From Fig. A-1,

$$\bar{i}_g = \bar{i}_{svc} + \bar{i}_t \quad (\text{A-5})$$

Separating into real and imaginary parts, (A-5) can be expressed as,

$$i_{gd} = i_{svcd} + i_{td} \quad (\text{A-6})$$

$$i_{gq} = i_{svcq} + i_{tq} \quad (\text{A-7})$$

For small variations,

$$\Delta i_{gd} = \Delta i_{svcd} + \Delta i_{td} \quad (\text{A-8})$$

$$\Delta i_{gq} = \Delta i_{svcq} + \Delta i_{tq} \quad (\text{A-9})$$

Alternatively, (A-5) can be re-written as,

$$\bar{i}_g = \bar{Y}_{svc} \bar{v}_{svc} + \frac{(\bar{v}_{svc} - \bar{v}_{\infty})}{jX_{l2}} \quad (\text{A-10})$$

where

$$\bar{i}_{svc} = \bar{Y}_{svc} \bar{v}_{svc} \quad (\text{A-11})$$

$$\bar{Y}_{svc} = j(B_C - B_L(\alpha)) = jB_{svc} \quad (\text{A-12})$$

It must be noted that for a given operating condition $B_{svco} = (B_C - B_{Lo}(\alpha))$.

From 2-30 and 2-31 in Chapter 2,

$$B_L(\alpha) = \frac{2}{\pi X_L} \left\{ (\pi - \alpha) + \frac{1}{2} \sin(2\alpha) \right\} \quad (\text{A-13})$$

$$B_C = 2\pi fC \quad (\text{A-14})$$

For small variations,

$$\Delta B_{svc} = -\Delta B_L(\alpha) = F(\alpha)\Delta\alpha \quad (\text{A-15})$$

where

$$F(\alpha) = \frac{2}{\pi X_L} - \frac{2}{\pi X_L} \cos(2\alpha) \quad (\text{A-16})$$

It is noted that $F(\alpha)$ is a non-linear component due to the term $\cos(2\alpha)$. This non-linearity, however, is cancelled out by an ideal, linearised block in the SVC model. Therefore, $F(\alpha)$ can be assumed to have a constant value of $2/(\pi X_L)$.

From (A-11), it can be separated into real and imaginary parts as follows,

$$i_{svcd} = B_{svc} v_{svcq} \quad (\text{A-17})$$

$$i_{svcq} = -B_{svc} v_{svcd} \quad (\text{A-18})$$

Applying a small perturbation, (A-17) and (A-18) can be expressed as,

$$\Delta i_{svcd} = B_{svco} \Delta v_{svcq} + v_{svcqo} \Delta B_{svc} \quad (\text{A-19})$$

$$\Delta i_{svcq} = -(B_{svco} \Delta v_{svcd} + v_{svcdo} \Delta B_{svc}) \quad (\text{A-20})$$

From the vector diagram in Fig. A-1, an expression for \bar{I}_g can be obtained as,

$$\bar{I}_g = \frac{\bar{e}_t - \bar{v}_{svc}}{jX_{t1}} \quad (\text{A-21})$$

Separating into real and imaginary parts,

$$i_{gd} X_{t1} = e_{tq} - v_{svcq} \quad (\text{A-22})$$

$$i_{gq} X_{t1} = v_{svcd} - e_{td} \quad (\text{A-23})$$

From the vector diagram in Fig. A-1, an expression for \bar{I}_t can be obtained as,

$$\bar{I}_t = \frac{\bar{v}_{svc} - \bar{v}_{\infty}}{jX_{t2}} \quad (\text{A-24})$$

Separating into real and imaginary parts,

$$i_{td} X_{t2} = v_{svcq} - v_{\infty q} \quad (\text{A-25})$$

$$i_{tq} X_{t2} = v_{\infty d} - v_{svcd} \quad (\text{A-26})$$

Re-arranging (A-22) by making use of (A-6) and (A-25) yields,

$$e_{tq} = i_{gd} (X_{t1} + X_{t2}) - i_{svcd} X_{t2} + v_{\infty q} \quad (\text{A-27})$$

Substituting the stator voltage equation (2-9), in Chapter 2, into (A-27) gives,

$$i_{gd} = \left[\frac{E_q'' - v_{\infty q} + i_{svcd} X_{t2}}{X_d'' + X_{t1} + X_{t2}} \right] \quad (\text{A-28})$$

Re-arranging (A-23) by making use of (A-7) and (A-26) yields,

$$e_{td} = v_{\infty d} - i_{gq} (X_{t1} + X_{t2}) + i_{svcq} X_{t2} \quad (\text{A-29})$$

Substituting the stator voltage equation (2-8), in Chapter 2, into (A-29) gives,

$$i_{gq} = \left[\frac{v_{\infty d} - E_d'' + i_{svcq} X_{t2}}{X_q'' + X_{t1} + X_{t2}} \right] \quad (\text{A-30})$$

Separating (A-10) into real and imaginary parts,

$$i_{gq} X_{t2} = v_{\infty d} - (1 - X_{t2} B_{svc}) v_{svcd} \quad (\text{A-31})$$

$$i_{gd} X_{t2} = (1 - X_{t2} B_{svc}) v_{svcq} - v_{\infty q} \quad (\text{A-32})$$

Substituting (A-22) into (2-9) gives,

$$i_{gd} = \left[\frac{E_q'' - v_{svcq}}{X_d'' + X_{t1}} \right] \quad (\text{A-33})$$

Substituting (A-33) into (A-32), linearising and incorporating (A-3) gives,

$$\Delta v_{svcq} = \left[\frac{X_{t2}}{\Delta_d''} \right] \Delta E_q'' - \left[\frac{(X_d'' + X_{t1})v_{\infty do}}{\Delta_d''} \right] \Delta \delta + \left[\frac{X_{t2}(X_d'' + X_{t1})v_{svcqo}}{\Delta_d''} \right] \Delta B_{svc} \quad (\text{A-34})$$

where

$$\Delta_d'' = X_{t2} + (X_d'' + X_{t1})(1 - X_{t2}B_{svco}) \quad (\text{A-35})$$

Substituting (A-23) into (2-8) gives,

$$i_{gq} = \left[\frac{v_{svcd} - E_d''}{X_q'' + X_{t1}} \right] \quad (\text{A-36})$$

Substituting (A-36) into (A-31), linearising and incorporating (A-4) gives,

$$\Delta v_{svcd} = \left[\frac{X_{t2}}{\Delta_q''} \right] \Delta E_d'' + \left[\frac{(X_q'' + X_{t1})v_{\infty qo}}{\Delta_q''} \right] \Delta \delta + \left[\frac{X_{t2}(X_q'' + X_{t1})v_{svcdo}}{\Delta_q''} \right] \Delta B_{svc} \quad (\text{A-37})$$

where

$$\Delta_q'' = X_{t2} + (X_q'' + X_{t1})(1 - X_{t2}B_{svco}) \quad (\text{A-38})$$

Re-arranging (A-28) by making use of (A-19) and (A-34) gives,

$$\Delta i_{gd} = \left[\frac{1 - X_{t2}B_{svco}}{\Delta_d''} \right] \Delta E_q'' + \left[\frac{v_{\infty do}}{\Delta_d''} \right] \Delta \delta - \left[\frac{X_{t2}v_{svcqo}}{\Delta_d''} \right] \Delta B_{svc} \quad (\text{A-39})$$

Re-arranging (A-30) by making use of (A-20) and (A-37) gives,

$$\Delta i_{gq} = \left[\frac{v_{\infty qo}}{\Delta_q''} \right] \Delta \delta - \left[\frac{1 - X_{t2}B_{svco}}{\Delta_q''} \right] \Delta E_d'' + \left[\frac{X_{t2}v_{svcdo}}{\Delta_q''} \right] \Delta B_{svc} \quad (\text{A-40})$$

D-axis Flux Linkage Voltage Equation:

Transient Voltage Equation

Transforming the transient voltage equation (2-6) into the S domain, and for small variations,

$$(1 + \tau'_{do}s)\Delta E_q' = \Delta E_{fd} - (X_d - X_d')\Delta i_{gd} \quad (\text{A-41})$$

Re-arranging (A-41) by making use of (A-15) and (A-39) gives,

$$\Delta E_q' = \frac{1}{1 + \tau'_{do}s} (\Delta E_{fd} - C_1 \Delta E_q'' - C_2 \Delta \delta + C_3 \Delta \alpha) \quad (\text{A-42})$$

where

$$C_1 = \left[\frac{(X_d - X_d')(1 - X_{t2}B_{svco})}{\Delta_d''} \right] \quad (\text{A-43})$$

$$C_2 = \left[\frac{(X_d - X_d')v_{\infty do}}{\Delta_d''} \right] \quad (\text{A-44})$$

$$C_3 = \frac{2}{\pi X_L} \left[\frac{X_{t2}(X_d - X'_d)v_{svco}}{\Delta''_d} \right] \quad (\text{A-45})$$

Subtransient Voltage Equation:

Transforming the subtransient voltage equation (2-10) into the S domain, and for small variations,

$$(1 + \tau''_{do}s)\Delta E''_q = C_4\Delta E_{fd} - C_5\Delta i_{gd} + C_6\Delta E'_q \quad (\text{A-46})$$

where

$$C_4 = \left[\frac{\tau''_{do}}{\tau'_{do}} \right] \quad (\text{A-47})$$

$$C_5 = \left[(X'_d - X''_d) + \frac{\tau''_{do}}{\tau'_{do}}(X_d - X'_d) \right] \quad (\text{A-48})$$

$$C_6 = \left[1 - \frac{\tau''_{do}}{\tau'_{do}} \right] \quad (\text{A-49})$$

Re-arranging (A-46) by making use of (A-15), (A-39) and (A-42) gives,

$$C_7(s)\Delta E''_q = C_8(s)\Delta E_{fd} - C_9(s)\Delta\delta + C_{10}(s)\Delta\alpha \quad (\text{A-50})$$

where

$$C_7(s) = \left[\frac{\Delta_d + \{ \tau'_{do}\Delta'_d + \tau''_{do}(\Delta''_d + (X_d - X'_d)(1 - X_{t2}B_{svco})) \} s + \{ \tau'_{do}\tau''_{do}\Delta''_d \} s^2}{\Delta''_d(1 + \tau'_{do}s)} \right] \quad (\text{A-51})$$

$$\Delta_d = X_{t2} + (X_d + X_{t1})(1 - X_{t2}B_{svco}) \quad (\text{A-52})$$

$$\Delta'_d = X_{t2} + (X'_d + X_{t1})(1 - X_{t2}B_{svco}) \quad (\text{A-53})$$

$$C_8(s) = \left[\frac{1 + \tau''_{do}s}{1 + \tau'_{do}s} \right] \quad (\text{A-54})$$

$$C_9(s) = v_{\infty do} \left[\frac{(X_d - X''_d) + \{ \tau'_{do}(X'_d - X''_d) + \tau''_{do}(X_d - X'_d) \} s}{\Delta''_d(1 + \tau'_{do}s)} \right] \quad (\text{A-55})$$

$$C_{10}(s) = \frac{2X_{t2}v_{svco}}{\pi X_L} \left[\frac{(X_d - X''_d) + \{ \tau'_{do}(X'_d - X''_d) + \tau''_{do}(X_d - X'_d) \} s}{\Delta''_d(1 + \tau'_{do}s)} \right] \quad (\text{A-56})$$

or

$$\Delta E''_q = g_3(s)\Delta E_{fd} - g_4(s)\Delta\delta + g_{svco}(s)\Delta\alpha \quad (\text{A-57})$$

where

$$g_3(s) = \left[\frac{\Delta''_d(1 + \tau''_{do}s)}{\Delta_d + \{ \tau'_{do}\Delta'_d + \tau''_{do}(\Delta''_d + (X_d - X'_d)(1 - X_{t2}B_{svco})) \} s + \{ \tau'_{do}\tau''_{do}\Delta''_d \} s^2} \right] \quad (\text{A-58})$$

$$g_4(s) = \left[\frac{v_{\infty do} \left((X_d - X''_d) + \{ \tau'_{do}(X'_d - X''_d) + \tau''_{do}(X_d - X'_d) \} s \right)}{\Delta_d + \{ \tau'_{do}\Delta'_d + \tau''_{do}(\Delta''_d + (X_d - X'_d)(1 - X_{t2}B_{svco})) \} s + \{ \tau'_{do}\tau''_{do}\Delta''_d \} s^2} \right] \quad (\text{A-59})$$

$$g_{svc2}(s) = \frac{2}{\pi X_L} \left[\frac{X_{t2} v_{svcqo} \left((X_d - X_d'') + \{ \tau'_{do} (X_d' - X_d'') + \tau''_{do} (X_d - X_d') \} s \right)}{\Delta_d + \{ \tau'_{do} \Delta_d' + \tau''_{do} (\Delta_d'' + (X_d - X_d')(1 - X_{t2} B_{svco})) \} s + \{ \tau'_{do} \tau''_{do} \Delta_d'' \} s^2} \right] \quad (A-60)$$

Q-axis Flux Linkage Voltage Equation:

Transforming the subtransient voltage equation (2-11) into the S domain, and for small variations,

$$(1 + \tau''_{qo} s) \Delta E_d'' = (X_q - X_q'') \Delta i_{gq} \quad (A-61)$$

Re-arranging (A-61) by making use of (A-15) and (A-40),

$$\Delta E_d'' = g_{4d}(s) \Delta \delta + g_{svc2d}(s) \Delta \alpha \quad (A-62)$$

or

$$\Delta E_d'' = \frac{1}{1 + \tau''_q s} (K_{4d} \Delta \delta + K_{svc2d} \Delta \alpha) \quad (A-63)$$

where

$$g_{4d}(s) = \left[\frac{K_{4d}}{(1 + \tau''_q s)} \right] \quad (A-64)$$

$$g_{svc2d}(s) = \left[\frac{K_{svc2d}}{(1 + \tau''_q s)} \right] \quad (A-65)$$

$$K_{4d} = \left[\frac{(X_q - X_q'') v_{\infty qo}}{\Delta_q} \right] \quad (A-66)$$

$$\Delta_q = X_{t2} + (X_q + X_{t1})(1 - X_{t2} B_{svco}) \quad (A-67)$$

$$K_{svc2d} = \frac{2}{\pi X_L} \left[\frac{X_{t2} (X_q - X_q'') v_{svcdo}}{\Delta_q} \right] \quad (A-68)$$

$$\tau''_q = \left[\frac{\Delta_q''}{\Delta_q} \tau''_{qo} \right] \quad (A-69)$$

Generator Terminal Voltage Equation:

The generator terminal voltage in equation (2-2) can be expressed in terms of d and q -axis components, as shown in (A-70),

$$e_t^2 = e_{td}^2 + e_{tq}^2 \quad (A-70)$$

Applying a small perturbation,

$$\Delta e_t = \frac{e_{tdo}}{e_{to}} \Delta e_{td} + \frac{e_{tqo}}{e_{to}} \Delta e_{tq} \quad (A-71)$$

Substituting (A-39) into (2-9) gives,

$$\Delta e_{tq} = \left[\frac{X_{t2} + X_{t1}(1 - X_{t2} B_{svco})}{\Delta_d''} \right] \Delta E_q'' - \left[\frac{X_d' v_{\infty do}}{\Delta_d''} \right] \Delta \delta + \left[\frac{X_d'' X_{t2} v_{svcqo}}{\Delta_d''} \right] \Delta B_{svc} \quad (A-72)$$

Substituting (A-40) into (2-8) gives,

$$\Delta e_{td} = \left[\frac{X_{t2} + X_{t1}(1 - X_{t2}B_{svco})}{\Delta_q''} \right] \Delta E_d'' + \left[\frac{X_q'' v_{\infty qo}}{\Delta_q''} \right] \Delta \delta + \left[\frac{X_q'' X_{t2} v_{svcd o}}{\Delta_q''} \right] \Delta B_{svc} \quad (\text{A-73})$$

Re-arranging (A-71) by making use of (A-15), (A-72), and (A-73) yields,

$$\Delta e_t = K_5 \Delta \delta + K_6 \Delta E_q'' + K_{6d} \Delta E_d'' + K_{svc3} \Delta \alpha \quad (\text{A-74})$$

where

$$K_5 = \left[\frac{e_{tdo}}{e_{to}} \cdot \frac{X_q'' v_{\infty qo}}{\Delta_q''} - \frac{e_{tqo}}{e_{to}} \cdot \frac{X_d'' v_{\infty do}}{\Delta_d''} \right] \quad (\text{A-75})$$

$$K_6 = \left[\frac{e_{tqo}}{e_{to}} \cdot \frac{X_{t2} + X_{t1}(1 - X_{t2}B_{svco})}{\Delta_d''} \right] \quad (\text{A-76})$$

$$K_{6d} = \left[\frac{e_{tdo}}{e_{to}} \cdot \frac{X_{t2} + X_{t1}(1 - X_{t2}B_{svco})}{\Delta_q''} \right] \quad (\text{A-77})$$

$$K_{svc3} = \frac{2}{\pi X_L} \left[\frac{e_{tdo}}{e_{to}} \cdot \frac{X_{t2} X_q'' v_{svcd o}}{\Delta_q''} + \frac{e_{tqo}}{e_{to}} \cdot \frac{X_{t2} X_d'' v_{svcq o}}{\Delta_d''} \right] \quad (\text{A-78})$$

SVC Terminal Voltage Equation:

Similarly to the generator terminal voltage, the SVC terminal voltage can be expressed in terms of d and q -axis components,

$$v_{svc}^2 = v_{svcd}^2 + v_{svcq}^2 \quad (\text{A-79})$$

Applying a small perturbation, it can be expressed as (A-80),

$$\Delta e_t = \frac{e_{tdo}}{e_{to}} \Delta e_{td} + \frac{e_{tqo}}{e_{to}} \Delta e_{tq} \quad (\text{A-80})$$

Re-arranging (A-80) by making use of (A-15) and (A-34), (A-37) yields,

$$\Delta V_{svc} = K_{5n} \Delta \delta + K_{6n} \Delta E_q'' + K_{6dn} \Delta E_d'' + K_{svc3n} \Delta \alpha \quad (\text{A-81})$$

where

$$K_{5n} = \left[\frac{v_{svcd o}}{v_{svco}} \cdot \frac{(X_q'' + X_{t1}) v_{\infty qo}}{\Delta_q''} - \frac{v_{svcq o}}{v_{svco}} \cdot \frac{(X_d'' + X_{t1}) v_{\infty do}}{\Delta_d''} \right] \quad (\text{A-82})$$

$$K_{6n} = \left[\frac{v_{svcq o}}{v_{svco}} \cdot \frac{X_{t2}}{\Delta_d''} \right] \quad (\text{A-83})$$

$$K_{6dn} = \left[\frac{v_{svcd o}}{v_{svco}} \cdot \frac{X_{t2}}{\Delta_q''} \right] \quad (\text{A-84})$$

$$K_{svc3n} = \frac{2}{\pi X_L} \left[\frac{v_{svcd o}^2}{v_{svco}} \cdot \frac{X_{t2} (X_q'' + X_{t1})}{\Delta_q''} + \frac{v_{svcq o}^2}{v_{svco}} \cdot \frac{X_{t2} (X_d'' + X_{t1})}{\Delta_d''} \right] \quad (\text{A-85})$$

Electrical Power Equation:

The synchronous generator active power in equation (2-20) can be expressed as,

$$P_e = e_{td}i_{gd} + e_{tq}i_{gq} \quad (\text{A-86})$$

or

$$P_e = v_{\infty d}i_{td} + v_{\infty q}i_{tq} \quad (\text{A-87})$$

For small perturbations, the electrical power in (A-87) can be expressed as,

$$\Delta P_e = v_{\infty do}\Delta i_{td} + i_{tdo}\Delta v_{\infty d} + v_{\infty qo}\Delta i_{tq} + i_{tqo}\Delta v_{\infty q} \quad (\text{A-88})$$

Re-arranging (A-8) by making use of (A-19), (A-34) and (A-39), gives,

$$\Delta i_{td} = \left[\frac{1}{\Delta_d''} \right] \Delta E_q'' + \left[\frac{(1 - (X_d'' + X_{t1})B_{svco})v_{\infty do}}{\Delta_d''} \right] \Delta \delta + \left[\frac{(X_d'' + X_{t1})v_{svco}}{\Delta_d''} \right] \Delta B_{svc} \quad (\text{A-89})$$

Re-arranging (A-9) by making use of (A-20), (A-37) and (A-49) gives,

$$\Delta i_{tq} = \left[\frac{(1 - (X_q'' + X_{t1})B_{svco})v_{\infty qo}}{\Delta_q''} \right] \Delta \delta - \left[\frac{1}{\Delta_q''} \right] \Delta E_d'' - \left[\frac{(X_q'' + X_{t1})v_{svco}}{\Delta_q''} \right] \Delta B_{svc} \quad (\text{A-90})$$

Re-arranging (A-88) by making use of (A-15), (A-89) and (A-90) yields,

$$\Delta P_e = K_1 \Delta \delta + K_2 \Delta E_q'' - K_{2d} \Delta E_d'' + K_{svcl} \Delta \alpha \quad (\text{A-91})$$

where

$$K_1 = \left[\frac{(1 - (X_{t1} + X_d'')B_{svco})v_{\infty do}^2}{\Delta_d''} + \frac{(1 - (X_{t1} + X_q'')B_{svco})v_{\infty qo}^2}{\Delta_q''} + i_{tdo}v_{\infty qo} - i_{tqo}v_{\infty do} \right] \quad (\text{A-92})$$

$$K_2 = \left[\frac{v_{\infty do}}{\Delta_d''} \right] \quad (\text{A-93})$$

$$K_{2d} = \left[\frac{v_{\infty qo}}{\Delta_q''} \right] \quad (\text{A-94})$$

$$K_{svcl} = \frac{2}{\pi X_L} \left[\frac{(X_{t1} + X_d'')v_{\infty do}v_{svco}}{\Delta_d''} - \frac{(X_{t1} + X_q'')v_{\infty qo}v_{svco}}{\Delta_q''} \right] \quad (\text{A-95})$$

Swing equation:

Transforming the swing equation (2-21) and (2-22) into S domain, for small variations,

$$\Delta \omega = \frac{1}{2Hs} (\Delta P_m - \Delta P_e - D\Delta \omega) \quad (\text{A-96})$$

$$\Delta \delta = \frac{\omega_o}{s} \Delta \omega \quad (\text{A-97})$$

The transfer-function block diagram model of the synchronous generator-SVC system for Model 1 is shown in Fig. A-2. It is realised by combining (A-57), (A-63), (A-74), (A-81), (A-91), (A-96) and (A-97).

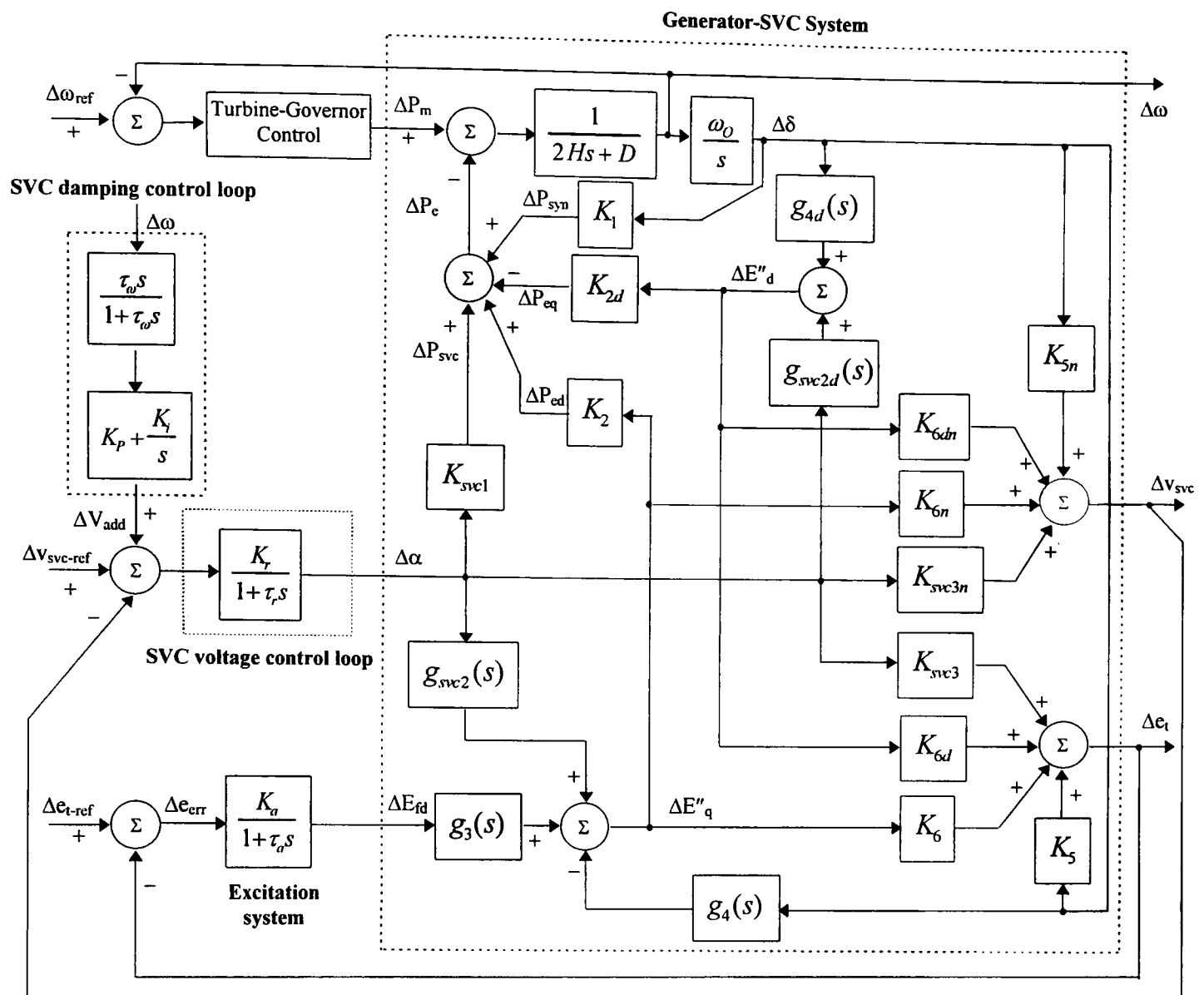


Figure A-2 Block-diagram model of synchronous generator-SVC system with Model 1

A-2 Model 2

Substituting (2-4) into (A-27) gives,

$$i_{gd} = \left[\frac{E'_q - v_{\infty q} + i_{svcd} X_{t2}}{X'_d + X_{t1} + X_{t2}} \right] \quad (A-98)$$

Substituting (A-22) into (2-4) gives,

$$i_{gd} = \left[\frac{E'_q - v_{svcq}}{X'_d + X_{t1}} \right] \quad (A-99)$$

Substituting (A-99) into (A-32), linearising and incorporating (A-4) gives,

$$\Delta v_{svcq} = \left[\frac{X_{t2}}{\Delta'_d} \right] \Delta E'_q - \left[\frac{(X'_d + X_{t1}) v_{\infty do}}{\Delta'_d} \right] \Delta\delta + \left[\frac{X_{t2} (X'_d + X_{t1}) v_{svcqo}}{\Delta'_d} \right] \Delta B_{svc} \quad (A-100)$$

Re-arranging (A-98) by making use of (A-19) and (A-100) gives,

$$\Delta i_{gd} = \left[\frac{(1 - X_{t2} B_{svco})}{\Delta'_d} \right] \Delta E'_q + \left[\frac{v_{\infty do}}{\Delta'_d} \right] \Delta\delta - \left[\frac{X_{t2} v_{svcqo}}{\Delta'_d} \right] \Delta B_{svc} \quad (A-101)$$

D-axis Flux Linkage Voltage Equation:

Re-arranging (A-41) by making use of (A-15) and (A-101) gives,

$$\Delta E'_q = g_3(s)\Delta E_{fd} - g_4(s)\Delta\delta + g_{svc2}(s)\Delta\alpha \quad (\text{A-102})$$

or

$$\Delta E'_q = \frac{K_3}{1 + K_3\tau'_{do}s} (\Delta E_{fd} - K_4\Delta\delta + K_{svc2}\Delta\alpha) \quad (\text{A-103})$$

where

$$g_3(s) = \left[\frac{K_3}{1 + K_3\tau'_{do}s} \right] \quad (\text{A-104})$$

$$g_4(s) = \left[\frac{K_3K_4}{1 + K_3\tau'_{do}s} \right] \quad (\text{A-105})$$

$$g_{svc2}(s) = \left[\frac{K_3K_{svc2}}{1 + K_3\tau'_{do}s} \right] \quad (\text{A-106})$$

$$K_3 = \left[\frac{\Delta'_d}{\Delta_d} \right] \quad (\text{A-107})$$

$$K_4 = \left[\frac{(X_d - X'_d)v_{\infty do}}{\Delta'_d} \right] \quad (\text{A-108})$$

$$K_{svc2} = \frac{2}{\pi X_L} \left[\frac{X_{t2}(X_d - X'_d)v_{svcqo}}{\Delta'_d} \right] \quad (\text{A-109})$$

Generator Terminal Voltage Equation:

Substituting (A-101) into (2-4) gives,

$$\Delta e_{tq} = \left[\frac{X_{t2} + X_{t1}(1 - X_{t2}B_{svco})}{\Delta'_d} \right] \Delta E'_q - \left[\frac{X'_d v_{\infty do}}{\Delta'_d} \right] \Delta\delta + \left[\frac{X'_d X_{t2} v_{svcqo}}{\Delta'_d} \right] \Delta B_{svc} \quad (\text{A-110})$$

Re-arranging (A-71) by making use of (A-15), (A-73) and (A-110) gives,

$$\Delta e_t = K_5\Delta\delta + K_6\Delta E'_q + K_{6d}\Delta E''_d + K_{svc3}\Delta\alpha \quad (\text{A-111})$$

where

$$K_5 = \left[\frac{e_{tdo}}{e_{tqo}} \cdot \frac{X''_q v_{\infty qo}}{\Delta''_q} - \frac{e_{tqo}}{e_{tdo}} \cdot \frac{X'_d v_{\infty do}}{\Delta'_d} \right] \quad (\text{A-112})$$

$$K_6 = \left[\frac{e_{tqo}}{e_{tdo}} \cdot \frac{X_{t2} + X_{t1}(1 - X_{t2}B_{svco})}{\Delta'_d} \right] \quad (\text{A-113})$$

$$K_{6d} = \left[\frac{e_{tdo}}{e_{tqo}} \cdot \frac{X_{t2} + X_{t1}(1 - X_{t2}B_{svco})}{\Delta''_q} \right] \quad (\text{A-114})$$

$$K_{svc3} = \frac{2}{\pi X_L} \left[\frac{e_{tdo}}{e_{tqo}} \cdot \frac{X_{t2} X''_q v_{svcd o}}{\Delta''_q} + \frac{e_{tqo}}{e_{tdo}} \cdot \frac{X_{t2} X'_d v_{svcqo}}{\Delta'_d} \right] \quad (\text{A-115})$$

SVC Terminal Voltage Equation:

Re-arranging (A-80) by making use of (A-15), (A-37) and (A-100) gives,

$$\Delta v_{svc} = K_{5n} \Delta \delta + K_{6n} \Delta E'_q + K_{6dn} \Delta E''_d + K_{svc3n} \Delta \alpha \quad (\text{A-116})$$

where

$$K_{5n} = \left[\frac{v_{svcd0}}{v_{svco}} \cdot \frac{(X''_q + X_{t1})v_{\infty q0}}{\Delta''_q} - \frac{v_{svcq0}}{v_{svco}} \cdot \frac{(X'_d + X_{t1})v_{\infty d0}}{\Delta'_d} \right] \quad (\text{A-117})$$

$$K_{6n} = \left[\frac{v_{svcq0}}{v_{svco}} \cdot \frac{X_{t2}}{\Delta'_d} \right] \quad (\text{A-118})$$

$$K_{6dn} = \left[\frac{v_{svcd0}}{v_{svco}} \cdot \frac{X_{t2}}{\Delta''_q} \right] \quad (\text{A-119})$$

$$K_{svc3n} = \frac{2}{\pi X_L} \left[\frac{v_{svcd0}^2}{v_{svco}} \cdot \frac{X_{t2}(X''_q + X_{t1})}{\Delta''_q} + \frac{v_{svcq0}^2}{v_{svco}} \cdot \frac{X_{t2}(X'_d + X_{t1})}{\Delta'_d} \right] \quad (\text{A-120})$$

Electrical Power Equation:

Re-arranging (A-8) by making use of (A-19), (A-100) and (A-101) gives,

$$\Delta i_{td} = \left[\frac{1}{\Delta'_d} \right] \Delta E'_q + \left[\frac{(1 - (X'_d + X_{t1})B_{svco})v_{\infty d0}}{\Delta'_d} \right] \Delta \delta + \left[\frac{(X'_d + X_{t1})v_{svcq0}}{\Delta'_d} \right] \Delta B_{svc} \quad (\text{A-121})$$

Re-arranging (A-88) by making use of (A-15), (A-90) and (A-121) gives,

$$\Delta P_e = K_1 \Delta \delta + K_2 \Delta E'_q - K_{2d} \Delta E''_d + K_{svc1} \Delta \alpha \quad (\text{A-122})$$

where

$$K_1 = \left[\frac{(1 - (X_{t1} + X'_d)B_{svco})v_{\infty d0}^2}{\Delta'_d} + \frac{(1 - (X_{t1} + X''_q)B_{svco})v_{\infty q0}^2}{\Delta''_q} + i_{td0}v_{\infty q0} - i_{tq0}v_{\infty d0} \right] \quad (\text{A-123})$$

$$K_2 = \left[\frac{v_{\infty d0}}{\Delta'_d} \right] \quad (\text{A-124})$$

$$K_{2d} = \left[\frac{v_{\infty q0}}{\Delta''_q} \right] \quad (\text{A-125})$$

$$K_{svc1} = \frac{2}{\pi X_L} \left[\frac{(X'_d + X_{t1})v_{svcq0}v_{\infty d0}}{\Delta'_d} - \frac{(X''_q + X_{t1})v_{svcd0}v_{\infty q0}}{\Delta''_q} \right] \quad (\text{A-126})$$

The transfer-function block diagram model of the synchronous generator-SVC system for Model 2 is shown in Fig. A-3. It is realised by combining (A-63), (A-96), (A-97), (A-103), (A-111), (A-116) and (A-122).

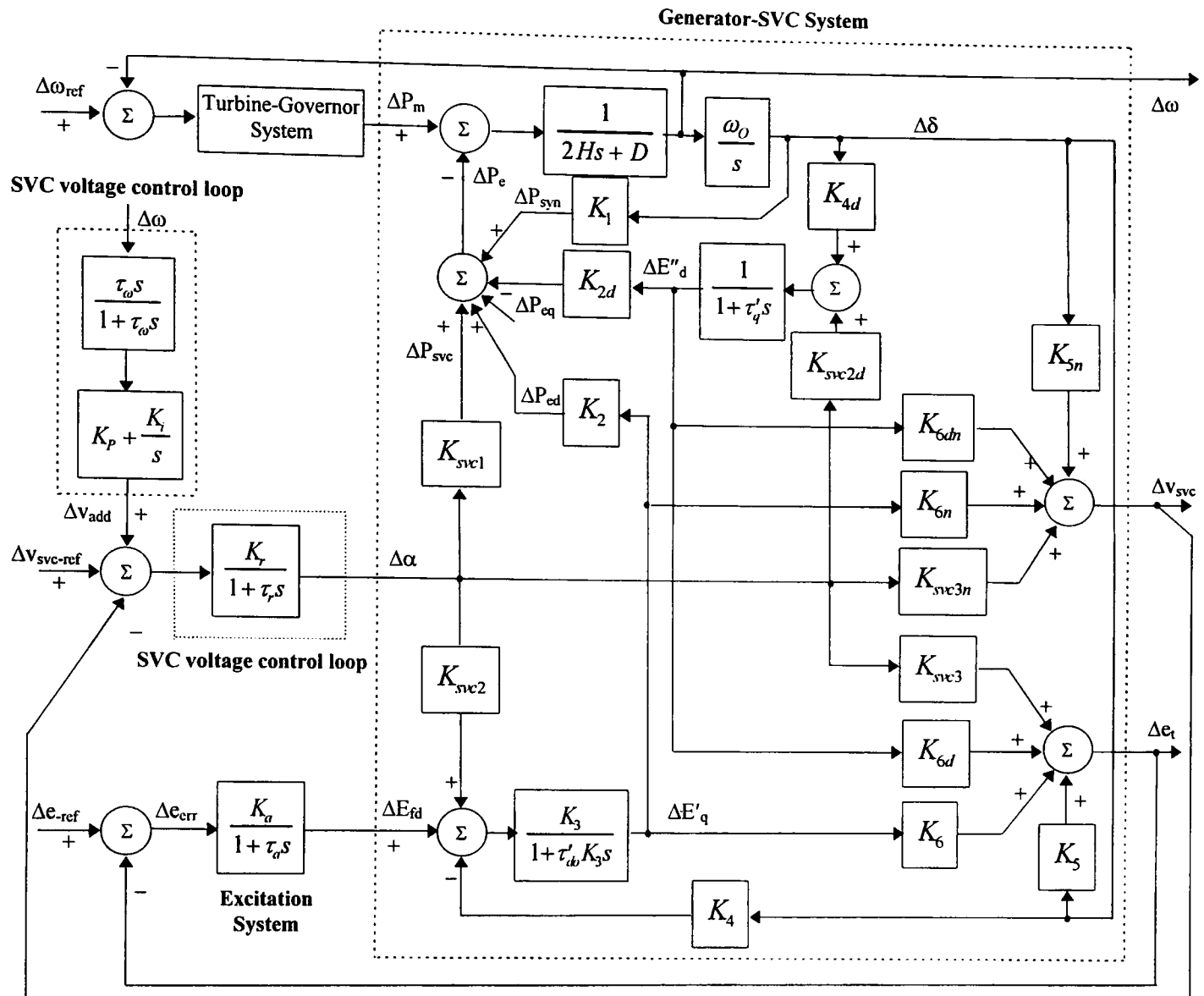


Figure A-3 Block-diagram model of synchronous generator-SVC system with Model 2

A-3 Model 3

Substituting (2-5) into (A-30) gives,

$$i_{gq} = \left[\frac{v_{\infty d} + i_{svdq} X_{t2}}{X_q + X_{t1} + X_{t2}} \right] \quad (\text{A-127})$$

Substituting (A-23) into (2-5) gives,

$$i_{gq} = \left[\frac{v_{svcd}}{X_q + X_{t1}} \right] \quad (\text{A-128})$$

Substituting (A-128) into (A-31), linearising and incorporating (A-4) gives,

$$\Delta v_{svcd} = \left[\frac{(X_q + X_{t1})v_{\infty qo}}{\Delta_q} \right] \Delta \delta + \left[\frac{X_{t2}(X_q + X_{t1})v_{svcdo}}{\Delta_q} \right] \Delta B_{svc} \quad (\text{A-129})$$

Re-arranging (A-127) by making use of (A-20) and (A-129) gives,

$$\Delta i_{gq} = \left[\frac{v_{\infty qo}}{\Delta_q} \right] \Delta \delta + \left[\frac{X_{t2}v_{svcdo}}{\Delta_q} \right] \Delta B_{svc} \quad (\text{A-130})$$

Generator Terminal Voltage Equation:

Substituting (A-130) into (2-5) gives,

$$\Delta e_{td} = \left[\frac{X_q v_{\infty qo}}{\Delta_q} \right] \Delta \delta + \left[\frac{X_q X_{t2} v_{svcd o}}{\Delta_q} \right] \Delta B_{svc} \quad (\text{A-131})$$

Re-arranging (A-71) by making use of (A-15), (A-110) and (A-131) yields,

$$\Delta e_t = K_5 \Delta \delta + K_6 \Delta E'_q + K_{sv3} \Delta \alpha \quad (\text{A-132})$$

where

$$K_5 = \left[\frac{e_{tdo}}{e_{to}} \cdot \frac{X_q v_{\infty qo}}{\Delta_q} - \frac{e_{tqo}}{e_{to}} \cdot \frac{X'_d v_{\infty do}}{\Delta'_d} \right] \quad (\text{A-133})$$

$$K_6 = \left[\frac{e_{tqo}}{e_{to}} \cdot \frac{X_{t2} + X_{t1}(1 - X_{t2} B_{svco})}{\Delta'_d} \right] \quad (\text{A-134})$$

$$K_{sv3} = \frac{2}{\pi X_L} \left[\frac{e_{tdo}}{e_{to}} \cdot \frac{X_{t2} X_q v_{svcd o}}{\Delta_q} + \frac{e_{tqo}}{e_{to}} \cdot \frac{X_{t2} X'_d v_{svcd o}}{\Delta'_d} \right] \quad (\text{A-135})$$

SVC Terminal Voltage Equation:

Re-arranging (A-80) by making use of (A-15), (A-100) and (A-129) yields,

$$\Delta v_{svc} = K_{5n} \Delta \delta + K_{6n} \Delta E'_q + K_{sv3n} \Delta \alpha \quad (\text{A-136})$$

where

$$K_{5n} = \left[\frac{v_{svcd o}}{v_{svco}} \cdot \frac{(X_q + X_{t1}) v_{\infty qo}}{\Delta_q} - \frac{v_{svcd o}}{v_{svco}} \cdot \frac{(X'_d + X_{t1}) v_{\infty do}}{\Delta'_d} \right] \quad (\text{A-137})$$

$$K_{6n} = \left[\frac{v_{svcd o}}{v_{svco}} \cdot \frac{X_{t2}}{\Delta'_d} \right] \quad (\text{A-138})$$

$$K_{sv3n} = \frac{2}{\pi X_L} \left[\frac{v_{svcd o}^2}{v_{svco}} \cdot \frac{X_{t2} (X_q + X_{t1})}{\Delta_q} + \frac{v_{svcd o}^2}{v_{svco}} \cdot \frac{X_{t2} (X'_d + X_{t1})}{\Delta'_d} \right] \quad (\text{A-139})$$

Electrical Power Equation:

Re-arranging (A-9) by making use of (A-20), (A-129) and (A-130) gives,

$$\Delta i_{tq} = \left[\frac{(1 - (X_q + X_{t1}) B_{svco}) v_{\infty qo}}{\Delta_q} \right] \Delta \delta - \left[\frac{(X_q + X_{t1}) v_{svcd o}}{\Delta_q} \right] \Delta B_{svc} \quad (\text{A-140})$$

Re-arranging (A-88) by making use of (A-15), (A-121) and (A-140) yields

$$\Delta P_e = K_1 \Delta \delta + K_2 \Delta E'_q + K_{sv1} \Delta \alpha \quad (\text{A-141})$$

where

$$K_1 = \left[\frac{(1 - (X_{t1} + X'_d) B_{svco}) v_{\infty do}^2}{\Delta'_d} + \frac{(1 - (X_{t1} + X_q) B_{svco}) v_{\infty qo}^2}{\Delta_q} + i_{tdo} v_{\infty qo} - i_{tqo} v_{\infty do} \right] \quad (\text{A-142})$$

$$K_2 = \left[\frac{v_{\infty do}}{\Delta'_d} \right] \quad (\text{A-143})$$

$$K_{svc1} = \frac{2}{\pi X_L} \left[\frac{(X_{l1} + X'_d)v_{\infty do} v_{svcqo}}{\Delta'_d} - \frac{(X_{l1} + X_q)v_{\infty qo} v_{svcd0}}{\Delta_q} \right] \quad (\text{A-144})$$

The transfer-function block diagram model of the synchronous generator-SVC system for Model 3 is shown in Fig. A-4. It is realised by combining (A-96), (A-97), (A-103), (A-132), (A-136) and (A-141).

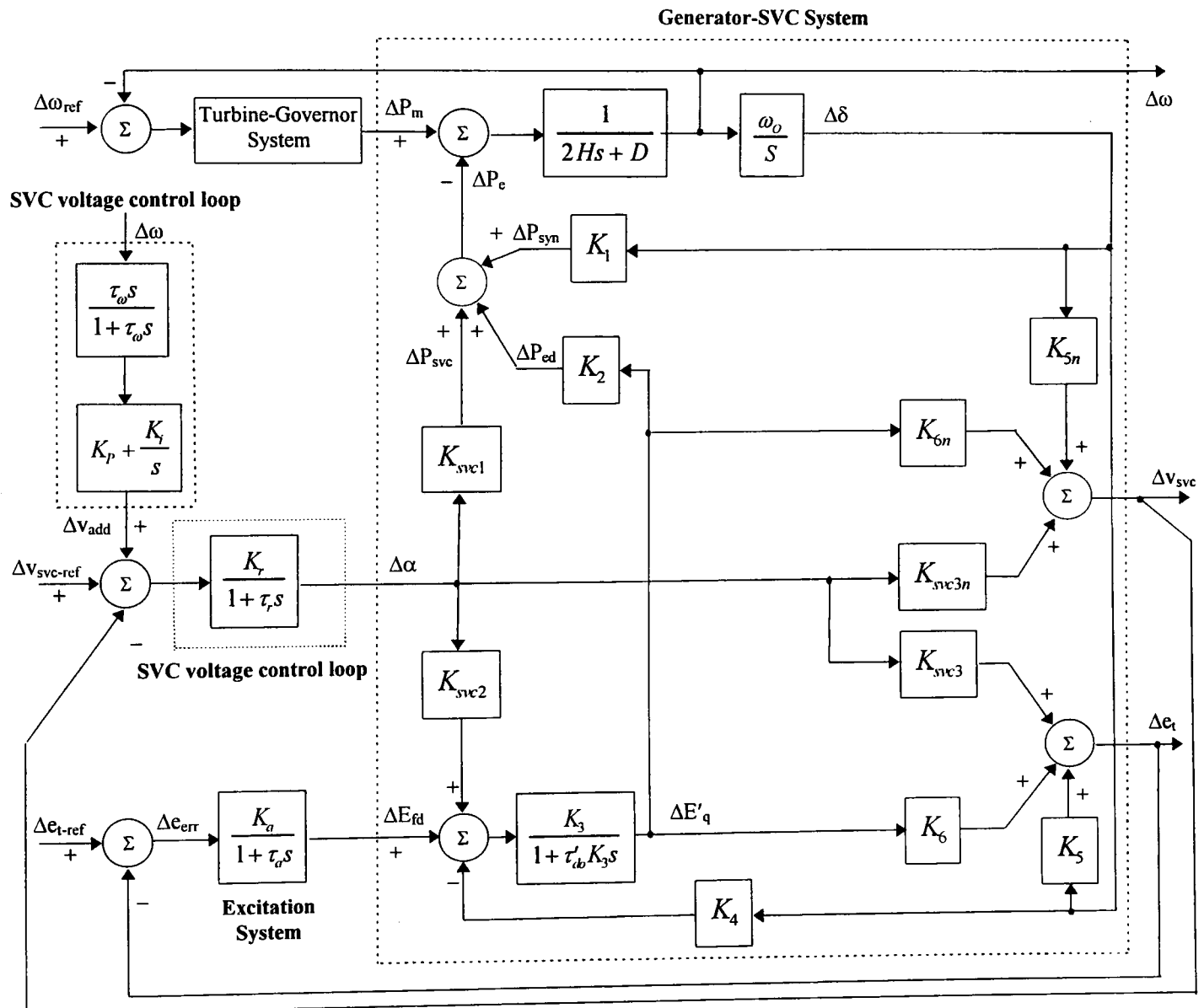


Figure A-4 Block-diagram model of synchronous generator-SVC system with Model 3

Appendix B

Derivation of the Small-Signal Transfer Function Block Diagram Model of the n Synchronous Generator and m SVC Systems

This appendix derives the transfer function block diagram model for n -synchronous generators, m SVCs. The Mathematical representations of the power system elements in Chapter 2 are used in the derivation process.

Starting with the re-arrangement (2-8) and (2-9) by making use of (2-1) gives,

$$\bar{e}_t = \bar{E}'' + (X_q'' - X_d'')i_{gq} - jX_d''\bar{i}_g \quad (\text{B-1})$$

For the i^{th} machine, (B-1) can be written as,

$$\bar{e}_{ti} = \bar{E}_i'' + (X_{qi}'' - X_{di}'')i_{gqi} - jX_{di}''\bar{i}_{gi} \quad (\text{B-2})$$

Re-arranging (B-2) by making use of (2-13) and (2-16), the generator's terminal voltage of the i^{th} machine in common co-ordinates is given by,

$$\bar{E}_{ti} = e^{j(\delta_i - \pi/2)} \left(\bar{E}_i'' + (X_{qi}'' - X_{di}'')i_{gqi} \right) - jX_{di}''\bar{i}_{gi} \quad (\text{B-3})$$

For a n machine system, the generator's terminal voltage in (B-3) can be written in matrix form as,

$$[\bar{E}_t] = [e^{j(\delta - \pi/2)}] \left\{ [\bar{E}''] + [X_q'' - X_d''] [i_{gq}] \right\} - [jX_d''] [\bar{I}_g] \quad (\text{B-4})$$

where $[e^{j(\delta - \pi/2)}]$, $[jX_d'']$ and $[X_q'' - X_d'']$ are diagonal matrices.

For small variations, (B-4) can be expressed as,

$$[\Delta \bar{E}_t] = [e^{j(\delta - \pi/2)}] \left\{ [\Delta \bar{E}''] + [X_q'' - X_d''] [\Delta i_{gq}] + j \left[[\bar{E}''] + [X_q'' - X_d''] [i_{gq}] \right] [\Delta \delta] \right\} - [jX_d''] [\Delta \bar{I}_g] \quad (\text{B-5})$$

where $[i_{gq}]$ is a diagonal matrix.

The incorporation of m SVCs into the power system networks introduces m SVC nodes, which are retained for explicit representation together with the n machine nodes. The admittance matrix $[\bar{Y}]$ in (2-24) for n generator nodes plus the m SVC nodes can be expressed as follows,

$$\begin{bmatrix} \bar{I}_g \\ \dots \\ 0 \end{bmatrix} = \begin{bmatrix} \bar{Y}_{nn} & \vdots & \bar{Y}_{nm} \\ \dots & \dots & \dots \\ \bar{Y}_{mn} & \vdots & \bar{Y}_{mm} + \bar{Y}_{svc} \end{bmatrix} \begin{bmatrix} \bar{E}_t \\ \dots \\ \bar{V}_{svc} \end{bmatrix} \quad (\text{B-6})$$

B-6) may be alternatively expressed as,

$$[\bar{I}_g] = [\bar{Y}_{nm}] [\bar{E}_t] + [\bar{Y}_{nm}] [\bar{V}_{svc}] \quad (\text{B-7})$$

$$[\bar{Y}_{mn}] [\bar{E}_t] + [\bar{Y}_{mm} + \bar{Y}_{svc}] [\bar{V}_{svc}] = [0] \quad (\text{B-8})$$

It is noted that the dimensions of $[\bar{I}_g]$, and $[\bar{E}_t]$ are $n \times 1$ and $[\bar{V}_{svc}]$ is $m \times 1$

For small variations, (B-7) and (B-8) can be expressed as,

$$[\Delta \bar{I}_g] = [\bar{Y}_{nm}] [\Delta \bar{E}_t] + [\bar{Y}_{nm}] [\Delta \bar{V}_{svc}] \quad (\text{B-9})$$

$$[\bar{Y}_{mn} + \bar{Y}_{svc}] [\Delta \bar{V}_{svc}] = -[\bar{Y}_{mn}] [\Delta \bar{E}_t] - [\Delta \bar{Y}_{svc}] [\bar{V}_{svc}] \quad (\text{B-10})$$

From (2-29), \bar{Y}_{svc} can be expressed as,

$$\bar{Y}_{svc} = j(B_C - B_L(\alpha)) \quad (\text{B-11})$$

where

$$B_L(\alpha) = \frac{2}{\pi X_L} \left\{ (\pi - \alpha) + \frac{1}{2} \sin(2\alpha) \right\} \quad (\text{B-12})$$

$$B_C = 2\pi fC \quad (\text{B-13})$$

It is noted that for a given operating condition $\bar{Y}_{svc} = j(B_C - B_L(\alpha_o))$.

For small variations,

$$\Delta \bar{Y}_{svc} = -j\Delta B_L(\alpha) = j \left\{ \frac{2}{\pi X_L} - \frac{2}{\pi X_L} \cos(2\alpha) \right\} \Delta \alpha \quad (\text{B-14})$$

The non-linear term can be neglected (see previous discussion in Appendix A), therefore,

$$\Delta \bar{Y}_{svc} = jK\Delta \alpha \quad (\text{B-15})$$

where

$$K = \frac{2}{\pi X_L} \quad (\text{B-16})$$

For m SVC, $\Delta \bar{Y}_{svc}$ in (B-15) can be written in matrix form as,

$$[\Delta \bar{Y}_{svc}] = [jK][\Delta \alpha] \quad (\text{B-17})$$

Re-arranging (B-10) by making use of (B-17) gives,

$$[\Delta \bar{V}_{svc}] = -[\bar{Y}_{mm} + \bar{Y}_{svc}]^{-1} \left[[\bar{Y}_{mn}] [\Delta \bar{E}_t] + [jK][\Delta \alpha][\bar{V}_{svc}] \right] \quad (\text{B-18})$$

Re-arranging (B-9) by making use of (B-18) gives,

$$[\Delta \bar{I}_g] = [\bar{Y}_a][\Delta \bar{E}_t] - [\bar{Y}_b][jK][\Delta \alpha][\bar{V}_{svc}] \quad (\text{B-19})$$

where

$$[\bar{Y}_a] = [\bar{Y}_{nn}] - [\bar{Y}_{nm}] [\bar{Y}_{mm} + \bar{Y}_{svc}]^{-1} [\bar{Y}_{mn}] \quad (\text{B-20})$$

$$[\bar{Y}_b] = [\bar{Y}_{nm}] [\bar{Y}_{mm} + \bar{Y}_{svc}]^{-1} \quad (\text{B-21})$$

Re-arranging (B-19) by making use of (B-5) gives,

$$[\Delta \bar{I}_g] = [\bar{Y}_g] [e^{j(\delta - \pi/2)}] \left\{ [\Delta \bar{E}''] + [X_q'' - X_d''] [\Delta i_{gq}] + j [\bar{E}''] + [X_q'' - X_d''] [i_{gq}] \right\} [\Delta \delta] - [\bar{Y}_s] [jK] [\Delta \alpha] [\bar{V}_{svc}] \quad (\text{B-22})$$

where

$$[\bar{Y}_g] = \left[[\bar{Y}_a]^{-1} + [jX_d''] \right]^{-1} \quad (\text{B-23})$$

$$[\bar{Y}_s] = [\bar{Y}_g] [\bar{Y}_a]^{-1} [\bar{Y}_b] \quad (\text{B-24})$$

For the i^{th} machine of the n machine system in $D-Q$ co-ordinates, the generator armature current in (B-22) can be re-written as,

$$\Delta \bar{I}_{gi} = \sum_{j=1}^n \bar{Y}_{gij} e^{j(\delta_j - \pi/2)} \left\{ \Delta \bar{E}_j'' + (X_{qj}'' - X_{dj}'') \Delta i_{gqj} + j \left(\bar{E}_j'' + (X_{qj}'' - X_{dj}'') i_{gqj} \right) \Delta \delta_j \right\} - \sum_{j=1}^m \bar{Y}_{sij} \bar{V}_{svcj} (jK_j) \Delta \alpha_j \quad (\text{B-25})$$

It is noted that in (B-25) the term $j=i$ is included.

Changing from $D-Q$ to d_i-q_i co-ordinates for the i^{th} machine gives,

$$\bar{i}_{gi} = e^{j(-\delta_i + \pi/2)} \bar{I}_{gi} \quad (\text{B-26})$$

For small variations, (B-26) can be expressed as,

$$\Delta \bar{i}_{gi} = e^{j(-\delta_i + \pi/2)} \Delta \bar{I}_{gi} - j \bar{I}_{gi} \Delta \delta_i \quad (\text{B-27})$$

Re-expression (B-27) by making use of (B-25), $\Delta \bar{I}_{gi}$ in d_i-q_i axis is given by,

$$\Delta \bar{i}_{gi} = \sum_{j=1}^n \bar{Y}_{gij} e^{j\delta_{ji}} \left\{ \Delta \bar{E}_j'' + (X_{qj}'' - X_{dj}'') \Delta i_{gqj} + j \left(\bar{E}_j'' + (X_{qj}'' - X_{dj}'') i_{gqj} \right) \Delta \delta_{ji} \right\} - \sum_{j=1}^m \bar{Y}_{sij} e^{j(-\delta_i + \pi/2)} (jK_j) \bar{V}_{svcj} \Delta \alpha_j \quad (\text{B-28})$$

where

$$\delta_{ji} = \delta_j - \delta_i \quad (\text{B-29})$$

$$\Delta \delta_{ji} = \Delta \delta_j - \Delta \delta_i \quad (\text{B-30})$$

Let us assume that,

$$\bar{Y}_{gij} = Y_{gij} e^{j\beta_{ij}} \quad (\text{B-31})$$

$$\bar{Y}_{sij} = Y_{sij} e^{j\gamma_{ij}} \quad (\text{B-32})$$

Re-arranging (B-28) by making use of (B-29)-(B-32) gives,

$$\Delta \bar{i}_{gi} = \sum_{j=1}^n Y_{gij} e^{j(\delta_{ji} + \beta_{ij})} \left\{ \Delta \bar{E}_j'' + (X_{qj}'' - X_{dj}'') \Delta i_{gqj} + j \left(\bar{E}_j'' + (X_{qj}'' - X_{dj}'') i_{gqj} \right) \Delta \delta_{ji} \right\} - \sum_{j=1}^m Y_{sij} e^{j(-\delta_i + \gamma_{ij} + \pi/2)} (jK_j) \bar{V}_{svcj} \Delta \alpha_j \quad (\text{B-33})$$

The generator armature current of the i^{th} machine in (B-33) can be decomposed in d_i - q_i axis as,

$$\begin{aligned} \Delta i_{gdi} = & \sum_{j=1}^n Y_{gij} \left\{ C_{gij} \left(\Delta E_{dj}'' + (X_{qj}'' - X_{dj}'') \Delta i_{gqj} \right) - S_{gij} \Delta E_{qj}'' - \left(S_{gij} \left(E_{dj}'' + (X_{qj}'' - X_{dj}'') i_{gqj} \right) + C_{gij} E_{qj}'' \right) \Delta \delta_{ji} \right\} \\ & + \sum_{j=1}^m Y_{sij} B_{ij} K_j \Delta \alpha_j \end{aligned} \quad (\text{B-34})$$

$$\begin{aligned} \Delta i_{gqi} = & \sum_{j=1}^n Y_{gij} \left\{ S_{gij} \left(\Delta E_{dj}'' + (X_{qj}'' - X_{dj}'') \Delta i_{gqj} \right) + C_{gij} \Delta E_{qj}'' - \left(S_{gij} E_{qj}'' - C_{gij} \left(E_{dj}'' + (X_{qj}'' - X_{dj}'') i_{gqj} \right) \right) \Delta \delta_{ji} \right\} \\ & + \sum_{j=1}^m Y_{sij} A_{ij} K_j \Delta \alpha_j \end{aligned} \quad (\text{B-35})$$

where

$$C_{gij} = \cos(\delta_{ji} + \beta_{ij}) \quad (\text{B-36})$$

$$S_{gij} = \sin(\delta_{ji} + \beta_{ij}) \quad (\text{B-37})$$

$$C_{sij} = \cos(\delta_i + \gamma_{ij}) \quad (\text{B-38})$$

$$S_{sij} = \sin(\delta_i + \gamma_{ij}) \quad (\text{B-39})$$

$$A_{ij} = S_{sij} V_{svcdj} + C_{sij} V_{svcqj} \quad (\text{B-40})$$

$$B_{ij} = C_{sij} V_{svcdj} - S_{sij} V_{svcqj} \quad (\text{B-41})$$

For n machines, (B-34) and (B-35) can be expressed in matrix form as,

$$[\Delta i_{gd}] = [K_{Rd}] [\Delta \delta] + [K_{Dd}] [\Delta E_q''] + [K_{Qd}] [\Delta E_d''] + [C_{Qd}] [\Delta i_{gq}] + [K_{Ad}] [\Delta \alpha] \quad (\text{B-42})$$

$$[C_{Qq}] [\Delta i_{gq}] = [K_{Rq}] [\Delta \delta] + [K_{Dq}] [\Delta E_q''] + [K_{Qq}] [\Delta E_d''] + [K_{Aq}] [\Delta \alpha] \quad (\text{B-43})$$

where

$$K_{Rdij} = -Y_{gij} \left\{ C_{gij} E_{qj}'' + S_{gij} \left(E_{dj}'' + (X_{qj}'' - X_{dj}'') i_{gqj} \right) \right\} \quad \text{for } j \neq i \quad (\text{B-44})$$

$$K_{Rqij} = -Y_{gij} \left\{ S_{gij} E_{qj}'' - C_{gij} \left(E_{dj}'' - (X_{qj}'' - X_{dj}'') i_{gqj} \right) \right\} \quad \text{for } j \neq i \quad (\text{B-45})$$

$$K_{Rdii} = - \sum_{j \neq i}^n K_{Rdij} \quad (\text{B-46})$$

$$K_{Rqii} = - \sum_{j \neq i}^n K_{Rqij} \quad (\text{B-47})$$

$$K_{Ddij} = -Y_{gij} S_{gij} \quad \text{for } j=1 \rightarrow n \quad (\text{B-48})$$

$$K_{Dqij} = Y_{gij} C_{gij} \quad \text{for } j=1 \rightarrow n \quad (\text{B-49})$$

$$K_{Qdij} = Y_{gij} C_{gij} \quad \text{for } j=1 \rightarrow n \quad (\text{B-50})$$

$$K_{Qqij} = Y_{gij} S_{gij} \quad \text{for } j=1 \rightarrow n \quad (\text{B-51})$$

$$C_{Qdij} = Y_{gij} C_{gij} (X_{qj}'' - X_{dj}'') \quad \text{for } j=1 \rightarrow n \quad (\text{B-52})$$

$$C_{Qqij} = -Y_{gij} S_{gij} (X_{qj}'' - X_{dj}'') \quad \text{for } j \neq i \quad (\text{B-53})$$

$$C_{Qqii} = 1 + C_{Qqii} \quad \text{for } j = i \quad (\text{B-54})$$

$$K_{Adj} = Y_{sij} B_{ij} K_j \quad \text{for } j = 1 \rightarrow m \quad (\text{B-55})$$

$$K_{Aqij} = Y_{sij} A_{ij} K_j \quad \text{for } j = 1 \rightarrow m \quad (\text{B-56})$$

Re-arranging (B-42) and (B-43) gives,

$$[\Delta i_{gd}] = [D_d][\Delta E_q''] + [Q_d][\Delta E_d''] + [R_d][\Delta \delta] + [A_d][\Delta \alpha] \quad (\text{B-57})$$

$$[\Delta i_{gq}] = [D_q][\Delta E_q''] + [Q_q][\Delta E_d''] + [R_q][\Delta \delta] + [A_q][\Delta \alpha] \quad (\text{B-58})$$

where

$$[R_q] = [C_{Qq}]^{-1} [K_{Rq}] \quad (\text{B-59})$$

$$[D_q] = [C_{Qq}]^{-1} [K_{Dq}] \quad (\text{B-60})$$

$$[Q_q] = [C_{Qq}]^{-1} [K_{Qq}] \quad (\text{B-61})$$

$$[A_q] = [C_{Qq}]^{-1} [K_{Aq}] \quad (\text{B-62})$$

$$[R_d] = [K_{Rd}] + [C_{Qd}][R_q] \quad (\text{B-63})$$

$$[D_d] = [K_{Dd}] + [C_{Qd}][D_q] \quad (\text{B-64})$$

$$[Q_d] = [K_{Qd}] + [C_{Qd}][Q_q] \quad (\text{B-65})$$

$$[A_d] = [K_{Ad}] + [C_{Qd}][A_q] \quad (\text{B-66})$$

Electrical power equation:

As shown in (2-20), the electrical power of a synchronous generator can be expressed as,

$$P_{ei} = e_{td} i_{gd} + e_{tq} i_{gq} \quad (\text{B-67})$$

Re-arranging (B-67) by making use of (2-8) and (2-9), the electrical power for the i^{th} machine may be expressed as,

$$P_{ei} = E_{di}'' i_{di} + E_{qi}'' i_{qi} + i_{qi} (X_{qi}'' - X_{di}'') i_{di} \quad (\text{B-68})$$

For small variation, (B-68) can be written in matrix form for n machines as follows,

$$[\Delta P_e] = [i_d][\Delta E_d''] + [i_q][\Delta E_q''] + \left[[E_d''] + [i_q][X_q'' - X_d''] \right] [\Delta i_d] + \left[[E_q''] + [i_d][X_q'' - X_d''] \right] [\Delta i_q] \quad (\text{B-69})$$

Substituting (B-57) and (B-58) into (B-69) gives,

$$[\Delta P_e] = [K_1][\Delta \delta] + [K_2][\Delta E_q''] + [K_{2d}][\Delta E_d''] + [K_{svcl}][\Delta \alpha] \quad (\text{B-70})$$

where

$$[K_1] = [Q_t][R_q] + [D_t][R_d] \quad (\text{B-71})$$

$$[K_2] = [i_q] + [Q_t][D_q] + [D_t][D_d] \quad (\text{B-72})$$

$$[K_{2d}] = [i_d] + [Q_t][Q_q] + [D_t][Q_d] \quad (\text{B-73})$$

$$[K_{svcl}] = [Q_t][A_q] + [D_t][A_d] \quad (\text{B-74})$$

$$[Q_t] = [E_q''] + [i_d][X_q'' - X_d''] \quad (\text{B-75})$$

$$[F_t] = [E_d''] + [i_q][X_q'' - X_d''] \quad (\text{B-76})$$

For the i^{th} machine, (B-70) may be expressed as,

$$\begin{aligned} \Delta P_{ei} = & K_{1ii}\Delta\delta_i + \sum_{j \neq i}^n K_{1ij}\Delta\delta_j + K_{2ii}\Delta E_{qi}'' + \sum_{j \neq i}^n K_{2ij}\Delta E_{qj}'' + K_{2dii}\Delta E_{di}'' + \sum_{j \neq i}^n K_{2dij}\Delta E_{dj}'' \\ & + K_{svclii}\Delta\alpha_i + \sum_{j \neq i}^m K_{svclij}\Delta\alpha_j \end{aligned} \quad (\text{B-77})$$

where

$$K_{1ii} = Q_t R_{qii} + D_t R_{dii} \quad (\text{B-78})$$

$$K_{1ij} = Q_t R_{qij} + D_t R_{dij} \quad (\text{B-79})$$

$$K_{2ii} = i_{qi} + Q_t D_{qii} + D_t D_{dii} \quad (\text{B-80})$$

$$K_{2ij} = Q_t D_{qij} + D_t D_{dij} \quad (\text{B-81})$$

$$K_{2dii} = i_{di} + Q_t Q_{qii} + D_t Q_{dii} \quad (\text{B-82})$$

$$K_{2dij} = Q_t Q_{qij} + D_t Q_{dij} \quad (\text{B-83})$$

$$K_{svclii} = Q_t A_{qii} + D_t A_{dii} \quad (\text{B-84})$$

$$K_{svclij} = Q_t A_{qij} + D_t A_{dij} \quad (\text{B-85})$$

$$D_t = E_{di}'' + (X_{qi}'' - X_{di}'')i_{qi} \quad (\text{B-86})$$

$$Q_t = E_{qi}'' + (X_{qi}'' - X_{di}'')i_{di} \quad (\text{B-87})$$

D-axis flux linkage equation:

Transforming the d -axis flux linkages in equations (2-6) and (2-10) into S domain and expressing the result in matrix form for n machines gives,

$$[1] + [\tau'_{do}]s [\Delta E_q'] = [\Delta E_{fd}] - [X_d - X'_d][\Delta i_{gd}] \quad (\text{B-88})$$

$$[1] + [\tau''_{do}]s [\Delta E_q''] = [1] + [\tau'_{do}]s [\Delta E_q'] - [X'_d - X_d][\Delta i_{gd}] \quad (\text{B-89})$$

Re-arranging (B-88)-(B-89) gives,

$$[C_3(s)][\Delta E_q''] = [C_1(s)][\Delta E_{fd}] - [C_2(s)][\Delta i_{gd}] \quad (\text{B-90})$$

where

$$[C_1(s)] = [1] + [\tau''_{do}]s \quad (\text{B-91})$$

$$[C_2(s)] = [X_d - X'_d] + [\tau'_{do}[X'_d - X_d] + \tau''_{do}[X_d - X'_d]]s \quad (\text{B-92})$$

$$[C_3(s)] = [1] + [\tau'_{do} + \tau''_{do}]s + [\tau'_{do}\tau''_{do}]s^2 \quad (\text{B-93})$$

where $[1]$ is a unit matrix and $[\tau'_{do}]$ is a diagonal matrix.

Re-arranging (B-90) by making use of (B-57) gives,

$$\begin{aligned} [[C_2(s)][D_d] + [C_3(s)]][\Delta E_q''] &= [C_1(s)][\Delta E_{fd}] - [C_2(s)][[R_d][\Delta\delta] + [Q_d][\Delta E_d'']] \\ &\quad + [A_d][\Delta\alpha] \end{aligned} \quad (\text{B-94})$$

For the i^{th} machine, (B-94) may be expressed as,

$$\begin{aligned} \Delta E_{qi}'' &= g_{3ii}(s)\Delta E_{fdi} - \sum_{j \neq i}^n g_{3ij}(s)\Delta E_{qj}'' - g_{4ii}(s)\Delta\delta_i - \sum_{j \neq i}^n g_{4ij}(s)\Delta\delta_j - g_{7ii}(s)\Delta E_{di}'' \\ &\quad - \sum_{j \neq i}^n g_{7ij}(s)\Delta E_{dj}'' - g_{\text{svc}2ii}(s)\Delta\alpha_i - \sum_{j \neq i}^m g_{\text{svc}2ij}(s)\Delta\alpha_j \end{aligned} \quad (\text{B-95})$$

where

$$g_{3ii}(s) = \frac{1 + \tau_{doi}''s}{\Delta(s)} \quad (\text{B-96})$$

$$g_{3ij}(s) = \frac{\{(X_{di} - X_{di}'')\} + (\tau_{doi}'(X_{di}' - X_{di}'') + \tau_{doi}''(X_{di} - X_{di}'))s}{\Delta(s)} D_{dij} \quad (\text{B-97})$$

$$g_{4ii}(s) = \frac{\{(X_{di} - X_{di}'')\} + (\tau_{doi}'(X_{di}' - X_{di}'') + \tau_{doi}''(X_{di} - X_{di}'))s}{\Delta(s)} R_{dii} \quad (\text{B-98})$$

$$g_{4ij}(s) = \frac{\{(X_{di} - X_{di}'')\} + (\tau_{doi}'(X_{di}' - X_{di}'') + \tau_{doi}''(X_{di} - X_{di}'))s}{\Delta(s)} R_{dij} \quad (\text{B-99})$$

$$g_{7ii}(s) = \frac{\{(X_{di} - X_{di}'')\} + (\tau_{doi}'(X_{di}' - X_{di}'') + \tau_{doi}''(X_{di} - X_{di}'))s}{\Delta(s)} Q_{dii} \quad (\text{B-100})$$

$$g_{7ij}(s) = \frac{\{(X_{di} - X_{di}'')\} + (\tau_{doi}'(X_{di}' - X_{di}'') + \tau_{doi}''(X_{di} - X_{di}'))s}{\Delta(s)} Q_{dij} \quad (\text{B-101})$$

$$g_{\text{svc}2ii}(s) = \frac{\{(X_{di} - X_{di}'')\} + (\tau_{doi}'(X_{di}' - X_{di}'') + \tau_{doi}''(X_{di} - X_{di}'))s}{\Delta(s)} A_{dii} \quad (\text{B-102})$$

$$g_{\text{svc}2ij}(s) = \frac{\{(X_{di} - X_{di}'')\} + (\tau_{doi}'(X_{di}' - X_{di}'') + \tau_{doi}''(X_{di} - X_{di}'))s}{\Delta(s)} A_{dij} \quad (\text{B-103})$$

$$\begin{aligned} \Delta(s) &= \{1 + (X_{di} - X_{di}'')D_{dii}\} \\ &\quad + \{(\tau_{doi}' + \tau_{doi}'') + (\tau_{doi}'(X_{di}' - X_{di}'') + \tau_{doi}''(X_{di} - X_{di}'))D_{dii}\}s + \{\tau_{doi}'\tau_{doi}''\}s^2 \end{aligned} \quad (\text{B-104})$$

Q-axis flux linkage equation:

Transforming the q -axis flux linkages in equation (2-11) into S domain and expressing the result in matrix form for n machines gives,

$$[[1] + [\tau_{qo}''s]][\Delta E_d''] = [X_q - X_q''][\Delta i_{gq}] \quad (\text{B-105})$$

Re-arranging (B-105) by making use of (B-58) gives,

$$[[1] - [X_q - X_q'']][Q_q] + [\tau_{qo}''s][\Delta E_d''] = [X_q - X_q''][[R_q][\Delta\delta] + [D_q][\Delta E_q'']] + [A_q][\Delta\alpha] \quad (\text{B-106})$$

$$\begin{aligned} \Delta E''_{di} = & - \sum_{j \neq i}^n g_{7dij}(s) \Delta E''_{dj} + g_{4dii}(s) \Delta \delta_i + \sum_{j \neq i}^n g_{4dij}(s) \Delta \delta_j + g_{3dii}(s) \Delta E''_{qi} \\ & + \sum_{j \neq i}^n g_{3dij}(s) \Delta E''_{qj} + g_{svc2dii}(s) \Delta \alpha_i - \sum_{j \neq i}^m g_{svc2dij}(s) \Delta \alpha_j \end{aligned} \quad (B-107)$$

where

$$g_{7dij}(s) = \frac{(X_{qi} - X''_{qi}) Q_{qij}}{1 - (X_{qi} - X''_{qi}) Q_{qii} + \tau''_{qoi} s} \quad (B-108)$$

$$g_{3dii}(s) = \frac{(X_{qi} - X''_{qi}) D_{qii}}{1 - (X_{qi} - X''_{qi}) Q_{qii} + \tau''_{qoi} s} \quad (B-109)$$

$$g_{3dij}(s) = \frac{(X_{qi} - X''_{qi}) D_{qij}}{1 - (X_{qi} - X''_{qi}) Q_{qii} + \tau''_{qoi} s} \quad (B-110)$$

$$g_{4dii}(s) = \frac{(X_{qi} - X''_{qi}) R_{qii}}{1 - (X_{qi} - X''_{qi}) Q_{qii} + \tau''_{qoi} s} \quad (B-111)$$

$$g_{4dij}(s) = \frac{(X_{qi} - X''_{qi}) R_{qij}}{1 - (X_{qi} - X''_{qi}) Q_{qii} + \tau''_{qoi} s} \quad (B-112)$$

$$g_{svc2dii}(s) = \frac{(X_{qi} - X''_{qi}) A_{qii}}{1 - (X_{qi} - X''_{qi}) Q_{qii} + \tau''_{qoi} s} \quad (B-113)$$

$$g_{svc2dij}(s) = \frac{(X_{qi} - X''_{qi}) A_{qij}}{1 - (X_{qi} - X''_{qi}) Q_{qii} + \tau''_{qoi} s} \quad (B-114)$$

Generator terminal voltage equation:

For small variations, the generator terminal voltage can be written in matrix form for n machine as,

$$[\Delta e_t] = [e_t]^{-1} \left[[e_{td}] [\Delta e_{td}] + [e_{tq}] [\Delta e_{tq}] \right] \quad (B-115)$$

The generator terminal voltages equations in d -axis and q -axis, (2-8) and (2-9), can be written in matrix form for n machines as,

$$[\Delta e_{tq}] = [\Delta E''_q] - [X''_d] [\Delta i_{gd}] \quad (B-116)$$

$$[\Delta e_{td}] = [\Delta E''_d] + [X''_q] [\Delta i_{gq}] \quad (B-117)$$

Substituting (B-57) into (B-116) gives,

$$[\Delta e_{tq}] = \left[[1] - [X''_d] [D_d] \right] [\Delta E''_q] - [X''_d] [Q_d] [\Delta E''_d] - [X''_d] [R_d] [\Delta \delta] - [X''_d] [A_d] [\Delta \alpha] \quad (B-118)$$

Substituting (B-58) into (B-117) gives,

$$[\Delta e_{td}] = \left[[1] + [X''_q] [Q_q] \right] [\Delta E''_d] + [X''_q] [D_q] [\Delta E''_q] + [X''_q] [R_q] [\Delta \delta] + [X''_q] [A_q] [\Delta \alpha] \quad (B-119)$$

Substituting (B-118) and (B-119) into (B-115) gives,

$$[\Delta e_t] = [K_5] [\Delta \delta] + [K_6] [\Delta E''_q] + [K_{6d}] [\Delta E''_d] + [K_{svc3}] [\Delta \alpha] \quad (B-120)$$

where

$$[K_5] = [e_t]^{-1} \left[[e_{td}] [X''_q] [R_q] - [e_{tq}] [X''_d] [R_d] \right] \quad (B-121)$$

$$[K_6] = [e_t]^{-1} \left[[e_{td}] [X_q''] [D_q] + [e_{tq}] \left[[1] - [X_d''] \right] [D_d] \right] \quad (\text{B-122})$$

$$[K_{6d}] = [e_t]^{-1} \left[[e_{td}] \left[[1] + [X_q''] \right] [Q_q] - [e_{tq}] [X_d''] [Q_d] \right] \quad (\text{B-123})$$

$$[K_{svc3}] = [e_t]^{-1} \left[[e_{td}] [X_q''] [A_q] - [e_{tq}] [X_d''] [A_d] \right] \quad (\text{B-124})$$

For the i^{th} machine, (B-120) may be expressed as,

$$\begin{aligned} \Delta e_{ti} = & K_{5ii} \Delta \delta_i + \sum_{j \neq i}^n K_{5ij} \Delta \delta_j + K_{6ii} \Delta E_{qi}'' + \sum_{j \neq i}^n K_{6ij} \Delta E_{qj}'' + K_{6dii} \Delta E_{di}'' + \sum_{j \neq i}^n K_{6dij} \Delta E_{dj}'' \\ & + K_{svc3ii} \Delta \alpha_i + \sum_{j \neq i}^m K_{svc3ij} \Delta \alpha_j \end{aligned} \quad (\text{B-125})$$

where

$$K_{5ii} = e_{ti}^{-1} \left(e_{tdi} X_{qi}'' R_{qii} - e_{tqi} X_{di}'' R_{dii} \right) \quad (\text{B-126})$$

$$K_{5ij} = e_{ti}^{-1} \left(e_{tdi} X_{qi}'' R_{qij} - e_{tqi} X_{di}'' R_{dij} \right) \quad (\text{B-127})$$

$$K_{6ii} = e_{ti}^{-1} \left(e_{tdi} X_{qi}'' D_{qii} - e_{tqi} (1 - X_{di}'') D_{dii} \right) \quad (\text{B-128})$$

$$K_{6ij} = e_{ti}^{-1} \left(e_{tdi} X_{qi}'' D_{qij} - e_{tqi} X_{di}'' D_{dij} \right) \quad (\text{B-129})$$

$$K_{6dii} = e_{ti}^{-1} \left(e_{tdi} (1 - X_{qi}'') Q_{qii} - e_{tqi} X_{di}'' Q_{dii} \right) \quad (\text{B-130})$$

$$K_{6dij} = e_{ti}^{-1} \left(e_{tdi} X_{qi}'' Q_{qij} - e_{tqi} X_{di}'' Q_{dij} \right) \quad (\text{B-131})$$

$$K_{svc3ii} = e_{ti}^{-1} \left(e_{tdi} X_{qi}'' A_{qii} - e_{tqi} X_{di}'' A_{dii} \right) \quad (\text{B-132})$$

$$K_{svc3ij} = e_{ti}^{-1} \left(e_{tdi} X_{qi}'' A_{qij} - e_{tqi} X_{di}'' A_{dij} \right) \quad (\text{B-133})$$

SVC terminal voltage equation:

For small variations, the SVC terminal voltage for m SVC can be written in matrix form as,

$$[\Delta V_{svc}] = [V_{svc}]^{-1} \left[[V_{svcD}] [\Delta V_{svcD}] + [V_{svcQ}] [\Delta V_{svcQ}] \right] \quad (\text{B-134})$$

Re-arranging (B-9) by making use of (B-5) gives,

$$\begin{aligned} [\Delta \bar{E}_t] = & [\bar{Y}_c] [jX_d'']^{-1} \left[e^{j(\delta - \pi/2)} \right] \left\{ [\Delta \bar{E}''] + [X_q'' - X_d''] [\Delta i_{gq}] + j \left[[\bar{E}''] + [X_q'' - X_d''] [i_{gq}] \right] [\Delta \delta] \right\} \\ & - [\bar{Y}_c] [\bar{Y}_{nm}] [\Delta \bar{V}_{svc}] \end{aligned} \quad (\text{B-135})$$

where

$$[\bar{Y}_c] = \left[[jX_d'']^{-1} + [\bar{Y}_{nm}] \right]^{-1} \quad (\text{B-136})$$

Re-arranging (B-10) by making use of (B-135) gives,

$$\begin{aligned} [\Delta \bar{V}_{svc}] = & -[\bar{Y}_c] \left[e^{j(\delta - \pi/2)} \right] \left\{ [\Delta \bar{E}''] + [X_q'' - X_d''] [\Delta i_{gq}] + j \left[[\bar{E}''] + [X_q'' - X_d''] [i_{gq}] \right] [\Delta \delta] \right\} \\ & - [\bar{Y}_d] [\Delta \bar{Y}_{svc}] [\bar{V}_{svc}] \end{aligned} \quad (\text{B-137})$$

where

$$[\bar{Y}_d] = \left[[\bar{Y}_{mm} + \bar{Y}_{svc}] - [\bar{Y}_{mn}] [\bar{Y}_c] [\bar{Y}_{nm}] \right]^{-1} \quad (\text{B-138})$$

$$[\bar{Y}_e] = [\bar{Y}_d] [\bar{Y}_{mn}] [\bar{Y}_c] [jX_d'']^{-1} \quad (\text{B-139})$$

For the i^{th} SVC in D - Q co-ordinates, the SVC terminal voltage can be re-written as,

$$\begin{aligned} \Delta \bar{V}_{svci} = & - \sum_{j=1}^n \bar{Y}_{ej} e^{j(\delta_j - \pi/2)} \left(\Delta \bar{E}_j'' + (X_{qj}'' - X_{dj}'') \Delta i_{gj} + j \left(\bar{E}_j'' + (X_{qj}'' - X_{dj}'') i_{gj} \right) \Delta \delta_j \right) \\ & - \sum_{j=1}^m \bar{Y}_{dij} \Delta \bar{V}_{svcj} \bar{V}_{svcj} \end{aligned} \quad (\text{B-140})$$

Let us assume that,

$$\bar{Y}_{ej} = Y_{ej} e^{j\theta_{ij}} \quad (\text{B-141})$$

$$\bar{Y}_{dij} = Y_{dij} e^{j\phi_{ij}} \quad (\text{B-142})$$

Re-arranging (B-140) by making use of (B-141), (B-142) and (B-15) gives,

$$\begin{aligned} \Delta \bar{V}_{svci} = & - \sum_{j=1}^n Y_{ej} e^{j(\delta_j + \theta_{ij} - \pi/2)} \left(\Delta \bar{E}_j'' + (X_{qj}'' - X_{dj}'') \Delta i_{gj} + j \left(\bar{E}_j'' + (X_{qj}'' - X_{dj}'') i_{gj} \right) \Delta \delta_j \right) \\ & - \sum_{j=1}^m Y_{dij} e^{j\phi_{ij}} \bar{V}_{svcj} (jK_j) \Delta \alpha_j \end{aligned} \quad (\text{B-143})$$

The SVC terminal voltage of the i^{th} SVC in (B-143) can be decomposed in D - Q axes as,

$$\begin{aligned} \Delta V_{svcDi} = & \sum_{j=1}^n Y_{ej} \left(-C_{fij} \Delta E_{qj}'' - S_{fij} \left(\Delta E_{dj}'' + (X_{qj}'' - X_{dj}'') \Delta i_{gj} \right) \right. \\ & \left. + \left(S_{fij} E_{qj}'' - C_{fij} \left(E_{dj}'' + (X_{qj}'' - X_{dj}'') i_{gj} \right) \right) \Delta \delta_j \right) + \sum_{j=1}^m Y_{dij} K_j a_{ij} \Delta \alpha_j \end{aligned} \quad (\text{B-144})$$

$$\begin{aligned} \Delta V_{svcQi} = & \sum_{j=1}^n Y_{ej} \left(-S_{fij} \Delta E_{qj}'' + C_{fij} \left(\Delta E_{dj}'' + (X_{qj}'' - X_{dj}'') \Delta i_{gj} \right) \right. \\ & \left. - \left(C_{fij} E_{qj}'' + S_{fij} \left(E_{dj}'' + (X_{qj}'' - X_{dj}'') i_{gj} \right) \right) \Delta \delta_j \right) - \sum_{j=1}^m Y_{dij} K_j b_{ij} \Delta \alpha_j \end{aligned} \quad (\text{B-145})$$

where

$$C_{fij} = \cos(\theta_{ij} + \delta_j) \quad (\text{B-146})$$

$$S_{fij} = \sin(\theta_{ij} + \delta_j) \quad (\text{B-147})$$

$$C_{lij} = \cos(\phi_{ij}) \quad (\text{B-148})$$

$$S_{lij} = \sin(\phi_{ij}) \quad (\text{B-149})$$

$$a_{ij} = S_{lij} V_{svcDj} + C_{lij} V_{svcQj} \quad (\text{B-150})$$

$$b_{ij} = C_{lij} V_{svcDj} - S_{lij} V_{svcQj} \quad (\text{B-151})$$

For m SVCs, (B-144) and (B-145) can be expressed in matrix form as,

$$[\Delta V_{svcD}] = [S_{Rd}] [\Delta \delta] + [S_{Dd}] [\Delta E_q''] + [S_{Qd}] [\Delta E_d''] + [S_{CQd}] [\Delta i_q] + [S_{Ad}] [\Delta \alpha] \quad (\text{B-152})$$

$$[\Delta V_{svcQ}] = [S_{Rq}] [\Delta \delta] + [S_{Dq}] [\Delta E_q''] + [S_{Qq}] [\Delta E_d''] + [S_{CQq}] [\Delta i_q] + [S_{Aq}] [\Delta \alpha] \quad (\text{B-153})$$

where

$$S_{Rdij} = Y_{eij} \left(S_{fij} E_{qj}'' - C_{fij} \left(E_{dj}'' + (X_{qj}'' - X_{dj}'') i_{gqj} \right) \right) \quad \text{for } j=1 \rightarrow n \quad (\text{B-154})$$

$$S_{Rqij} = Y_{eij} \left(-C_{fij} E_{qj}'' - S_{fij} \left(E_{dj}'' + (X_{qj}'' - X_{dj}'') i_{gqj} \right) \right) \quad \text{for } j=1 \rightarrow n \quad (\text{B-155})$$

$$S_{Ddij} = -Y_{eij} C_{fij} \quad \text{for } j=1 \rightarrow n \quad (\text{B-156})$$

$$S_{Dqij} = -Y_{eij} S_{fij} \quad \text{for } j=1 \rightarrow n \quad (\text{B-157})$$

$$S_{Qdij} = -Y_{eij} S_{fij} \quad \text{for } j=1 \rightarrow n \quad (\text{B-158})$$

$$S_{Qqij} = Y_{eij} C_{fij} \quad \text{for } j=1 \rightarrow n \quad (\text{B-159})$$

$$S_{CQdij} = -Y_{eij} S_{fij} (X_{qj}'' - X_{dj}'') \quad \text{for } j=1 \rightarrow n \quad (\text{B-160})$$

$$S_{CQqij} = Y_{eij} C_{fij} (X_{qj}'' - X_{dj}'') \quad \text{for } j=1 \rightarrow n \quad (\text{B-161})$$

$$S_{Adij} = Y_{dij} a_{ij} K_j \quad \text{for } j=1 \rightarrow m \quad (\text{B-162})$$

$$S_{Aqij} = -Y_{dij} b_{ij} K_j \quad \text{for } j=1 \rightarrow n \quad (\text{B-163})$$

Re-arranging (B-152) and (B-153) by making use of (B-58) gives,

$$[\Delta V_{svcD}] = [T_{Rd}] [\Delta \delta] + [T_{Dd}] [\Delta E_q''] + [T_{Qd}] [\Delta E_d''] + [T_{Ad}] [\Delta \alpha] \quad (\text{B-164})$$

$$[\Delta V_{svcQ}] = [T_{Rq}] [\Delta \delta] + [T_{Dq}] [\Delta E_q''] + [T_{Qq}] [\Delta E_d''] + [T_{Aq}] [\Delta \alpha] \quad (\text{B-165})$$

where

$$[T_{Rd}] = [S_{Rd}] + [S_{CQd}] [R_q] \quad (\text{B-166})$$

$$[T_{Rq}] = [S_{Rq}] + [S_{CQq}] [R_q] \quad (\text{B-167})$$

$$[T_{Dd}] = [S_{Dd}] + [S_{CQd}] [D_q] \quad (\text{B-168})$$

$$[T_{Dq}] = [S_{Dq}] + [S_{CQq}] [D_q] \quad (\text{B-169})$$

$$[T_{Qd}] = [S_{Qd}] + [S_{CQd}] [Q_q] \quad (\text{B-170})$$

$$[T_{Qq}] = [S_{Qq}] + [S_{CQq}] [Q_q] \quad (\text{B-171})$$

$$[T_{Ad}] = [S_{Ad}] + [S_{CQd}] [A_q] \quad (\text{B-172})$$

$$[T_{Aq}] = [S_{Aq}] + [S_{CQq}] [A_q] \quad (\text{B-173})$$

Re-arranging (B-134) by making use of (B-164) and (B-165) gives,

$$[\Delta V_{svc}] = [K_{5n}] [\Delta \delta] + [K_{6n}] [\Delta E_q''] + [K_{6dn}] [\Delta E_d''] + [K_{svc3n}] [\Delta \alpha] \quad (\text{B-174})$$

where

$$[K_{5n}] = [V_{svc}]^{-1} \left[[V_{svcD}] [T_{Rd}] + [V_{svcQ}] [T_{Rq}] \right] \quad (\text{B-175})$$

$$[K_{6n}] = [V_{svc}]^{-1} \left[[V_{svcD}] [T_{Dd}] + [V_{svcQ}] [T_{Dq}] \right] \quad (\text{B-176})$$

$$[K_{6dn}] = [V_{svc}]^{-1} \left[[V_{svcD}] [T_{Qd}] + [V_{svcQ}] [T_{Qq}] \right] \quad (\text{B-177})$$

$$[K_{svc3n}] = [V_{svc}]^{-1} \left[[V_{svcD}] [T_{Ad}] + [V_{svcQ}] [T_{Aq}] \right] \quad (\text{B-178})$$

For the i^{th} SVC, (B-174) may be expressed as,

$$\begin{aligned} \Delta V_{svci} = & K_{5nii} \Delta \delta_i + \sum_{j \neq i}^n K_{5nij} \Delta \delta_j + K_{6nii} \Delta E''_{qi} + \sum_{j \neq i}^n K_{6nij} \Delta E''_{qj} \\ & + K_{6dnii} \Delta E''_{di} + \sum_{j \neq i}^n K_{6dnij} \Delta E''_{dj} + K_{svc3nii} \Delta \alpha_i + \sum_{j \neq i}^m K_{svc3nij} \Delta \alpha_j \end{aligned} \quad (\text{B-179})$$

where

$$K_{5nii} = V_{svci}^{-1} \left(V_{svcDi} T_{Rdii} + V_{svcQi} T_{Rqii} \right) \quad (\text{B-180})$$

$$K_{5nij} = V_{svci}^{-1} \left(V_{svcDi} T_{Rdij} + V_{svcQi} T_{Rqij} \right) \quad (\text{B-181})$$

$$K_{6nii} = V_{svci}^{-1} \left(V_{svcDi} T_{Ddii} + V_{svcQi} T_{Dqii} \right) \quad (\text{B-182})$$

$$K_{6nij} = V_{svci}^{-1} \left(V_{svcDi} T_{Ddij} + V_{svcQi} T_{Dqij} \right) \quad (\text{B-183})$$

$$K_{6dnii} = V_{svci}^{-1} \left(V_{svcDi} T_{Qdii} + V_{svcQi} T_{Qqii} \right) \quad (\text{B-184})$$

$$K_{6dnij} = V_{svci}^{-1} \left(V_{svcDi} T_{Qdij} + V_{svcQi} T_{Qqij} \right) \quad (\text{B-185})$$

$$K_{svc3nii} = V_{svci}^{-1} \left(V_{svcDi} T_{Adii} + V_{svcQi} T_{Aqii} \right) \quad (\text{B-186})$$

$$K_{svc3nij} = V_{svci}^{-1} \left(V_{svcDi} T_{Adj} + V_{svcQi} T_{Aqj} \right) \quad (\text{B-187})$$

The transfer function block diagram which represents n synchronous generators and m SVCs is shown in Fig. B-1. It is realised by combining equations (B-77), (B-95), (B-107), (B-125), and (B-179).

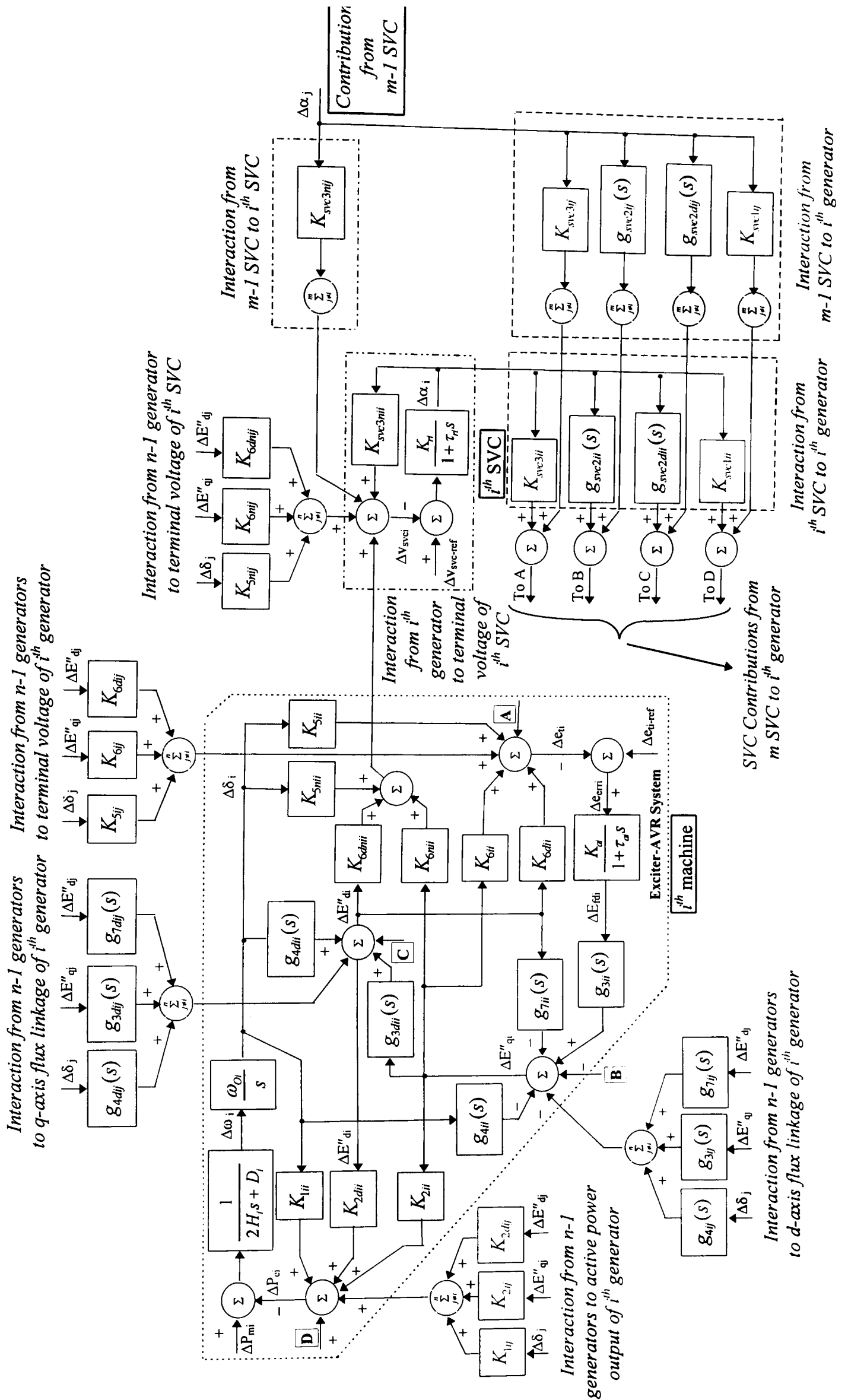


Figure B-1 Transfer function block diagram model of n machine and m SVC system

Appendix C

Derivation of the Small-Signal Transfer-Function Block Diagram Models of the Synchronous Generators-TCSC System

This appendix presents the derivation of the transfer function block diagram model of a synchronous machine and a TCSC system. The system is shown in Fig. 7-1 of Chapter 7. The model $(2d,1q)$, corresponding to a salient-pole machine is used in the derivations.

The vector diagram of the system can be drawn as shown in Fig. C-1.

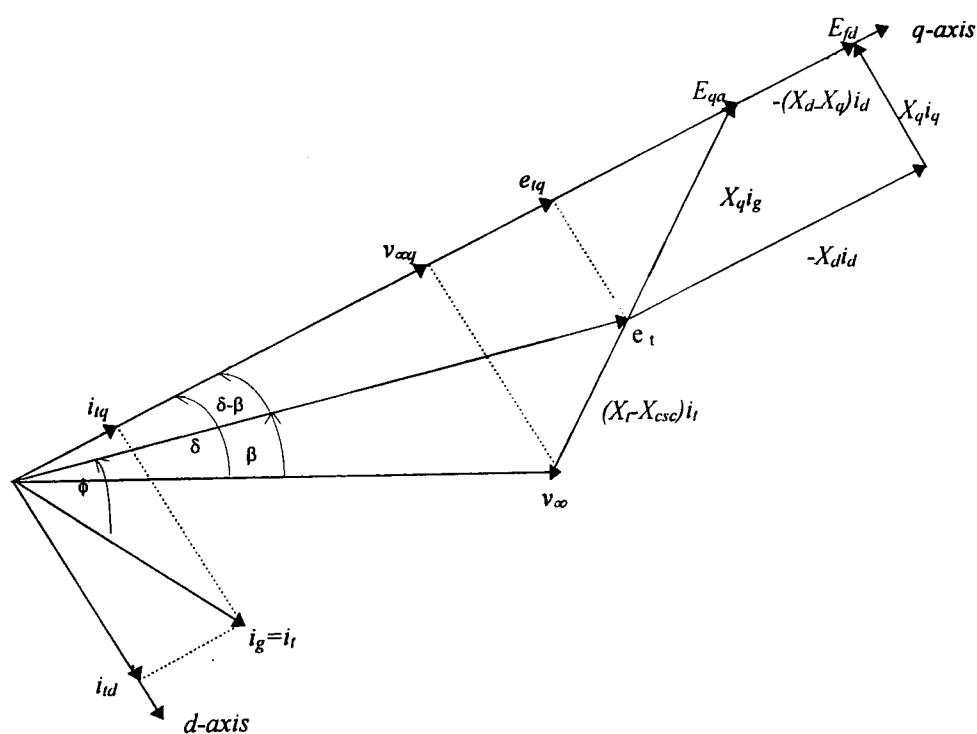


Figure C-1 Vector diagram of a synchronous generator-TCSC system

For the vector diagram in Fig. C-1, with the rotor position taken as the reference, an incremental change of the infinite-bus voltage is given by,

$$\Delta V_{\infty q} = -V_{\infty d0} \Delta \delta \quad (C-1)$$

$$\Delta V_{\infty d} = V_{\infty q0} \Delta \delta \quad (C-2)$$

According to equation (2-32), the total reactance (X_{csc}) of the TCSC can be expressed as,

$$X_{\text{csc}} = X_c - C_1[2(\pi - \alpha) + \sin(2(\pi - \alpha))] + C_2 \cos^2(\pi - \alpha)[\lambda \tan(\lambda(\pi - \alpha)) - \tan(\pi - \alpha)] \quad (\text{C-3})$$

where

$$C_1 = \frac{X_C + X_{LC}}{\pi} \quad (\text{C-4})$$

$$C_2 = \frac{4X_{LC}^2}{\pi X_L} \quad (\text{C-5})$$

$$\lambda = \frac{\omega_o}{\omega} = \sqrt{\frac{X_C}{X_L}} \quad (\text{C-6})$$

$$X_{LC} = \frac{X_C X_L}{X_C - X_L} \quad (\text{C-7})$$

$$\omega_o^2 = \frac{1}{LC} = \omega^2 \frac{X_C}{X_L} \quad (\text{C-8})$$

For small perturbations, variations in the TCSC's total reactance in (C-3) are given by,

$$\Delta X_{\text{csc}} = \left\{ 2C_1(1 + \cos 2\alpha) - C_2 \sin 2\alpha \left[\lambda \frac{\sin(\lambda(\pi - \alpha))}{\cos(\lambda(\pi - \alpha))} - \frac{\sin(\pi - \alpha)}{\cos(\pi - \alpha)} \right] - C_2 \left[\frac{\lambda^2 \cos^2(\pi - \alpha)}{\cos^2(\lambda(\pi - \alpha))} - 1 \right] \right\} \Delta \alpha \quad (\text{C-9})$$

$$\Delta X_{\text{csc}} = F(\alpha) \Delta \alpha \quad (\text{C-10})$$

From the vector diagram in Fig. C-1, \bar{i}_g can be expressed as,

$$\bar{i}_g = \frac{\bar{e}_t - \bar{v}_\infty}{j(X_t - X_{\text{csc}})} \quad (\text{C-11})$$

Separating into real and imaginary parts,

$$i_{gd}(X_t - X_{\text{csc}}) = e_{tq} - v_{\infty q} \quad (\text{C-12})$$

$$i_{gq}(X_t - X_{\text{csc}}) = v_{\infty d} - e_{td} \quad (\text{C-13})$$

Substituting (2-9) into (C-12) gives,

$$i_{gd} = \frac{E_q'' - v_{\infty q}}{X_d'' + X_t - X_{\text{csc}}} \quad (\text{C-14})$$

Substituting (2-8) into (C-13) gives,

$$i_{gq} = \frac{v_{\infty d} - E_d''}{X_q'' + X_t - X_{\text{csc}}} \quad (\text{C-15})$$

By applying a small perturbation, (C-14) and (C-15) can be expressed as,

$$\Delta i_{gd} = \left[\frac{1}{\Lambda_d''} \right] \Delta E_q'' + \left[\frac{V_{\infty do}}{\Lambda_d''} \right] \Delta \delta + \left[\frac{i_{gdo}}{\Lambda_d''} \right] \Delta X_{csc} \quad (C-16)$$

$$\Delta i_{gq} = - \left[\frac{1}{\Lambda_q''} \right] \Delta E_d'' + \left[\frac{V_{\infty qo}}{\Lambda_q''} \right] \Delta \delta + \left[\frac{i_{gqo}}{\Lambda_q''} \right] \Delta X_{csc} \quad (C-17)$$

where

$$\Lambda_d'' = X_d'' + X_t - X_{csc} \quad (C-18)$$

$$\Lambda_q'' = X_q'' + X_t - X_{csc} \quad (C-19)$$

D-axis Flux Linkage Voltage Equation:

Transient Voltage Equation

Transforming the transient voltage equation (2-6) into the S domain, and for small variations,

$$(1 + \tau'_{do}s) \Delta E_q' = \Delta E_{fd} - (X_d - X_d') \Delta i_{gd} \quad (C-20)$$

Re-arranging (C-20) by making use of (C-16) gives,

$$\Delta E_q' = \frac{1}{1 + \tau'_{do}s} (\Delta E_{fd} - C_1 \Delta E_q'' - C_2 \Delta \delta - C_3 \Delta X_{csc}) \quad (C-21)$$

where

$$C_1 = \left[\frac{X_d - X_d'}{\Lambda_d''} \right] \quad (C-22)$$

$$C_2 = \left[\frac{(X_d - X_d') v_{\infty do}}{\Lambda_d''} \right] \quad (C-23)$$

$$C_3 = \left[\frac{(X_d - X_d') i_{gdo}}{\Lambda_d''} \right] \quad (C-24)$$

Subtransient Voltage Equation:

Transforming the subtransient voltage equation (2-10) into the S domain, and re-arranging by making use of (C-20) gives,

$$(1 + \tau''_{do}s) \Delta E_q'' = C_4 \Delta E_{fd} - C_5 \Delta i_{gd} + C_6 \Delta E_q' \quad (C-25)$$

where

$$C_4 = \left[\frac{\tau''_{do}}{\tau'_{do}} \right] \quad (C-26)$$

$$C_5 = \left[(X_d' - X_d'') + \frac{\tau''_{do}}{\tau'_{do}} (X_d - X_d') \right] \quad (C-27)$$

$$C_6 = \left[1 - \frac{\tau''_{do}}{\tau'_{do}} \right] \quad (C-28)$$

Re-arranging (C-25) by making use of (C-21), (C-16) and (C-10) gives,

$$C_7(s)\Delta E_q'' = C_8(s)\Delta E_{fd} - C_9(s)\Delta\delta - C_{10}(s)\Delta\alpha \quad (C-29)$$

where

$$C_7(s) = \left[\frac{\Lambda_d + \left\{ \tau'_{do}\Lambda'_d + \tau''_{do}(\Lambda''_d + (X_d - X'_d)) \right\} s + \left\{ \tau'_{do}\tau''_{do}\Lambda''_d \right\} s^2}{\Lambda''_d(1 + \tau'_{do}s)} \right] \quad (C-30)$$

$$\Lambda_d = X_d + X_t - X_{csc} \quad (C-31)$$

$$C_8(s) = \left[\frac{1 + \tau''_{do}s}{1 + \tau'_{do}s} \right] \quad (C-32)$$

$$C_9(s) = v_{\infty do} \left[\frac{(X_d - X''_d) + \left\{ \tau'_{do}(X'_d - X''_d) + \tau''_{do}(X_d - X'_d) \right\} s}{\Lambda''_d(1 + \tau'_{do}s)} \right] \quad (C-33)$$

$$C_{10}(s) = i_{gd} \left[\frac{(X_d - X''_d) + \left\{ \tau'_{do}(X'_d - X''_d) + \tau''_{do}(X_d - X'_d) \right\} s}{\Lambda''_d(1 + \tau'_{do}s)} \right] F(\alpha) \quad (C-34)$$

or

$$\Delta E_q'' = g_3(s)\Delta E_{fd} - g_4(s)\Delta\delta - g_{csc2}(s)\Delta\alpha \quad (C-35)$$

where

$$g_3(s) = \left[\frac{\Lambda''_d(1 + \tau''_{do}s)}{\Lambda_d + \left\{ \tau'_{do}\tau''_{do}\Lambda''_d + \tau'_{do}(X'_d - X''_d) + \tau''_{do}(X_d - X'_d) \right\} s + \left\{ \tau'_{do}\tau''_{do}\Lambda''_d \right\} s^2} \right] \quad (C-36)$$

$$g_4(s) = \left[\frac{v_{\infty do} \left((X_d - X''_d) + \left\{ \tau'_{do}(X'_d - X''_d) + \tau''_{do}(X_d - X'_d) \right\} s \right)}{\Lambda_d + \left\{ \tau'_{do}\tau''_{do}\Lambda''_d + \tau'_{do}(X'_d - X''_d) + \tau''_{do}(X_d - X'_d) \right\} s + \left\{ \tau'_{do}\tau''_{do}\Lambda''_d \right\} s^2} \right] \quad (C-37)$$

$$g_{csc2}(s) = \left[\frac{i_{gd} \left((X_d - X''_d) + \left\{ \tau'_{do}(X'_d - X''_d) + \tau''_{do}(X_d - X'_d) \right\} s \right)}{\Lambda_d + \left\{ \tau'_{do}\tau''_{do}\Lambda''_d + \tau'_{do}(X'_d - X''_d) + \tau''_{do}(X_d - X'_d) \right\} s + \left\{ \tau'_{do}\tau''_{do}\Lambda''_d \right\} s^2} \right] F(\alpha) \quad (C-38)$$

Q-axis Flux Linkage Voltage Equation:

Transforming the subtransient voltage equation (2-11) into the S domain, and for small variations,

$$(1 + \tau''_{qo}s)\Delta E_d'' = (X_q - X''_q)\Delta i_{gq} \quad (C-39)$$

Re-arranging (C-61) by making use of (C-15) and (C-40) gives,

$$\Delta E_d'' = g_{4d}(s)\Delta\delta + g_{csc2d}(s)\Delta\alpha \quad (C-40)$$

or

$$\Delta E_d'' = \frac{1}{1 + \tau''_{qo}s} (K_{4d}\Delta\delta + K_{csc2d}\Delta\alpha) \quad (C-41)$$

where

$$g_{4d}(s) = \left[\frac{K_{4d}}{(1 + \tau_q''s)} \right] \quad (C-42)$$

$$g_{svc2d}(s) = \left[\frac{K_{csc2d}}{(1 + \tau_q''s)} \right] \quad (C-43)$$

$$K_{4d} = \left[\frac{(X_q - X_q'')v_{\infty qo}}{\Lambda_q} \right] \quad (C-44)$$

$$\Lambda_q = X_q + X_t - X_{csc} \quad (C-45)$$

$$K_{csc2d} = \left[\frac{(X_q - X_q'')i_{gqo}}{\Lambda_q} \right] F(\alpha) \quad (C-46)$$

$$\tau_q'' = \left[\frac{\Lambda_q''}{\Lambda_q} \tau_{qo}'' \right] \quad (C-47)$$

Generator Terminal Voltage Equation:

The generator's terminal voltage in equation (2-2) can be expressed in terms of d and q -axis components for small variations as follows,

$$\Delta e_t = \frac{e_{tdo}}{e_{to}} \Delta e_{td} + \frac{e_{tqo}}{e_{to}} \Delta e_{tq} \quad (C-48)$$

Substituting (C-16) into (2-9) gives,

$$\Delta e_{tq} = \left[\frac{X_t - X_{csc}}{\Lambda_d''} \right] \Delta E_d'' - \left[\frac{X_d'' v_{\infty do}}{\Lambda_d''} \right] \Delta \delta - \left[\frac{X_d'' i_{gdo}}{\Lambda_d''} \right] \Delta X_{csc} \quad (C-49)$$

Substituting (C-40) into (2-8) gives,

$$\Delta e_{td} = \left[\frac{X_t - X_{csc}}{\Lambda_q''} \right] \Delta E_d'' + \left[\frac{X_q'' v_{\infty qo}}{\Lambda_q''} \right] \Delta \delta + \left[\frac{X_q'' i_{gqo}}{\Lambda_q''} \right] \Delta X_{csc} \quad (C-50)$$

Re-arranging (C-48) by making use of (C-49), (C-50) and (C-10) yields,

$$\Delta e_t = K_5 \Delta \delta + K_6 \Delta E_d'' + K_{6d} \Delta E_d'' + K_{csc3} \Delta \alpha \quad (C-51)$$

where

$$K_5 = \left[\frac{e_{tdo}}{e_{to}} \cdot \frac{X_q'' v_{\infty qo}}{\Lambda_q''} - \frac{e_{tqo}}{e_{to}} \cdot \frac{X_d'' v_{\infty do}}{\Lambda_d''} \right] \quad (C-52)$$

$$K_6 = \left[\frac{e_{tqo}}{e_{to}} \cdot \frac{X_t - X_{csc}}{\Lambda_d''} \right] \quad (C-53)$$

$$K_{6d} = \left[\frac{e_{tdo}}{e_{to}} \cdot \frac{X_t - X_{csc}}{\Lambda_q''} \right] \quad (C-54)$$

$$K_{csc3} = \left[\frac{e_{tdo}}{e_{to}} \cdot \frac{X_q'' i_{gqo}}{\Lambda_q''} - \frac{e_{tqo}}{e_{to}} \cdot \frac{X_d'' i_{gdo}}{\Lambda_d''} \right] F(\alpha) \quad (C-55)$$

Electrical Power Equation:

The active power output of a synchronous generator, equation (2-20), can be expressed as,

$$P_e = v_{\infty d} i_{td} + v_{\infty q} i_{tq} \quad (\text{C-56})$$

For small perturbations, the electrical power in (C-56) can be expressed as,

$$\Delta P_e = v_{\infty do} \Delta i_{td} + i_{tdo} \Delta v_{\infty d} + v_{\infty qo} \Delta i_{tq} + i_{tqo} \Delta v_{\infty q} \quad (\text{C-57})$$

Re-arranging (C-57) by making use of (C-16), (C-17) and (C-10) yields,

$$\Delta P_e = K_1 \Delta \delta + K_2 \Delta E_q'' - K_{2d} \Delta E_d'' + K_{\text{csc}1} \Delta \alpha \quad (\text{C-58})$$

where

$$K_1 = \left[\frac{v_{\infty do}^2}{\Lambda_d''} + \frac{v_{\infty qo}^2}{\Lambda_q''} + i_{tdo} v_{\infty qo} - i_{tqo} v_{\infty do} \right] \quad (\text{C-59})$$

$$K_2 = \left[\frac{v_{\infty do}}{\Lambda_d''} \right] \quad (\text{C-60})$$

$$K_{2d} = \left[\frac{v_{\infty qo}}{\Lambda_q''} \right] \quad (\text{C-61})$$

$$K_{\text{csc}1} = \left[\frac{v_{\infty do} i_{gdo}}{\Lambda_d''} + \frac{v_{\infty qo} i_{gqo}}{\Lambda_q''} \right] F(\alpha) \quad (\text{C-62})$$

TCSC Current Equation:

similarly to the generator terminal voltage, the current across the TCSC can be expressed in terms of d and q -axis components, for small variations, as follows,

$$\Delta i_{\text{csc}} = \frac{i_{tdo}}{i_{to}} \Delta i_{td} + \frac{i_{tqo}}{i_{to}} \Delta i_{tq} \quad (\text{A-63})$$

Re-arranging (A-63) by making use of (A-16) and (A-17), (A-10) yields,

$$\Delta i_{\text{csc}} = K_{5n} \Delta \delta + K_{6n} \Delta E_q'' - K_{6dn} \Delta E_d'' + K_{\text{csc}3n} \Delta \alpha \quad (\text{A-64})$$

where

$$K_{5n} = \left[\frac{i_{tdo}}{i_{to}} \cdot \frac{v_{\infty do}}{\Lambda_d''} + \frac{i_{tqo}}{i_{to}} \cdot \frac{v_{\infty qo}}{\Lambda_q''} \right] \quad (\text{A-65})$$

$$K_{6n} = \left[\frac{i_{tdo}}{i_{to}} \cdot \frac{1}{\Lambda_d''} \right] \quad (\text{A-66})$$

$$K_{6dn} = \left[\frac{i_{tqo}}{i_{to}} \cdot \frac{1}{\Lambda_q''} \right] \quad (\text{A-67})$$

$$K_{\text{csc}3n} = \left[\frac{i_{tdo}^2}{i_{to}} \cdot \frac{1}{\Lambda_d''} + \frac{i_{tqo}^2}{i_{to}} \cdot \frac{1}{\Lambda_q''} \right] F(\alpha) \quad (\text{A-68})$$

The transfer function block diagram of the synchronous generator-TCSC system shown in Fig. C-2 is realised by combining equation (C-35), (C-41), (C-51) and (C-64).

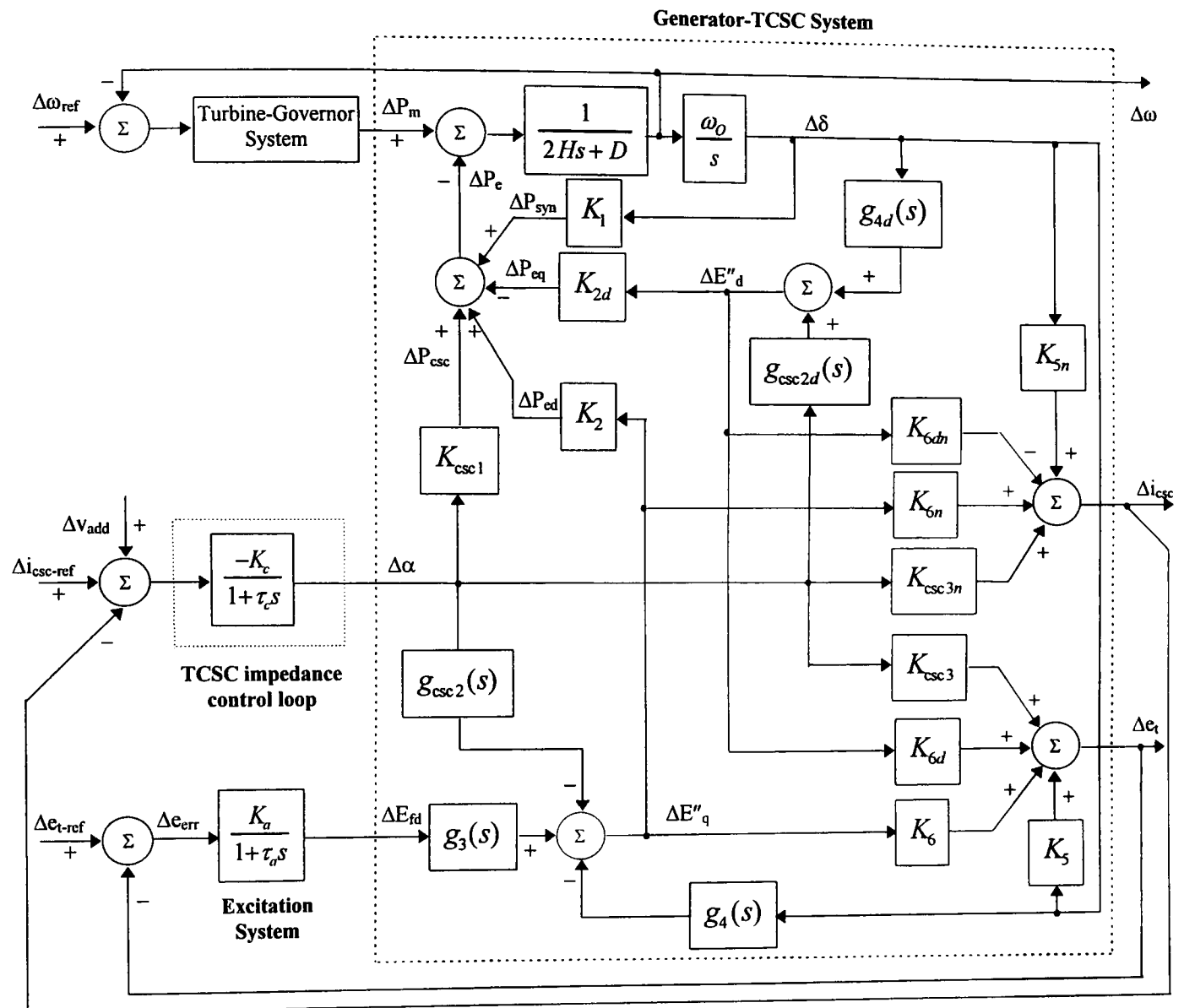


Figure C-2 Block diagram model of synchronous generator and TCSC System

Appendix D

System Parameters

Synchronous generator parameters

Direct axis:

| | |
|----------------------------|------------------------|
| Synchronous reactance | $X_d = 1.445$ p.u. |
| Transient reactance | $X'_d = 0.316$ p.u. |
| Subtransient reactance | $X''_d = 0.179$ p.u. |
| Transient time constant | $\tau'_{do} = 5.26$ s |
| Subtransient time constant | $\tau''_{do} = 5.26$ s |

Quadrature axis:

| | |
|----------------------------|-------------------------|
| Synchronous reactance | $X_q = 0.959$ p.u. |
| Subtransient reactance | $X''_q = 0.162$ p.u. |
| Subtransient time constant | $\tau''_{qo} = 0.159$ s |
| Stator resistance | $R_a = 0$ |
| Inertia constant | $H = 4.27$ s |
| Damping coefficient | $D = 0$ |
| Nominal frequency | $f_o = 50$ Hz |

Excitation control system

$$g_{avr}(s) = K_a / (1 + s\tau_a)$$

| | |
|---------------------------------|-------------------|
| Voltage regulator time constant | $\tau_a = 0.05$ s |
| Voltage regulator gain | $K_a = 100$ |

Thyristor-controlled reactor system

SVC

| | |
|----------------------|------------------|
| Inductive reactance | $X_L = 2.5$ p.u. |
| Capacitive reactance | $X_C = 2.5$ p.u. |

TCSC

| | |
|----------------------|---------------------|
| Inductive reactance | $X_L = 0.005$ p.u. |
| Capacitive reactance | $X_C = 0.0025$ p.u. |